Universitat Autònoma de Barcelona

Aptasensors based on Electrochemical Impedance Spectroscopy

Cristina Ocaña Tejada

Doctoral Thesis

Doctoral Studies in Chemistry

Supervisor: Manel del Valle Zafra

Departament de Química

Facultat de Ciències

2015

Thesis submitted to aspire for the Doctor Degree

Cristina Ocaña Tejada

Supervisor's Approval:

Dr. Manel del Valle Zafra

Professor of Analytical Chemistry

Bellaterra (Cerdanyola del Vallès), 4th June 2015

Acknowledgments

The present dissertation has been carried out at the laboratories of the Grup de Sensors i Biosensors of the Departament de Química from Universitat Autònoma de Barcelona, thanks to the FPI fellowship and *Estancias Breves* Grant provided by Ministry of Science and Innovation (MCINN), and the financial support of the Projects; “Estrategias en el desarrollo y aplicación de lenguas electrónicas empleando biosensors y nuevos materiales de reconocimiento” (MCINN CTQ2010-17099), and “ Electronic tongue fingerprinting: aplicaciones en el campo alimentario y de seguridad” (MCINN, CTQ2013-41577-P).

Grup de Sensors i Biosensors

Unitat de Química Analítica

Departament de Química

Universitat Autónoma de Barcelona

Edifici Cn, 08193, Bellaterra.

A mi familia

A person who never made
a mistake never tried anything new

Albert Einstein

TABLE OF CONTENTS

Table of contents

LIST OF ABBREVIATIONS AND SYMBOLS

List of abbreviations and symbols

α	Constant Phase Element exponent
σ	Warburg coefficient
φ	Phase angle
ω	Radial frequency
Δ	Difference between R_{ct} values
Δ_{ratio}	Signal for representation of the results
AbCyt *c*	Antibody of Cytochrome c
AC	Alternating Current
AgNPs	Silver Nanoparticles
AIV	Avian Influenza Virus
AMP	Adenosine monophosphate
Apt	Aptamer
AptCyt *c*	Aptamer of Cytochrome c
AptCyt *c* Bio	Aptamer of Cytochrome c biotinylated
AptCyt *c* NH_2	Aptamer of Cytochrome c aminated
AptThr	Aptamer of Thrombin
AptThrBio	Aptamer of Thrombin biotinylated
AuNPs	Gold nanoparticles
Av	Avidin
AvGEC	Avidin Graphite Epoxy Composite
BSA	Bovin Serum Albumin
C	Capacitance
CdSe	Cadmium Selenide
CdTe	Cadmium Telluride
CFU	Colony-Forming Unit
CNT	Carbon Nanotube

CPE	Constant Phase Element
CV	Cyclic Voltammetry
Cyt *c*	Cytochrome c
DNA	Desoxyribonucleic Acid
Dox	Doxorubicin
DPV	Diferential Pulse Voltammetry
E	Potential
EDAC	1-Ethyl-3-[dimethylaminopropyl]carbodiimide
EIS	Electrochemical Impedance Spectroscopy
FET	Field-Effect Transistor
GCE	Glassy Carbon Electrode
GEC	Graphite Epoxy Composite
HIV-1	Human Immunodeficiency Virus 1
HIV-RT	Reverse transcriptase of the type 1 human deficiency virus
HRP	Horse Radish Peroxidase
I	Current Intensity
IFN-ɣ	Interferon-gamma
IgE	Immunoglobulin E
IgG	Immunoglobulin G
ISFET	Ion-Sensitive Field-Effect Transistor
IUPAC	International Union of Pure and Applied Chemistry
LSAW	Leaky Surface Acoustic Wave
MAB	Molecular Aptamer Beacon
MCE	Mercaptoethanol
min	Minutes
MRI	Magnetic Resonance Imaging
MWCNT	Multi Walled Carbon Nanotube
NHS	N-Hydroxysuccinimide
NTA	Nitrilotriacetic acid

OTA	Ochratoxin A
PBS	Phosphate Buffer Saline
PCR	Polymerase Chain Reaction
PDGF	Platelet-derived Growth Factor
PEG	Poly(ethylene glycol)
ProThr	Prothrombin
PVC	Poly(vinyl chloride)
Q	Symbol use for CPE
QD	Quantum dot
QCM	Quartz Crystal Microbalance
R	Resistance
R_{ct}	Electron transfer Resistance
rGO	Reduced Graphene Oxide
RNA	Ribonucleic Acid
R_s	Resistance of the solution
RSD	Relative Standard Deviation
SAM	Self-Assembled Monolayers
SAW	Surface Acoustic Wave
SDS	Sodium dodecylsulfate
SELEX	Systematic Evolution of Ligands by Exponential Enrichment
SEM	Scanning Electron Microscopy
SERS	Surface-enhanced Raman Spectroscopy
SPE	Screen printed electrode
SPR	Surface Plasmon Resonance
Strep	Streptavidin
Strep-AuNPs	Streptavidin gold nanoparticles
SWCNT	Single Wall Carbon Nanotube
SWV	Squarewave Voltammetry
TEM	Transmission Electron Microscopy

Thr	Thrombin
TSC	Trisodium citrate buffer
W	Warburg
Z	Impedance
Z_i	Imaginary part of impedance
ZnS	Zinc sulphide
Z_r	Real part of impedance

SUMMARY

Summary

In the recent years, due to the need for rapid diagnosis and improvements in sensing, new recognition elements are employed in biosensors. One kind of these new recognition elements are aptamers. Aptamers are synthetic strands of DNA or RNA which are selected in vitro and have the ability to bind to proteins, ions, whole cells, drugs and low molecular weight ligands recognizing their target with high affinity and specificity. Several aptamer-based biosensors, also called aptasensors, have been recently developed. Among all the transduction techniques employed in biosensors, Electrochemical Impedance Spectroscopy has widely used as a tool for characterizing sensor platforms and for studying biosensing events at the surface of the electrodes. The important feature presented by this technique is that it does not require any labelled species for the transduction; thus, this detection technique can be used for designing label-free protocols thus avoiding more expensive and time-consuming assays.

The main aim of this PhD work was the development of aptasensors using the electrochemical impedance technique previously mentioned for protein detection. For that, different types of electrodes were used, such as Graphite Epoxy Composite electrodes (GECs), Avidin Graphite Epoxy Composite electrodes (AvGECs) and commercial Multi-Walled carbon nanotubes screen printed electrodes (MWCNT-SPE).

The work was divided in two main parts according to the detection of the two different proteins.

The first part was focused on thrombin detection. First of all, different impedimetric label-free aptasensors based on several aptamer immobilization techniques such as wet physical adsorption, avidin-biotin affinity and covalent bond via electrochemical activation of the electrode surface and via electrochemical grafting were developed and evaluated. Then, AvGECs electrodes

were compared as a platform for genosensing and aptasensing. With the aim to amplying the obtained impedimetric signal using AvGECs, an aptamer sandwich protocol for thrombin detection was used including streptavidin gold-nanoparticles (Strep-AuNPs) and silver enhancement treatment.

The second part of the study was based on cytochrome c detection. Firstly, a simple label-free aptasensor for the detection of this protein using a wet physical adsorption immobilization technique was performed. Finally, with the goal to amplify the impedimetric signal, a hybrid aptamer-antibody sandwich assay using MWCNT-SPE for the detection of the target protein was carried out.

In this way, the thesis explores and compares a wide scope of immobilization procedures, the use of label-free or nanocomponent modified biomolecules in different direct or amplified protocols, and the use of direct recognition and sandwich alternatives to enhance sensitivity and/or selectivity of the assay.

RESUMEN

Resumen

En los últimos años, debido a la necesidad de análisis rápidos y de mejoras en sensado, se han utilizado nuevos elementos de reconocimiento en biosensores. Uno de estos nuevos elementos de reconocimiento son los aptámeros. Los aptámeros son cadenas sintéticas de ADN o ARN las cuáles son seleccionadas *in vitro* y tienen la habilidad de unirse a proteínas, iones, células, fármacos y ligandos de bajo peso molecular reconociendo a sus moléculas diana con alta afinidad y especificidad. Diversos biosensores basados en aptámeros, también llamados aptasensores, han sido desarrollados recientemente. De entre todas las técnicas de transducción utilizadas, la Espectrocopía Electroquímica de Impedancia ha sido ampliamente utilizada como herramienta para caracterizar superficies de sensores y estudiar eventos de biosensado en la superficie de electrodos. La característica más importante que presenta está técnica es que no requiere ninguna especie marcada para la transducción; por lo tanto, está técnica de detección puede utilizarse para diseñar protocolos directos sin etiquetaje, evitando ensayos más caros y laboriosos.

El principal objetivo de esta tesis doctoral fue el desarrollo de aptasensores utilizando la técnica electroquímica de impedancia mencionada anteriormente para la detección de proteínas. Para ello, diferentes tipos de electrodos fueron utilizados, tales como electrodos de compósito grafito-epoxi, electrodos de biocompósito grafito-epoxi modificados con moléculas de avidina y electrodos comerciales serigrafiados de nanotubos de carbono de pared múltiple.

El trabajo se dividió principalmente en dos partes de acuerdo con la detección de dos proteínas diferentes.

La primera parte se focalizó en la detección de trombina. Antes de nada, se compararon y evaluaron varios aptasensores de detección directa sin etiquetaje basados en diferentes técnicas de inmovilización de los aptámeros, tales como: adsorción física húmeda, afinidad avidina-biotina y enlace covalente

mediante activación electroquímica de la superficie del electrodo y mediante inserción electroquímica. Posteriormente, los electrodos de biocompósito fueron comparados como plataformas en genosensado y aptasensado. Con la finalidad de amplificar la señal impedimétrica obtenida utilizando electrodos de biocompósito, un protocolo sándwich fue empleado incuyendo nanopartículas de oro modificadas con estreptavidina y tratamiento amplificador de plata.

La segunda parte del estudio se basó en la detección de citocromo c. Primeramente, se realizó un simple aptasensor de detección directa de ésta proteína sin etiquetaje utilizando la técnica de inmovilización de adsorción física húmeda. Finalmente, y con el objetivo de amplificar la señal impedimétrica, se desarrolló un ensayo tipo sándwich hibrido de aptámero y anticuerpo utilizando electrodos serigrafiados de nanotubos de carbono de pared múltiple para la detección de la proteína.

De esta manera, la tesis explora y compara una amplia gama de procedimientos de inmovilización, el uso de detección directa sin etiquetas o nanomaterial modificado con biomoléculas en diferentes protocolos directos o de amplificación, y el uso de reconocimiento directo y sándwich para amplificar la sensibilidad y/o la selectividad del ensayo.

RESUM

Resum

En els últims anys, a causa de la necessitat de diàgnostics ràpids i de millores en sensat, s'han utilitzat nous elements de reconeixement en biosensors. Un tipus d'aquests nous elements de reconeixement són els aptàmers. Els aptàmers són cadenes sintètiques de ADN o ARN les quals són seleccionades *in vitro* i tenen la capacitat d'unir-se a proteïnes, ions, cèl.lules, fàrmacs i lligands de baix pes molecular, reconeixent les seves molècules diana amb alta afinitat i especificitat. Diversos biosensors basats en aptàmers, també anomenats aptasensors, han sigut desenvolupats recentment. D'entre totes les tècniques de transducció utilitzades en biosensors, l'Espectrocòpia Electroquímica d'Impedància ha sigut àmpliament emprada como a eina per caracteritzar la superficies de sensors i estudiar esdeveniments en el biosensat en la superficie d'elèctrodes. La característica més important que presenta aquesta tècnica és que no requereix cap espècie marcada per a la transducció, per tant, aquesta tècnica de detecció pot utilitzar-se per dissenyar protocols de detecció directa sense marcatge, evitant assajos més cars i laboriosos.

El principal objectiu d'aquesta tesi doctoral va ser el desenvolupament d'aptasensors utilitzant la tècnica electroquímica d'impedància esmentada anteriorment. Per a això, diferents tipus d'elèctrodes van ser utilitzats, tals com elèctrodes de compòsit grafit-epoxi, elèctrodes de biocompòsit grafit-epoxi modificats amb molècules d'avidina i elèctrodes comercials serigrafiats de nanotubs de carboni de paret múltiple.

El treball es va dividir principalmente en dues parts d'acord amb la detecció de dues proteïnes diferents.

La primera part es va focalitzar en la detecció de trombina. Primer de tot, es van comparar i avaluar diversos aptasensors de detecció directa sense marcatge basat en diferents tècniques d'immobilització dels aptàmers, tals com: adsorció física humida, afinitat avidina-biotina i enllaç covalent mitjançant

activació electroquímica de la superfície de l'elèctrode i mitjançant inserció electroquímica. Posteriorment, els elèctrodes de biocompòsit van ser comparats com a plataformes en genosensat i aptasensat. Amb la finalitat d'amplificar el senyal impedimètric obtingut utilitzant elèctrodes de biocompòsit, un protocol sandwich va ser emprat incloent nanopartícules d'or modificades amb estreptavidina i tractament amplificador de plata.

La segona part de l'estudi es va basar en la detecció de citocrom c. Primerament, es va realitzar un simple aptasensor de detecció directa sense marcatge per a la detecció d'aquesta proteïna utilitzant la tècnica d'immobilització d'adsorció física humida. Finalment, i amb l'objectiu d'amplificar el senyal impedimètric, es va desenvolupar un assaig tipus sandwich híbrid d'aptàmer i anticòs utilitzant elèctrodes serigrafiats de nanotubs de carboni de paret múltiple.

D'aquesta manera, la tesi explora i compara una àmplia gamma de procediments d'immobilització, l'ús de detecció directa sense marcatge o nanomaterial modificat amb biomolècules en diferents protocols directes o d'amplificació, i l'ús de reconeixement directe i sandwich per amplificar la sensibilitat i/o la selectivitat de l'assaig.

CHAPTER 1. INTRODUCTION

1. Introduction

1.1. Biosensors

In recent years, the importance of monitoring and controlling many different parameters in fields such as clinical diagnoses, food industry, environment, forensics or drug development has been increasing. Thus, there is a need to have reliable analytical devices capable to carry out fast and accurate analyses. Conventional methods provide high sensitivity and selectivity but they are expensive, time consuming and require highly trained personal. One way to overcome many disadvantages of these methods is to develop biosensors.

1.1.1 Brief history of Biosensors

The history of biosensors started with the development of enzyme electrodes by the Professor Leland C Clark Jnr. In 1962, Clark published his paper on the oxygen electrode [21]. The concept was illustrated by an experiment in which glucose oxidase was entrapped at a Clark oxygen electrode using dialysis membrane. A few years later, in 1975 Clark's biosensor became commercial reality with the successful re-launch of the Yellow Springs Instrument Company (Ohio) glucose analyser based on the amperometric detection of hydrogen peroxide.

After Clark published his enzyme electrode paper, Garry A. Rechnitz with S. Katz published one of the first papers in the area of biosensors with the direct potentiometric determination of urea after urease hydrolysis in 1963. In 1969 the potentiometric urea electrode was introduced by George Guilbault and Joseph Moltavo using immobilized urease and a pH-sensitive sensor [64]. Then, in 1973 Ph. Racinee and W. Mindt developed the first lactate electrode [127]. In 1976, Clemens and his co-workers incorporated an electrochemical glucose biosensor bedside an artificial pancreas, and a few years later this biosensor was marketed by Miles Laboratories [22, 149]. Finally, Karl Cammann introduced the term “biosensor” in 1977 [19], but it was not until 1997 when IUPAC introduced for the first time the definition for biosensors in analogy to the definition of chemosensors [156].

Nowadays, as can be seen in Figure 1.1, the work on biosensors and papers published continues to make progress using different biological elements in combination with various types of transducers.

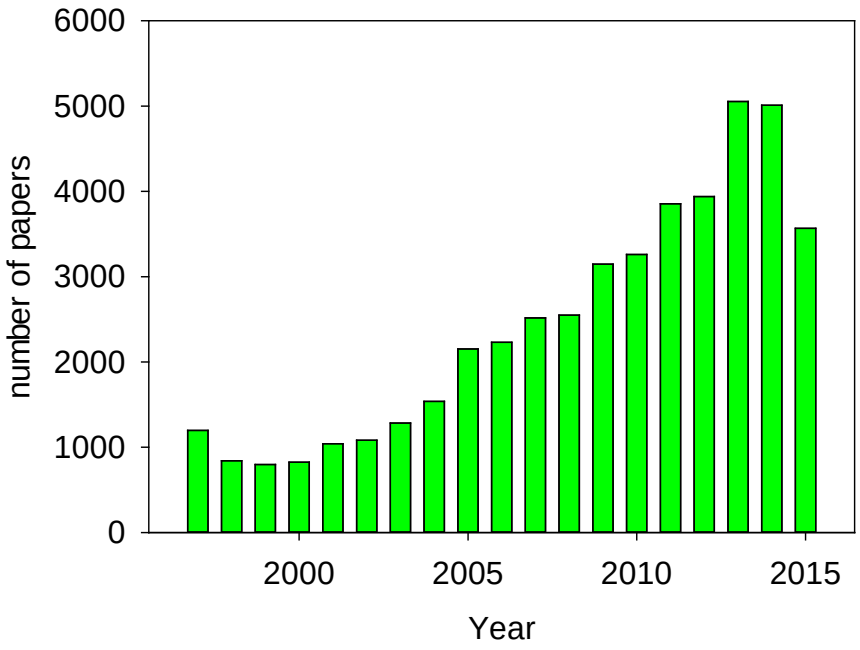

Figure 1.1. Number of biosensors' publications published from 1995 to 2015 (Science Direct-May 2015).

In commercial term, biosensors are quickly acquiring popularity in the global market due to their wide variety of applications in the fields of medical diagnostics, pharmaceuticals, biodefense, food industry and industrial processes. The greatest application for biosensors continues to be blood glucose devices. However, the market is changing towards other applications such as infectious disease screening, cholesterol testing, blood gas analyses, pregnancy testing and applications in industrial biology, food toxicity detection and military field [186].

1.1.2. Definition and classification

Several definitions have been proposed to define biosensors, but according to the IUPAC in 1999, a biosensor is an independently integrated receptor transducer device, which is capable of providing selective quantitative

or semi-quantitative analytical information using a biological recognition element [181].

The term biosensors means that the device is a combination of three parts: (i) a biorecognition element or bioreceptor, (ii) a sensor element also called transducer and (iii) a signal processing system. The basic concepts of a biosensors' operation can be illustrated in Figure 1.2. A bioreceptor generally consists of an immobilized biocomponent that is able to detect the specific target analyte. On the other hand, the transducer is a converter. The reaction between the analyte and the bioreceptor causes a chemical change, and this change is converted into an electrical signal by the transducer. Finally, the electrical signal is amplified and sent to a microelectronics and data processor.

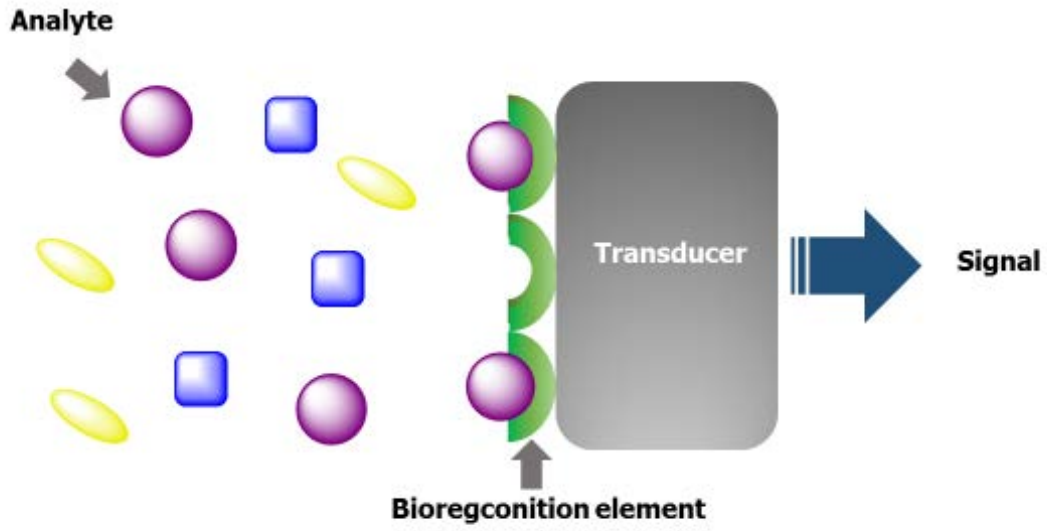

Figure 1.2. Schematic representation of a biosensor.

Biosensors can be classified either by the type biorecognition element that they utilize or by the type of transduction they employ. Most forms of transduction can be categorized in one of four main groups: optical, calorimetric, piezoelectric and electrochemical, as indicated in Figure 1.3. In

addition, this group can be further divided into two general categories; label (indirect detection) and label-free types (direct detection).

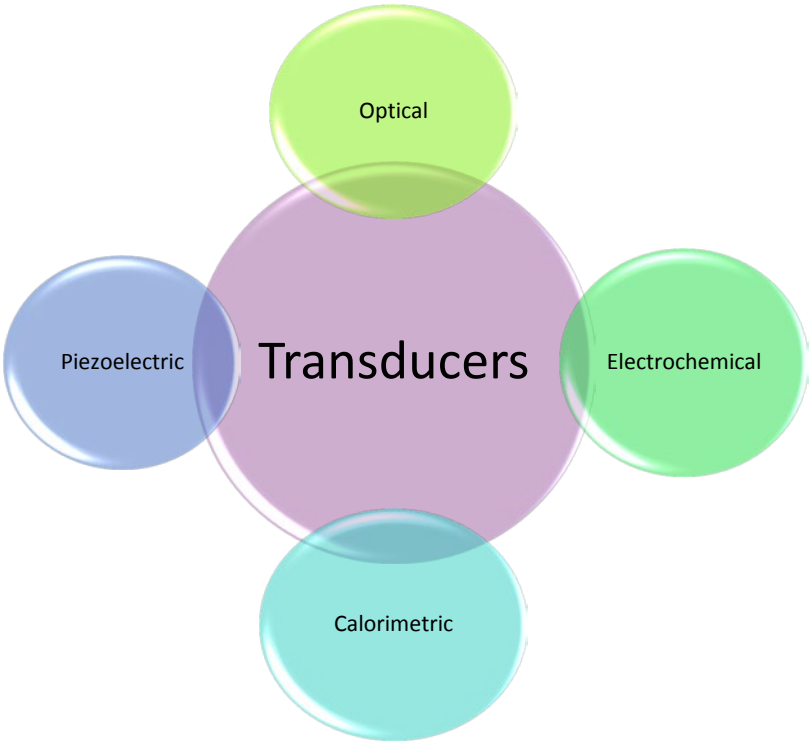

Figure 1.3. Classification of transducers used in biosensors.

Among all types, electrochemical biosensors are especially attractive because of the remarkable high sensitivity, low cost, fast-response and experimental simplicity. Moreover, they are the most frequently used in commercialized biosensors, for instance for blood glucose testing. The small size of electrodes and the possibility to miniaturization permit the construction of hand devices or/and in field devices.

As mentioned above, biosensors also can be classified depending on the type of bioreceptor used. Generally they can be divided into five major groups: enzyme based sensors, nucleic acid based sensors (called genosensors), cell based sensors, immunosensors and biomimetic sensors, see Figure 1.4.

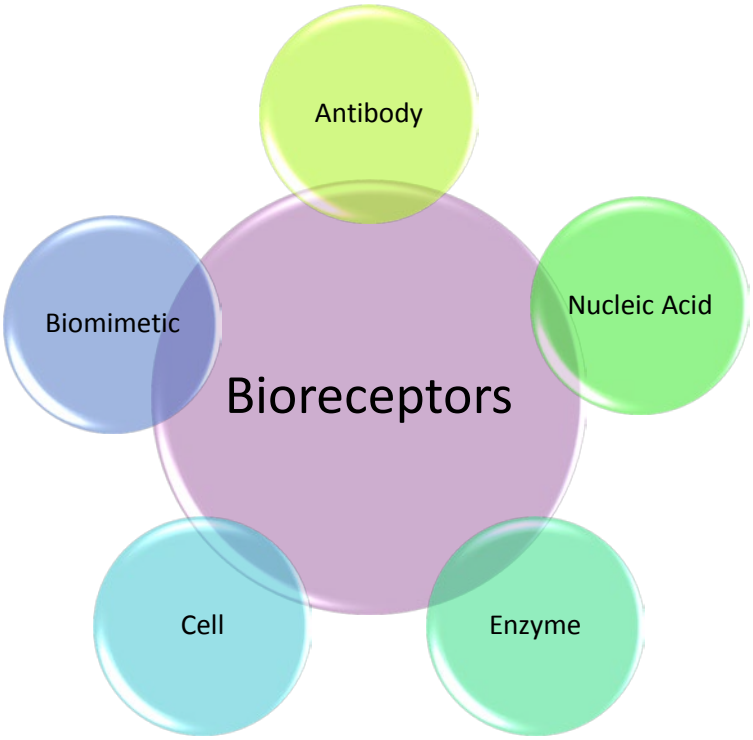

Figure 1.4. Classification of bioreceptors used in biosensors.

1.2. Aptamer

Since Watson and Crick proposed the double helix structure of DNA in 1953 [194], the development of DNA based sensors or genosensors has been increasing [10, 122, 191]. Recently, synthetic DNA/RNA structures called aptamers have attracted more and more interest.

The word aptamer derives from the Latin word *aptus*, which means to fit, and the Greek *meros*, meaning region [47, 175]. Nucleic acid aptamers are single artificial strands of DNA or RNA with a length in the range of 10-100 nucleotides, which are selected in vitro and have the ability to bind to proteins, ions, whole cells, drugs and low molecular weight ligands, ranging from low nanomolar (nM) to picomolar (pM), and recognizing their target with high affinity and specificity, often matching or even exceeding those of antibodies

[132]. Complementary base pairing defines aptamer secondary structure, consisting primary short helical arms and single stranded loops. Several secondary motifs have been described in the literature, such as hairpin structure, pseudoknot or G-quadruplex [155]. This class of functional nucleic acids can fold into complex three-dimensional shapes [68, 144, 145] in aqueous solutions, forming binding pockets and clefs for the specific recognition and thigh binding of any given molecular target [70].

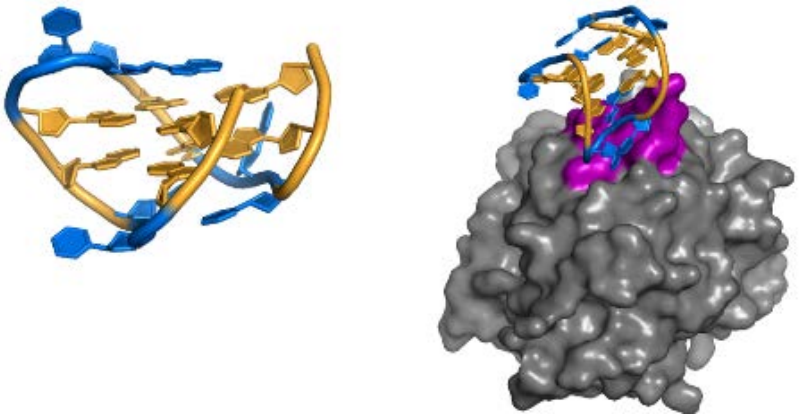

(A) (B)

Figure 1.5. A) A double G-quadruplex Thrombin aptamer and B) Thrombin aptamer bound to exosite 1 (magenta) of thrombin (adapted from [162]).

The aptamer generation emerged in 1990 [47, 188]. Thuerk and Gold described a new in vitro selection and amplification method, named SELEX (Systematic Evolution of Ligands by Exponential Enrichment). They used a combinatorial nucleic acid library to select RNA oligonucleotides that binds very tightly and selectivity to a certain non-nucleic acid target [188]. In the same

year, Ellington and Szostak used a similar selection method to isolate RNA molecules from a random sequence RNA library which can recognize and bind small organic dyes [47]. Two years later, the successful selection of single stranded DNA aptamers from a chemically synthesized pool of random sequence DNA molecules could be shown. Since its discovery, aptamer technology has received tremendous interest in scientific and industrial fields such as pharmaceutical, medicinal,...and is often modified to make the selection process more efficient and less time consuming, and to select aptamers with particular binding features for different molecules and for different applications.

1.2.1 Types of aptamers

Initially, aptamer were developed with DNA or RNA molecules for a direct interaction with a target. Nevertheless, lately additional functionalities have been incorporated to aptamers.

1.2.1.1 Molecular Aptamer Beacon

Molecular aptamer beacons (MAB) are DNA sequences composed of one target-recognition region, flanked by two short complementary stem sequences, which force the entire sequence to form a stem–loop structure in the absence of a target, also described as a hairpin [98, 176, 214]. The formation of the stem–loop structure brings in closeness the quencher and fluorophore, which are located at opposite ends of the MAB, by which fluorescence is quenched effectively. In the presence of a target molecule, biorecognition between the target and the loop sequence of the MAB takes place, conformational changes open the hairpin and fluorescence is restored due to the spatial separation of the fluorophore and quencher [30].

1.2.1.2. Spiegelmers

The word *spiegelmers* comes from the German word Spiegel, which means mirror. *Spiegelmers* are L-enantiomeric RNA or DNA oligonucleotides in which the mirror-image configuration of the nucleotides prevents nuclease degradation [197]. They are immunologically inert and show high biostability without any further chemical modifications, thus Spiegelmers are very well suitable for *in vitro* and *in vivo* applications [134].

1.2.1.3 Multivalent circular DNA aptamer

Multivalent circular aptamers or *captamers* are simple DNA aptamers with a large molecular framework in the form of a multivalent circle [13]. It is considered that these circular species increase the conformational stability and improve activity through a reduction in misfolding and a substantial degree of nucleolytic stabilization. Moreover, they are multitasking, thus they can simultaneously or alternatively bind to different molecular targets [41].

1.2.1.4 Peptide aptamer

Peptide aptamer are protein-based agents that are selected for specific binding to a given target protein under intracellular conditions. Generally, a peptide aptamer consists of a short variable peptide domain presented in the context of a supporting protein scaffold [24, 54]. It has been shown to possess the capability to specifically block the function of its target protein in vitro, as well as in living cells. It can be used to validate therapeutic targets at the intracellular level and also possess therapeutic potential as lead structures for drug design and as a basis for the development of protein drugs [71].

1.2.1.5 Aptazymes

Aptazymes are chimeric molecules that contain two functional regions: a ligand-binding motif that is responsive to a target of interest and a catalytic element that can accelerate a chemical reaction under determinate conditions [73].

1.2.2 SELEX

The SELEX process is characterized by iterative cycles of in vitro selection and amplification. The basic stages in a SELEX process are shown in Figure 1.6.

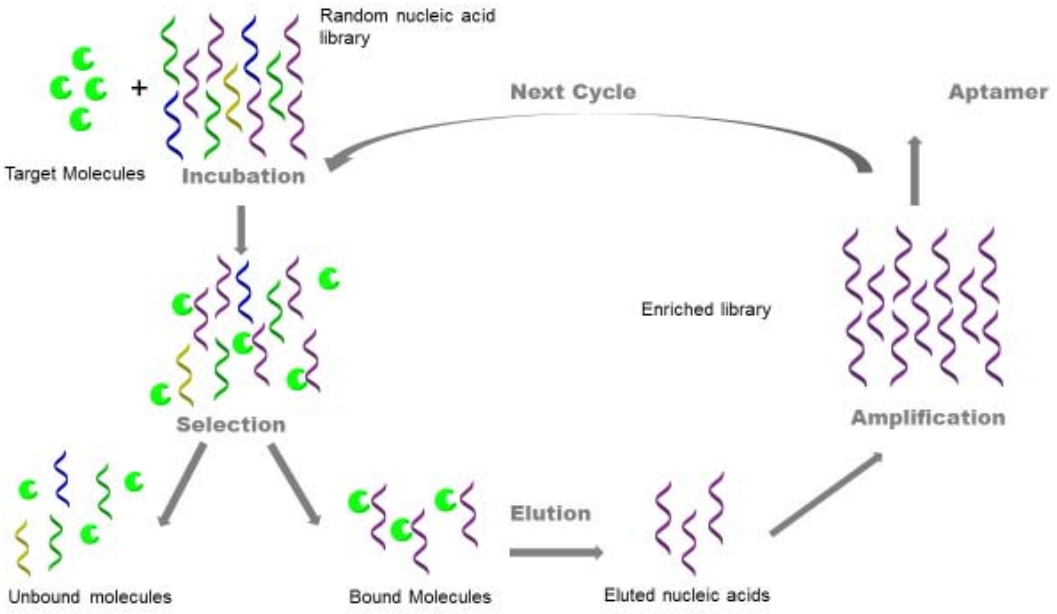

Figure 1.6. Scheme of SELEX process.

The process starts with the synthesis of a single-stranded library of oligonucleotides, consisting of about 10^{13} to 10^{15} different sequence motifs [78]. Each oligonucleotide comprises a central region of random sequence flanked by a 5' and a 3' region of defined sequence. Each member in a library is a unique linear oligomer. The chemically synthesized single-strand DNA pool is amplified by Polymerase Chain Reaction (PCR) in order to generate a double-

stranded DNA pool [183]. Several modifications of the random libraries have been developed. Essentially, modifications can improve aptamer potency by increasing the affinity of aptamers to targets by providing higher stability or by offering nuclease resistance (in the case of RNA aptamers) [63].

In the screening stage, the starting library is incubated with a target of interest in a buffer solution of election at a given temperature. During this step, a small fraction of the individual sequences interacts with the target, and these sequences are isolated from the rest of the library by filtration through nitrocellulose (for protein target) or by affinity chromatography (normally for small molecules target) [79]. The population of sequences after being isolated, it is amplified in order to achieve an enriched library to be used for the next selection and amplification cycle. The enrichment of the high affinity sequences requires several iterations under stringent conditions. In general, 8-15 cycles are required to obtain an oligonucleotide population that is dominated by those sequences which bind the target best [174]. Once obtained the sequence by cloning, the aptamer can be generated by chemical synthesis. In order to validate its specificity and affinity for the target, its binding activity can be checked by different methods.

Aptamers obtain from SELEX process are full-length sequences. In most cases, the fixed sequences regions used for primer binding are not important for aptamer function and consequently they can be removed. Technological advances in this process have allowed to eliminate the fixed regions in random sequences libraries, producing shorter aptamer sequences [80].

It is worth mentioning that the RNA SELEX is more complex than DNA SELEX because additional in vitro transcription steps are needed before and after each PCR amplification [174].

SELEX is a highly complex process, that takes a long time, months, nevertheless this process was automated in 1998 [27]. Improvements upon

around this process have increased binding efficiency of aptamers. Many variants of SELEX method have been developed, some of which are summarized in Table 1.1.

Table 1.1. Different variants of SELEX.

METHOD	DESCRIPTION	APPLICATION	REFERENCE
TOGGLE SELEX	Change of targets during the process	Aptamers with different specificity levels	[196]
CONDITIONAL SELEX	Selection in specific conditions	Aptamer which bind the target depending on a specific condition	[192]
TAILORED SELEX	Use of libraries that lack fixed border sequences	Aptamers of small size	[189]
CELL SELEX	Whole cells are used as target	Aptamer for cellular markers	[129]
GENOMIC SELEX	Libraries are based on genomic sequences	Genomic sequences for different molecules	[166]
MIRROR-IMAGES SELEX	Use of natural compound's enantiomers	Spiegelmers	[152]
PRIMER-FREE SELEX	Elimination of primer prior the selection step	Elimination of the effect of primers	[141]

1.2.3. Biorecognition event between aptamer and target

As already mentioned above, aptamers form characteristic three-dimensional structures, such as stems, loops, hairpins, triplexes or quadruplexes. This tertiary conformational structure furnishes the key for understanding molecular interaction between the aptamer and the target. Several mechanisms for binding affinity, target specificity, thermodynamics and kinetics are used in order to determine how aptamers interact, associate and dissociate with their target molecules [167].

There are some different interactions between aptamer with small and large targets. Small molecules are bound by fitting into the aptamer conformation by the formation of intermolecular hydrogen bonds. In this model, aptamers fold into a binding pocket on association with the target and unfold on dissociation of hydrogen bonds. However, for larger targets, for instance proteins or cells, the aptamer binding site is induced to fit better into the surface of the target by noncovalent ligations such as hydrogen bonds, electrostatic interactions, base stacking effects and hydrophobicity [167]. In addition, water molecules facilitate the contact by filing the empty spaces at the protein-aptamer interfaces [188]

1.2.4 Aptamers versus Antibodies

It is well known that antibodies and aptamers can bind the relative target with high specificity and affinity. However, aptamers offer numerous advantages over antibodies that make them very promising in several applications, see Table 1.2.

Table 1.2. Advantages of aptamers versus antibodies.

APTAMER	ANTIBODY
In vitro production	*In vivo* production
Automated synthesis and screening	Production process complicated and expensive
Identification of small molecules, toxins and drugs	Limited to molecules that produce an immuno-response. Small molecules require conjugation to a hapten
Can function at different T and pH	Only works under physiological conditions
Production highly reproducible and produces pure product	Variations in lot to lot
Easily labeled in precise locations	Labeling can cause loss of afinity
Easy transportation and storage	Sensitive to temperature and humidity changes

The main advantage of aptamers over antibodies is that aptamers are isolated by *in vitro* methodologies that are independent of animals, and an *in vitro* combinatorial library can be generated for any target including toxins or small molecules. Moreover, the aptamer selection process can be manipulated to obtain aptamers which bind a specific region of the target under different conditions [183]. In addition, aptamer can be easily functionalized by their ends to facilitate immobilization on supports.

By contrast, the generation of antibodies are *in vivo*. The animal immune system selects the sites on the target protein to which the antibodies bind, thus limiting the extent to which the antibodies can be functionalized and applied.

After selection, aptamers are produced by chemical synthesis with extreme accuracy and reproducibility. They are purified under denaturing conditions to a very high degree of purity [80]. Besides, through chemical synthesis, modifications in the aptamer can be introduced to enhance the affinity, stability and specificity of the molecules. However, the production and identification of monoclonal antibodies are laborious, expensive and requires screening of a large number of colonies [168].

Another advantage that aptamers have over antibodies can be seen in their higher temperature and pH stability. Aptamers are very stable and can recover their native, active conformation after thermal denaturation. They are stable to long-term storage and can be transported at room temperature. Whilst antibodies are temperature and pH sensitive proteins that can suffer irreversible denaturation, and they also have a limited shelf life [80].

Although aptamers present all these properties, mainly RNA aptamers are nuclease-sensitive which is very critical for their use in *ex vivo* and *in vivo* applications [50]. However, chemical modification of the ribose ring at the 2'-position improves the stability of these aptamers [150].

1.2.4 Applications of aptamers

Due to the several advantages that aptamers possess, they have been used in numerous applications [155, 175, 183].

1.2.4.1 Therapeutic applications

One of the first applications of aptamers was in therapeutics. Their advantages of small size, quick elimination, biocompatibility, low production cost and no cross reactivity with antibody binding receptor make them good candidates for this application. The majority of therapeutics aptamers inhibit target molecules [48] with high affinity and selectivity, and some act as receptor agonists [124]. One of the most successful therapeutic application of an aptamer has been carried out for the treatment of age-related macular degeneration [164]. Antivascular endothelial growth factor participates in the growth of abnormal new blood vessels in the eyes causing vision loss. A therapeutic aptamer was developed with the aim to inhibit this abnormal growth by OSI Pharmaceuticals under the name Macugen®. This aptamer was approved for patients with neovascular age-related macular degeneration by the Food and Drug Administration.

Another possibility is to use aptamers as targeting molecules in drug delivery. Huang et al. proposed the conjugation of doxorubicin (Dox) with an aptamer as a delivery agent. Dox is a polyclyclic antibiotic very used in the treatment of various leukemias and lymphomas. It intercalates into DNA and blocks its replication. The Dox molecule was attached to the aptamer via hydrazine linker. The aptamer-Dox complex retained aptamer's binding properties and interacted with the T-cell acute lymphoblastic leukemia with high affinity. In addition, the cytotoxic effect of Dox was preserved. It was conjectured that the covalent bond between the aptamer and Dox was hydrolyzed in the acidic environment of the endosome and the realesed Dox would then be free to enter the nucleous [72].

1.2.4.2 Separation techniques

Other aptamer area of increasing interest in the field of pharmaceuticals or biological analysis is the separation techniques, such as chromatography, affinity chromatography, capillary electrophoresis and mass spectroscopy. The relatively small size of aptamers and their easy of chemical conjugation to chromatographic supports make high-density aptamer columns useful. Other features of aptamers which make them suitable candidates for these applications include their good stability, high purity, and desirable binding properties. Obviously, the other property used is the reversibility of the target binding, normally forced by changes in pH, salinity, etc. of the reaction media.

One example was the purification of human L-selectin by affinity chromatography. It was performed with a streptavidin-sepharose column conjugated with biotinylated DNA aptamers selected against selectin (Kd = 2 nM), showing excellent purification efficiency with about 1500-fold purification and an 83 % recovery in a single step [158].

Pavski and Le reported a non-competitive capillary electrophoresis/LIF (CE/LIF) using a specific aptamer for the reverse transcriptase of the type 1 human deficiency virus (HIV-RT). The approach was based on the use of a fluorescently labelled DNA aptamer and could quantify HIV-RT up to 50nM with high selectivity [147].

1.2.4.3 Bio-Imaging

Another application of aptamer is in bio-imaging. The conjugation of aptamers with nanomaterials such quantum dots (QD), gadolinium,... or simple fluorophores as imaging agents represents a powerful diagnostic tool for the detection of several diseases in early stage [168, 200].

Hwand et al. developed a cancer-specific multimodal imaging probe base on cobalt-ferrite nanoparticle protected by a silica shell and coated by fluorescent rhodamine. They demonstrate that the aptamer multimodal nanoparticle system enabled the targeted fluorescence imaging of nucleolide and Magnetic Resonance Imaging (MRI) *in vivo* and *in vitro* [76]. Chen et al. reported a prion protein aptamer modified silver nanoparticles (AgNPs) that could be used as targeted contrast imaging agents for dark-field light scattering and Transmission Electronic Microscopy (TEM). The complex could be internalized into plasma membrane, lysosome and endocytic structure through aptamer mediated endocytosis [34].

1.2.4.4 Diagnostics

The most dynamic field in aptamer research seems to be diagnostics. Several researchers make effort to develop sensitive, time-efficient and inexpensive methods to detect particular molecules, proteins, toxins,... even cells. Biosensors using aptamers as a biological recognition element are called aptasensors. Due to the wide spectrum of potential aptamer targets they have been using in numerous applications, see Figure 1.7.

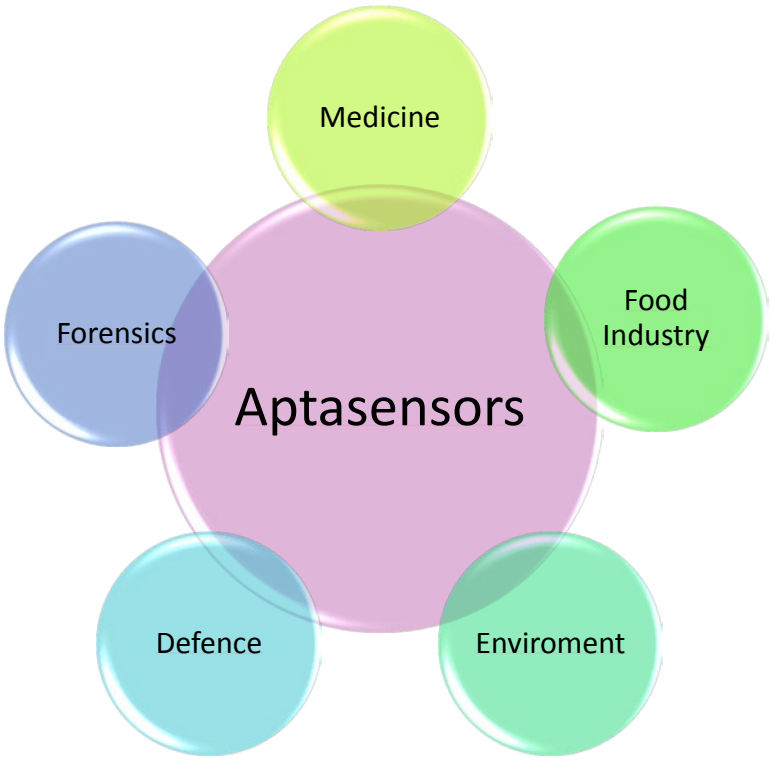

Figure 1.7. Scheme of the principal applications of aptasensors.

1.3 Aptasensors

Aptasensors (or genosensors of aptamers) are devices capable of providing an analytical signal from the binding event between a target molecule and an aptamer. They combine a biological recognition element (aptamer) that confers selectivity, with a transducer that confers sensitivity and generates an electrical signal from the recognition event.

The first use of aptamers as biorecognition element in biosensors was reported in 1996, with an optical biosensor based on fluorescently labeled aptamers for Immunoglobulin G (IgG) detection [39]. Few months later, Conrad and Ellington developed a radiolabeled aptamer for different protein kinase C isozymes detection [25], and Drolet et al. reported an enzyme-linked sandwich assay which used a fluorescently labeled SELEX derived oligonulceotides [42]. After that, several aptasensor papers have been published using different types of transductors. Table 1.3 shows a sample of potential targets, transductions

methods and sensitivities of different aptasensors. One of the features that can be derived is the low detection limits that are achieved, for very different targets, from potassium ion to tumoral cells.

Table 1.3. Different aptasensors from the literature using different transducers.

TRANSDUCER	TRANSDUCTION TECHNIQUE	LABEL	TARGET	LOD	REFERENCE
OPTICAL	Fluorescence	Berberine	Potassium ion	31 nM	[66]
OPTICAL	Fluorescence	Tb^{3+}	Ochratoxin A	20 pg/ml	[209]
OPTICAL	SPR	No	Lysozyme	2.4 nM	[126]
OPTICAL	Colorimetric	AuNPs	Bisphenol A	0.1 ng/ml	[125]
PIEZOELECTRIC	QCM	No	HIV-1 Tat protein	0.25 ppm	[128]
PIEZOELECTRIC	SAW	No	Human breast cancer cells	32 cells/ml	[29]
ELECTROCHEMICAL	DPV	AgNPs	Cocaine	150pM	[160]
ELECTROCHEMICAL	DPV	Alkaline phosphatase	IgE	300 ng/ml	[142]
ELECTROCHEMICAL	Voltammetry	No	Platelet-derived	50 pM	[93]

			growth factor		
ELECTROCHEMICAL	EIS	No	17β-estradiol	5 fM	[88]
ELECTROCHEMICAL	EIS	No	Thrombin	0.2 nM	[208]

Fluorescence labels have been widely used in aptasensors. Stojanovic et al. described an aptasensor for cocaine detection. They engineered anti-cocaine aptamer to obtain a partially folded structure with a ligand-induced binding pocket based on terminal stem-closure. When double-end labeled, aptamer could detect cocaine concentrations through changes in fluorescence [171]. Lee and Walt reported an aptasensor for thrombin detection using a microarray format. Thrombin was detected by displacement of fluorescein conjugated thrombin from the aptamer linked to silica microspheres in a fiber-optic biosensors system [96].

Quartz Crystal Microbalance (QCM) and Surface Plasmon Resonance (SPR) were widely used as label-free methods. In 2004, Minunni et al. reported an aptasensor for HIV-Tat protein detection based on piezoelectric quartz crystals [128]. Taking advantage of SPR technique, Chuang et al. reported a membrane-based microfluidic device integrated sensor for interferon-gamma (IFN-γ) detection. Using a bi-functional, hairpin-shaped aptamer as the sensing probe, they specifically detected the IFN-γ and amplified the signal by binding the streptavidin [36].

In 2005, the first electrochemical aptasensor was described, based on a sandwich format, where aptamers were labeled with glucose oxidase for the detection of Thr by amperometry [184]. Lai et al. designed an electrochemical aptasensor for the detection of platelet-derived growth factor (PDGF) directly in

blood serum. The aptasensor approach employed alternating current voltammetry to monitor target-induced folding in a methylene blue-modified, PDGF-binding aptamer [93]. An et al. developed a liquid-ion gated field-effect transistor (FET)-type flexible graphene aptasensor with high sensitivity and selectivity for Hg. The field-induced responses from the graphene aptasensor had excellent sensing performance, and Hg^{2+} ions with very low concentration could be detected, 10 pM [3].

1.3.1. The biosensing event in aptasensors

The biosensing event in aptasensors basically consists in three steps, as indicated Figure 1.8.

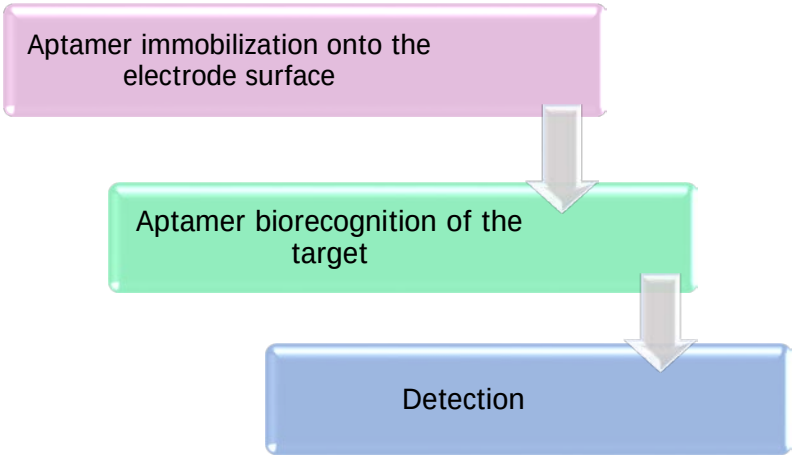

Figure 1.8. Scheme of the principal steps in the construction of aptasensors.

In some cases, additional steps are required for amplifying the obtained signal.

1.3.2. Aptamer immobilization techniques on the electrode surface

As mentioned in the previous section, the first step in the protocol for aptasensing is the immobilization of aptamers onto the electrode surface. The control of this step is essential in order to ensure high orientation, reactivity, accessibility and stability of the surface-aptamer. The achievement of high sensitivity and selectivity requires minimization of nonspecific adsorption and the stability of the immobilized aptamers [133].

Several electrode materials such as glassy carbon, carbon paste, graphite composites, graphite, carbon nanotubes, graphene, gold,... are used in aptasensors as sensing platforms. Some of them are explain in Section 1.5.1.

It is important to mention that previous to the aptamer immobilization, a pretreatment of the solution of the aptamer is required in order to promote the loose conformation of the aptamer.

The most common immobilization techniques used in aptasensors are shown in Table 1.4, and they are described in detail below.

Table 1.4. Summary of some immobilization techniques.

IMMOBILIZATION TECHNIQUE	INTERACTION OR REACTION	ADVANTAGES	DISADVANTAGES	REFERENCE
PHYSICAL ADSORPTION	Hydrophobic interaction	Simple Fast Low cost Direct method	Desorption by change of ionic strength, pH, reagents Random orientation	[113, 137]
COVALENT BINDING	Chemical binding	Good stability High binding strength Use during long term	Use of linker molecules Slow, irreversible Expensive	[85, 101, 157]
AVIDIN-BIOTIN AFFINITY	Specific interaction	Good orientation High specificity and functionality Well-controlled	Expensive Use of biocompatible linker	[65, 120]
SELF-ASSEMBLED MONOLAYERS (SAM)	Chemical binding or adsorption	Good orientation High sensitivity Well-ordered	Use of linker molecules	[99, 173]

1.3.2.1 Adsorption

This immobilization technique is based on a direct adsorption of aptamer through weak, labile bonds with active substrate sites. The physical adsorption could be either wet or dry. In the first case, a solution of aptamer is incubated onto the electrode surface and then it is let dry. While in the second case, the electrode is left in contact with a solution of aptamer for a specific time. Du et al. reported a dual-analyte logic aptasensor for thrombin and lysozyme detection. They immobilized a mix thrombin and lysozyme aptamer by wet physical adsorption onto graphene/glassy carbon electrodes [43]. Labeled Ochratoxin A (OTA) was immobilized onto nano-graphite surface by physical adsorption for OTA detection using a fluorescence transducer [195].

Adsorption is the simplest method to immobilize aptamers on the electrode surfaces because it does not require additional reagents or special nucleic acid modifications, therefore resulting in a rapid, simple and low cost protocol for the aptamer immobilization. However, it has some drawbacks, aptamer orientation is random and the attachment of aptamers to the electrode surface is weak. Due to this weak attachment aptamers can be removed by some buffers or reagents when performing the assay.

1.3.2.2 Covalent binding

Immobilization of aptamers onto the electrode surface is usually carried out by means of covalent binding between a molecule attached to the electrode surface and a reactive group of the aptamer. Different types of covalent binding technique have been reported in the literature [18, 157, 199], considering that aptamers can be easily functionalized by their ends to facilitate the immobilization (eg. –amino, -tiol, biotinia, etc.). However, the most used protocol is based on the formation of a covalent bond between the aptamer and the electrode surface through the activation of a carboxylic acid with carbodiimide 1-(3-dimethylaminopropyl)-3-ethyl carbodiimide (EDC) and N-

hydroxysulfosuccinimide (NHS) for reaction with an amine group. For instance, Chen H. et al. immobilized NH_2-terminated aptamer on an activated glassy carbon electrode by the formation of amide bond for adenosine triphosphate detection[31]. Rohrback F. et al. developed an aptasensor based on covalently immobilization of lysozyme aptamer modified with amine group on the surface of multiwalled carbon nanotube-modified screen-printed electrode [157].

This method provides the benefits by structural flexibility and chemical stability, thus improving biorecognition efficiency. However, it presents some drackbacks, it requires chemical modifications of the surface, which make the assay time consuming, and aptamers have to be modified, which make the assay more expensive than others immobilization techniques.

1.3.2.3 Streptavidin (or Avidin)-Biotin Affinity

Several researchers have been taken advantage of the strong complex formed by streptavidin or avidin with biotin in order to immobilized bioreceptors onto electrode surface [17, 151]. Streptavidin and avidin are large tetrameric molecules (70 KDa) with four identical binding sites, and biotin is a small molecule that binds with high affinity binding site with an affinity constant of $1 \cdot 10^{-15}$ M^{-1} [45]. The stability of this interaction is nearly equal to that of a covalent bond. Actually, this interaction can only be broken under very extreme conditions. This is a two steps method, where the solid surface is first modified with streptavidin or avidin (deposition by physical adsorption or covalent interaction or immobilization into a composite material), followed by step of biotinylated aptamers are added to form the complex.

Zhang K. et al. immobilized biotinylated aptamer of thrombin onto a microplate modified covalently with biotin and then with streptavidin [210]. Bai et al. reported an SPR aptasensor for avian influenza virus based on biotinylated aptamer immobilized on a gold surface modified with streptavidin [6].

This immobilization technique provides a good orientation of the aptamers onto the electrode surface, which causes a high specificity. However, streptavidin and avidin are expensive and it requires biotinylated aptamers which increases the production cost.

1.3.2.4 Self-Assembled Monolayers (SAM)

Self-assembled monolayers (SAM) technique is a spontaneously formation of monolayers by adsorption or chemical binding of molecules from a homogeneous solution onto a substrate. Several kinds of SAMs have been reported. However, in aptasensors most common protocols are based on the adsorption of sulfur-based compounds such as thiols, disulphides, ... on gold [110, 212]. An example reported in the literature is the immobilization of thiol-aptamer by self-assembly on gold surface. The thiol groups demonstrate affinity towards the noble metal surface allowing the formation of covalent bonds between the sulfur and gold atoms [9, 193]. In addition, various oligo(ethylene glycol) (EG) mixtures of different molar ratios of EG_6-COOH and EG_3-OH were used for the formation of SAM in the construction of an aptasensor for IgE detection [89].

SAM method is one of the simplest techniques to provide a reproducible, ultrathin, and well-ordered layer suitable for further modification with aptamers, which improve sensitivity, speed, and reproducibility. However, the use of linker molecules make the assay expensive.

1.3.3. Types and formats of detection

After aptamer immobilization and target biorecognition, the following step in the construction of aptasensor is the detection. Different types and formats of detection can be used in aptasensing.

1.3.3.1 Label-free or labeled detection

Aptasensors that use label-free transduction methods do not require a label aptamer to signal the presence of target on the sensor surface, thereby enabling the use of unmodified samples, with the possibility of real time measurement. Label-free detection methods greatly simplify the time, effort and money required for assay development. There are few techniques and transducers making possible the label-free detection. Between them once can list SPR, Electrochemical Impedance Spectroscopy (EIS), Field Effect Transistor (FET) and Piezoelectric transduction.

On the other hand, labeled methods require a labeled aptamer to signal the presence of target on the sensor surface. Fluorophores, enzymes or metal nanoparticles are some examples of labels. Typically, optical methods imply labeled species. Different label-based aptasensors have been reported [2, 111, 195, 202].

1.3.3.2 Format of detection (configuration assay)

Basically, aptasensors can be divided into three different assay formats: direct, sandwich or competitive.

-Direct format

This format consists on the direct or simple interaction of a label or label-free aptamer with its target. For small molecular targets, they are often covered within the binding pockets of aptamer structures, see Figure 1.8 (A). By contrast, protein or big targets are structurally more complicated than smaller targets and they allow the interaction of several discriminatory contacts such as hydrogen bonds, electrostatic interactions, shape complementary, etc., [169] see Figure 1.8 (B). Several aptasensors based on this approach have been used for the detection of targets such as lysozyme [102], Immunoglobulin E [185],

thrombin [154], cocaine [159] or cancer cells [51] . This format is simple, fast and cheap. However, sometimes there are problems of sensitivity or selectivity.

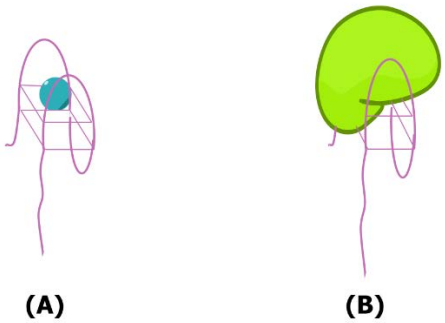

Figure 1.8. Aptamer-based assay direct formats. (A) Small molecule target hidden within the binding pockets of aptamer structure (B) Protein or big target locally exposed with the binding pocket of aptamer structure.

-Sandwich format

Sandwich format is based on the immobilization of an aptamer onto the electrode surface followed by an incubation with the target protein and in a last step with a second aptamer, Figure 1.9 (A). Generally, first and second aptamer have different nucleic acid sequences. However, in limited cases, for instance dimeric proteins contain two identical binding sites, thus allowing the use of a single aptamer. In case when there are no two aptamers for the target of interest, it is possible to use an antibody as a second aptamer, Figure 1.9 (B).

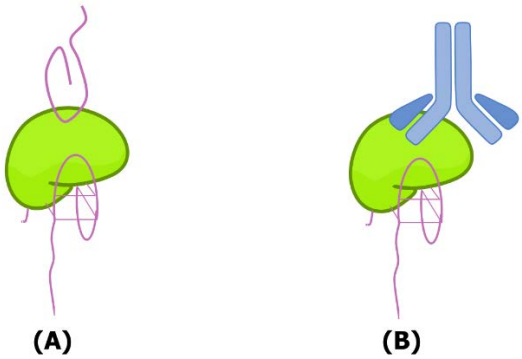

Figure 1.9. (A) Aptamer sandwich format, (B) Aptamer-antibody sandwich format assay.

The use of sandwich format enables detection of the target with very high sensitivity and selectivity. However, several incubation steps are required, which make the assay time-consuming. In addition, an extra aptamer or antibody is needed, which make the assay expensive [140].

-Competitive format

In competitive assays only one aptamer is required and the time necessary for the assay is fast. As can be seen in Figure 1.10, the format consists on the immobilization of the target onto the electrode surface, followed by exposure to different concentration of the target and a fixed concentration of the aptamer, leading to a competition for the aptamer.

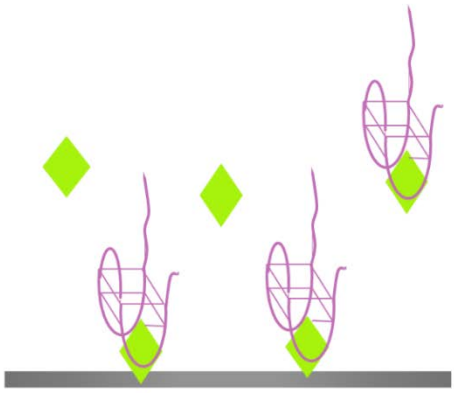

Figure 1.10. Competitive format assay.

1.3.4. Detection techniques

Most aptasensors in the literature depend on the transduction technique employed can be classified in optical, piezoelectric or electrochemical.

1.3.4.1 Optical aptasensors

This method of transduction has been employed in many aptasensors due to the many different types of spectroscopy such as absorption, fluorescence, phosphorescence, Raman, Surface-enhanced Raman Spectroscopy (SERS), refraction and dispersion spectroscopy. However, the surface plasmon resonance (SPR) or fluorescence are the most popular methods available for optical aptasensors.

-Fluorescence

A fluorescence aptasensor detects the change in frequency of electromagnetic radiation emission which is caused by previous absorption of radiation and also by generation of an excited state lasting for a short time. In this approach, the simplest format is to label the aptamers with a quencher and a fluorophore. Furthermore, different complicated formats utilizing quaternary structural reorganization, such as molecular aptamer beacon, which results in the assembly or disassembly of aptamer were also developed.

Verdian-Doghaei et al. developed a biosensor based on a quadruplex-forming aptamer for the determination of potassium ion. The aptamer was used as a molecular recognition element. It was adjacent to two arm fragments and a dual-labeled oligonucleotide serving as a signal transduction probe which is complementary of the arm fragment sequence. In the presence of potassium, the aptamer was displaced from the signal transduction probe, which was accompanied by decreased signal. The concentration of potassium was proportional to the quenching percentage of fluorescence intensity [190]. Chen et al. reported a signal-on fluorescent biosensor for detection of OTA based on fluorescent DNA-scaffolded silver-nanocluster, structure-switching of anti-OTA aptamer and magnetic beads [33].

Fluorescence technology provides high sensitivity, high efficiency and simple operation.

-*Surface Plasmon Resonance*

Surface Plasmon Resonance aptasensors use surface plasmon waves to detect changes when the target interacts with the aptamer. When the immobilized aptamer recognizes its target, it produces a change in the refractive index at the sensor surface. This produces a variation in the propagation constant of the surface plasmon wave and the variation is measure to produce a reading.

Golub et al. developed an aptasensor for cocaine detection. Supramolecular AuNPs-aptamer subunits-cocaine complex generated on the Au support allowed the SPR detection of cocaine through the reflectance changes stimulated by the electronic coupling between the localized plasmon of the AuNPs and the surface plasmon wave [58]. Bai et al. reported an aptasensor for avian influenza virus (AIV) using a SPR transductor. The immobilized aptamers captured AIV H5N1 in a sample solution, which caused an increase in the refraction index [6].

An important advantage of using SPR is that it is able to provide label-free biosensing which makes it really attractive for real time monitoring.

1.3.4.2. Piezoelectric aptasensors

Piezoelectric aptasensors are based on the principle of coupling the aptamer with a piezoelectric component. Several materials exhibit the piezoelectric effect, such as quartz, tourmaline, lithium niobate or tantalite, etc. However, the properties of quartz are the main reason for its common application in biosensing [148]. The most important transducer in this field are represented by Quartz Crystal Microbalance (QCM) and Surface Acoustic Wave (SAW).

-Quartz Crystal Microbalance (QCM)

Aptasensors based on QCM transduction detect changes in frequency of a gold-plated quartz crystal due to changes in mass on the surface of the crystal. Aptamers are immobilized on the quartz oscillator surface, and target solutions are injected. When targets are recognised by the aptamers, the effective mass of the oscillator increases, resulting in the decrease in the resonance frequency of the oscillator [138].

Zheng et al. developed an aptamer-based gold nanoparticles (AuNPs)-enhanced sensing strategy for detection of adenosine [213]. The QCM crystal was modified with a layer of thiolated linker aptamer, which can be partly base-paired with the detection part containing the adenosine aptamer sequence. In the presence of adenosine, the aptamer bound with adenosine, which restrained the reporter part carrying AuNPs to combine with the random coiled detection part. Therefore, when the concentration of adenosine is low, more amount of AuNPs combined to the crystal [213]. Zhang et al. reported a novel quartz crystal microbalance (QCM) assay for lysozyme detection. In order to enhance the sensitivity of this aptasensor, biocatalytic precipitation reaction combined with strand-scission cycle and rolling circle amplification were applied together [211].

The advantages of using this type of transduction are label-free detection, simplicity of use, cost effectiveness and real time monitoring. However, there are some drawbacks needing to be overcome such as lack of specificity and sensitivity.

-Surface Acoustic Wave (SAW)

Surface acoustic wave (SAW) aptasensors are based on horizontally polarized surface shear waves, which allow direct and label free detection in real time. Signal response changes result from mass increase and viscoelasticity

changes on the biosensor surface. All types of binding reactions can be detected by determining resonant frequency changes of an oscillator [94]. Chang et al. designed an aptasensor array for human breast cancer cells based on Leaky Surface acoustic wave (LSAW). In this methodology, every resonator crystal unit of the LSAW aptasensor array had an individual oscillator circuit to work without mutual interference, and could oscillate independently with the phase shift stability of ±0.15° in air phase and ±0.3° in liquid phase. The aptamer was assembled to the gold electrode surface of 100 MHz $LiTaO_3$ piezoelectric crystal, which could effectively captured target cells based on the specific interaction between aptamer and the overexpression of MUC1 protein on tumor cell surface. The aptamer-cell complexes increased the mass loading of LSAW aptasensor and led to phase shifts of LSAW [29].

1.3.4.3. Electrochemical detection

Electrochemical techniques have been extensively recognized as a powerful tool for fast access to biochemical information in aptamer-target complex due to their high sensitivity, fast response, easy operation, possibility of minituarization, relatively compact, as well as low production cost [69].

According to the IUPAC, electrochemical techniques include amperometry, potentiometry, conductometry and semiconductor field-effect transistor [181].

-Amperometry

Amperometric aptasensors are focused on the measurement of current as a function of time resulting from the oxidation and reduction of redox species in a biochemical reaction that mainly depends on the concentration of an analyte with a fixed potential [148]. When the current is measured at a constant potential, this is referred to as amperometry. However, when the current is measured during controlled variations of the potential, this is referred

to as voltammetry [61]. Normally, it utilizes mediator or redox species in order to participate in the redox reaction with the biological component and help in the faster electron transfer.

Luo et al. designed a sensitive amperometric aptasensor to detect toxin A of *Clostridium difficile* based on a horseradish peroxidase (HRP) labeled aptamer-DNA duplex. In the absence of toxin, the aptamer-DNA duplex modified the electrode surface with HRP, so that an amperometric response was induced based on the electrocatalytic properties of thionine. This was mediated by the electrons that were generated in the enzymatic reaction of hydrogen peroxide under HRP catalysis. After the specific recognition of the toxin, an aptamer-toxin A complex was produced rather than the aptamer-DNA duplex, forcing the HRP-labeled aptamer to dissociate from the electrode surface, which reduced the catalytic capacity of HRP and reduced the response current [117]. Bai et al. reported an aptasensor based on direct electron transfer and electrocatalysis of HRP using exonuclease-catalyzed target recycling and hybridization chain reaction (HCR) for signal amplification for sensitive detection of thrombin [7].

The main advantage of this class of transducer is the type of instrument used for these measurements, which is very easy to obtain and can be inexpensive and compact, thus this allowing for the possibility of *in situ* measurements. However, some limitations for this signal transduction mechanism are: the potential interferences to the response, if several electroactive compounds generate false current values, and it requires labels to generate the amperometric signal which makes expensive the assay.

-Potentiometry

This technique measures differences in potential that it generated across an ion selective membrane separating two solutions at virtually zero current flow. In these types of aptasensors, the biological recognition element converts

the recognition process into a potential signal to provide an analytical signal [148]. Düzgün et al. demonstrated the feasibility to potentiometrically detect large analytes such as proteins using a nanostructured hybrid material (based on carbon nanotubes) that incorporates aptamers of thrombin[44]. In addition, Zelada-Guillén et al. showed that the same strategy could be applied to quantify bacteria in real samples [206].

The main advantages of this detection system are simplicity use, low cost, and real-time detection which make it highly valuable for different types of applications.

-Field-Effect Principles (FET)

FET is a type of transduction that uses an electric field to control the conductivity of a channel between two electrodes in a semiconducting material [61]. Althought, there are different types of FET transductors, in biosensing application ion-selective field-effect transistor (ISFET) is the most used.

Goda and Miyahara developed biosensors based on an aptamer-modified field-effect transistor (FET) for the detection of lysozyme and thrombin. The aptamer-based potentiometry was achieved in a multi-parallel way using a microelectrodes array format of the gate electrode. A change in the gate potential was monitored in real-time after introduction of a target protein at various concentrations to the functionalized electrodes in a buffer solution. Specific protein binding altered the charge density at the gate/solution interface because of the intrinsic local net-charges of the captured protein[56]. Zayats et al. reported a label-free, reagentless ISFET aptamer-based sensing device. Upon binding to adenosine monophosphate (AMP), an AMP aptamer released a hybridized short complementary oligonucleotide, which in turn affected the charges associated with the gate and altered the source-to-drain current. This approach demonstrated a sensitivity limit of 5×10^{-5} M, requiring only a 4 min response time.

-Conductometry

This transduction technique provides information about the ability of an electrolyte solution to conduct an electric current between electrodes. The major advantage of conductometric biosensors are that no reference electrode is required, it is cheap, and there is the possibility of minituarization [61]. Unfortunately, they have some drawbacks, low sensitivity and strongly dependent on the response to buffer capacity.

-Electrochemical Impedance Spectroscopy

Electrochemical impedance spectroscopy (EIS) is one of the most powerful tool for directly probing the interfacial reaction mechanisms and monitoring the dynamics of biomolecular interactions [62].

Compared to other electrochemical methods, EIS has been used in numerous studies, such as immunosensing [97, 103, 106] and genosensing [15, 16, 146], because of its high sensitivity, simplicity use, capacity for label-free detection and cost-efficient technique.

A detail explanation of this technique is given in the followed section.

1.4. Electrochemical Impedance Spectroscopy (EIS)

The term impedance was introduced by the electrical engineer, physicist and mathematician Olivier Heaviside in 1886, who adapted complex numbers to the study of electrical circuits [123].

EIS is one of the most effective and reliable methods to extract information about electrochemical characteristics of electrochemical systems [20], thus it is widely applied in many fields, e.g. corrosion, electrode kinetics,

membranes, batteries and cells, interfaces, biochemistry, solid-state electrochemistry.

Basically, there are two modes of performance the method:

-Electrochemical Impedance Spectroscopy or Impedance Voltammetry, which is based on measuring the impedance as a function of the frequency of a small sinusoidal potential perturbation superimposed on a potential bias.

-Alternating Current Polarography or Alternating Current Voltammetry, which consists on applying superposition of a single-frequency sinusoidal potential on a scanned or stepped direct potential and measuring the sinusoidal current response as a function of the direct potential.

Basically, EIS is based on applying an AC potential to an electrochemical cell and measuring the current through the cell. When a process occurs in a electrochemical cell, it can be modelled using combination of resistors, capacitors,... using the principle of the equivalent circuits. This principle consists on obtaining values of electrical parameters such as resistance, capacitance, etc. when an experimental spectra is fitted with a theorical curve corresponding to the selected circuit model.

If it is applied a sinusoidal potential excitation E_t:

$$E_t = E_o \cdot \sin(\omega \cdot t) \qquad (1.1)$$

Where E_t is the potential at time t, E_o is the amplitude of the signal and $\omega = 2\pi f$ is the radial frequency (f is the frequency expressed in Hertz (Hz)).

An AC current signal with a current intensity I_t is obtained in response to this potential applied. I_t also depending on t with the same frequency but with

an amplitude I_o and a phase angle φ depending on the impedance of the system, as shown in Figure 1.11.

$$I_t = I_o \cdot \sin(\omega \cdot t + \varphi) \qquad (1.2)$$

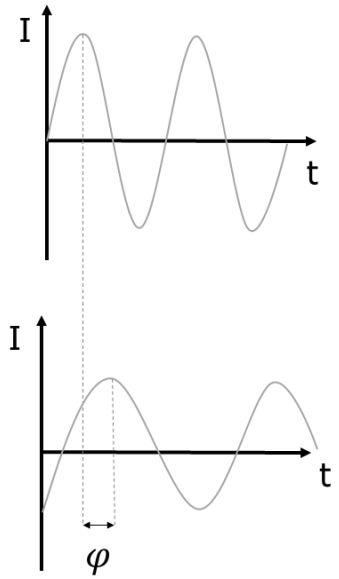

Figure 1.11. AC excitation signal applied and sinusoidal current response in the system under study.

To calculate the impedance of the system, an expression analogous to Ohm's Law is used:

$$Z = \frac{E_t}{I_t} = \frac{E_o \cdot \sin(\omega \cdot t)}{I_o \cdot \sin(\omega \cdot t + \varphi)} = Z_o \cdot \frac{\sin(\omega \cdot t)}{\sin(\omega \cdot t + \varphi)} \qquad (1.3)$$

According to Euler's expression:

$$\exp(j\varphi) = \cos\varphi + j \sin\varphi \qquad (1.4)$$

A common way to represent the impedance vector model is to use complex notation:

$$E(t) = E_o \cdot \exp(j\omega \cdot t) \qquad (1.5)$$

$$I(t) = I_o \cdot \exp(j\omega \cdot t - j\varphi) \qquad (1.6)$$

Therefore impedance is represented as:

$$Z = \frac{E}{I} = Z_o \exp(j\varphi) = Z_o \ (\cos\varphi + jsin\,\varphi) = Z_r + jZ_i \qquad (1.7)$$

where Z_r is the real part of the impedance and Z_i the imaginary part.

In order to acquire an impedimetric spectrum, an AC excitation signal is applied to the system within a certain frequency range, obtaining an AC current response for each analysed frequency value.

The most common graphical representation of impedimetric data is the "Nyquist Diagram", in which the imaginary part of the impedance Z_i is plotted versus the real part Z_r. In this plot, each point correspond to a different frequency. In Figure 1.12 is represented a Nyquist diagram, where the impedance vector with magnitude $|Z|$ ($|Z|$ correspond to Z_o) forms with the X-axis an angle corresponding to the phase angle φ. The high frequency data are represented on the left part of the diagram whilst the low frequency are on the right one.

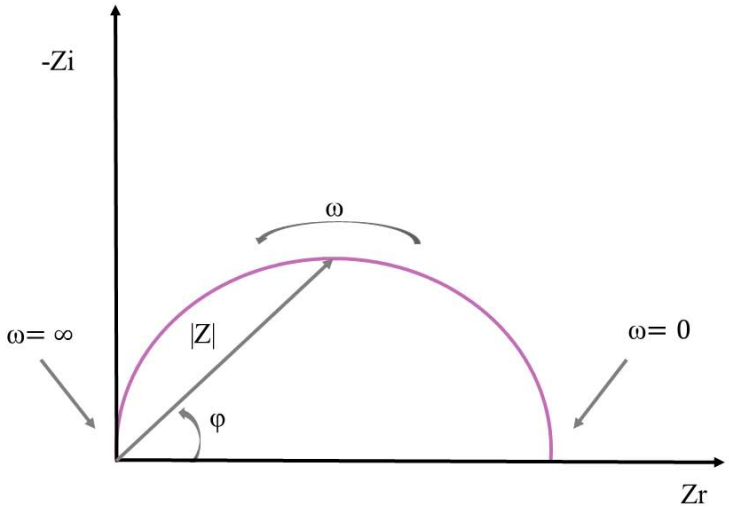

Figure 1.12. Nyquist diagram representing the impedance vector in the complex plane.

Another way of representation data is "Bode Diagram" where the modulus of the impedance (Log|Z|) and the phase angle (φ) between the AC potential and the AC current as a function of the frequency (log ω) are plotted. As shown in Figure 1.13, the impedance data which are frequency independent represent the behavior of the resistive processes (phase angles close to 0) whereas the ones that are dependent on the frequency are more related to capacitive or diffusive processes (phase angles between -90º or -45º). Each type of representation can be chosen according to different experiment and needs for parameter visualization.

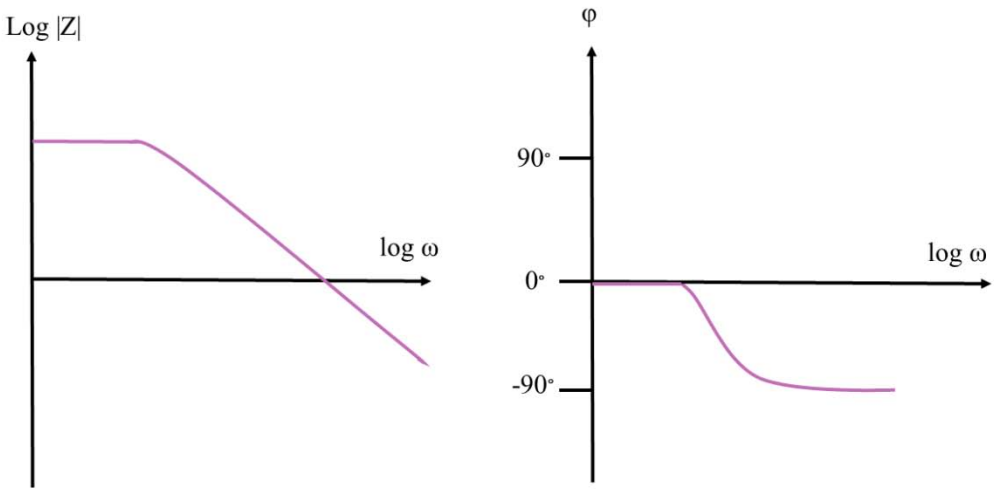

Figure 1.13. Bode diagrams.

The interpretation of impedimetric spectra consists on the correlation among the obtained data with equivalent circuits formed by basic electrical elements (resistance, capacitor, inductance,...).

Figure 1.14 shows an example of Nyquist diagram to a simple equivalent circuit formed by resistance R_1 in series with the parallel combination of a capacitance C and another R_2 ($R_1(R_2C)$). This important circuit is observed for very well behaved electrochemical reaction occurring onto a metallic electrode. The impedance spectra is represented by a semicircle beginning in the point corresponding to R_1 value (a) and ending in the point (b) corresponding to the equal $R_1 + R_2$. The value of capacitance of the capacitor C is obtained by the maximum value of imaginary impedance in the spectrum. Most of impedance spectra corresponding to electrochemical systems can be fitted to this type of equivalent circuit. In that cases, the parameter R_1 represents the resistance of the solution (R_s), R_2 corresponds to the resistance (R_{ct}) to the charge transfer between the solution and the electrode surface and C is the capacitance of the double layer due to the interface between the electrode and the electrolytic solution.

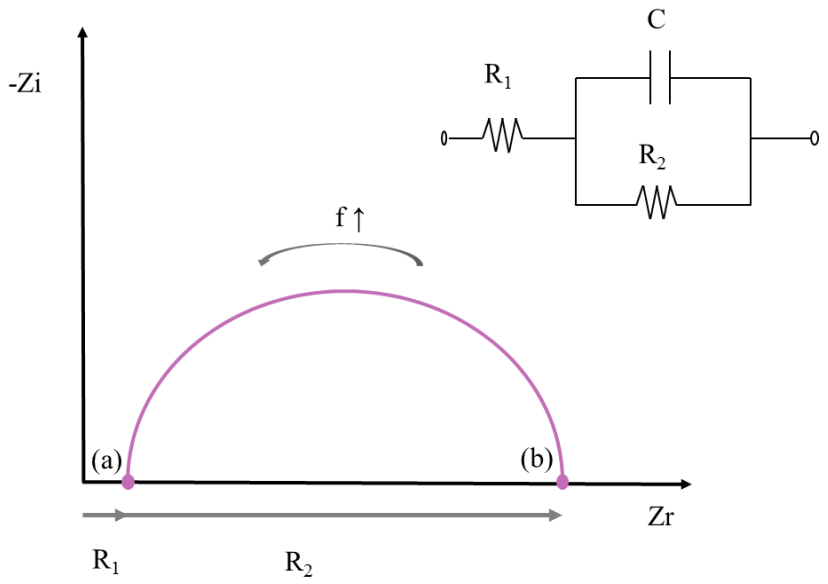

Figure 1.14. Nyquist diagram and the corresponding equivalent circuit.

A Warburg impedance parameter should be considered when it is recorded at low frequencies. This parameter is related to the mass transfer between the solution and the electrode surface and can be modelled as a frequency dependent reactance with equal real and imaginary components.

$$Z_w = \sigma \cdot (\omega)^{-\frac{1}{2}} \cdot (1 - j) \qquad (1.8)$$

Where ω is the radial frequency and σ is the Warburg coefficient (constant for a defined system).

The Warburg impedance appears on a Nyquist diagram as a diagonal line with a slope of 45°. In an electrochemical system or process it represents the diffusion of electrochemical species in the solution. Figure 1.15 shows the impedimetric spectra and the most favourite model of equivalent circuit for a simple electrochemical reaction called Randles equivalent circuit [5] .

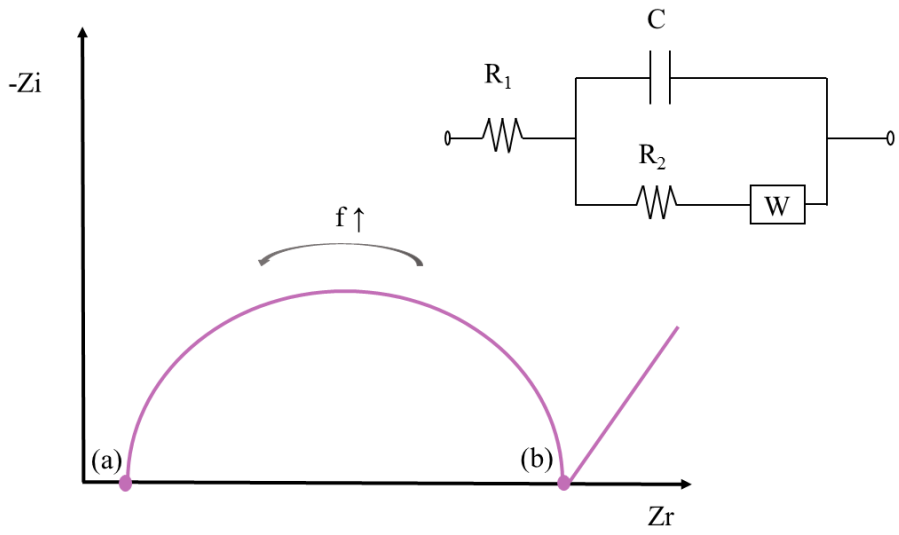

Figure 1.15. Nyquist diagram and the corresponding equivalent Randles circuit.

In some cases, the semicercles of Nyquist diagrams present a depressed and not completely symmetric shape, this is due to the non-ideal behavior of most capacitors in electrochemical systems. In order to fit better the experimental data to the theoretical curves, a Constant Phase Element (CPE) is used instead of a capacitor. The impedance of a CPE is represented by:

$$Z_{CPE} = (j \cdot \omega)^{-\alpha} / C \qquad (1.9)$$

Where ω is radial frequency, C is capacitance and α is a exponent, $\alpha(0-1)$. In a constant phase element, the exponent α is lower than 1, even though α = 1 corresponds to the ideal capacitor.

As mentioned above, EIS is a widely used technique in several fields. In biosensing, due to its ability of directly probing the interfacial properties of a modified electrode, this technique is rapidly developing as a tool for studying biorecognition events at the electrode surface [87].

1.4.1. Impedimetric aptasensors

Recently, among the different electrochemical techniques available, impedance has widely been used in aptasensors. This can be due to the fact that it allows to perform label-free detection which makes the assay rapid, simple and low cost. However, sometimes labelling are required in order to increase selectivity (e.g. using sandwich approach) and enhance sensivity (e.g. using a label that can significantly amplify the impedimetric response).

Two different types of impedance measurements can be performed: non-Faradaic and Faradaic measurements.

In the first case the parameter of interest in the study is the capacitance of the double layer former between the solution and the electrode surface. In this type of measurement no additional reagents is required. After each modification of the electrode surface, a variation in the capacitance value can be observed due to the displacement of water and ions from the surface upon the biomolecule binding [38].

In the second one, redox species are added to the bulk solution, which are alternatively oxidized and reduced by the transfer of an electron to and from the working conductive electrode [38]. After each step of the biosensing event, variations of the charge transfer resistance between the solution and the electrons surface could be observed due to repulsion/attraction of the redox marker or/and sterical hindrance.

In aptasensing, Faradaic impedance is more used than non-Faradaic.

Many impedimetric aptasensors have been presented in the literature, including label-free or labeled detection. Table 1.5 shows some examples.

Table 1.5. Examples of different impedimetric aptasensors

LABEL-FREE	TARGET	LOD	REFERENCE
√	Anatoxin A	0.5 nM	[46]
√	Sodium diclofenac	0.27 µM	[86]
√	Progesterone	0.90 ng/ml	[26]
√	Adenosine	16.5 nM	[112]
X	Angiogenin	0.064 pM	[35]
X	Mucin 1 protein	0.1 nM	[109]
X	Immunoglobulin E	6 pM	[163]

Taking advantage of label-free detection Zhang et al. designed an aptasensor for cocaine based on the formation of a supramolecular aptamer fragments/substrate complex. An anticocaine aptamer was divided into two fragments, Cx and Cy. Three different sensing interfaces were fabricated by immobilizing Cx or Cy on a gold electrode through modifying their 5′ or 3′ end with a thiolated group followed by the treatment with mercaptoethanol (MCE). The interfacial electron transfer resistance was found to depend strongly on the cocaine concentration [207]. Moreover, Xu et al. developed a label-free aptasensor for thrombin detection based on electropolymerized film. Firstly, a poly(pyrrole-nitrilotriacetic acid) (poly(pyrrole-NTA)) film was electrogenerated onto the surface of electrodes followed by complexation of Cu^{2+} ions. Then, the

histidine labeled thrombin aptamer was immobilized with specific orientation onto the electrode through coordination of the histidine groups on the NTA–Cu^{2+} complex. The aptasensor was applied for the detection and quantification of thrombin without a labeling step [201].

1.5. Nanomaterials used in impedimetric aptasensors

In the last decades, in order to satisfy the growing demands for ultrasensitive detection, researchers have developed many techniques to enhance the response of the aptasensors by modifying with different functional materials. Thanks to the continuous development of the nanotechnology, different nanomaterials have been used, some of them are shown in figure 1.19. These nanomaterials present several characteristics such as biological compatibility, high surface area, chemical stability, excellent catalytic activity, nontoxicity and conductivity.

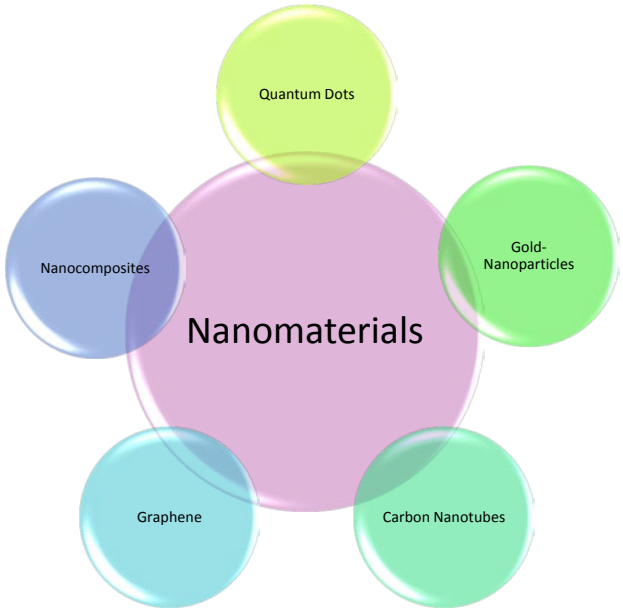

Figure 1.19. Scheme of different nanomaterials used in impedimetric aptasensors.

The use of nanomaterials in impedimetric aptasensors implies two different aspects. Some are used as a materials for the construction of new sensing platforms with the aim of improving the electrochemical response. Others are used as labels in order to obtain a significant signal amplification [14]. In addition, some of them can be used in both cases. Table 1.6 shows different nanomaterials and their uses.

Table 1.6. Different nanomaterials and their uses in impedimetric aptasensors.

TYPE OF NANOMATERIAL	SENSING PLATFORM	LABEL
CARBON NANOTUBES	√	√
QUANTUM DOTS	X	√
GOLD-NANOPARTICLES	√	√
GRAPHENE	√	√
NANOCOMPOSITES	√	X

A detailed description of the most commonly used nanomaterials as sensing platforms and as labels in impedimetric aptasensors, their general properties and their most successful application in impedimetric aptasensors are given in following sections.

1.5.1. Nanomaterials to construct sensing platforms

It is well known that the correct immobilization of aptamers and the amount of them influence the accuracy and the sensitivity of aptasensors. Due to their excellent and unique properties, several nanomaterials have been employed as a material to construct sensing platforms. They provide high surface area with abundant binding points, synergic effect among catalytic activity, conductivity and biocompatibility.

1.5.1.1 Carbon Nanotubes

Carbon Nanotubes (CNT) are one of the most known and used nanomaterial since its discovery in 1991 by Iijima [77]. They offer unique advantages or properties, such as high surface to volume ratio, high thermal and electrical conductivity, chemical stability, biocompatibility and anisotropic behavior [59]. Thus, they are attracting much interest among all applied sciences and technologies, especially in the construction of sensing platforms.

CNT are related with fullerene molecules. They are composed of graphene sheets which are wound into a cylindrical shape. They may be closed at either end with caps containing pentagonal rings, or they may be left open [153]. Depending on the synthesis conditions, either single or multiwall carbon nanotubes are formed. Single-Walled Carbon Nanotubes (SWCNT) are single cylinders of graphite sheet and Multi-Walled Carbon Nanotubes (MWCNT) are multi concentric cylinders of graphite sheets [57], see Figure 1.20.

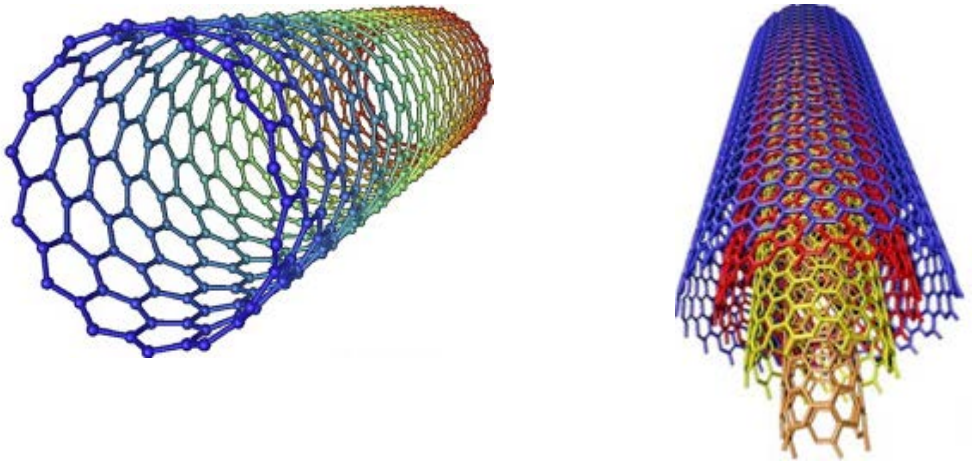

(A) (B)

Figure 1.20. Scheme of: A) a single-walled carbon nanotube (adapted from [180]) and B) a multi-walled carbon nanotube (adapted from([204])).

Park et al. developed an electrochemical aptasensor for thrombin detection using SWCNT casted Glassy Carbon Electrodes (GCE). The new platform formed by SWCNT casted o the GCE provided a suitable conducting matrix for aptamer immobilization through π-stacking and electrochemical detection [143]. Kara et al. described an impedimetric aptasensor for label-free detection of thrombin using screen printed electrodes (SPE) modified with MWCNT as the supports to enhance the surface of the electrodes compare with bare SPE [85]. Furthemore, Rohrbach et al. took advantage of the same MWCNT properties and they developed an impedimetric aptasensor for lysozyme detection using modified SPE [157].

1.5.1.2 Gold nanoparticles

Gold nanoparticles (AuNPs) is one of the most studied nanomaterials available for biosensors [198]. AuNPs introduces many advantages to the biosensors, encompassing their ability to provide an efficient loading platform

for immobilizing biological material and further improve electron transfer between the active site and electrode [153]. Catalysis is another useful and advantageous property to take into account for synthesis or chemically amplified detection. In addition, nanoparticles have also been used as labels in electrochemical aptasensing, this function is covered below.

Evtugyn et al. developed an impedimetric aptasensor for OTA detection on the base of aptamer carrier based on Au nanoparticles suspended in the dendrimeric hydrophilic polymer Boltorn H30®. Measurements of electrochemical properties of the modifier confirmed the high activity of AuNPs in the electron transduction as well as improvement of the aptasensor characteristics in comparison with Boltorn H30® and bare gold electrode [49]. In addition, Xie et al. described a label-free aptasensor for lysozyme detection using SPE modified with AuNPs. The modification of the electrode surface with AuNPs caused an increase of the active surface area, from 0.72mm^2 to 1.33mm^2 [199].

1.5.1.3 Graphene

Graphene is a new form of carbon nanomaterials with unique physical and chemical properties [135], such as large specific surface area [172], high electrical conductivity [170], excellent thermal stability with oxidation resistance temperature, high thermal conductivity [55], remarkable mechanical strength [95], and outstanding optical transmittance [53]. In addition, it also shows great electrochemical properties, including wide electrochemical potential windows, low charge-transfer resistance, and excellent electrochemical activity [165].

Graphene is basically a single layer of carbon atoms organized in a closely packed honeycomb two-dimensional lattice. Moreover, all the properties aforesaid, graphene and its associated materials such as reduced graphene oxide (rGO) [118], graphene nanoflakes [130] and graphene platelets [37], are

capable of adsorbing oligonucleotides due to the strong unique π-π interactions between the nanomaterial and the nitrogenous based of nucleotides. Consequently, they are commonly used in biosensing technology [114, 116]. For instance, Loo et al. presented an impedimetric aptasensor for thrombin detection comparing SPE modified with different carbon materials as a graphite oxide, graphene oxide, thermally reduced graphene oxide and electrochemically rGO. The SPE modified with graphene oxide was the most sensitive surface for the detection of thrombin with the adopted protocol [113].

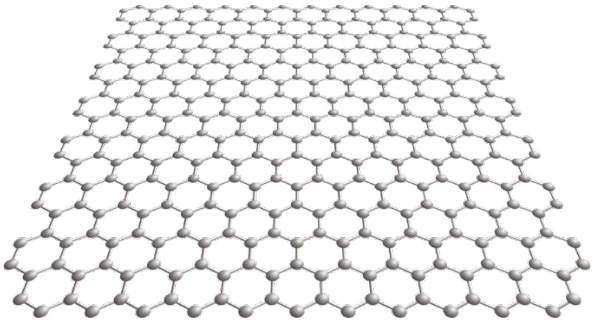

Figure 1.20. A structure of a sheet of graphene.

1.5.1.4. Nanocomposites

As its name indicates, a nanocomposite is a composite in which at least one of the phases shows dimensions in the nanometer range [161]. The integration of nanomaterials into matrix allows to exploit the synergistic effect of this new nano-matrix which could greatly improve the sensitivity of aptasensors. For instance, Liu et al. described a label-free aptamer-based sensor for dopamine detection using graphene-polyaniline nanocomposite film. Authors attributed to the high obtained sensitivity to the nanocomposite film. This could enhance the conductivity of the electrode to accelerate the probe to reach the electrode surface [108]. In addition, Jia et al. presented an aptasensor for the ultrasensitive detection of *Staphylococcus aureus* using a nanocomposite prepared from reduced graphene oxide and AuNPs. The

nanocomposite increased electron transfer and the electrochemical signal, obtaining a detection limit of 10 CFU [81].

1.5.2. Nanomaterials as label for signal amplification

The most common nanomaterials used as a label in impedimetric aptasensors are given next

1.5.2.1 Quantum Dots

Quantum dots (QDs) are semiconductor nanocrystals of semiconductor materials with CdSe/ZnS core-shell [23], see Figure 1.21. They have attracted remarkable attention in the fields of nanotechnology and biotechnology, especially in fluorescence based biological imaging applications. In impedimetric aptasensing, QDs are used as a label to enhance the impedimetric response. For example, Li et al. fabricated an electrochemical aptasensor based on quantum dots-coated silica nanospheres and the gold nanoparticles modified screen printed electrode. The screen-printed gold electrode was modified with AuNPs, the aptamer of thrombin was covalently bound to cadmium telluride (CdTe) QDs on the surface of silica nanoparticles. Enhanced sensitivity was also achieved by an increase of CdTe QDs loading aptamer [100].

.

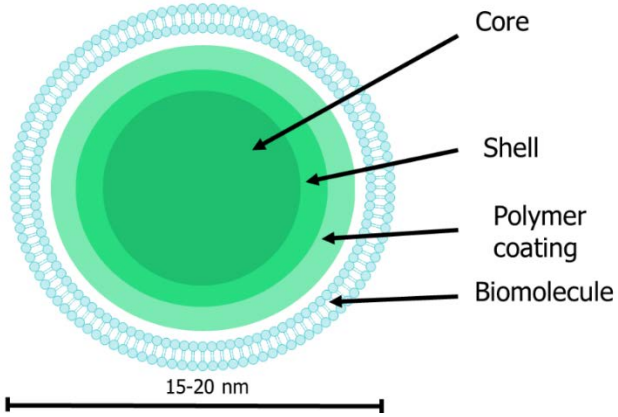

Figure 1.21. Scheme of the QD's structure.

1.5.2.2 Gold nanoparticles

Another interesting application of AuNPs in impedimetric aptasensors is to be used as a label in order to enhance the impedimetric signal. Several strategies has been used in the literature. For instance, Liu et al. proposed AuNPs modified with aptamer of tumor marker as amplification strategy. This may result in an obvious EIS signal change of the modified electrode, and offering a significant amplification for the detection of tumor marker [109]. Deng et al. developed an amplification strategy based on an aptamer sandwich approach for thrombin detection, aptamer/thrombin/aptamer-functionalized AuNPs. In detail, the strategy consisted on three cascade steps: (1) Apt-AuNPs as the first-level signal enhancer; (2) the steric-hindrance between the enlarged Apt-AuNPs as the second-level signal amplification; (3) the electrostatic-repulsion between sodium dodecylsulfate (SDS) stabilized Apt-AuNPs and the redox probe $[Fe(CN)_6]^{3-/4-}$ as the third-level signal amplification. Enlargement of Apt-AuNPs integrated with negatively charged surfactant (SDS) capping improved the sensitivity of the impedimetric aptasensor [40].

1.6. Signal Amplification methods using EIS

Despite the rapidity, lower costs and simplicity of label-free protocols, there are some cases where maximum sensitivity is of upper importance, and some additional amplification strategies are required. Different signal amplification methods used in impedance biosensors are explain in detail below.

1.6.1. Enzymes

Enzymes are currently the most used labels for biosensing. A general protocol to use enzymes is the sandwich approach, where the second aptamer

or antibody are label with them. A sterical hindrance generated by enzyme can strongly influence the impedimetric response.

1.6.2. Insoluble product

This strategy is based on the production of an insoluble product onto the electrode surface by enzymatic reaction. This precipitate causes a big increase of impedance signal, which improve sensitivity. Several enzymes and different substrates have been used in the literature [83]. For instance, Yang et al. used this strategy for the detection of α-fetoprotein. They developed an impedimetric sandwich immunosensor based on functionalized nanomaterial labels and bienzyme (horseradish peroxidase and glucose oxidase). The enzymes linked to functionalized nanomaterials as biocatalysts could accelerate the oxidation of 4-chloro-1-naphthol by H_2O_2 to yield the insoluble product on the electrode surface. The mass loading of the precipitates on the device led to a significant enhanced signal [203]. As the same way, Kaatz et al. propose an amplification strategy for linear single-strand probe detection based in two insoluble dyes which are generated by enzymatic reaction. As the previous example, these precipitate on the surface thus increasing the impedance signal in the presence of the ferri/ferrocyanide redox couple [83].

1.6.3. Gold Nanoparticles

One of the most common signal amplification method in impedimetric biosensors is the use of AuNPs. The different sterical hindrance and/or electrostatic repulsion generated by presence of nanoparticles onto the electrode surface can strongly influence the impedimetric response. It is worth mentioning that it is common to enhance the signal amplification of AuNPs with catalytic silver or gold deposition onto the surface of the AuNPs. These treatments are called: Silver Enhancement Treatment and Gold Enhancement treatment. In both methods, silver or gold ions are chemically reduced to metal atoms on the AuNPs surface in the presence of a reducing agent. Special care

has to be taken in controlling the deposition time and temperature so as to achieve a low-background and reproducible detection.

There are several examples of electrochemical assays using this treatments in the literature [8, 91, 104, 107] . For instance, Ye et al. proposed a nanoporous alumina membrane based sensing platform with gold nanoparticle tags amplification for DNA sensing. DNA hybridization in the nanopores induced blockage in the nanopores, which could be detected by EIS. The blockage signal could be further amplified by AuNPs and silver enhancement treatment to reach a limit of detection of 50 pM [205].

1.6.4. Nanoplatforms

Recently, nanoplatforms have been used as a label in biosensing application, in a similar manner as gold nanoparticles are utilized. These nanoplatforms can be made of graphene oxide [115], CNT, CuO, etc.

One reported application of nanoplatforms is the use of reduced graphene oxide in an impedimetric aptasensor for OTA detection based on a sandwich protocol. The thiolated capture DNA was immobilized on a gold electrode to capture the aptamer, then the sensing interface was incubated with OTA, followed by AuNPs–rGO functionalized reporter DNA hybridized with the residual aptamers. By using the AuNPs–rGO as an signal amplified platform, a single hybridization event between aptamer and reporter DNA was translated into more than 10^7 redox events, leading to a substantial increase in charge-transfer resistance by 7~ orders of magnitude compared with that of the free aptamer modified electrode [82]. Such an approach has demonstrated the capability of graphene based nanoplatforms to achieve a substantial amplification.

1.7. Aptamer targets

Since its discovery in 1990, aptamers have been selected for a wide spectrum of targets, more than 100 targets approximately [90]. The wide spectrum of targets includes almost any class of protein (enzymes, viral proteins, membrane proteins,...) [67, 92, 131], toxins [177, 178], drugs [74, 119], small organic compounds, ions [190] and even living cells [60]. However, large molecules such proteins are the best suited targets in the SELEX process, because they provide a large surface for interaction with aptamers [90].

The main targets used in this PhD thesis are explain in detail next.

1.7.1. Thrombin

Thrombin (Thr) (or factor IIa) is a serine protease enzyme of the chymotrypsin family. This family includes enzymes involved in digestion and degradative process, blood cogulation, cell-mediated immunity and cell deth, fibrinolysis, fertilization, and embryonic development [187]. This protein is composed by two active chains, an A-chain of 49 residues and a B-chain of 259 residues (Mw 32000 Da) [11]. Thr is generated in blood from its inactive precursor prothrombin (or factor II) and plays two important and opposite functions in thrombosis and haemostasis. Thrombin acts as a procoagulant factor when it converts fibrinogen into an insoluble fibrin clot that anchors platelets to the sites of lesion and initiates processes of wound repair. Moreover, it activates the transglutaminase factor XIII which stabilizes the fibrin clot, inhibits the fibrinolysis and activates factors V, VIII and XI [187]. In contrast, thrombin also acts as an anticoagulant through activation of protein C and release plasminogen activators from endothelial cells, which promote fibrinolytic cascade [182], see Figure 1.16.

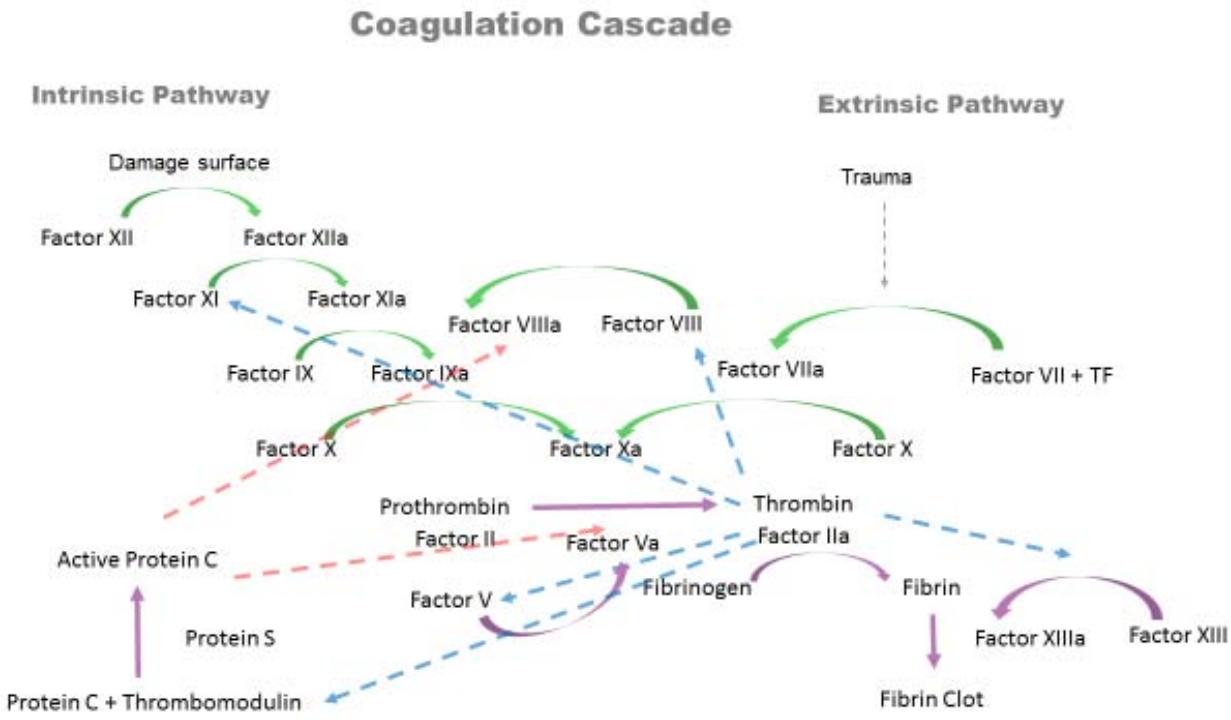

Figure 1.16. Scheme of Coagulation Cascade. Blue arrows correspond to principal activated functions of thrombin and red arrows correspond to anticoagulation function of active Protein C.

Thrombus are formed when an alteration occurs in these mechanisms. Different cardiovascular diseases such as stroke, myocardial infarction, deep-vein thrombosis and pulmonary embolism appear as consequence of the formation of thrombus [182].

As already mentioned above, thrombin is not present in blood under normal condition, but can reach low micromolar concentration during the coagulation process. However, when there isn't hemostatic process, concentrations of thrombin in the picomolar range in blood are associated with several diseases previously mentioned [12].

1.7.1.1. Aptamer of thrombin

The aptamer of thrombin (AptThr) was the first in vitro selected aptamer targeted toward a protein with not known physiological binding to nucleic acids

[13]. The folding between AptThr and Thr is well-defined in solution. When the aptamer interacts with thrombin, it forms a unimolecular DNA quadruplex consisting of two G-quartets connected by two loops and one TGT loop. A TT loop is formed between the two TT loops across the diagonal of the top G-quartet [121], as indicated Figure 1.17.

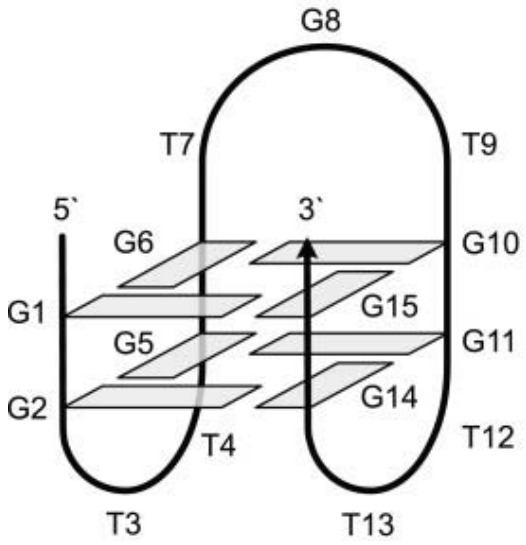

Figure 1.17. Quadruplex structure of thrombin aptamer (adapted from [105]).

This aptamer has been extensively applied as an inhibitor of thrombin activity in therapeutic [13, 179], as an imaging agent to detect thrombus, and recently as a biorecognition element for thrombin detection [32, 52, 136, 154]. Besides the different cardiovascular disease that thrombin can produce in picomolar concentration range, it is also considered an useful tumor marker for cancer pulmonary metastasis, thus an aptasensor for thrombin detection could be a useful diagnostic tool.

1.7.2. Cytochrome c

Cytochrome c (Cyt *c*) is a small protein (Mw~ 12000 Da), highly soluble (~100 $g \cdot L^{-1}$) and positively charged with a pI of 10.0-10.5. It is formed by one polypeptide chain linked to a heme C group, i.e., a protoporphyrin IX with a

coordinated iron ion, as indicated Figure 1.18 (A). The heme group is covalently linked to the Cyt *c* peptide chain through thioether bonds with cysteine residues. The heme iron is a hexacordinate configuration with His18 and Met80 as amino acid ligands, see Figure 1.18 (B). The heme iron-Met80 bond causes the weak 695 nm absorption band in the spectrum of Cyt *c* in the oxidized state [75].

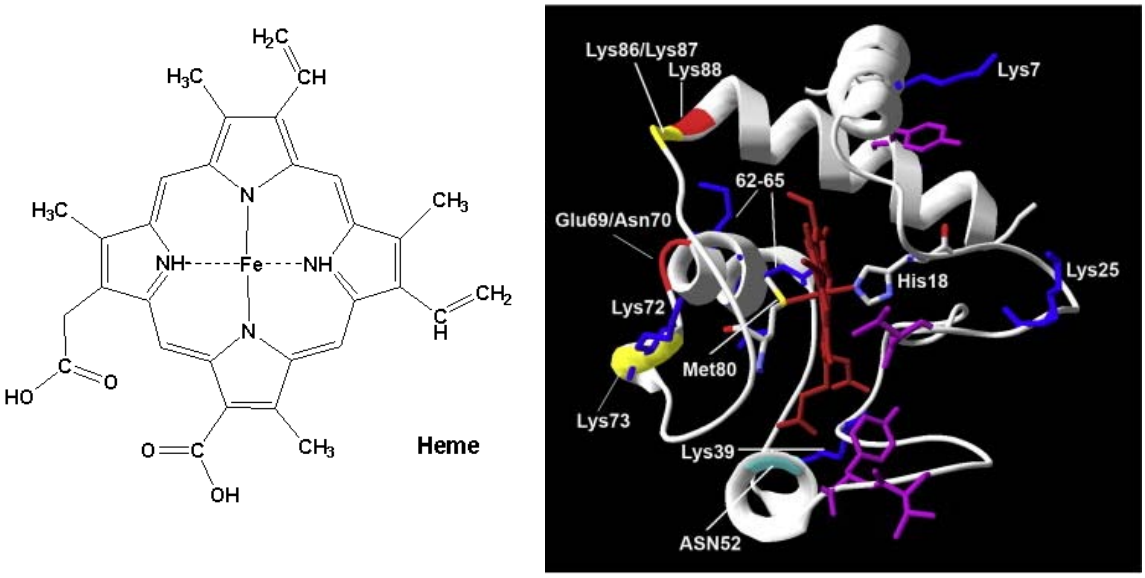

(A) (B)

Figure 1.18. A) Structure of heme group, B) Stereo view of cytochrome *c* structure of the conventional structure (adopted from [75]).

Cyt *c* is a multi-functional enzyme which is involved in life and death decisions of the cells. It plays an important role in electron transfer as part of the mitochondrial electron transport chain [75]. Cyt *c* uses its heme group as a redox intermediate to shuttle electrons between Complex III and Complex IV. It is also essential for the apoptosis process in the cells [139]. This process, apoptosis or programmed cell death, is a crucial mechanism of animal life that eliminates unwanted cells and is vital for embryonic development, homeostasis and immune defense. When a cell receives an apoptotic stimulus, Cyt *c* is

released into the cytosol where it binds with apoptotic protease-activating factor 1 [75], initiating the apoptotic mechanism.

Some problems in tissues and in skeletal muscles such as heart, liver, brain [1],... and Leighis syndrome [28] and infantile mitochondrial myopathy [4] are related to Cyt *c* deficiency.

Moreover, an increment of Cyt *c* concentration are associated to the pathogenesis of diabetes-specific microvascular diseases and neurodegenerative diseases, such as Alzheimer's disease, Huntington's disease, muscular dystrophies, and in models of cerebral ischemia [84]. Consequently, the absolute quantification of Cyt *c* release is great important as a preclinical indicator of these diseases.

1.8. References

[1] U.N. Abdulhag, D. Soiferman, O. Schueler-Furman, C. Miller, A. Shaag, O. Elpeleg, S. Edvardson, A. Saada, Mitochondrial complex IV deficiency, caused by mutated COX6B1, is associated with encephalomyopathy, hydrocephalus and cardiomyopathy, European Journal of Human Genetics 23 (2015) 159-164.

[2] M. Alibolandi, F. Hadizadeh, F. Vajhedin, K. Abnous, M. Ramezani, Design and fabrication of an aptasensor for chloramphenicol based on energy transfer of CdTe quantum dots to graphene oxide sheet, Materials Science and Engineering: C 48 (2015) 611-619.

[3] J.H. An, S.J. Park, O.S. Kwon, J. Bae, J. Jang, High-performance flexible graphene aptasensor for mercury detection in mussels, ACS Nano 7 (2013) 10563-10571.

[4] F. Baertling, M. A.M. van den Brand, J.L. Hertecant, A. Al-Shamsi, L. P. van den Heuvel, F. Distelmaier, E. Mayatepek, J.A. Smeitink, L.G.J. Nijtmans, R.J.T. Rodenburg, Mutations in COA6 cause cytochrome c oxidase deficiency and neonatal hypertrophic cardiomyopathy, Human Mutation 36 34-38.

[5] E.B. Bahadir, M.K. Sezginturk, A review on impedimetric biosensors, Artificial Cells, Nanomedicine and Biotechnology (2014) 1-15.

[6] H. Bai, R. Wang, B. Hargis, H. Lu, Y. Li, A SPR aptasensor for detection of avian influenza virus H5N1, Sensors (Basel) 12 (2012) 12506-12518.

[7] L. Bai, Y. Chai, R. Yuan, Y. Yuan, S. Xie, L. Jiang, Amperometric aptasensor for thrombin detection using enzyme-mediated direct electrochemistry and DNA-based signal amplification strategy, Biosensors and Bioelectronics 50 (2013) 325-330.

[8] Y.H. Bai, J.Y. Li, J.J. Xu, H.Y. Chen, Ultrasensitive electrochemical detection of DNA hybridization using Au/Fe3O4 magnetic composites combined with silver enhancement, Analyst 135 (2010) 1672-1679.

[9] T. Bao, H. Shu, W. Wen, X. Zhang, S. Wang, A sensitive electrochemical aptasensor for ATP detection based on exonuclease III-assisted signal amplification strategy, Analytica Chimica Acta.

[10] S. Barreda-García, M.J. González-Álvarez, N. de-los-Santos-Álvarez, J.J. Palacios-Gutiérrez, A.J. Miranda-Ordieres, M.J. Lobo-Castañón, Attomolar quantitation of Mycobacterium tuberculosis by asymmetric helicase-dependent isothermal DNA-amplification and electrochemical detection, Biosensors and Bioelectronics 68 (2015) 122-128.

[11] R. Becker, F. Spencer, Thrombin: Structure, Biochemistry, Measurement, and Status in Clinical Medicine, Journal of Thrombosis and Thrombolysis 5 (1998) 215-229.

[12] J. Bichler, J.A. Heit, W.G. Owen, Detection of Thrombin in human blood by ex-vivo hirudin, Thrombosis Research 84 (1996) 289-294.

[13] L.C. Bock, L.C. Griffin, J.A. Latham, E.H. Vermaas, J.J. Toole, Selection of single-stranded DNA molecules that bind and inhibit human thrombin, Nature 355 (1992) 564-566.

[14] A. Bonanni, M. del Valle, Use of nanomaterials for impedimetric DNA sensors: A review, Analytica Chimica Acta 678 (2010) 7-17.

[15] A. Bonanni, M.J. Esplandiu, M.I. Pividori, S. Alegret, M. del Valle, Impedimetric genosensors for the detection of DNA hybridization, Analytical Bioanalytical Chemistry 385 (2006) 1195-1201.

[16] A. Bonanni, M. Isabel Pividori, M. Del Valle, DNA polymorphism sensitive impedimetric detection on gold-nanoislands modified electrodes, Talanta 136 (2015) 95-101.

[17] A. Bonanni, M.I. Pividori, M. del Valle, Application of the avidin-biotin interaction to immobilize DNA in the development of electrochemical impedance genosensors, Analytical Bioanalytical Chemistry 389 (2007) 851-861.

[18] I. Bravo, T. García-Mendiola, M. Revenga-Parra, F. Pariente, E. Lorenzo, Diazonium salt click chemistry based multiwall carbon nanotube electrocatalytic platforms, Sensors and Actuators B: Chemical.

[19] K. Cammann, Bio-sensors based on ion-selective electrodes, Fresenius' Zeitschrift für Analytische Chemie 287 (1977) 1-9.

[20] F.Ç. Cebeci, E. Sezer, A.S. Sarac, A novel EDOT–nonylbithiazole–EDOT based comonomer as an active electrode material for supercapacitor applications, Electrochimica Acta 54 (2009) 6354-6360.

[21] L.C. Clark, Lyons, C., Electode system for continous monitoring in cardiovascular surgery, Annals of the New York Academy of Science 102 (1962) 29-45.

[22] A.H. Clemens, P.H. Chang, R.W. Myers, Development of an automatic system of insulin infusion controlled by blood sugar, its system for the determination of glucose and control algorithms, Journees annuelles de diabetologie de l"Hotel-Dieu (1976) 269-278.

[23] S. Coe, W.-K. Woo, M. Bawendi, V. Bulovic, Electroluminescence from single monolayers of nanocrystals in molecular organic devices, Nature 420 (2002) 800-803.

[24] P. Colas, B. Cohen, T. Jessen, I. Grishina, J. McCoy, R. Brent, Genetic selection of peptide aptamers that recognize and inhibit cyclin-dependent kinase 2, Nature 380 (1996) 548-550.

[25] R. Conrad, A.D. Ellington, Detecting Immobilized Protein Kinase C Isozymes with RNA Aptamers, Analytical Biochemistry 242 (1996) 261-265.

[26] G. Contreras Jiménez, S. Eissa, A. Ng, H. Alhadrami, M. Zourob, M. Siaj, Aptamer-based label-free impedimetric biosensor for detection of progesterone, Analytical Chemistry 87 (2015) 1075-1082.

[27] J.C. Cox, P. Rudolph, A.D. Ellington, Automated RNA selection, Biotechnology Progress 14 (1998) 845-850.

[28] O. Chai, J. Milgram, M.H. Shamir, O. Brenner, Polioencephalomyelopathy in a mixed breed dog resembling Leigh's disease, Canadian Veterinary Journal 56 (2015) 59-62.

[29] K. Chang, Y. Pi, W. Lu, F. Wang, F. Pan, F. Li, S. Jia, J. Shi, S. Deng, M. Chen, Label-free and high-sensitive detection of human breast cancer cells by aptamer-based leaky surface acoustic wave biosensor array, Biosensors and Bioelectronics 60 (2014) 318-324.

[30] W.T. Chaoyung J. Y, Molecular beacons, Springer-Verlag Berlin and Heidelberg GmbH & Co. K, Berlin, 2013.

[31] H. Chen, Q. Chen, Y. Zhao, F. Zhang, F. Yang, J. Tang, P. He, Electrochemiluminescence aptasensor for adenosine triphosphate detection using host–guest recognition between metallocyclodextrin complex and aptamer, Talanta 121 (2014) 229-233.

[32] H. Chen, F. Yuan, S. Wang, J. Xu, Y. Zhang, L. Wang, Aptamer-based sensing for thrombin in red region via fluorescence resonant energy transfer between NaYF4: Yb,Er upconversion nanoparticles and gold nanorods, Biosensors and Bioelectronics 48 (2013) 19-25.

[33] J. Chen, X. Zhang, S. Cai, D. Wu, M. Chen, S. Wang, J. Zhang, A fluorescent aptasensor based on DNA-scaffolded silver-nanocluster for ochratoxin A detection, Biosensors and Bioelectronics 57 (2014) 226-231.

[34] L.Q. Chen, S.J. Xiao, L. Peng, T. Wu, J. Ling, Y.F. Li, C.Z. Huang, Aptamer-based silver nanoparticles used for intracellular protein imaging and single nanoparticle spectral analysis, Journal of Physical Chemistry B 114 (2010) 3655-3659.

[35] Z. Chen, C. Zhang, X. Li, H. Ma, C. Wan, K. Li, Y. Lin, Aptasensor for electrochemical sensing of angiogenin based on electrode modified by cationic polyelectrolyte-functionalized graphene/gold nanoparticles composites, Biosensors and Bioelectronics 65 (2015) 232-237.

[36] T.L. Chuang, C.C. Chang, Y. Chu-Su, S.C. Wei, X.H. Zhao, P.R. Hsueh, C.W. Lin, Disposable surface plasmon resonance aptasensor with membrane-based sample handling design for quantitative interferon-gamma detection, Lab on a Chip - Miniaturisation for Chemistry and Biology 14 (2014) 2968-2977.

[37] F.L. D. W. Wang, Z. S. Wu, W. C. Ren and H. M. Cheng, Electrochemical interfacial capacitance in multilayer graphene sheets: dependence on number of stacking layers, Electrochemical Communications (2009) 1729-1732.

[38] J.S. Daniels, N. Pourmand, Label-Free Impedance Biosensors: Opportunities and Challenges, Electroanalysis 19 (2007) 1239-1257.

[39] K.A. Davis, B. Abrams, Y. Lin, S.D. Jayasena, Use of a high affinity DNA ligand in flow cytometry, Nucleic Acids Research 24 (1996) 702-706.

[40] C. Deng, J. Chen, Z. Nie, M. Wang, X. Chu, X. Chen, X. Xiao, C. Lei, S. Yao, Impedimetric Aptasensor with Femtomolar Sensitivity Based on the Enlargement of Surface-Charged Gold Nanoparticles, Analytical Chemistry 81 (2008) 739-745.

[41] D.A. Di Giusto, S.M. Knox, Y. Lai, G.D. Tyrelle, M.T. Aung, G.C. King, Multitasking by multivalent circular DNA aptamers, Chembiochem 7 (2006) 535-544.

[42] D.W. Drolet, L. Moon-McDermott, T.S. Romig, An enzyme-linked oligonucleotide assay, Nature Biotechnology 14 (1996) 1021-1025.

[43] M. Du, T. Yang, C. Zhao, K. Jiao, Electrochemical logic aptasensor based on graphene, Sensors and Actuators B: Chemical 169 (2012) 255-260.

[44] A. Duzgun, A. Maroto, T. Mairal, C. O'Sullivan, F.X. Rius, Solid-contact potentiometric aptasensor based on aptamer functionalized carbon nanotubes for the direct determination of proteins, Analyst 135 (2010) 1037-1041.

[45] R.C. Eberson, Miller J.A., Moran J.R.,Ward M.D. , Journa of American Chemistry Society 112 (1990) 3239-3243.

[46] R. Elshafey, M. Siaj, M. Zourob, DNA aptamers selection and characterization for development of label-free impedimetric aptasensor for neurotoxin anatoxin-a, Biosensors and Bioelectronics 68 (2015) 295-302.

[47] A.D. Ellington, J.W. Szostak, In vitro selection of RNA molecules that bind specific ligands, Nature 346 (1990) 818-822.

[48] C.L. Esposito, S. Catuogno, V. de Franciscis, L. Cerchia, New insight into clinical development of nucleic acid aptamers, Discovery Medicine 11 (2011) 487-496.

[49] G. Evtugyn, A. Porfireva, V. Stepanova, M. Kutyreva, A. Gataulina, N. Ulakhovich, V. Evtugyn, T. Hianik, Impedimetric aptasensor for ochratoxin a determination based on Au nanoparticles stabilized with hyper-branched polymer, Sensors (Switzerland) 13 (2013) 16129-16145.

[50] M. Famulok, G. Mayer, M. Blind, Nucleic acid aptamers - From selection in vitro to applications in vivo, Accounts of Chemical Research 33 (2000) 591-599.

[51] L. Feng, Y. Chen, J. Ren, X. Qu, A graphene functionalized electrochemical aptasensor for selective label-free detection of cancer cells, Biomaterials 32 (2011) 2930-2937.

[52] H. Fu, C. Ge, W. Cheng, C. Luo, D. Zhang, L. Yan, Y. He, G. Yi, A Hairpin Electrochemical Aptasensor for sensitive and specific detection of thrombin based on homogenous target recognition, Electroanalysis 25 (2013) 1223-1229.

[53] H. Gao, H. Duan, 2D and 3D graphene materials: Preparation and bioelectrochemical applications, Biosensors and Bioelectronics 65 (2015) 404-419.

[54] C.R. Geyer, R. Brent, Selection of genetic agents from random peptide aptamer expression libraries, Methods in Enzymology 328 (2000) 171-208.

[55] S. Ghosh, I. Calizo, D. Teweldebrhan, E.P. Pokatilov, D.L. Nika, A.A. Balandin, W. Bao, F. Miao, C.N. Lau, Extremely high thermal conductivity of graphene: Prospects for thermal management applications in nanoelectronic circuits, Applied Physics Letters 92 (2008) -.

[56] T. Goda, Y. Miyahara, Label-free and reagent-less protein biosensing using aptamer-modified extended-gate field-effect transistors, Biosensors and Bioelectronics 45 (2013) 89-94.

[57] Y. Gogotsi, Carbon Nanomaterials, CRC Press Taylor and Francis, Boca Raton, US, 2006.

[58] E. Golub, G. Pelossof, R. Freeman, H. Zhang, I. Willner, Electrochemical, Photoelectrochemical, and Surface Plasmon Resonance Detection of Cocaine Using Supramolecular Aptamer Complexes and Metallic or Semiconductor Nanoparticles, Analytical Chemistry 81 (2009) 9291-9298.

[59] R.N. Goyal, S. Chatterjee, A.R.S. Rana, The effect of modifying an edge-plane pyrolytic graphite electrode with single-wall carbon nanotubes on its use for sensing diclofenac, Carbon 48 (2010) 4136-4144.

[60] J.C. Graham, H. Zarbl, Use of Cell-SELEX to Generate DNA Aptamers as Molecular Probes of HPV-Associated Cervical Cancer Cells, PLoS ONE 7 (2012) e36103.

[61] D. Grieshaber, R. MacKenzie, J. Vörös, E. Reimhult, Electrochemical Biosensors - Sensor Principles and Architectures, Sensors (Basel, Switzerland) 8 (2008) 1400-1458.

[62] K.H.-S. Gu M., Biosensors based on aptamers and enzymes, Springer-Verlag Berlina and Heidelberg GmbH & Co.K, Berlin, 2014.

[63] Y.S.K.a.M.B. Gu, Advanced in Aptamer Screening and Small Molecules Aptasensors, Adv. Biochem. Eng. Biotechnol. 140 (2013) 29-67.

[64] G.G. Guilbault, J.G. Montalvo, Urea-specific enzyme electrode, Journal of the American Chemical Society 91 (1969) 2164-2165.

[65] X. Guo, F. Wen, N. Zheng, Q. Luo, H. Wang, H. Wang, S. Li, J. Wang, Development of an ultrasensitive aptasensor for the detection of aflatoxin B1, Biosensors and Bioelectronics 56 (2014) 340-344.

[66] Y. Guo, Y. Chen, Y. Wei, H. Li, C. Dong, Label-free fluorescent aptasensor for potassium ion using structure-switching aptamers and berberine, Spectrochimica Acta Part A: Molecular and Biomolecular Spectroscopy 136, Part C (2015) 1635-1641.

[67] M. Hanazato, G. Nakato, F. Nishikawa, K. Hase, S. Nishikawa, H. Ohno, Selection of an aptamer against mouse GP2 by SELEX, Cell Structure and Function 39 (2014) 23-29.

[68] T. Hermann, D.J. Patel, Adaptive recognition by nucleic acid aptamers, Science 287 (2000) 820-825.

[69] F.J. Hernandez, V.C. Ozalp, Graphene and Other Nanomaterial-Based Electrochemical Aptasensors, Biosensors 2 (2012) 1-14.

[70] J. Hesselberth, M.P. Robertson, S. Jhaveri, A.D. Ellington, In vitro selection of nucleic acids for diagnostic applications, Journal of Biotechnology 74 (2000) 15-25.

[71] F. Hoppe-Seyler, I. Crnkovic-Mertens, E. Tomai, K. Butz, Peptide aptamers: specific inhibitors of protein function, Current Molecular Medicine 4 (2004) 529-538.

[72] H. Huang, G. Jie, R. Cui, J.-J. Zhu, DNA aptamer-based detection of lysozyme by an electrochemiluminescence assay coupled to quantum dots, Electrochemistry Communications 11 (2009) 816-818.

[73] J. Huang, Y. He, X. Yang, K. Wang, K. Quan, X. Lin, Split aptazyme-based catalytic molecular beacons for amplified detection of adenosine, Analyst 139 (2014) 2994-2997.

[74] L. Huang, X. Yang, C. Qi, X. Niu, C. Zhao, X. Zhao, D. Shangguan, Y. Yang, A label-free electrochemical biosensor based on a DNA aptamer against codeine, Analytica Chimica Acta 787 (2013) 203-210.

[75] M. Hüttemann, P. Pecina, M. Rainbolt, T.H. Sanderson, V.E. Kagan, L. Samavati, J.W. Doan, I. Lee, The multiple functions of cytochrome c and their regulation in life and death decisions of the mammalian cell: From respiration to apoptosis, Mitochondrion 11 (2011) 369-381.

[76] W. Hwang do, H.Y. Ko, J.H. Lee, H. Kang, S.H. Ryu, I.C. Song, D.S. Lee, S. Kim, A nucleolin-targeted multimodal nanoparticle imaging probe for tracking cancer cells using an aptamer, Journal of Nuclear Medicine 51 (2010) 98-105.

[77] S. Iijima, Helical microtubules of graphitic carbon, Nature 354 (1991) 56-58.

[78] D. Irvine, C. Tuerk, L. Gold, SELEXION. Systematic evolution of ligands by exponential enrichment with integrated optimization by non-linear analysis, Journal of Molecular Biology 222 (1991) 739-761.

[79] S.D. Jayasena, Aptamers: an emerging class of molecules that rival antibodies in diagnostics, Clinical Chemistry 45 (1999) 1628-1650.

[80] S.D. Jayasena, Aptamers: An emerging class of molecules that rival antibodies in diagnostics, Clinical Chemistry 45 (1999) 22.

[81] F. Jia, N. Duan, S. Wu, X. Ma, Y. Xia, Z. Wang, X. Wei, Impedimetric aptasensor for Staphylococcus aureus based on nanocomposite prepared from reduced graphene oxide and gold nanoparticles, Microchimica Acta 181 (2014) 967-974.

[82] L. Jiang, J. Qian, X. Yang, Y. Yan, Q. Liu, K. Wang, K. Wang, Amplified impedimetric aptasensor based on gold nanoparticles covalently bound graphene sheet for the picomolar detection of ochratoxin A, Analytica Chimica Acta 806 (2014) 128-135.

[83] M. Kaatz, H. Schulze, I. Ciani, F. Lisdat, A.R. Mount, T.T. Bachmann, Alkaline phosphatase enzymatic signal amplification for fast, sensitive impedimetric DNA detection, Analyst 137 (2012) 59-63.

[84] B. Kadenbach, S. Arnold, I. Lee, M. Hüttemann, The possible role of cytochrome c oxidase in stress-induced apoptosis and degenerative diseases, Biochimica et Biophysica Acta (BBA) - Bioenergetics 1655 (2004) 400-408.

[85] P. Kara, A. de la Escosura-Muñiz, M. Maltez-da Costa, M. Guix, M. Ozsoz, A. Merkoçi, Aptamers based electrochemical biosensor for protein detection using carbon nanotubes platforms, Biosensors and Bioelectronics 26 (2010) 1715-1718.

[86] L. Kashefi-Kheyrabadi, M.A. Mehrgardi, Design and construction of a label free aptasensor for electrochemical detection of sodium diclofenac, Biosensors and Bioelectronics 33 (2012) 184-189.

[87] E. Katz, I. Willner, Probing biomolecular interactions at conductive and semiconductive surfaces by impedance spectroscopy: Routes to impedimetric immunosensors, DNA-Sensors, and enzyme biosensors, Electroanalysis 15 (2003) 913-947.

[88] H. Ke, M. Liu, L. Zhuang, Z. Li, L. Fan, G. Zhao, A Fetomolar Level 17β-estradiol Electrochemical Aptasensor Constructed On Hierachical Dendritic Gold Modified Boron-Doped Diamond Electrode, Electrochimica Acta 137 (2014) 146-153.

[89] Y.H. Kim, J.P. Kim, S.J. Han, S.J. Sim, Aptamer biosensor for lable-free detection of human immunoglobulin E based on surface plasmon resonance, Sensors and Actuators B: Chemical 139 (2009) 471-475.

[90] Y.S. Kim, M.B. Gu, Advances in aptamer screening and small molecule aptasensors, Advances in biochemical engineering/biotechnology 140 (2014) 29-67.

[91] Y.-J. Ko, J.-H. Maeng, Y. Ahn, S.-Y. Hwang, N.G. Cho, S.-H. Lee, Real-time immunoassay with a PDMS–glass hybrid microfilter electro-immunosensing chip using nanogold particles and silver enhancement, Sensors and Actuators B: Chemical 132 (2008) 327-333.

[92] E. Kraus, W. James, A.N. Barclay, Cutting edge: novel RNA ligands able to bind CD4 antigen and inhibit CD4+ T lymphocyte function, Journal of Immunology 160 (1998) 5209-5212.

[93] R.Y. Lai, K.W. Plaxco, A.J. Heeger, Aptamer-based electrochemical detection of picomolar platelet-derived growth factor directly in blood serum, Analytical Chemistry 79 (2007) 229-233.

[94] K. Lange, F.J. Gruhl, M. Rapp, Surface Acoustic Wave (SAW) biosensors: coupling of sensing layers and measurement, Methods in Molecular Biology 949 (2013) 491-505.

[95] C. Lee, X. Wei, J.W. Kysar, J. Hone, Measurement of the elastic properties and intrinsic strength of monolayer graphene, Science 321 (2008) 385-388.

[96] M. Lee, D.R. Walt, A fiber-optic microarray biosensor using aptamers as receptors, Analytical Biochemistry 282 (2000) 142-146.

[97] H. Li, J. Yan, W. Ou, H. Liu, S. Liu, Y. Wan, Construction of a biotinylated cameloid-like antibody for lable-free detection of apolipoprotein B-100, Biosensors and Bioelectronics 64 (2015) 111-118.

[98] J. Li, Z.C. Cao, Z. Tang, K. Wang, W. Tan, Molecular beacons for protein-DNA interaction studies, Methods in molecular biology (Clifton, N.J.) 429 (2008) 209-224.

[99] W. Li, Z. Nie, X. Xu, Q. Shen, C. Deng, J. Chen, S. Yao, A sensitive, label free electrochemical aptasensor for ATP detection, Talanta 78 (2009) 954-958.

[100] Y. Li, L. Deng, C. Deng, Z. Nie, M. Yang, S. Si, Simple and sensitive aptasensor based on quantum dot-coated silica nanospheres and the gold screen-printed electrode, Talanta 99 (2012) 637-642.

[101] Y. Li, L. Deng, C. Deng, Z. Nie, M. Yang, S. Si, Simple and sensitive aptasensor based on quantum dot-coated silica nanospheres and the gold screen-printed electrode, Talanta 99 (2012) 637-642.

[102] Y. Li, H. Qi, Q. Gao, C. Zhang, Label-free and sensitive electrogenerated chemiluminescence aptasensor for the determination of lysozyme, Biosensors and Bioelectronics 26 (2011) 2733-2736.

[103] D. Lin, T. Tang, D. Jed Harrison, W.E. Lee, A.B. Jemere, A regenerating ultrasensitive electrochemical impedance immunosensor for the detection of adenovirus, Biosensors and Bioelectronics 68 (2015) 129-134.

[104] L. Lin, Y. Liu, L. Tang, J. Li, Electrochemical DNA sensor by the assembly of graphene and DNA-conjugated gold nanoparticles with silver enhancement strategy, Analyst 136 (2011) 4732-4737.

[105] B. Liu, D. Li, Structural transformation induced by locked nucleic acid or 2'-O-methyl nucleic acid site-specific modifications on thrombin binding aptamer, Chemistry Central Journal 8 (2014) 19.

[106] L. Liu, D. Xu, Y. Hu, S. Liu, H. Wei, J. Zheng, G. Wang, X. Hu, C. Wang, Construction of an impedimetric immunosensor for label-free detecting carbofuran residual in agricultural and environmental samples, Food Control 53 (2015) 72-80.

[107] R. Liu, Y. Zhang, S. Zhang, W. Qiu, Y. Gao, Silver Enhancement of Gold Nanoparticles for Biosensing: From Qualitative to Quantitative, Applied Spectroscopy Reviews 49 (2013) 121-138.

[108] S. Liu, X. Xing, J. Yu, W. Lian, J. Li, M. Cui, J. Huang, A novel label-free electrochemical aptasensor based on graphene-polyaniline composite film for dopamine determination, Biosensors and Bioelectronics 36 (2012) 186-191.

[109] X. Liu, Y. Qin, C. Deng, J. Xiang, Y. Li, A simple and sensitive impedimetric aptasensor for the detection of tumor markers based on gold nanoparticles signal amplification, Talanta 132 (2015) 150-154.

[110] Y. Liu, T. Kwa, A. Revzin, Simultaneous detection of cell-secreted TNF-α and IFN-γ using micropatterned aptamer-modified electrodes, Biomaterials 33 (2012) 7347-7355.

[111] Y.M. Liu, M. Zhou, Y.Y. Liu, K.J. Huang, J.T. Cao, J.J. Zhang, G.F. Shi, Y.H. Chen, A novel sandwich electrochemiluminescence aptasensor based on molybdenum disulfide nanosheet-graphene composites and Au nanoparticles for signal amplification, Analytical Methods 6 (2014) 4152-4157.

[112] Z. Liu, R. Yuan, Y. Chai, Y. Zhuo, C. Hong, X. Yang, H. Su, X. Qian, Highly sensitive, reusable electrochemical aptasensor for adenosine, Electrochimica Acta 54 (2009) 6207-6211.

[113] A.H. Loo, A. Bonanni, M. Pumera, Impedimetric thrombin aptasensor based on chemically modified graphenes, Nanoscale 4 (2012) 143-147.

[114] A.H. Loo, A. Bonanni, M. Pumera, Inherently electroactive graphene oxide nanoplatelets as labels for specific protein-target recognition, Nanoscale 5 (2013) 7844-7848.

[115] A.H. Loo, A. Bonanni, M. Pumera, Thrombin aptasensing with inherently electroactive graphene oxide nanoplatelets as labels, Nanoscale 5 (2013) 4758-4762.

[116] C.-H. Lu, H.-H. Yang, C.-L. Zhu, X. Chen, G.-N. Chen, A Graphene Platform for Sensing Biomolecules, Angewandte Chemie International Edition 48 (2009) 4785-4787.

[117] P. Luo, Y. Liu, Y. Xia, H. Xu, G. Xie, Aptamer biosensor for sensitive detection of toxin A of Clostridium difficile using gold nanoparticles synthesized by Bacillus stearothermophilus, Biosensors and Bioelectronics 54 (2014) 217-221.

[118] Y.M.Z.a.S.J.D. M. Zhou, Electrochemical sensing and biosensing platform based on chemically reduced graphene oxide, Analytical Chemistry 81 (2009) 5603-5613.

[119] P.d.P. M.N Stojanovic, W. Landry American Chemistry Society 122 (2000) 11547.

[120] W. Ma, H. Yin, L. Xu, Z. Xu, H. Kuang, L. Wang, C. Xu, Femtogram ultrasensitive aptasensor for the detection of OchratoxinA, Biosensors and Bioelectronics 42 (2013) 545-549.

[121] R.F. Macaya, P. Schultze, F.W. Smith, J.A. Roe, J. Feigon, Thrombin-binding DNA aptamer forms a unimolecular quadruplex structure in solution, Proceedings of the National Academy of Sciences of the United States of America 90 (1993) 3745-3749.

[122] C.L. Manzanares-Palenzuela, N. de-los-Santos-Álvarez, M.J. Lobo-Castañón, B. López-Ruiz, Multiplex electrochemical DNA platform for femtomolar-level quantification of genetically modified soybean, Biosensors and Bioelectronics 68 (2015) 259-265.

[123] J.R. McDonald, Impedance Spectroscopy, John Wiley, New York, 1987.

[124] J.O. McNamara, D. Kolonias, F. Pastor, R.S. Mittler, L. Chen, P.H. Giangrande, B. Sullenger, E. Gilboa, Multivalent 4-1BB binding aptamers costimulate CD8+ T cells and inhibit tumor growth in mice, Journal of Clinical Investigation 118 (2008) 376-386.

[125] Z. Mei, H. Chu, W. Chen, F. Xue, J. Liu, H. Xu, R. Zhang, L. Zheng, Ultrasensitive one-step rapid visual detection of bisphenol A in water samples by label-free aptasensor, Biosensors and Bioelectronics 39 (2013) 26-30.

[126] I. Mihai, A. Vezeanu, C. Polonschii, C. Albu, G.L. Radu, A. Vasilescu, Label-free detection of lysozyme in wines using an aptamer based biosensor and SPR detection, Sensors and Actuators, B: Chemical 206 (2014) 198-204.

[127] W. Mindt, P. Racine, Stimulating electrode with low energy consumption, Medical and Biological Engineering 11 (1973) 659-660.

[128] M. Minunni, S. Tombelli, A. Gullotto, E. Luzi, M. Mascini, Development of biosensors with aptamers as bio-recognition element: The case of HIV-1 Tat protein, Biosensors and Bioelectronics 20 (2004) 1149-1156.

[129] K.N. Morris, K.B. Jensen, C.M. Julin, M. Weil, L. Gold, High affinity ligands from in vitro selection: Complex targets, Proceedings of the National Academy of Sciences 95 (1998) 2902-2907.

[130] P.P. N. G. Shang, M. McMullan, M. Chu, A. Stamboulis, A. Potenza, S. S. Chesi and H. Marchetto, Catalyst-free efficient growth, orientation and biosensing properties of multilayer graphene nanoflake films with sharp edge planes, Advanced Functional Materials (2008) 3506-3514.

[131] P. Nadal, A. Pinto, M. Svobodova, N. Canela, C.K. O'Sullivan, DNA aptamers against the lup an 1 food allergen, PLoS ONE 7 (2012).

[132] S.M. Nimjee, C.P. Rusconi, B.A. Sullenger, Aptamers: An emerging class of therapeutics, Annual Review of Medicine, Annual Reviews, Palo Alto, 2005, pp. 555-583.

[133] S. Nimse, K. Song, M. Sonawane, D. Sayyed, T. Kim, Immobilization Techniques for Microarray: Challenges and Applications, Sensors 14 (2014) 22208-22229.

[134] V. Ninichuk, S. Clauss, O. Kulkarni, H. Schmid, S. Segerer, E. Radomska, D. Eulberg, K. Buchner, N. Selve, S. Klussmann, H.-J. Anders, Late Onset of Ccl2 Blockade with the Spiegelmer mNOX-E36–3'PEG Prevents Glomerulosclerosis and Improves Glomerular Filtration Rate in db/db Mice, The American Journal of Pathology 172 (2008) 628-637.

[135] K.S. Novoselov, A.K. Geim, S.V. Morozov, D. Jiang, Y. Zhang, S.V. Dubonos, I.V. Grigorieva, A.A. Firsov, Electric field effect in atomically thin carbon films, Science 306 (2004) 666-669.

[136] C. Ocaña, M. Del Valle, Signal amplification for thrombin impedimetric aptasensor: Sandwich protocol and use of gold-streptavidin nanoparticles, Biosensors and Bioelectronics 54 (2014) 408-414.

[137] C. Ocaña, M. Pacios, M. del Valle, A Reusable Impedimetric Aptasensor for Detection of Thrombin Employing a Graphite-Epoxy Composite Electrode, Sensors 12 (2012) 3037-3048.

[138] H. Ogi, Wireless-electrodeless quartz-crystal-microbalance biosensors for studying interactions among biomolecules: A review, Proceedings of the Japan Academy. Series B, Physical and Biological Sciences 89 (2013) 401-417.

[139] Y.-L.P. Ow, D.R. Green, Z. Hao, T.W. Mak, Cytochrome c: functions beyond respiration, Nature Reviews Molecular Cell Biology 9 (2008) 532-542.

[140] I. Palchetti, M. Mascini, Electrochemical nanomaterial-based nucleic acid aptasensors, Analytical Bioanalytical Chemistry 402 (2012) 3103-3114.

[141] W. Pan, P. Xin, G.A. Clawson, Minimal primer and primer-free SELEX protocols for selection of aptamers from random DNA libraries, Biotechniques 44 (2008) 351-360.

[142] K.I. Papamichael, M.P. Kreuzer, G.G. Guilbault, Viability of allergy (IgE) detection using an alternative aptamer receptor and electrochemical means, Sensors and Actuators B: Chemical 121 (2007) 178-186.

[143] K. Park, S.J. Kwon, J. Kwak, A Label-Free Electrochemical Aptasensor for Thrombin Using a Single-Wall Carbon Nanotube (SWCNT) Casted Glassy Carbon Electrode (GCE), Electroanalysis 26 (2014) 513-520.

[144] D.J. Patel, Structural analysis of nucleic acid aptamers, Current Opinion in Chemical Biology 1 (1997) 32-46.

[145] D.J. Patel, A.K. Suri, Structure, recognition and discrimination in RNA aptamer complexes with cofactors, amino acids, drugs and aminoglycoside antibiotics, Reviews in Molecular Biotechnology 74 (2000) 39-60.

[146] M.K. Patel, M.A. Ali, S. Srivastava, V.V. Agrawal, S.G. Ansari, B.D. Malhotra, Magnesium oxide grafted carbon nanotubes based impedimetric genosensor for biomedical application, Biosensors and Bioelectronics 50 (2013) 406-413.

[147] V. Pavski, X.C. Le, Detection of Human Immunodeficiency Virus Type 1 Reverse Transcriptase Using Aptamers as Probes in Affinity Capillary Electrophoresis, Analytical Chemistry 73 (2001) 6070-6076.

[148] V. Perumal, U. Hashim, Advances in biosensors: Principle, architecture and applications, Journal of Applied Biomedicine 12 (2014) 1-15.

[149] E.F. Pfeiffer, W. Beischer, C. Thum, A.H. Clemens, The artificial endocrine pancreas in clinical medicine and in research, Journees annuelles de diabetologie de l"Hotel-Dieu (1976) 279-296.

[150] W.A. Pieken, D.B. Olsen, F. Benseler, H. Aurup, F. Eckstein, Kinetic characterization of ribonuclease-resistant 2'-modified hammerhead ribozymes, Science 253 (1991) 314-317.

[151] M.I. Pividori, A. Lermo, A. Bonanni, S. Alegret, M. del Valle, Electrochemical immunosensor for the diagnosis of celiac disease, Analytical Biochemistry 388 (2009) 229-234.

[152] W.G. Purschke, F. Radtke, F. Kleinjung, S. Klussmann, A DNA Spiegelmer to staphylococcal enterotoxin B, Nucleic Acids Research 31 (2003) 3027-3032.

[153] W. Putzbach, N.J. Ronkainen, Immobilization techniques in the fabrication of nanomaterial-based electrochemical biosensors: a review, Sensors (Basel, Switzerland) 13 (2013) 4811-4840.

[154] A. Radi, J.L. Acero Sánchez, E. Baldrich, C.K. O'Sullivan, Reusable Impedimetric Aptasensor, Analytical Chemistry 77 (2005) 6320-6323.

[155] F. Radom, P.M. Jurek, M.P. Mazurek, J. Otlewski, F. Jeleń, Aptamers: Molecules of great potential, Biotechnology Advances 31 (2013) 1260-1274.

[156] R. Renneberg, D. Pfeiffer, F. Lisdat, G. Wilson, U. Wollenberger, F. Ligler, A.P. Turner, Frieder Scheller and the short history of biosensors, Advances in Biochemical Engineering Biotechnology 109 (2008) 1-18.

[157] F. Rohrbach, H. Karadeniz, A. Erdem, M. Famulok, G. Mayer, Label-free impedimetric aptasensor for lysozyme detection based on carbon nanotube-modified screen-printed electrodes, Analytical Biochemistry 421 (2012) 454-459.

[158] T.S. Romig, C. Bell, D.W. Drolet, Aptamer affinity chromatography: combinatorial chemistry applied to protein purification, Journal of Chromatography B: Biomedical Sciences and Applications 731 (1999) 275-284.

[159] M. Roushani, F. Shahdost-fard, A highly selective and sensitive cocaine aptasensor based on covalent attachment of the aptamer-functionalized AuNPs onto nanocomposite as the support platform, Analytica Chimica Acta 853 (2015) 214-221.

[160] M. Roushani, F. Shahdost-Fard, A novel ultrasensitive aptasensor based on silver nanoparticles measured via enhanced voltammetric response of electrochemical reduction of riboflavin as redox probe for cocaine detection, Sensors and Actuators, B: Chemical 207 (2015) 764-771.

[161] R. Roy, R.A. Roy, D.M. Roy, Alternative perspectives on "quasi-crystallinity": Non-uniformity and nanocomposites, Materials Letters 4 (1986) 323-328.

[162] V.J. Ruigrok, M. Levisson, J. Hekelaar, H. Smidt, B.W. Dijkstra, J. van der Oost, Characterization of Aptamer-Protein Complexes by X-ray Crystallography and Alternative Approaches, International Journal of Molecular Sciences 13 (2012) 10537-10552.

[163] A. Salimi, S. Khezrian, R. Hallaj, A. Vaziry, Highly sensitive electrochemical aptasensor for immunoglobulin e detection based on sandwich assay using enzyme-linked aptamer, Analytical Biochemistry 466 (2013) 89-97.

[164] M. Sassanfar, J.W. Szostak, An RNA motif that binds ATP, Nature 364 (1993) 550-553.

[165] Y. Shao, J. Wang, H. Wu, J. Liu, I.A. Aksay, Y. Lin, Graphene Based Electrochemical Sensors and Biosensors: A Review, Electroanalysis 22 (2010) 1027-1036.

[166] T. Shtatland, S.C. Gill, B.E. Javornik, H.E. Johansson, B.S. Singer, O.C. Uhlenbeck, D.A. Zichi, L. Gold, Interactions of Escherichia coli RNA with bacteriophage MS2 coat protein: genomic SELEX, Nucleic Acids Research 28 (2000).

[167] T. Šmuc, I.-Y. Ahn, H. Ulrich, Nucleic acid aptamers as high affinity ligands in biotechnology and biosensorics, Journal of Pharmaceutical and Biomedical Analysis 81–82 (2013) 210-217.

[168] K.M. Song, S. Lee, C. Ban, Aptamers and their biological applications, Sensors (Basel) 12 (2012) 612-631.

[169] S. Song, L. Wang, J. Li, C. Fan, J. Zhao, Aptamer-based biosensors, TrAC Trends in Analytical Chemistry 27 (2008) 108-117.

[170] S. Stankovich, D.A. Dikin, R.D. Piner, K.A. Kohlhaas, A. Kleinhammes, Y. Jia, Y. Wu, S.T. Nguyen, R.S. Ruoff, Synthesis of graphene-based nanosheets via chemical reduction of exfoliated graphite oxide, Carbon 45 (2007) 1558-1565.

[171] d.P.P. Stojanovic M.N., Landry W., Aptamer-based folding fluorescent sensor for cocaine, Journal of American Chemistry Society 123 (2001) 4928-4931.

[172] M.D. Stoller, S. Park, Y. Zhu, J. An, R.S. Ruoff, Graphene-Based Ultracapacitors, Nano Letters 8 (2008) 3498-3502.

[173] X. Sun, B. Liu, C. Yang, C. Li, An extremely sensitive aptasensor based on interfacial energy transfer between QDS SAMs and GO, Spectrochimica Acta Part A: Molecular and Biomolecular Spectroscopy 131 (2014) 288-293.

[174] Z. Szeitner, J. András, R.E. Gyurcsányi, T. Mészáros, Is less more? Lessons from aptamer selection strategies, Journal of Pharmaceutical and Biomedical Analysis.

[175] W. Tan, H. Wang, Y. Chen, X. Zhang, H. Zhu, C. Yang, R. Yang, C. Liu, Molecular aptamers for drug delivery, Trends in Biotechnology 29 (2011) 634-640.

[176] W. Tan, K. Wang, T.J. Drake, Molecular beacons, Current Opinion in Chemical Biology 8 (2004) 547-553.

[177] J. Tang, J. Xie, N. Shao, Y. Yan, The DNA aptamers that specifically recognize ricin toxin are selected by two in vitro selection methods, Electrophoresis 27 (2006) 1303-1311.

[178] J. Tang, T. Yu, L. Guo, J. Xie, N. Shao, Z. He, In vitro selection of DNA aptamer against abrin toxin and aptamer-based abrin direct detection, Biosensors and Bioelectronics 22 (2007) 2456-2463.

[179] D.M. Tasset, M.F. Kubik, W. Steiner, Oligonucleotide inhibitors of human thrombin that bind distinct epitopes, Journal of Molecular Biology 272 (1997) 688-698.

[180] M. Terrones, Science and technology of the twenty-first century: synthesis, properties, and applications of carbon nanotubes, Annual Review of Materials Research 33 (2003).

[181] D.R. Thévenot, K. Toth, R.A. Durst, G.S. Wilson, Electrochemical biosensors: recommended definitions and classification, Biosensors and Bioelectronics 16 (2001) 121-131.

[182] P. Thiagarajan, A.S. Narayanan, Thrombin, eLS, John Wiley & Sons, Ltd, 2001.

[183] S. Tombelli, M. Minunni, M. Mascini, Analytical applications of aptamers, Biosensors and Bioelectronics 20 (2005) 2424-2434.

[184] S. Tombelli, M. Minunni, M. Mascini, Piezoelectric biosensors: Strategies for coupling nucleic acids to piezoelectric devices, Methods 37 (2005) 48-56.

[185] D.T. Tran, V. Vermeeren, L. Grieten, S. Wenmackers, P. Wagner, J. Pollet, K.P.F. Janssen, L. Michiels, J. Lammertyn, Nanocrystalline diamond impedimetric aptasensor for the label-free detection of human IgE, Biosensors and Bioelectronics 26 (2011) 2987-2993.

[186] Transparencymarketresearch, Biosensors Market (Technologies: Electrochemical, Optical, Thermal, Piezoelectric; Applications: Medical, Food Toxicity Detection, Industrial Process Control, Agriculture, Environment and Others; and End Users: Point of Care Testing, Home Healthcare Diagnostics, Research Laboratories, Security and Bio-defense, and Food Industry) - Global Industry Analysis, Size, Share, Growth, Trends and Forecast, 2014 - 2020, USA-Canada, 2014.

[187] M.E.M.a.N.E. Tsopanoglov, Thrombin: Physiology and Disease, Springer, New York, USA, 2009.

[188] C. Tuerk, L. Gold, Systemic evolution of ligands by exponential enrichment: RNA ligands to bacteriophage T4 DNA polymerase, Science 249 (1990) 505-510.

[189] A. Vater, F. Jarosch, K. Buchner, S. Klussmann, Short bioactive Spiegelmers to migraine-associated calcitonin gene-related peptide rapidly identified by a novel approach: Tailored-SELEX, Nucleic Acids Research 31 (2003) e130-e130.

[190] A. Verdian-Doghaei, M.R. Housaindokht, K. Abnous, A fluorescent aptasensor for potassium ion detection-based triple-helix molecular switch, Analytical Biochemistry 466 (2014) 72-75.

[191] D. Voccia, I. Palchetti, Photoelectrochemical biosensors for nucleic acid detection, Journal of Nanoscience and Nanotechnology 15 (2015) 3320-3332.

[192] M. Vuyisich, P.A. Beal, Controlling Protein Activity with Ligand-Regulated RNA Aptamers, Chemistry & Biology 9 (2002) 907-913.

[193] Y. Wang, J. Feng, Z. Tan, H. Wang, Electrochemical impedance spectroscopy aptasensor for ultrasensitive detection of adenosine with dual backfillers, Biosensors and Bioelectronics 60 (2014) 218-223.

[194] J.D. Watson, F.H.C. Crick, Molecular structure of nucleic acids: A structure for deoxyribose nucleic acid, Nature 171 (1953) 737-738.

[195] Y. Wei, J. Zhang, X. Wang, Y. Duan, Amplified fluorescent aptasensor through catalytic recycling for highly sensitive detection of ochratoxin A, Biosensors and Bioelectronics 65 (2015) 16-22.

[196] R. White, C. Rusconi, E. Scardino, A. Wolberg, J. Lawson, M. Hoffman, B. Sullenger, Generation of species cross-reactive aptamers using "toggle" SELEX, Molecular Therapy 4 (2001) 567-573.

[197] B. Wlotzka, S. Leva, B. Eschgfäller, J. Burmeister, F. Kleinjung, C. Kaduk, P. Muhn, H. Hess-Stumpp, S. Klussmann, In vivo properties of an anti-GnRH Spiegelmer: An example of an oligonucleotide-based therapeutic substance class, Proceedings of the National Academy of Sciences of the United States of America 99 (2002) 8898-8902.

[198] L. Wu, E. Xiong, X. Zhang, X. Zhang, J. Chen, Nanomaterials as signal amplification elements in DNA-based electrochemical sensing, Nano Today 9 (2014) 197-211.

[199] D. Xie, C. Li, L. Shangguan, H. Qi, D. Xue, Q. Gao, C. Zhang, Click chemistry-assisted self-assembly of DNA aptamer on gold nanoparticles-modified screen-printed carbon

electrodes for label-free electrochemical aptasensor, Sensors and Actuators B: Chemical 192 (2014) 558-564.

[200] H. Xing, N.Y. Wong, Y. Xiang, Y. Lu, DNA aptamer functionalized nanomaterials for intracellular analysis, cancer cell imaging and drug delivery, Current Opinion in Chemical Biology 16 (2012) 429-435.

[201] H. Xu, K. Gorgy, C. Gondran, A. Le Goff, N. Spinelli, C. Lopez, E. Defrancq, S. Cosnier, Label-free impedimetric thrombin sensor based on poly(pyrrole-nitrilotriacetic acid)-aptamer film, Biosensors and Bioelectronics 41 (2013) 90-95.

[202] N. Xu, Q. Wang, J. Lei, L. Liu, H. Ju, Label-free triple-helix aptamer as sensing platform for "signal-on" fluorescent detection of thrombin, Talanta 132 (2014) 387-391.

[203] F. Yang, J. Han, Y. Zhuo, Z. Yang, Y. Chai, R. Yuan, Highly sensitive impedimetric immunosensor based on single-walled carbon nanohorns as labels and bienzyme biocatalyzed precipitation as enhancer for cancer biomarker detection, Biosensors and Bioelectronics 55 (2014) 360-365.

[204] N. Yang, X. Chen, T. Ren, P. Zhang, D. Yang, Carbon nanotube based biosensors, Sensors and Actuators B: Chemical 207, Part A (2015) 690-715.

[205] W.W. Ye, J.Y. Shi, C.Y. Chan, Y. Zhang, M. Yang, A nanoporous membrane based impedance sensing platform for DNAsensing with gold nanoparticle amplification, Sensors and Actuators, B: Chemical 193 (2014) 877-882.

[206] G.A. Zelada-Guillén, S.V. Bhosale, J. Riu, F.X. Rius, Real-Time Potentiometric Detection of Bacteria in Complex Samples, Analytical Chemistry 82 (2010) 9254-9260.

[207] D.-W. Zhang, F.-T. Zhang, Y.-R. Cui, Q.-P. Deng, S. Krause, Y.-L. Zhou, X.-X. Zhang, A label-free aptasensor for the sensitive and specific detection of cocaine using supramolecular aptamer fragments/target complex by electrochemical impedance spectroscopy, Talanta 92 (2012) 65-71.

[208] H. Zhang, S. Shuang, L. Sun, A. Chen, Y. Qin, C. Dong, Label-free aptasensor for thrombin using a glassy carbon electrode modified with a graphene-porphyrin composite, Microchimica Acta 181 (2014) 189-196.

[209] J. Zhang, X. Zhang, G. Yang, J. Chen, S. Wang, A signal-on fluorescent aptasensor based on Tb3+ and structure-switching aptamer for label-free detection of Ochratoxin A in wheat, Biosensors and Bioelectronics 41 (2013) 704-709.

[210] K. Zhang, M. Xie, B. Zhou, Y. Hua, Z. Yan, H. Liu, L.-n. Guo, B. Wu, B. Huang, A new strategy based on aptasensor to time-resolved fluorescence assay for adenosine deaminase activity, Biosensors and Bioelectronics 41 (2013) 123-128.

[211] X. Zhang, J. Chen, H. Liu, S. Zhang, Quartz crystal microbalance detection of protein amplified by nicked circling, rolling circle amplification and biocatalytic precipitation, Biosensors and Bioelectronics 65 (2015) 341-345.

[212] X. Zhang, V.K. Yadavalli, Surface immobilization of DNA aptamers for biosensing and protein interaction analysis, Biosensors and Bioelectronics 26 (2011) 3142-3147.

[213] B. Zheng, S. Cheng, W. Liu, M.H.W. Lam, H. Liang, Small organic molecules detection based on aptamer-modified gold nanoparticles-enhanced quartz crystal microbalance with dissipation biosensor, Analytical Biochemistry 438 (2013) 144-149.

[214] J. Zhu, L. Zhang, Z. Zhou, S. Dong, E. Wang, Molecular aptamer beacon tuned DNA strand displacement to transform small molecules into DNA logic outputs, Chemical Communications 50 (2014) 3321-3323.

CHAPTER 2.OBJECTIVES OF THE RESEARCH

2. Objectives of the research

2.1. General Objectives

The development of aptasensors is of great interest nowadays in many fields. Consequently, the general aims of this PhD thesis were:

1. Design and development of aptasensors for protein detection using different electrodes materials and experimental procedures.

2. Use of Electrochemical Impedance Spectroscopy as highly sensitive transduction technique in aptasensing assays.

3. Employment of sandwich protocol and nanomaterials such as quantum dots, gold-nanoparticles and carbon nanotubes in order to improve the impedimetric response.

4. Application of the developed aptasensors in spiked serum samples.

2.2. Specific objectives

In order to carry out the main objectives, the following specific objectives were established according to the two different proteins detected:

A. Development of impedimetric aptasensors for thrombin detection

A.1 Development of label-free impedimetric aptasensors for thrombin detection

A.1.1. Comparison and evaluation of different aptamer immobilization techniques onto the electrode surface.

A.1.2. Evaluation of AvGEC electrodes as a platform for aptasensing and genosensing

A.2. Development of an impedimetric aptasensor based on aptamer sandwich protocol, gold nanoparticles and silver enhancement treatment.

A.2.2. Comparison of the analytical results obtained before and after each signal amplification step.

A.2.3. Evaluation of the selectivity of the aptasensor with possible interfering proteins and compounds.

A.2.4. Evaluation of the developed aptasensor with spiked serum samples.

B. Development of impedimetric aptasensors for cytochrome c detection

B.1. Development of label-free impedance aptasensors for cytochrome c based on physical adsorption of aptamer onto the surface of a GEC electrode.

B.1.1. Evaluation of the analytical characteristics of the aptasensor.

B.1.2. Comparison of the signal coming from cytochrome c to the ones coming from possible interfering proteins.

B.2. Development of an impedance aptamer-antibody sandwich assay for cytochrome c detection using MWCNT-SPEs.

B.2.1 Comparison of the analytical results obtained before and after each signal amplification step.

B.2.2. Evaluation of the selectivity of the aptamer-antibody assay with possible interfering proteins and compounds.

B.2.3. Evaluation of the developed aptasensor with spiked serum samples.

CHAPTER 3. EXPERIMENTAL

3. Experimental

3.1. Chemicals and buffers

Potassium dihydrogen phosphate, potassium ferricyanide $K_3[Fe(CN)_6]$,potassium ferrocyanide $K_4[Fe(CN)_6]$, perchloric acid, trisodium citrate, hydroxylamine chloride, sodium monophosphate, trisodium citrate, sodium nitrite, methanol, chloroauric acid, *N*-hydroxysuccinimide (NHS), *N*-(3-dimethylaminopropyl)-*N'*-ethylcabodiimide hydrochloride (EDC), streptavidin gold nanoparticles (strep-AuNPs), 625 nm streptavidin quantum dots (strep-AuNps), avidin (Av), fibrinogen (Fbr), cytochrome c (Cyt *c*) and thrombin (Thr), were purchased from Sigma Aldrich (St. Louis, MO, USA). Poly(ethylene glycol) 1000 (PEG), 4-aminobenzoic acid (ABA), sodium chloride and potassium chloride were obtained from Fluka (Buchs, Switzerland). Prothrombin (ProThr) was purchased from Apollo Scientific (Manchester, UK). LI silver enhancement kit was obtained

from Nanoprobes (Yaphank, New York). Human serum samples were provided from Hospital del Mar (Barcelona, Spain). All-solid-state electrodes (GECs and AvGECs) were prepared using 50 µm particle size graphite powder (Merck, Darmstadt, Germany), avidin and Epotek H77 resin and its corresponding hardener (both from Epoxy Technology, Billerica, MA, USA).

Other reagents were commercially available and were all of analytical reagent grade. All solutions were made up using sterilized Milli-Q water (Millipore, Billerica, MA, USA).

Aptamers and oligonucleotides used in this study were prepared by TIB-MOLBIOL (Berlin, Germany) and Sigma Aldrich (St. Louis, MO, USA). Their sequences and modifications are shown in Table 3.1. Aptamer and oligonucleotides stock solutions were diluted with sterilized and deionized water, separated in fractions of 100 µL and stored at a temperature of -20°C. When required, a single fraction was defrosted and used. As recommended, all aptamer and oligonucleotides solutions were utilized within six months after being frozen.

Table 3.1. Sequences of used aptamers and oligonucleotides and their modifications.

NAME	MODIFICATION	SEQUENCE
AptThr	-	5'-GGTTGGTGTGGTTGG-3'
AptThrNH_2	3'-NH_2	5'-GGTTGGTGTGGTTGG-3'
AptThrBio1	3'-Biotin	5'-GGTTGGTGTGGTTGG-3'
AptThrBio2	5'-Biotin	5'AGTCCGTGGTAGGGCAGGTTGGGGTGACT-3'
AptCyt *c*	-	5'-AGTGTGAAATATCTAAACTAAATGTGGAGGGT GGGACGGGAAGAAGTTTATTTTTCACACT-3′
AptCyt *c* NH_2	3'-NH_2	5'-AGTGTGAAATATCTAAACTAAATGTGGAGGGT GGGACGGGAAGAAGTTTATTTTTCACACT-3′
AptCyt *c* Bio	5'-Biotin	5'-AGTGTGAAATATCTAAACTAAATGTGG AGGGTGGGACGGGAAGAAGTTTATTTTTCACACT-3′
ProbeEH	5'-Biotin	5'-CCTCACTCTGAACTGGGGGCGAATC-3'
TargetEH	5'-Biotin	5'-GATTCGCCCCCAGTTCAGAGTGAGG-3'
Non complementary target	-	5'- GTACCAGCCCTTGTGATACAGCGGG-3'

The employed buffers are listed in Table 3.2

All solutions employed for the aptasensing and genosensing protocols were sterilized to prevent any degradation due to nucleases by use of a sterilizer at 20 bars and 125 ºC for 30 min.

Table 3.2. Names and compositions of the different buffer solutions employed in this thesis.

BUFFER NAME	PH	CHEMICAL COMPOSITION
PBS1	7.0	187 mM NaCl, 2.7 mM KCl, 8.1 mM $Na_2HPO_4 \cdot 2H_2O$, 1.76 mM KH_2PO_4
PBS2	7.0	10 mM sodium phosphate buffer
TSC1	7.0	0.75 M NaCl, 0.075 M trisodium citrate
TSC2	7.0	0.30 M NaCl, 0.030 M trisodium citrate
HYDROXYLAMINE CHLORIDE	6.0	0.4 mM $NH_2OH \cdot HCl$
TRIS	7.4	10 mM Tris
TRIETHYLAMMONIUM BICARBONATE	8	0.6 M triethylammoonium bicarbonate buffer

3.2. Equipment

AC impedance measurements were performed with an IM6e Impedance Measurement Unit (BAS-Zahner, Germany) or an Autolab PGStat 20 (Metrohm Autolab B.V, Utrecht, The Netherlands), see Figure 3.1. Thales and FRA software were used for the acquisition of the data and the control of the experiments, respectively. In addition, Zview (Scribner Associates Incorporated, Carolina, USA) software was used for data processing.

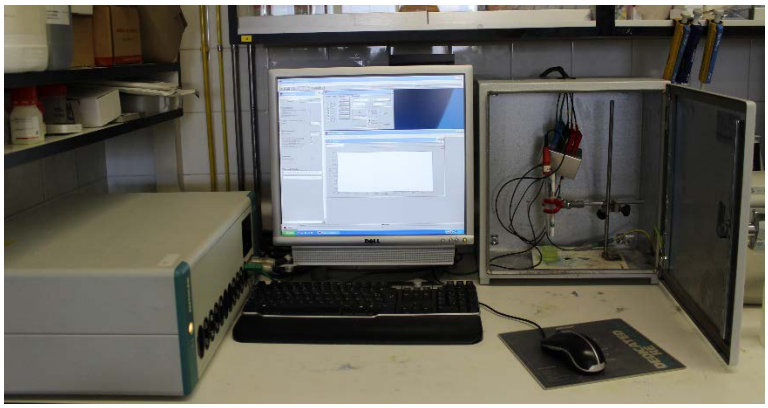

(A)

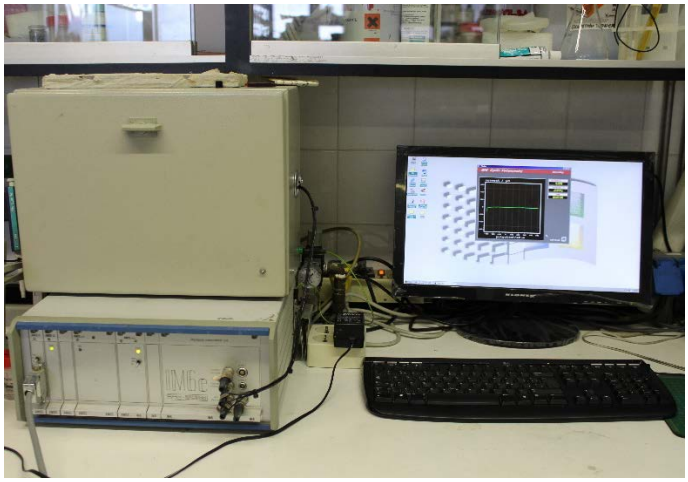

(B)

Figure 3.1. Equipment for Impedance measurement: (A) Autolab PGStat 20 and (B) BAS-Zahner IM6e.

Cyclic Voltammetry measurement were performed with an Autolab PGStat 20 (Metrohm Autolab B.V, Utrecht, The Netherlands). GPES software was used for the acquisition of the data and the control of the experiments.

A three electrode cell configuration was used to perform the impedance and cyclic voltammetry measurements: a platinum-ring auxiliary electrode (Crison 52–67 1, Barcelona, Spain), an Ag/AgCl pseudoreference electrode and the selected working electrode, see Figure 3.2.

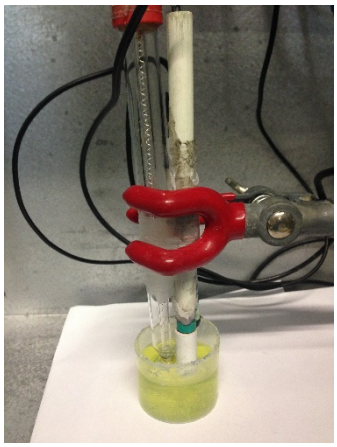

Figure 3.2. Electrochemical cell used.

A scanning electron microscope (SEM) (Merlin, Zeiss, Germany) was used to visualize silver enhanced strep-AuNPs and gold enhanced strep-AuNPs on the electrode surface, see Figure 3.3.

Figure 3.3. Merlin Scanning Electron Microscope.

A confocal microscope (SP5, Leica, Solms, Germany) was used to visualize strep-QDs on electrode surface, see Figure 3.4.

Figure 3.4. Confocal Microscope SP5.

Other equipment used:

- Eppendorf Thermomixer 5436 to control temperature incubations.
- pH-meter GLP22 (Crison 52–67 1, Barcelona, Spain).
- Vortex shaker MS3 basic (IKA, Staufen, Germany).
- Sterilizer CertoClav-Tisch-Autoclav 12L GS (Schaffhausen, Switzerland)

3.3. Electrodes

3.3.1. Graphite-epoxy composite electrodes (GEC)

All epoxy composite electrodes were prepared using a PVC tube body (6 mm i.d.) and a small copper disk soldered at the end of an electrical connector. Before iron soldering the copper disk, it was cleaned by dipping in Milli-Q water:HNO_3 (1:1) for a few seconds, in order to remove the copper oxide formed that can increase the electric current resistance reducing thus the sensitivity of the transducer. The conductive paste was deposited filling the cavity in the plastic

body, as shown in Figure 3.5. The obtained electrode was then cured in an oven to obtain a solid conductive paste.

(A) (B)

Figure 3.5. (A) Representation of electrodes components and (B) Conductive Paste.

Before each use, the electrode surface was smoothed with different abrasive sandpaper (nº220-400-600-800-1000-1200) and finally with alumina paper (polishing strips 301044-001, Orion) in order to obtain a smooth mirror finish with a fresh renewable surface.

Table 3.3. Compositions and experimental conditions used for the construction of each type of electrode (G=graphite, E= Epoxy resin, Av=Avidin).

	COMPOSITION (% W/W)			CURING PROTOCOL	
ELECTRODE	G	E	AV	Tª (ºC)	TIME (DAYS)
GEC	20	80		80	3
AvGEC	18	80	2	40	7

As shown in Table 3.3, the graphite-epoxy composite (GEC) paste was prepared by hand mixing the epoxy resin and the hardener at a 20:3 (w/w) ratio, according to the manufacturer, and the graphite powder. The resulting paste was thoroughly mixed by hand for about 1 hour, and then the composite material was cured at 80°C during 3 days.

The Avidin modified Graphite-Epoxy Composite Electrodes (AvGECs) were prepared using the same protocol, in this case, adding 2% of avidin, 18% of graphite and 80 % of epoxy resin. This mixture was thoroughly hand mixed to ensure the uniform dispersion of the avidin and graphite for throughout the resin about an hour and a half. Then, the biocomposite material was cured at 40°C during one week and then stored at 4°C before and after being used.

The reproducibility of the construction of both electrodes, GECs and AvGECs, as well as the polishing procedure have been previously reported [2, 3, 6].

3.3.2. Commercial Screen Printed Electrode

Multi-Walled Carbon Nanotubes screen printed electrodes (MWCNT-SPE) were supplied by Dropsens (Oviedo, Spain), see Figure 3.6.

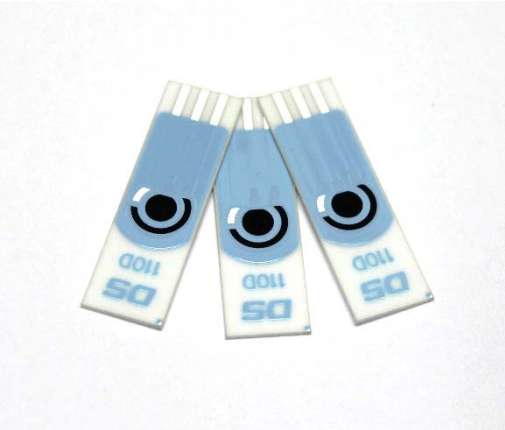

Figure 3.6. Multi-Walled Carbon Nanotubes screen printed electrodes (MWCNT-SPE).

3.4. Experimental Procedures

In this work, different procedures for thrombin and cytochrome c protein detection were employed in order to compare and optimize the obtained results.

3.4.1. Aptamer preconditioning

Before each aptamer immobilization technique, aptamer preconditioning is required in order to promote the loose conformation of the aptamer. For that, the aptamer solutions were heated at 80–90 °C for 3 min. And then, the solutions were dipped in a bath of cold water.

3.4.2. Aptasensors for thrombin detection

3.4.2.1. Label-free aptasensors for thrombin detection

Procedure 1-Aptasensor for thrombin detection based on physical adsorption as immobilization technique.

This analytical procedure consists of the immobilization of AptThr onto the GEC electrode surface using a wet physical adsorption technique, followed by a blocking step with PEG and the recognition of the target protein by the aptamer via incubation at room temperature.

In detail, the electrode was immersed in 160 µL of aptamer solution in Milli-Q water at the desired concentration, where the adsorption took place at room temperature for 15 min with soft stirring. Then, this was followed by two washing steps using PBS1 buffer solution for 10 min at room temperature, in order to remove unadsorbed aptamer.

After aptamer immobilization, the electrode was dipped in 160 µL of optimized PEG solution for 15 min at room temperature with soft stirring to minimize any possible nonspecific adsorption. This was followed by two washing steps using PBS1 buffer solution for 10 min.

The last step of the procedure is the recognition of the target protein by the immobilized aptamer. Consequently, the electrode was dipped in a solution with the desired concentration of thrombin. The incubation took place for 15 min at room temperature. After that, the biosensor was washed twice with PBS1

buffer solution for 10 min at room temperature to remove nonspecific adsorption of protein.

-Regeneration of thrombin aptamer

In order to regenerate the aptasensor, the aptamer-thrombin complex must be broken. For that, the electrode was dipped in a 2 M NaCl, heated at 42 °C while stirring for 20 min. Afterward, the electrode was washed twice with PBS1 buffer solution for 10 min.

Procedure 2- Aptasensor for thrombin detection using avidin-biotin affinity as immobilization technique.

This protocol is based on the immobilization of the aptamer of thrombin onto the transducer surface using the strong affinity between avidin and biotin, followed by a blocking step with PEG and the recognition of the target protein by the aptamer via incubation at room temperature.

Briefly, AvGEC electrode was dipped in 160 µL of AptThrBio1 solution for 15 min at room temperature with soft stirring. This was followed by two washing steps using PBS1 buffer solution for 10 min.

After aptamer immobilization, the electrode was dipped in 160 µL of PEG 40 mM for 15 min at room temperature with soft stirring to minimize any possible nonspecific adsorption. This was followed by two washing steps using PBS1 buffer solution for 10 min.

For recognition of Thr by the immobilized AptThr, the electrode was dipped in a solution with the desired concentration of Thr. The incubation took place for 15 min at room temperature. Then, the biosensor was washed twice with PBS1 buffer solution for 10 min at room temperature.

Procedure 3- Aptasensors for thrombin detection using covalent bond as immobilization technique.

Two different procedures were employed in this work with the aim to immobilized amino terminated aptamers onto the GEC electrode surface through amide bonds. In the first one, an electrochemical activation of the electrode surface was performed in order to create carboxylic groups required for the formation of amide bond via carbodiimide reaction. The second procedure consisted on the electrochemical deposition of diazonium salt onto the electrode surface (electrochemical grafting) for the formation of amide bond via the same carbodiimide reaction mentioned above. Both experimental procedures are described in more detail below.

-*Procedure 3.1- Electrochemical activation of the electrode surface*

In order to obtain an active surface with carboxyl groups, it was applied to the electrode a potencial of +0.8 V versus reference electrode Ag/AgCl/KCl (sat.) in 1 M $HClO_4$ solution during 5 h [7]. After that, the electrode was immersed in 160 µL of AptThrNH_2 in PBS1 solution with 1 mg of EDC and 0.5 mg of NHS during 24 h [5], with the goal of covalent immobilization of the aptamer through the amide bond formation. This step was followed by two washing steps using PBS1 buffer for 10 min.

After aptamer immobilization, the electrode was dipped in 160 µL of PEG 40 mM for 15 min at room temperature with soft stirring to minimize any possible nonspecific adsorption. This was followed by two washing steps using PBS1 buffer solution for 10 min.

The biorecogntion between aptamer and thrombin was performed when the electrode was dipped in a solution with the desired concentration of Thr. The incubation took place for 15 min at room temperature. Then, the biosensor was washed twice with PBS1 buffer solution for 10 min at room temperature.

-*Procedure 3.2- Electrochemical grafting of the electrode surface*

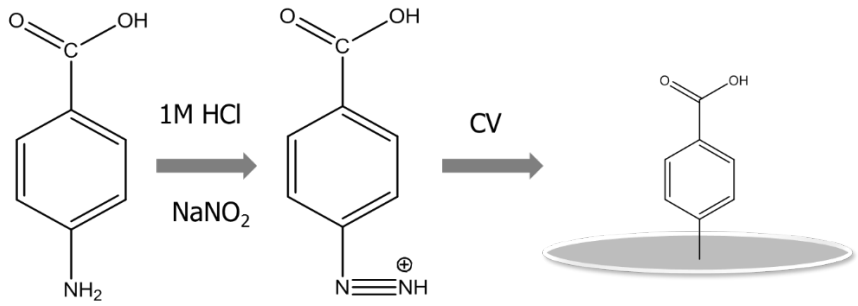

Figure 3.7. Scheme of deposition of diazonium salt onto the electrode surface (electrochemical grafting).

As can be seen in Figure 3.7, GEC electrodes were modified with diazonium salt. Firstly, 30 mg of ABA were dissolved in 3 mL of 1 M HCl and cooled with ice. Then, the diazonium salt was prepared by adding 2 mM $NaNO_2$ aqueous solution dropwise to this solution with constant stirring. Next, 570 µL of $NaNO_2$ solution was added to the ABA solution. The electrode was immersed in the solution and 200 successive voltammetric cycles ranging between 0.0 and -1.0 V (ν=200 mV·s^{-1}) were carried out [4]. The modified electrodes (benzoic acid modified carbon) were washed thoroughly with water and methanol and dried at room temperature. Finally, the electrodes were immersed in 160 µL of AptThrNH_2 with 1 mg of EDC and 0.5 mg of NHS during 12 h, with the goal of covalent immobilization of the aminated aptamer. This step was followed by two 10 min washing steps with PBS1 buffer solution [5].

After aptamer immobilization, the electrode was dipped in 160 µL of PEG 40 mM for 15 min at room temperature with soft stirring to minimize any possible nonspecific adsorption. This was followed by two washing steps using PBS1 buffer solution for 10 min.

The last step was the formation of the AptThr-Thr complex. For that, the electrode was dipped in a solution with the desired concentration of Thr. The

incubation took place for 15 min at room temperature. After that, the biosensor was washed twice with PBS1 buffer solution for 10 min at room temperature.

Procedure 4- Genosensor using avidin-biotin affinity as immobilization technique

This protocol was used for enterohaemoragic *Escherichia Coli O104:14* DNA testing.

The first step of the protocol was DNA hybrid formation in a solution containing the biotinylated probe and its complementary target. 30 pmol of biotinylated DNA probe and 30 pmol of its complementary target in 160 µL of TSC1 buffer were mixed in an Eppendorf tube. The hybridization took place in a thermomixer at 42ºC for 30 min with soft stirring.

Afterward, an avidin-modified electrode was dipped into an Eppendorf containing the biotinylated hybrid. The tube with the sensor was gently shaken for 20 min at 42 ºC. The previously formed biotinylated hybrid became immobilized onto the electrode surface due to the high affinity between the avidin exposed on the electrode surface and the biotin moiety on the biotinylated hybrid. This was followed by two washing steps with TSC2 at 42 ºC for 10 min.

In order to amplify the signal, strep-AuNPS and silver enhancement was used. AvGEC electrodes modified with biotinylated hybrid were incubated in an Eppendorf tube containing a solution of strep-AuNPs, 1:100 stock solution, in PBS2 buffer. The tube was then incubated at 42 ºC with soft stirring for 20 min. This step was followed by two gentle washing steps in PBS2 buffer for 10 min at 42 ºC.

Then, 20 µL of solution obtained by the combination of equal volumes of silver enhancer and initiator were deposited onto the electrode surface, and left for 7 min to react. The electrodes were then washed with MilliQ water in order to stop the reaction.

The negative control consisted of a non-biotinylated complementary target.

3.4.2.2 Aptasensor for thrombin detection using aptamer sandwich protocol, strep-AuNPs and silver enhancement treatment.

In this procedure, aptamer sandwich, strep-AuNPs and silver enhancement treatment were employed in order to amplify the obtained impedimetric signal. The scheme of experimental protocol is described in more detail below.

The first step consists of AptThrBio1 immobilization on the electrode surface. AvGEC electrode was immersed in a solution of AptThrBio1, where the avidin-biotin affinity interaction took place for 15 min at the electrode surface. This was followed by two washing steps using PBS1 buffer solution for 10 min, in order to remove any unadsorbed aptamer.

To minimize any possible nonspecific adsorption, the electrodes were dipped in 160 µL of PEG 40 mM for 15 min. This was followed by two washing steps using PBS1 buffer solution for 10 min.

The electrodes were dipped in a solution with the desired concentration of Thr or spiked sample. The incubation took place for 15 min. Then, the biosensors were washed twice with PBS1 buffer solution for 10 min.

In order to achieve the aptamer sandwich formation, the electrodes were dipped in 160 µl of PBS1 solution containing 12 pmols of AptThrBio2. The incubation took place for 15 min. This was followed by two washing steps using PBS1 buffer solution for 10 min.

AvGEC electrodes modified with the sandwich complex were incubated in 160 µL of strep-AuNPs, from a 1/100 dilution of the stock solution in PBS1 buffer. The tube was incubated at 25ºC with gentle stirring for 20 min. This step was followed by two gentle washing steps in PBS1 buffer for 10 min at 25ºC. In this way, nanoparticles were bound to sandwich through the formation of biotin-streptavidin complex. The optimal concentration of strep-AuNPs were optimized in previous studies [1].

-Silver enhancement treatment

Silver enhancement treatment was carried out either to be able to observe gold nanoparticles with SEM and to obtain a further signal amplification. In detail, 20 µl of a solution obtained by the combination of 10 µl of enhancer and 10 µl of initiator were deposited onto the electrode surface and left for 7 min to facilitate the reaction. Silver enhancement occurs during the catalytic reduction of silver from one solution (e.g. the enhancer) by another (e.g. the initiator) in the presence of gold nanoparticles. The reduction reaction causes silver to build up on the surface of the gold nanoparticles. After this catalytic silver reduction, the electrodes were thoroughly washed with deionized water to stop the reaction. The silver enhancing solution was prepared immediately before each use.

For silver enhancement treatment, the negative control used was a non-biotinylated AptCytc as aptamer without affinity.

- Visualization of aptamer sandwich using QDs

AvGEC electrodes modified with the biotin end aptamer sandwich were incubated in a solution of 40 nM of strep-QDs for 20 min at 25ºC with stirring. Then the electrodes were washed twice with 10mM PBS1 buffer. Negative controls were performed for the strep-QDs addition step either using AptCytc as noncomplementary target.

Aptamers and PEG concentrations have been optimized. For the optimization of aptamers concentration, different concentrations of aptamers were tested in order to ensure the full coverage of the electrode surface. For the optimization of PEG concentration, the concentration of aptamer was fixed at the optimized value and concentration of PEG was varied from 20mM to 50mM in PBS1 buffer solution.

In all the assays different selectivity experiments were carried out to verify selectivity characteristics of the assay with potentially interfering proteins instead of target protein.

3.4.3. Aptasensors for cytochrome c detection

3.4.3.1 Label-free aptasensor for cytochrome c detection based on physical adsorption technique.

This aptasensor is based on the same protocol used for thrombin detection using physical adsorption method as aptamer immobilization technique, see Section 3.4.2.1 Procedure 1.

3.4.3.2 Aptasensor for cytochrome c detection based on aptamer-antibody sandwich protocol

This procedure consists on the detection of Cyt *c* by using aptamer-antibody sandwich protocol, strep-AuNPs and silver enhancement treatment in order to amplify the impedimetric signal.

In detail, MWCNT-SPEs were modified with ABA by means of a one-step procedure. Firstly, 30 mg of ABA were dissolved in 3 mL of 1 M HCl and cooled with ice. Then, the diazonium salt was prepared by adding 570 µL of 2 mM $NaNO_2$ aqueous solution dropwise to the ABA solution, with constant stirring. The electrode was immersed in this solution, and 10 successive voltammetric cycles ranging between 0.0 and -1.0 V (ν=200 $mV \cdot s^{-1}$) were performed [4], generating a carbon-carbon bond and eliminating the azonium group. The modified electrodes (benzoic acid modified) were washed thoroughly with water and methanol and dried at room temperature. Finally, 60 µL of aptamer solution with 1 mg of EDC and 0.5 mg of NHS was placed on the modified electrode and left to react overnight, with the goal of covalent immobilization of the aptamer through the amide formation. This step was followed by two 10 min washing steps with PBS1 buffer solution.

In order to minimize any possible nonspecific adsorption of secondary species, 60 µl of PEG were dropped onto the electrodes and left to incubate during 15 min. This was followed by two washing steps using PBS1 buffer solution for 10 min.

60 µl of a solution with the desired concentration of Cyt *c* or spiked sample was dropped onto the electrodes. The incubation took place for 15 min. Then, the biosensors were washed twice with PBS1 buffer solution for 10 min.

In order to achieve the aptamer sandwich formation, the electrodes were dropped with 60 µl of AbCyt *c*, from a 1/500 dilution of the stock solution in PBS1 buffer soution. The incubation took place for 15 min. This was followed by two washing steps using PBS1 buffer solution for 10 min.

60 µL of strep-AuNPs, from a 1/100 dilution of the stock solution in phosphate buffer were dropped onto the electrodes. This step was followed by two gentle washing steps in phosphate buffer for 10 min at 25ºC. Negative controls were performed for the strep-AuNPs addition step using AptThr as an aptamer without affinity.

Silver enhancement treatment was carried out identical to the protocol 3.4.2.2. In this case, the negative control used was a biotinylated AptThr as aptamer without affinity.

- Gold enhancement treatment

The MWCNT screen-printed electrodes modified with sandwich and strep-AuNPs were immersed in a solution containing a mixture of 0.01% $HAuCl_4$ and 0.4 mM $NH_2OH{\cdot}HCl$ (pH 6.0) for 2 min at 25ºC, rinsed, and then treated for 2 additional min. In order to prevent the non-specific background of fine gold particles, the electrodes were rinsed with a solution of 0.6 M triethylammonium bicarbonate buffer after each amplification. Solutions were freshly prepared in a lightproof container before each use.

Aptamer, AbCyt *c* and PEG concentrations were optimized. For the optimization of aptamers concentration, different concentrations of aptamers

were tested in order to ensure the full coverage of the electrode surface. For the optimization of PEG concentration, the concentration of aptamer was fixed at the optimized value and concentration of PEG was varied from 20 mM to 50 mM in PBS1 buffer.

As in the case of Thr aptasensors, in all the assays selectivity experiments were carried out to verify selectivity characteristics of the assay with potentially interfering proteins instead of target protein.

3.4.4. Spiked samples preparation

3.4.4.1. Thrombin spiked samples

In order to validate the aptasensor based on a sandwich protocol, gold-nanoparticles and silver enhancement treatment in a real application, diluted human serum samples were spiked with different concentrations of thrombin. For that, human serum sample was diluted at 50 % with PBS1 buffer solution and then different concentrations of thrombin were spiked into the diluted serum.

3.4.4.2. Cytochrome c spiked samples

Aptasensor for cytochrome c detection based on aptamer-antibody sandwich protocol also was evaluated with human serum samples. Cyt *c* serum samples were prepared by adding small volume of extrinsic Cyt *c* solution in excess volume of undiluted serum samples.

In the case of the serum samples analysis, the blank assays corresponded to the serum sample without added extrinsic protein. All the experiment conditions were the same as the target detection.

3.5. Impedimetric Measurements

Impedance experiments were carried out at an applied potential of 0.17 V (vs. Ag/AgCl reference electrode), with a range of frequency of 50 KHz-0.05 Hz, an AC amplitude of 10 mV and a sampling rate of 10 points per decade above 66 Hz and 5 points per decade at the lower range. All measurements were performed in PBS1 buffer containing 0.01 M $K_3[Fe(CN)_6]/K_4[Fe(CN)_6]$ (1:1) mixture, used as a redox marker.

3.5.1. Data processing

After each modification of the electrode surface, an impedance measurement using a redox marker is recorded. The typical experimental spectrum obtained in all studied cases may be represented in the complex plane as a Nyquist diagram, as shown in Figure 3.8, where any diffusion component data points have been removed.

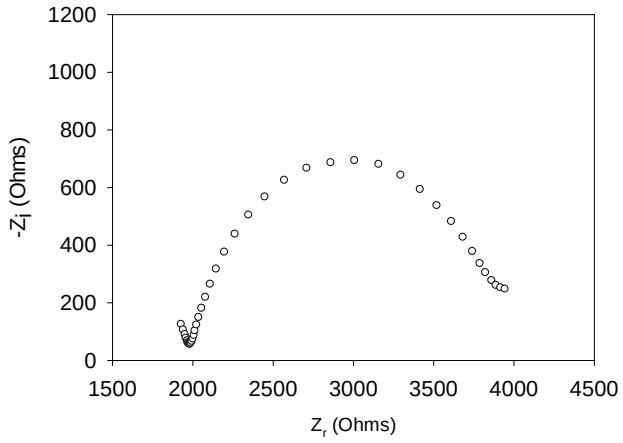

Figure 3.8. Typical Nyquist diagram obtained in experiments using $[Fe(CN)_6]^{3-/4-}$ as a redox marker.

The equivalent circuit proposed to best fit the experimental data is the one represented in Figure 3.9.

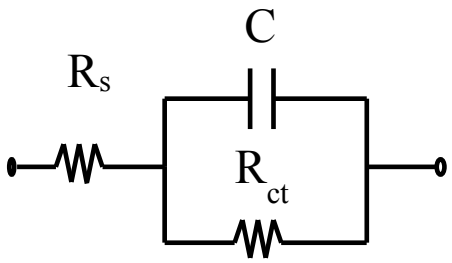

Figure 3.9. Equivalent circuit used to fit experimental data.

As indicated above, the interpretation of impedimetric spectra consists on the correlation among the obtained data with equivalent circuits formed by basic electrical elements. In this case, the resistance R_s corresponds to the resistance of the solution, R_{ct} represents the charge transfer resistance between the solution and the electrode surface, and CPE is associated to the capacitance of the double layer due to the interface between the electrode and the electrolytic solution. It is also important to point out that the contribution of the diffusion represented by Warburg impedance value wasn't taken into account in the selected equivalent circuit because in these studies the parameter of interest is represented by the charge transfer resistance R_{ct} (corresponding in the Nyquist diagram to the diameter of the semicircle).

After each performed fitting, the chi-square value provided by Zview software was thoroughly checked in order to evaluate the goodness of the fit. In all cases the calculated values for each circuit resulted <0.2, much lower than the tabulated value for 60 degrees of freedom (67.505 at 95% confidence level).

For all the different assays performed in this thesis, results were expressed as a relative R_{ct} variation.

-Δ and Δ_{ratio}

In order to compare the results obtained from the different electrodes used, and to obtain independent and reproducible results, a relative transformations of signals were needed [2].Thus, the Δ and Δ_{ratio} value were defined according to the following equations:

$$\Delta = R_{ct(\text{Bio-hybrid or Bio-hybrid + strep-AuNPs})} - R_{ct\ (\text{bare electrode})} \quad (3.1)$$

Where $R_{ct(\text{Bio-hybrid or Bio-hybrid + strep-AuNPs})}$ was the electron transfer resistance value measured after incubating with the biotynilated hybrid or with the biotynilated hybrid and the gold nanoparticles; and $R_{ct\ (\text{bare electrode})}$ was the electron transfer resistance of the blank electrode and buffer.

$$\Delta_{ratio} = \Delta_s / \Delta_p \quad (3.2)$$

$$\Delta_s = R_{ct\ (\text{aptamer-protein or sandwich or signal amplification treatment})} - R_{ct\ (\text{bare electrode})} \quad (3.3)$$

$$\Delta_p = R_{ct\ (\text{aptamer})} - R_{ct\ (\text{bare electrode})} \quad (3.4)$$

Where $R_{ct\ (\text{aptamer-protein or sandwich or signal amplification treatment})}$ was the electron transfer resistance value measured after incubating with the target protein or sandwich complex formation or a signal amplification method; $R_{ct\ (\text{aptamer})}$ was the electron transfer resistance after aptamer immobilization, and $R_{ct\ (\text{bare electrode})}$ was the electron transfer resistance of the blank electrode and buffer.

Figure 3.10 shows the different values of R_{ct} corresponding to the ones used in the previous equation 3.2, represented in the Nyquist diagram.

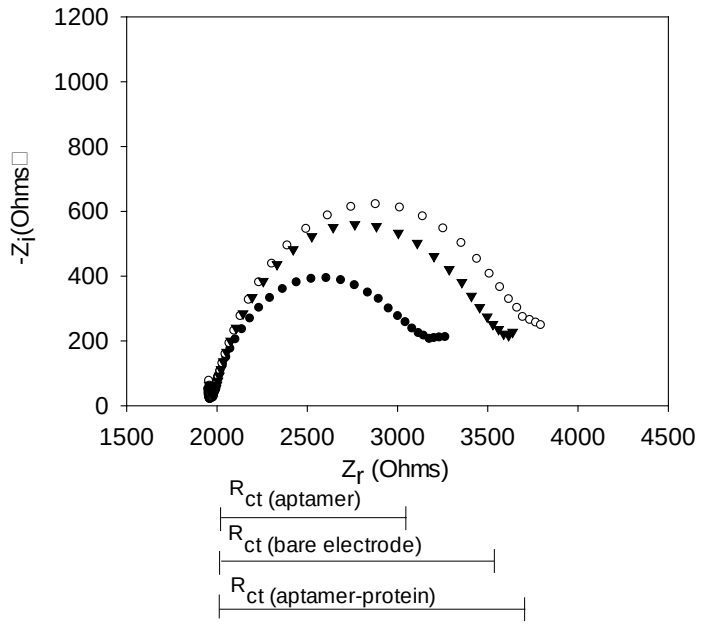

Figure 3.10. Nyquist diagrams and representation of charge transfer resistance value for a simple label-free assay.

3.6. Microscopy Studies

In this thesis, two different microscopy techniques were used with the aim to visualize the electrode surface and the different modifications performed.

3.6.1. Scanning Electron Microcopy

SEM images were taken at an acceleration voltage of 15 kV and resolution of 5.0 μm or at acceleration voltage of 20 kV and resolution of 10 μm.

3.6.2. Confocal Microscopy

Confocal images were collected at 625 nm and with excitation wavelength of 405 nm.

3.7. References

[1] A. Bonanni, M.J. Esplandiu, M. del Valle, Signal amplification for impedimetric genosensing using gold-streptavidin nanoparticles, Electrochimica Acta 53 (2008) 4022-4029.

[2] A. Bonanni, M.J. Esplandiu, M.I. Pividori, S. Alegret, M. del Valle, Impedimetric genosensors for the detection of DNA hybridization, Analytical Bioanalytical Chemistry 385 (2006) 1195-1201.

[3] A. Lermo, S. Campoy, J. Barbé, S. Hernández, S. Alegret, M.I. Pividori, In situ DNA amplification with magnetic primers for the electrochemical detection of food pathogens, Biosensors and Bioelectronics 22 (2007) 2010-2017.

[4] M. Moreno-Guzmán, I. Ojeda, R. Villalonga, A. González-Cortés, P. Yáñez-Sedeño, J.M. Pingarrón, Ultrasensitive detection of adrenocorticotropin hormone (ACTH) using disposable phenylboronic-modified electrochemical immunosensors, Biosensors and Bioelectronics 35 (2012) 82-86.

[5] M. Pacios, I. Martin-Fernandez, X. Borrissé, M.d. Valle, J. Bartrolí, E. Lora-Tamayo, P. Godignon, F. Perez-Murano, M.J. Esplandiu, Real time protein recognition in a liquid-gated carbon nanotube field-effect transistor modified with aptamers, Nanoscale (2012) 6.

[6] E. Williams, M.I. Pividori, A. Merkoçi, R.J. Forster, S. Alegret, Rapid electrochemical genosensor assay using a streptavidin carbon-polymer biocomposite electrode, Biosensors and Bioelectronics 19 (2003) 165-175.

[7] S. Yamazaki, Z. Siroma, T. Ioroi, K. Tanimoto, K. Yasuda, Evaluation of the number of carboxyl groups on glassy carbon after modification by 3,4-dihydroxybenzylamine, Carbon 45 (2007) 256-262.

CHAPTER 4. RESULTS AND DISCUSSION

4. Results and discussion

The results obtained during this PhD research are presented and discussed in the following sections.

The main results content in this PhD thesis have been presented in several international conferences:

a) XVI Transfrontaliar meeting of sensors and biosensors, Toulouse, France, September-2011.
b) Biosensors 2012, Cancún, Mexico, May-2012.
c) Nanomedicine Workshop UAB CEI, Bellaterra, Barcelona, Spain, Jun-2012.
d) XVII Transfrontier meeting of sensors and biosensors, Tarragona,Spain, September-2012.

e) Ibersensors, Puerto Rico, October-2012.
f) Nanorethinking workshop, Barcelona, Spain, November-2012.
g) COST Thematic Workshop, Biomimetic structures and DNA technology in biosensing, Bratislava, Slovakia, April-2013.
h) III International Conference on Bio-Sensing Technology, Sitges, Spain, May-2013.
i) COST Thematic Workshop, Bio-inspired Nanotechnologies for Biosensing, Sitges, Spain, May-2013.
j) XVIII Transfrontier meeting of sensors and biosensors, Alès ,France, September-2013.
k) Biosensors 2014, Melbourne, Australia, May-2014.
l) IV Jornades Doctorals del Departament de Química UAB, Bellaterra, Spain, May-2014.
m) XIX Transfrontier Meeting of Sensors and Biosensors 2014, Barcelona,Spain, September-2014.
n) III Workshop in Nanomedicine, Bellaterra, Barcelona, Spain, November-2014.
o) IV International Conference on Bio-Sensing Technology, Lisbon, Portugal, May-2015.

The list of articles originated from the work of this PhD thesis and accepted for the PhD Commission is the following:

Article 1. C. Ocaña, M. Pacios and M.del Valle, A reusable impedimetric aptasensor for detection of thrombin employing a graphite-epoxy composite electrode, Sensors 2012, 12, 3037-3048.

Article 2. C. Ocaña and M. del Valle, A comparison of four protocols for the immobilization of an aptamer on graphite composite electrodes, Micro Chimica Acta, 2014, 181, 355-363.

Article 3. C. Ocaña, C. Figueras and M. del Valle, Avidin epoxy-graphite composite electrode as platforms for genosensing and aptasensing, Journal of Nanoscience and Nanotechnology, 2014, 14, 1-9.

Article 4. C. Ocaña and M. del Valle, Signal amplification for thrombin impedimetric aptasensor: Sandwich protocol and use of gold-streptavidin nanoparticles, Biosensors and Bioelectronics, 2014, 54, 408-414.

Article 5. C. Ocaña, E. Arcay and M. del Valle, Label-free impedimetric aptasensor based on epoxy-graphite electrode for the recognition of cytochrome c, Sensors Actuators B, 2014, 191, 860-865.

Article 6. C. Ocaña, S. Lukic and M. del Valle, Aptamer-antibody sandwich assay for cytochrome c employing a MWCNT platform and the electrochemical impedance technique, Micro Chimica Acta, (submitted).

In addition, other articles related to this research work are included in the Annex Section.

Article 7. C.Ocaña, N. Malashikhina, M. del Valle and V. Pavlov, Label-free selective impedimetric detection of Cu^{2+} ions using catalytic DNA, Analyst, 2013, 138, 1995-1999.

Article 8. C. Ocaña and M. del Valle, Three different signal amplification strategies for the impedimetric detection of thrombin, Biosensors and Bioelectronics (draft).

The research was completed with a research stay of three months in Laboratoire IMAGES, Université de Perpignan Via Domitia, Perpignan, France; under the supervisor of Professor Jean-Louis Marty.

4.1. IMPEDIMETRIC APTASENSORS FOR THROMBIN DETECTION

4.1. Impedimetric aptasensors for thrombin detection

As mentioned in Section 1.7.1, thrombin is an important protein involved in blood coagulation. In pathological conditions is associated with various cardiovascular diseases, such as stroke, myocardial infarction, deep-vein thrombosis, pulmonary embolism, etc… In addition, it is also usually regarded as a tumor marker in the diagnosis of pulmonary metastasis. Consequently, the specific recognition and quantitative detection of thrombin is extremely important in both clinical practice and diagnostic application.

The main goal of this chapter is to develop and evaluated several impedimetric label-free aptasensor for the first time in our laboratory for thrombin detection based on different aptamer immobilization techniques such as physical adsorption, avidin-biotin affinity, and covalent bond via electrochemical activation of the electrode surface and via electrochemical grafting. With the aim to improve

the obtained impedimetric signals using AvGEC electrodes, a signal amplification strategy using aptamer sandwich, strep-AuNPs and silver enhancement treatment were performed. In addition, AvGECs electrodes were compared as a platform for genosensing and aptasensing. Thrombin aptamer was chosen as being one of the best studied and best functioning aptamers avalaible.

4.1.1. Label-free aptasensors for thrombin detection

4.1.1.1. Label-free aptasensor for thrombin detection based on physical adsorption immobilization technique

The whole biosensing principle of the impedimetric aptasensor is illustrated in Figure 4.1.1. Aptamer was immobilized onto the GEC electrode surface by wet physical adsorption technique. In order to avoid nonspecific adsorption, a blocking step with PEG was performed. Finally, Thr was recognized by the aptamer via incubation.

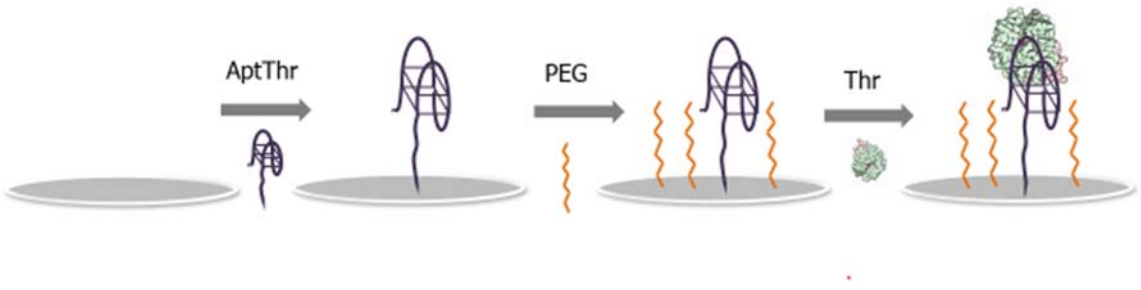

Figure 4.1.1. Scheme of the experimental protocol for the aptasensor for thrombin detection based on physical adsorption technique.

-Optimization of aptamer and PEG concentration

In order to generate a highly sensitive method with low detection limit for Thr detection, it was significant to choose optimal concentrations involved in the process of aptasensor construction and Thr detection.

Firstly, the influence of aptamer concentration was investigated by building its response curve, which was very essential to the sensitivity of the sensor. For this, increasing concentrations of AptThr was used to carry out the immobilization, evaluating the changes in the Δ_p.

Figure 4.1.2 shows the curve of AptThr adsorption onto the electrode surface. It can be observed that the difference in resistance (Δ_p) increased up to a value. This is due to the physical adsorption of the aptamer onto the electrode surface, which followed a Langmuir isotherm; in it, the variation of R_{ct} increases to reach a saturation value; the singular value of the exponential rise was chosen as the optimal concentration. This value corresponded to a concentration of aptamer of 1 µM.

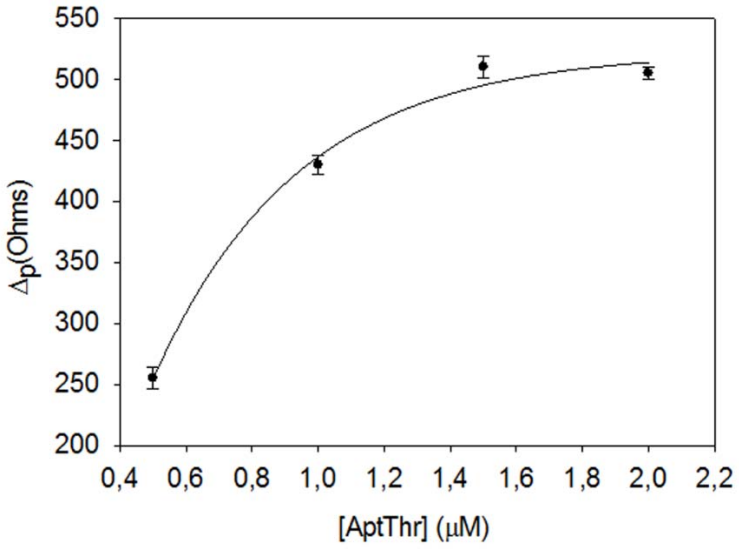

Figure 4.1.2. Optimization of the concentration of Apt-Thr. Uncertainty values corresponding to replicated experiments (n = 5).

In order to minimize any possible nonspecific adsorption onto the electrode surface, PEG was used as the blocking agent. After optimization of ApThr concentration, PEG concentrations were evaluated like in the previous case by construction of its calibration curve. As shown in Figure 4.1.3 there was an increase in resistance until the value of 40 mM of PEG where the saturation value is reached. Therefore, the optimal concentration of blocking agent was chosen as 40 mM.

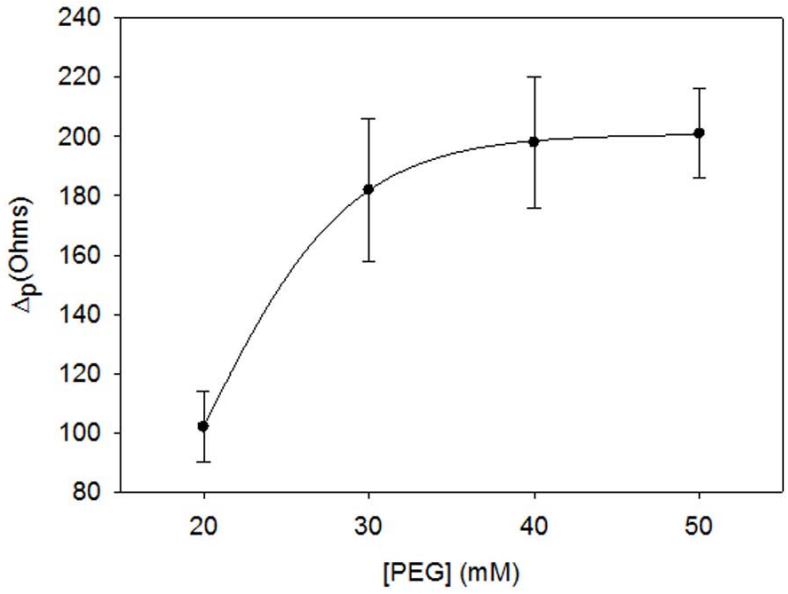

Figure 4.1.3. Optimization of the concentration of the blocking agent, PEG. Uncertainty values corresponding to replicated experiments (n = 5).

-Impedimetric response

With the optimized concentrations of aptamer and PEG and following the above experimental protocol for the detection of thrombin, the aptasensor response was initially evaluated. The aptamer of thrombin forms a single-strand oligonucleotide, a chain that recognizes the protein by a three-dimensional folding (quadriplex). During this folding, weak interactions between the aptamer and protein of the host-guest type are created, leading to complex AptThr-Thr.

One example of the obtained response after each biosensing step is shown in Figure 4.1.4. As can be seen, the resistance R_{ct} between the electrode surface and the solution is increased. This fact is due to the effect on the kinetics of the electron transfer redox marker $[Fe(CN)_6]^{3-}/[Fe(CN)_6]^{4-}$ which is delayed at the interface of the electrode, mainly caused by steric hindrance and electrostatic repulsion presented by the complex formed.

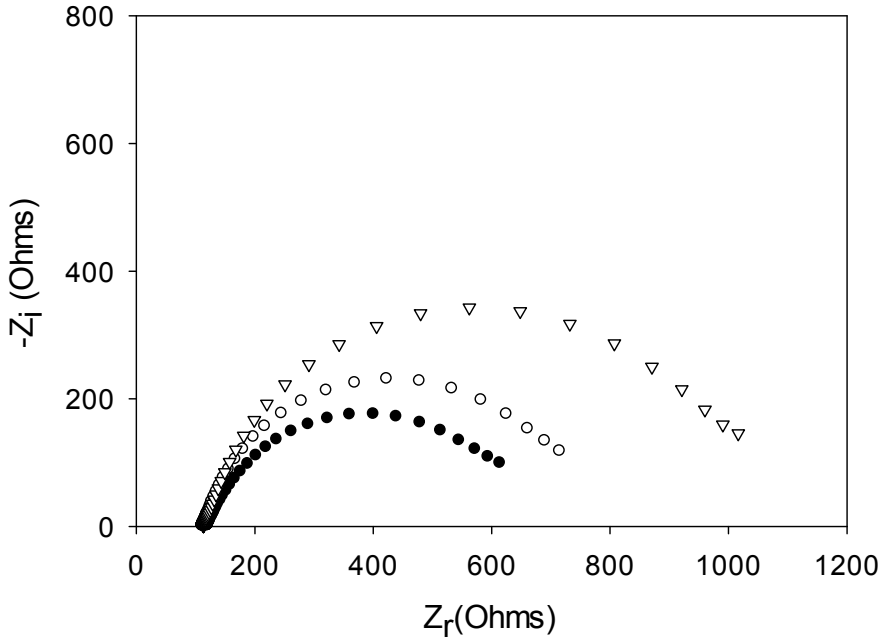

Figure 4.1.4. Nyquist Diagram of: (**a**) Bare electrode ●, (**b**) Aptamer of thrombin ○, and (**c**) AptThr-Thr 10 pM [Thr] ▽**.**

- Analytical performance of the aptasensor for detection of thrombin

New experiments with solutions containing different amount of thrombin were carried out and the corresponding calibration curve was built. Figure 4.1.5 shows the evolution of the Nyquist diagrams for the calibration of the aptasensor. There is a correct recognition of the protein by the aptamer; as by increasing thrombin concentration, the interfacial electron transfer resistance between the electrode surface and solution also increases, until reaching saturation. To

evaluate the linear range and detection limit of the AptThr-Thr system, the calibration curve was built, representing the analytical signal expressed as Δ_{ratio} *vs.* the protein concentration, Figure 4.1.6. As can be seen, a sigmoidal trend is obtained, where the central area could be approximated to a straight line, with a linear range from 7.5 pM to 75 pM for the protein. Moreover, a good linear relationship (r^2 = 0.9981) between the analytical signal (Δ_{ratio}) and the thrombin concentration in this range was obtained, according to the equation: $\Delta_{ratio} = 1.013 + 1.106 \cdot 10^{10}$ [Thr]. The EC_{50} was estimated as 44 pM and the detection limit, calculated as three times the standard deviation of the intercept obtained from the linear regression, was 4.5 pM. The reproducibility of the method showed a relative standard deviation (RSD) of 7.2 %, obtained from a series of 5 experiments carried out in a concentration of 75 pM Thr. These are satisfactory results for the detection of thrombin in real samples, given this level is exactly the concentration threshold when forming thrombus.

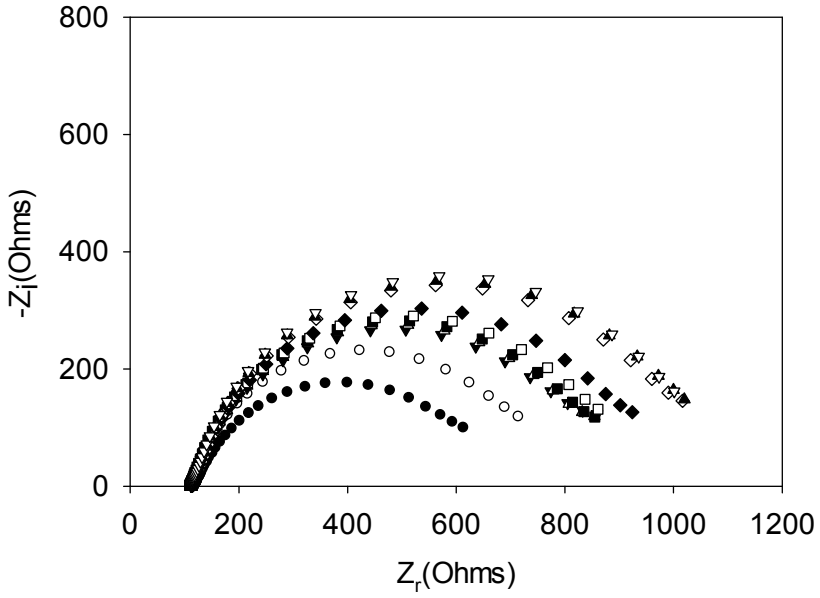

Figure 4.1.5. Nyquist diagrams for different concentrations of thrombin.● Electrode-buffer, ○ AptThr, ▼ $1 \cdot 10^{-12}$ M [Thr], Δ $2.5 \cdot 10^{-12}$ M [Thr], ■ $5.5 \cdot 10^{-12}$ M [Thr], □ $7.5 \cdot 10^{-12}$ M [Thr], ♦ $1 \cdot 10^{-11}$ M [Thr], ◇ $5 \cdot 10^{-11}$ M [Thr], ▲ $7.5 \cdot 10^{-11}$ M [Thr], ▽ $1 \cdot 10^{-10}$ M [Thr].

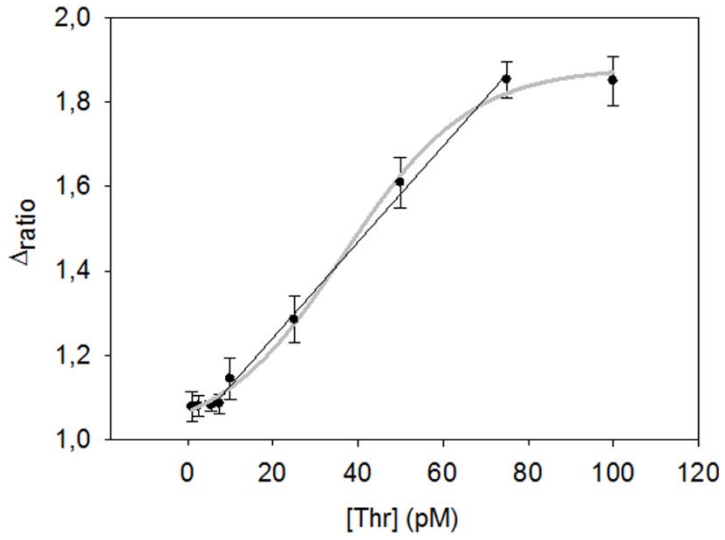

Figure 4.1.6. Calibration curve *vs.* thrombin concentration. ($\Delta_{ratio} = \Delta_s / \Delta_p$; $\Delta_s = R_{ct(\ AptThr\text{-}Thr)} - R_{ct\ (electrode\text{-}buffer)}$;$\Delta_p = R_{ct\ (AptThr)} - R_{ct(electrode\text{-}buffer)}$).

-Selectivity of Aptasensor

Thrombin is present in blood serum, a complex sample matrix, with hormones, lipids, blood cells and other proteins [23]. To study the selectivity of the system, we evaluated the response of the three proteins typically present in serum in major proportion such as Fbr, IgG and BSA. In the first case, we tested albumin protein, which is found in serum at a level from 3.500 to 5.000 mg/dL [24], representing more than 60% of the total protein present. To perform the test, the highest concentration in serum was used, that is 5.000 mg /dL. When the aptamer was incubated with this protein, electron interfacial resistance did not increase, in this case it was observed a slight decrease, see Figure 4.1.7. Afterwards, when the aptamer was incubated with thrombin, an increase in the resistance, and of expected magnitude, was observed. Therefore, it was proved that BSA was not recognized by the AptThr, and it did not interfere with aptamer-thrombin system.

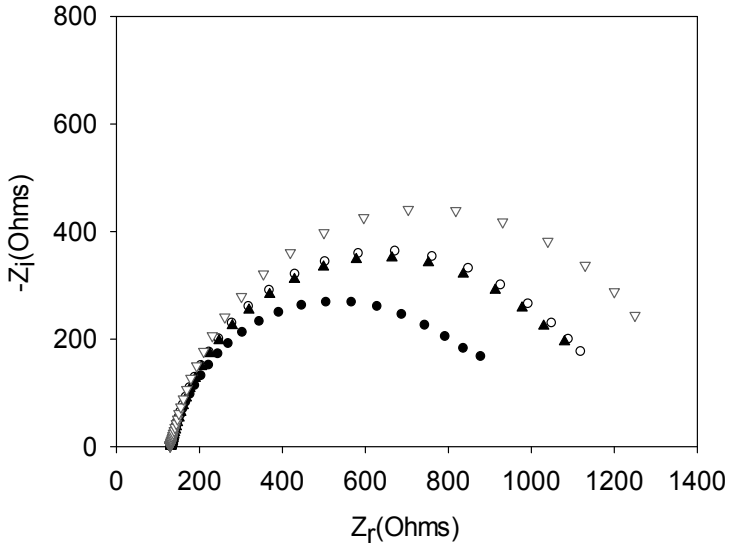

Figure 4.1.7. Nyquist Diagrams for: (●) Bare electrode, (o) AptThr, (▲) 5000 mg·dL^{-1} [BSA] and (▽) 100 pM [Thr].

In the second case, Fbr was evaluated as an interfering protein. Fbr is a fibrillar protein involved in the blood clotting process. By the action of thrombin, fibrinogen is degraded and results in the formation of a clot [25]. This protein is present in human serum in a concentration range of 200 to 400 mg/dL [26]. As can be seen in Figure 4.1.8., it was observed that the electron interfacial resistance increased as a result of some type of recognition by the AptThr. Therefore, this protein could act as an interference for the system.

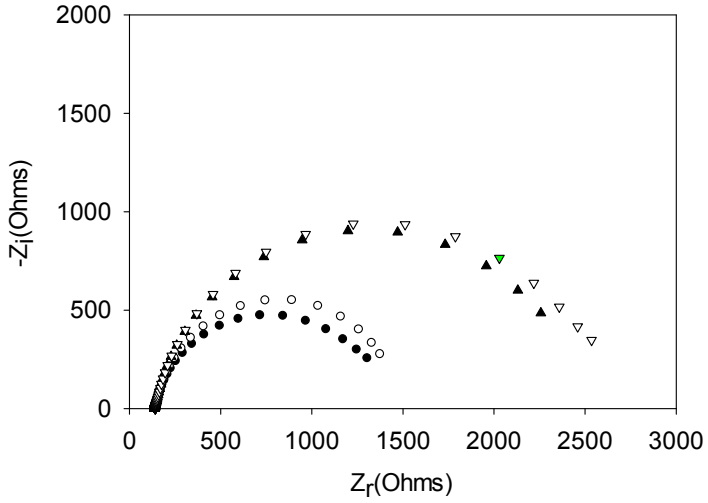

Figure 4.1.8. Nyquist Diagrams for: (●) Bare electrode, (o) AptThr, (▲) 400 mg·dL^{-1} [Fbr] and (▽) 100 pM [Thr].

In the last case, generic IgG was used. IgG is a globular protein that is synthesized in response to the invasion of any bacteria, virus or fungi. It is present in human serum over a range of concentrations from 950 mg/dL to 1.550 mg/dL in serum, with a normal value of 1.250 mg/dL. IgG also acted as interferent, which is proved from the increase of the resistance R_{ct}, as indicated Figure 4.1.9. This increase, as it also happened in the case of Fbr, may be due to some biological interaction between the aptamer and these proteins, not yet described.

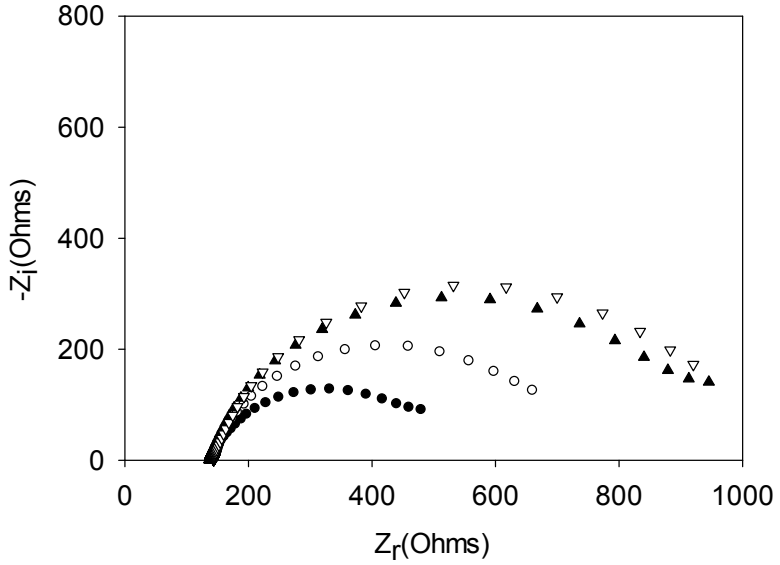

Figure 4.1.9. Nyquist Diagrams for: (●) Bare electrode, (o) AptThr, (▲) 400 mg·dL^{-1} [IgG] and (▽) 100 pM [Thr].

In the last two cases, the addition of Thr to the system increased the interfacial resistance between the electrode and the surface. This fact could be due to some phenomenon of partial displacement between thrombin and protein interferents that could take place.

-Selectivity of the aptasensor

Table 4.1.1. Summary of calibration results for thrombin and other major proteins presents in serum.

PROTEIN	REGRESSION PLOT	SENSITIVITY (M^{-1})	DETECTION LIMIT	TYPICAL CONC. IN SERUM
Thr	$\Delta_{ratio} = 1.013 + 1.106.10^{10}$ [Thr]	$1.106.10^{10}$	4.5 pM	0
Fbr	$\Delta_{ratio} = 1.007 + 3.698.10^{5}$ [Fbr]	$3.698.10^{5}$	2.0 μM	6–12 μM
IgG	$\Delta_{ratio} = 1.424 + 2.385.10^{4}$ [IgG]	$2.385.10^{4}$	10.0 μM	60–100 μM
BSA	No response	–	–	0.52–0.75 mM

To evaluate the sensitivity of the aptasensor we compared the calibration plots for the different proteins. Table 4.1.1 summarizes the parameters of the calibration curve of each protein and thrombin, as well as their respectives slopes and detection limits. The aptasensor showed the highest sensitivity for its target molecule, Thr, with its slope being 6 orders of magnitude greater than the slope for IgG and five orders of magnitude more than the one for Fbr, as shown in Figure 4.1.10. Therefore, it was demonstrated that the aptasensor showed a much higher sensitivity to Thr, regarding potential interfering proteins, which displayed this effect due to the high level of concentration in which they are present.

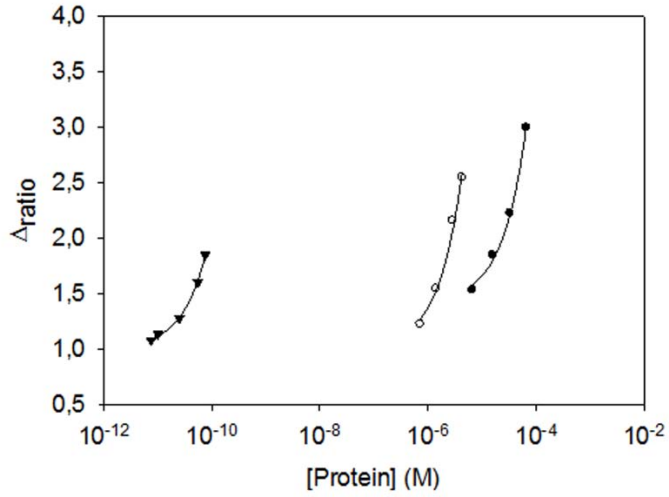

Figure 4.1.10. Response to proteins evaluated: IgG (●), Fbr (○) and Thr (▼).

-Regeneration of the aptasensor

In addition to response features, it was possible to regenerate the aptasensor by dissociating the AptThr-Thr complex, formed by weak interactions. It was achieved by stirring the aptasensor in saline media and increasing the temperature (42 °C). In this way, to show regeneration, three sensing cycles were performed with a blank measure in between each. Thr was added to the media and an increase of R_{ct} due to complex formation AptThr-Thr was recorded. Then, by adding a saline buffer, increasing the temperature and stirring, the complex dissociated and resistance decreased to the baseline value of the correspondent (AptThr), and so on. Values were calculated as Δ_{ratio} on every step of the process and represented in the bar chart as shown in Figure 4.1.11. In the third incubation with Thr, Δ_{ratio} was increased more than in the other incubations, this was because it was incubated with a higher concentration. This type of regeneration may be an alternative to the polishing surface renewal, a typical feature of graphite-epoxy composite electrodes; an important advantage is that it regenerates the electrode surface without removing the immobilized aptamer on the electrode surface, which means that their use is largely facilitated and that cost of each analysis is drastically reduced.

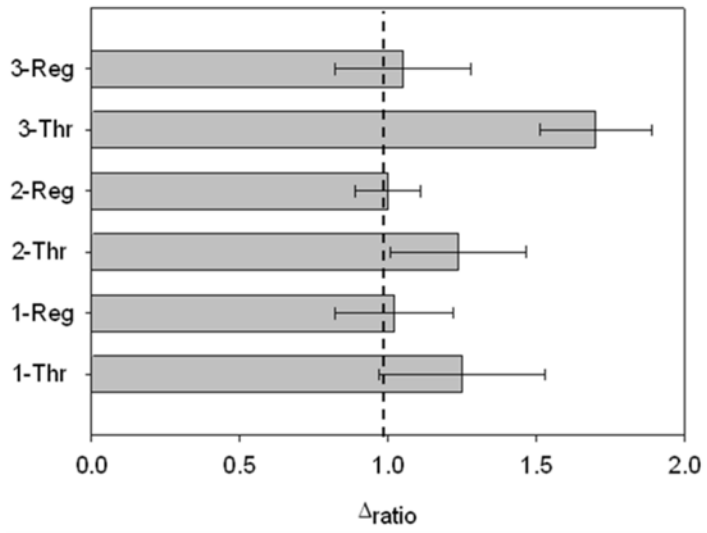

Figure 4.1.11. Signals obtained for three consecutive processes of regeneration. [Thr] used: 7.5 pM (1 and 2), and 75 pM (3). Uncertainty values corresponding to replicated experiments (n = 3).

4.1.1.2. Label-free aptasensor for thrombin detection based on avidin-biotin affinity immobilization technique

A label-free impedimetric aptasensor for thr detection was performed based on avidin-biotin affinity immobilization technique using AvGEC electrodes. The scheme of the experimental procedure is represented in Figure 4.1.12.

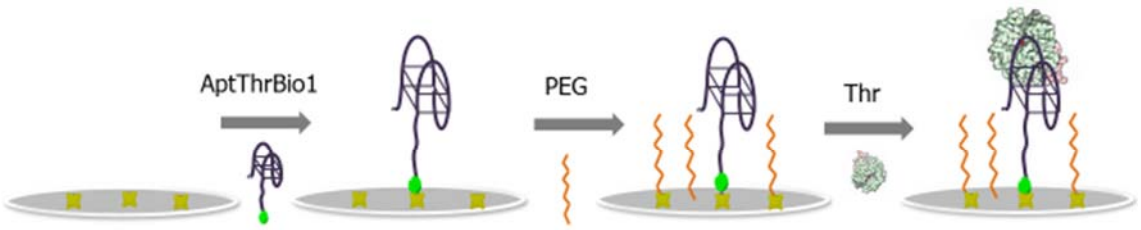

Figure 4.1.12. Scheme of the experimental protocol for the label-free aptasensor for thrombin detection based on avidin-biotin affinity method.

-Optimization of aptamer and PEG concentrations

EIS measurements with different concentrations of aptamer and PEG were carried out in order to optimize the aptamer and PEG concentration to be used in the protocol. Figure 4.1.12 shows the curve of AptThr fixation onto the electrode surface. In this graph, superposition of two behaviors can be noticed. First, the avidin-biotin interaction is detected, with almost a steady value of Δ_p 3 KΩ. After this, a monotonous increase for higher aptamer concentration can be also observed, which corresponds to simple non-specific adsorption on free surface sites. First behavior, follows Langmuir isotherm; in it, the variation of R_{ct} increases until a saturation value, chosen as the optimal concentration. This value corresponded to a concentration of aptamer of 35 pmols. To minimize any possible nonspecific adsorption onto the electrode surface, PEG was used as a blocking agent after aptamer fixation. Figure 4.1.13 shows the curve of PEG concentration on the electrode surface and, like the previous case, there is an increase in resistance until a value of 40 mM of PEG where the saturation value is reached. Therefore, the optimal concentration of blocking agent was chosen as 40 mM.

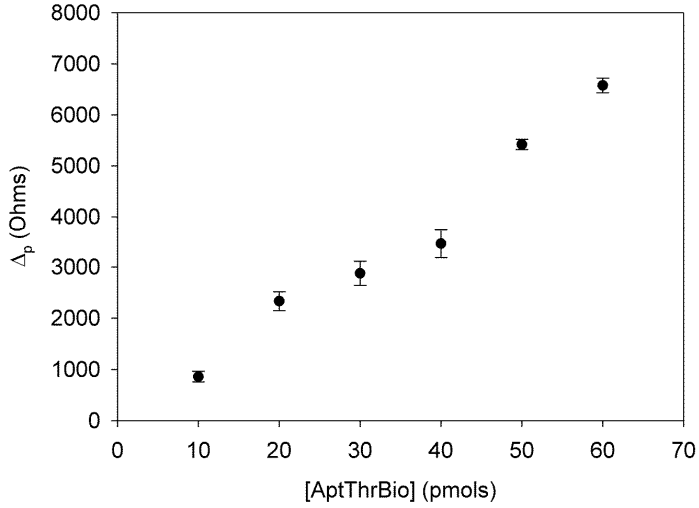

Figure 4.1.12. Optimization of the concentration of biotinylated aptamer for thrombin Apt-Thr. Uncertainty values corresponding to replicated experiments (n = 5).

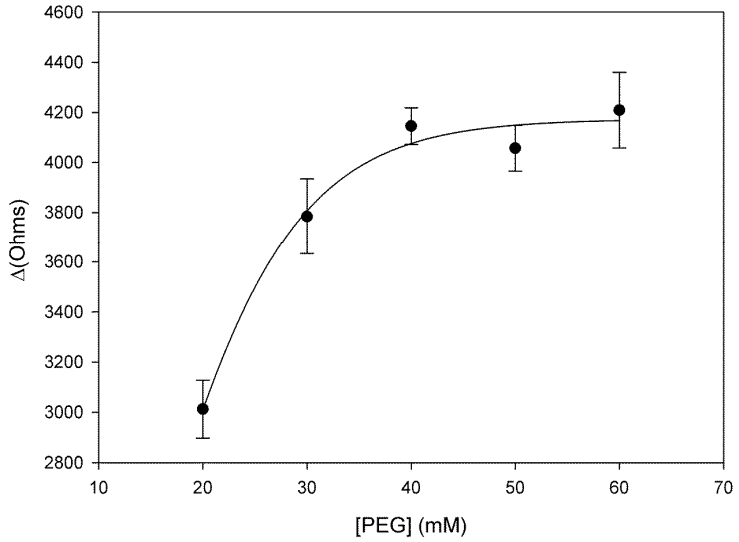

Figure 4.1.13 Optimization of the concentration of the blocking agent, PEG. Uncertainty values corresponding to replicated experiments (n = 5).

-Impedimetric response

After each step of the protocol, an EIS measurement was performed. As can be observed in Figure 4.1.14, the R_{ct} value diameter of the semicircle increased after each step. As mentioned above, this is attributable to the augmented difficulty of the redox reaction of $[Fe(CN)_6]^{3-/4-}$ to take place at electrode surface, due to the sensor surface alteration [21]. When an aptamer is immobilized on the sensor surface, an initial layer is formed and a negative charged interface is generated due to the presence of the negatively charged phosphate backbone of DNA. This fact produces a repulsion against the redox marker, also negatively charged, thus resulting in an inhibition of the electron transfer process and in an increment of the R_{ct} value. The aptamer-thrombin complex results in further increment of resistance value due to the hindrance caused by the formation of a double layer.

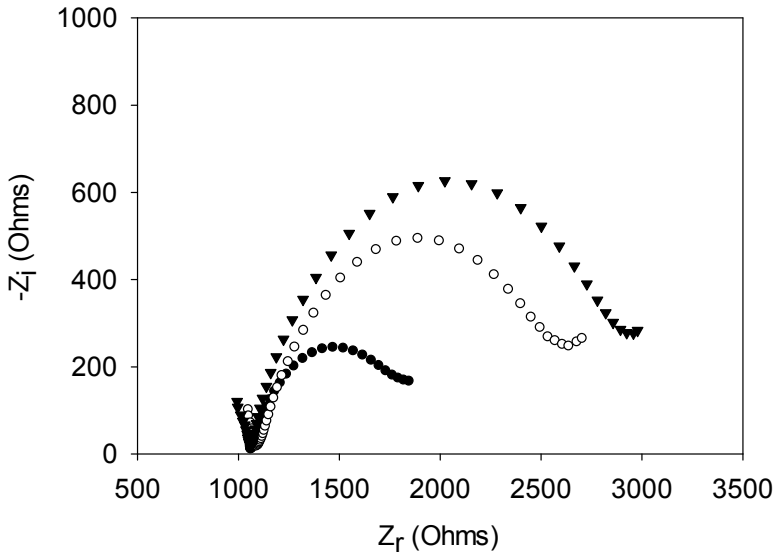

Figure 4.1.14. Nyquist Diagram of: (A) bare electrode (●), (B) AptThrBio1 (o) and (C) AptThrBio1-Thr (25 pM) (▼).

- Analytical performance of the aptasensor for detection of thrombin

The analytical performance of the aptasensor was evaluated with different concentrations of Thr. Figure 4.1.15 shows the calibration curve, representing the relative signal, Δ_{ratio}, versus the concentration of thrombin. As can be observed, a saturation curve is obtained, where the initial step could be approximated to a straight line, with a linear range from 0.75 pM to 100 pM for the protein. In addition, a good linear relationship (r^2 = 0.9921) between the analytical signal (Δ_{ratio}) and the thrombin concentration in this range was obtained, according to the equation: $\Delta_{ratio} = 1.053 + 1.530 \cdot 10^{10}$ [Thr]. The detection limit, calculated as three times the standard deviation of the intercept obtained from the linear regression, was 4.7 pM. The reproducibility of the method showed a relative standard deviation (RSD) of 4.9%, obtained from a series of 5 experiments carried out in a concentration of 75 pM Thr. These are satisfactory results for the detection of thrombin in real samples, given this level is exactly the concentration threshold for the formation of thrombus and for cancer marker.

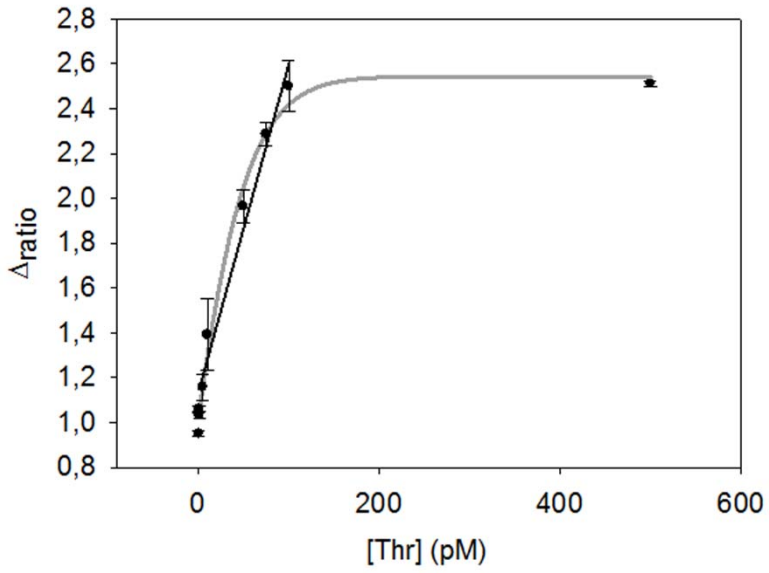

Figure 4.1.15. Calibration curve vs. thrombin concentration. ($\Delta_{ratio} = \Delta_s / \Delta_p$; $\Delta s = R_{ct(AptThrBio1-Thr)} - R_{ct\ (bare\ electrode)}$; $\Delta_p = R_{ct\ (AptThrBio1)} - R_{ct(bare\ electrode)}$).

-Selectivity of the aptasensor

Table 4.1.2. Summary of calibration results for thrombin and other major proteins presents in serum.

PROTEIN	REGRESSION PLOT	SENSITIVITY (M^{-1})	DETECTION LIMIT	TYPICAL CONC. IN SERUM
Thr	$\Delta_{ratio} = 1.053 + 1.530 \cdot 10^{10}[Thr]$	$1.530 \cdot 10^{10}$	4.7 pM	0
Fbr	$\Delta_{ratio} = 0.9857 + 1.499 \cdot 10^{4}[Fbr]$	$1.499 \cdot 10^{4}$	1.6 μM	6–12 μM
IgG	$\Delta_{ratio} = 0.6942 + 1.082 \cdot 10^{5}[IgG]$	$1.082 \cdot 10^{5}$	7.9 μM	60–100 μM
BSA	No response	–	–	0.52-0.75 μM

Concerning the selectivity of the system, the response of proteins typically present in serum such as Fbr, IgG and BSA we evaluated. As indicated on Table 4.1.2, the aptasensor exhibited the highest sensitivity for its target molecule, Thr, with its slope being five orders of magnitude greater than the slope for IgG and six orders of magnitude larger than the one for Fbr. Accordingly, it was confirmed

that the aptasensor showed a much higher sensitivity to Thr than the potential interfering proteins, which they may be present in serum in a higher concentration.

4.1.1.3. Label-free aptasensor for thrombin detection based on covalent bond immobilization technique via electrochemical activation of the electrode surface.

A schematic of the sensing principle is shown in Figure 4.1.16. In the development of this aptasensor an electrochemical activation of the surface was required in order to create carboxyl groups onto the electrode surface. Aminated thrombin aptamers were then immobilized onto the electrode surface through amide bond via carbodiimide reaction. Afterwards, a blocking step with PEG was carried out following by an incubation with the target protein.

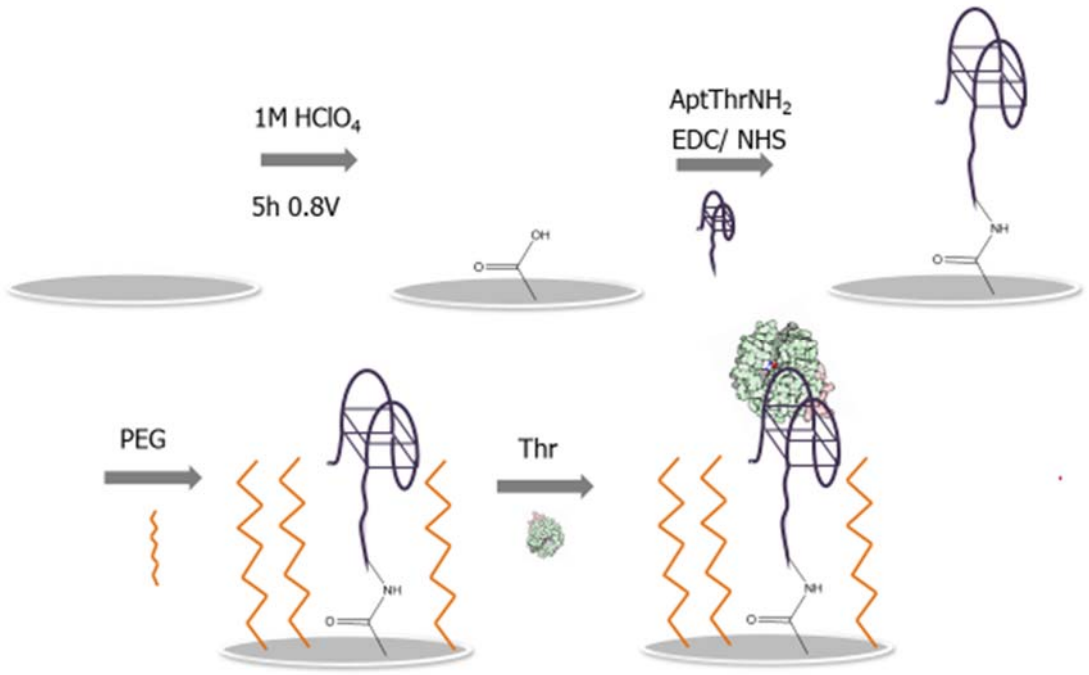

Figure 4.1.16. Scheme of experimental procedure for the label-free aptasensor for thrombin detection based on covalent bond immobilization technique via electrochemical activation of the electrode surface.

-Electrochemical activation of the electrode surface

This method consisted of the application of a potencial of +0.8 V to the carbon electrode surface for a duration of 5 hours in perchloric acid 1 M [44]. After that, the surface-confined carboxyl group were activated with EDC/NHS to link amino groups of the functionalized aptamers through the carbodiimide reaction [16], see Figure 4.1.17. Prior to selection of these conditions, other acidic media and electrolysis potentials and times were examinated, taking these as the best ones.

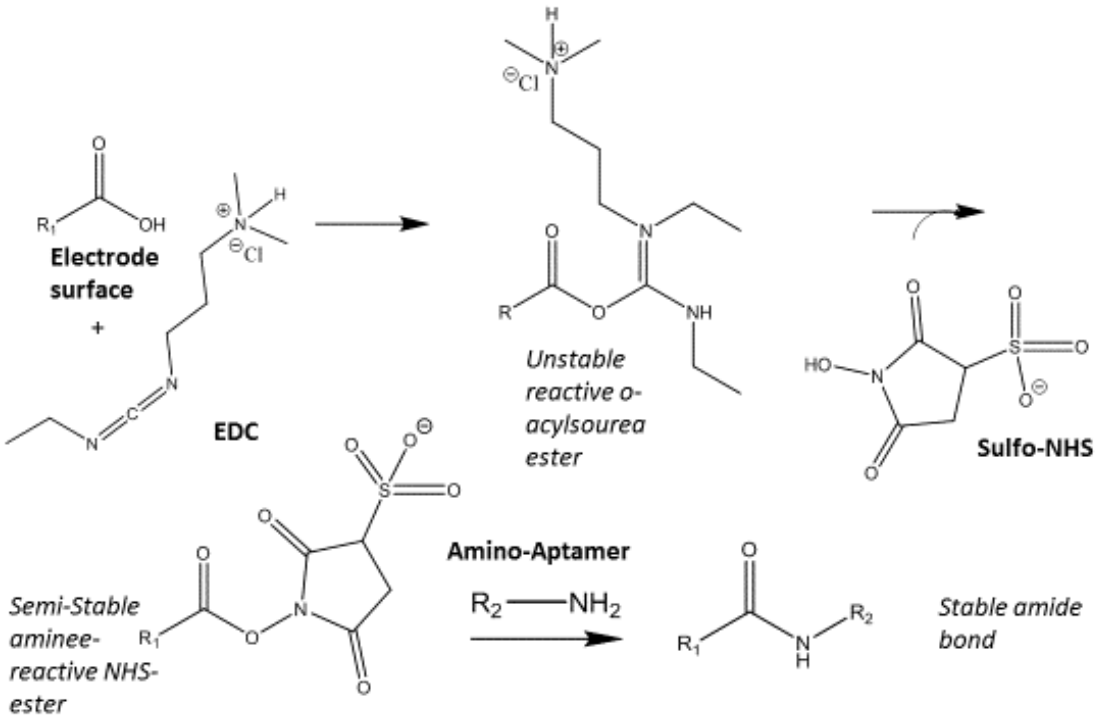

Figure 4.1.17. Mechanism of reaction between EDC-NHS and aminated aptamer.

As shown in the Figure, EDC reacts with a carboxylic group on the activated electrode surface, forming an amine-reactive o-acylsourea ester intermediate. This intermidate is unstable and has a short-lived in aqueous solution due to the fact that is susceptible of hydrolysis. The formation of an amine-reactive sulfo-NHS ester addition of NHS ester by addition of sulfo-NHS,

stabilize the intermediate and increase the yield of the amide reaction between the electrode surface and the aptamer.

-Optimization of aptamer and PEG concentrations

Once the electrodes surface were activated with carboxyl groups, aptamer and PEG concentrations were optimized separately by building its response curves. Figure 4.1.18 and 4.1.19 show the calibration curves of aptThrNH$_2$ and PEG respectively.

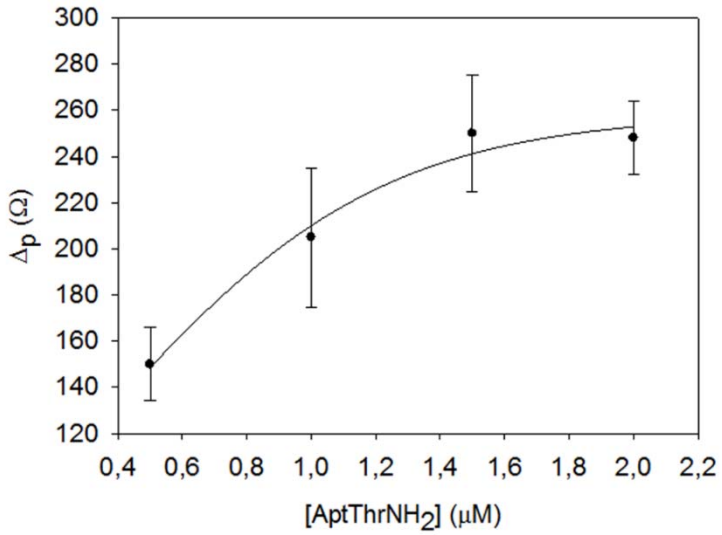

Figure 4.1.18. Optimization of the concentration of ApThrNH$_2$. Uncertainty values corresponding to replicated experiments (n=5).

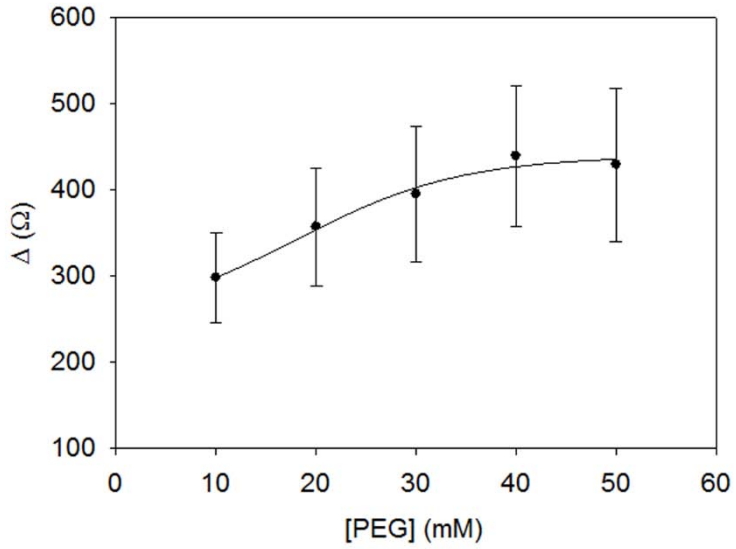

Figure 4.1.19. Optimization of the concentration of PEG. Uncertainty values corresponding to replicated experiments (n=5).

As in the previous procedures, the variation of R_{ct} in both cases increases until a saturation value, and these values were chosen as the optimal concentrations of $AptThrNH_2$ and PEG, 1.5 μM and 40 mM respectively.

-Impedimetric response

Impedance measurements were carried out after each step of the protocol. As indicated Figure 4.1.20, after the electrodes were funcionalized thorough electrochemical activation treatment, the R_{ct} decreased due to the formation of carboxyl groups on the electrode surface became very electroactive and did not repulsive interaction (electrostatic and steric) existed between the redox marker ions and the electrode surface. However, when $AptThrNH_2$ were immobilized, the R_{ct} increased due to electrostatic repulsion between the redox maker and the negatively charged phosphate groups of DNA skeleton, thus inhibiting the interfacial electron transfer process. Finally, after incubating with thrombin, the R_{ct} increased due to the hindrance caused by the formation of a double layer.

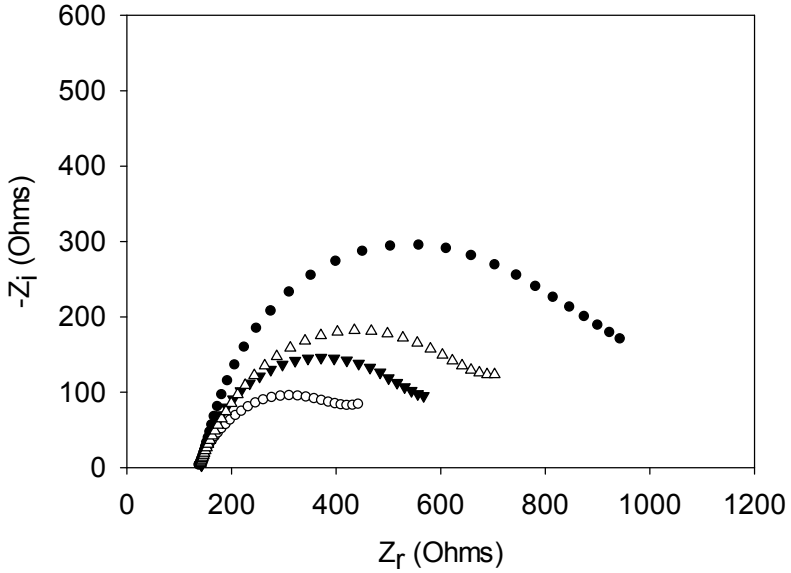

Figure 4.1.20. Nyquist Diagram of: (A) bare electrode (●), (B) electrochemical activation (o), (C) AptThrNH$_2$ (▼) and (D) AptThrNH$_2$ –Thr (75 pM)(Δ).

- Analytical performance of the aptasensor for detection of thrombin

Under the optimal experimental conditions, the EIS response for the detection of Thr with different concentrations were obtained. The calibration curve was shown in Figure 4.1.21, with concentrations of Thr ranging from 1 pM to 250 pM, the Δ_{ratio} exhibited a good linear relationship with the protein concentration between 1 pM to 100 pM. The equation of linear regression was $\Delta_{ratio} = 1.512 + 1.206 \cdot 10^{10}$ [Thr] with a limit of detection of 10.5 pM, calculated as three times the standard deviation of the intercept obtained from the linear regression. Moreover, a good reproducibility was obtained, 8.3 %, from a series of 5 experiments carried out in a concentration of 75 pM Thr. These results clearly indicated that the aptasensor could be used for Thr detection in serum samples.

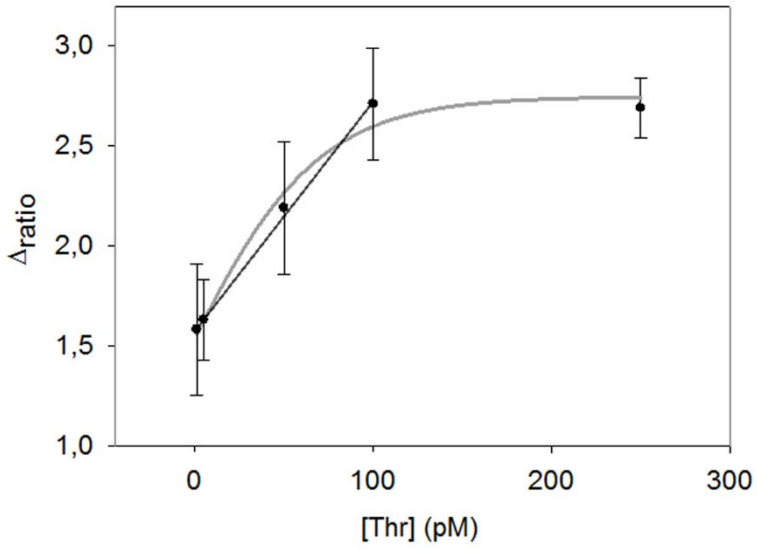

Figure 4.1.21. Calibration curve vs. thrombin concentration ($\Delta_{ratio} = \Delta_s / \Delta_p$; $\Delta s = R_{ct(AptThrBio1\text{-}Thr)} - R_{ct\ (bare\ electrode)}$; $\Delta_p = R_{ct\ (AptThrBio1)} - R_{ct(bare\ electrode)}$).

-Selectivity of the aptasensor

Table 4.1.3. Summary of calibration results for thrombin and other major proteins presents in serum.

PROTEIN	REGRESSION PLOT	SENSITIVITY (M^{-1})	DETECTION LIMIT	TYPICAL CONC. IN SERUM
Thr	$\Delta_{ratio} = 1.512 + 1.206 \cdot 10^{10}$ [Thr]	$1.206 \cdot 10^{10}$	10.5 pM	0
Fbr	$\Delta_{ratio} = 3.719 + 3.022 \cdot 10^{5}$ [Fbr]	$3.022 \cdot 10^{5}$	79.4 nM	6–12 μM
IgG	$\Delta_{ratio} = 1.559 + 1.132 \cdot 10^{4}$ [IgG]	$1.132 \cdot 10^{4}$	21.2 μM	60–100 μM
BSA	No response	–	–	0.52-0.75μM

The selectivity of the aptasensor was investigated by comparison of the sensing results of BSA, Fbr and IgG at serum concentration. As can be seen in Table 4.1.3, the aptasensor showed the highest sensitivity for its target molecule,

Thr, with its slope being six orders of magnitude greater than the slope for IgG and five orders of magnitude larger than the one for Fbr. Therefore, the above results confirmed that the aptasensor showed a much higher sensitivity to Thr than the potential interfering proteins, even though they are presents in serum with higher concentrations than thrombin. In addition, as in the previous aptasensors based on different immobilization techniques, BSA did not interfere with aptamer-thrombin system.

4.1.1.4. Label-free aptasensor for thrombin detection based on covalent bond immobilization technique via electrochemical grafting of the electrode surface

A label-free aptasensor for Thr detection based on aptamer immobilization via covalent bond through electrochemical grafting was performed. This technique is a simple way to produce stable carboxyl-derivatized conductive surfaces for the subsequent immobilization of aptamers (in this case). This was achieved through the use of 4-aminobenzoic acid and sodium nitrite to form a diazonium salt, which was immobilized on the electrode surface by its electrochemical reduction. Then, aminated thrombin aptamers were immobilized onto the electrode surface through amide bond via carbodiimide reaction, which was explained previously in Section 4.1.1.3. After that, a blocking step to avoid non-specific adsorption and an incubation step with thrombin protein were performed respectively, as indicated Figure 4.1.22.

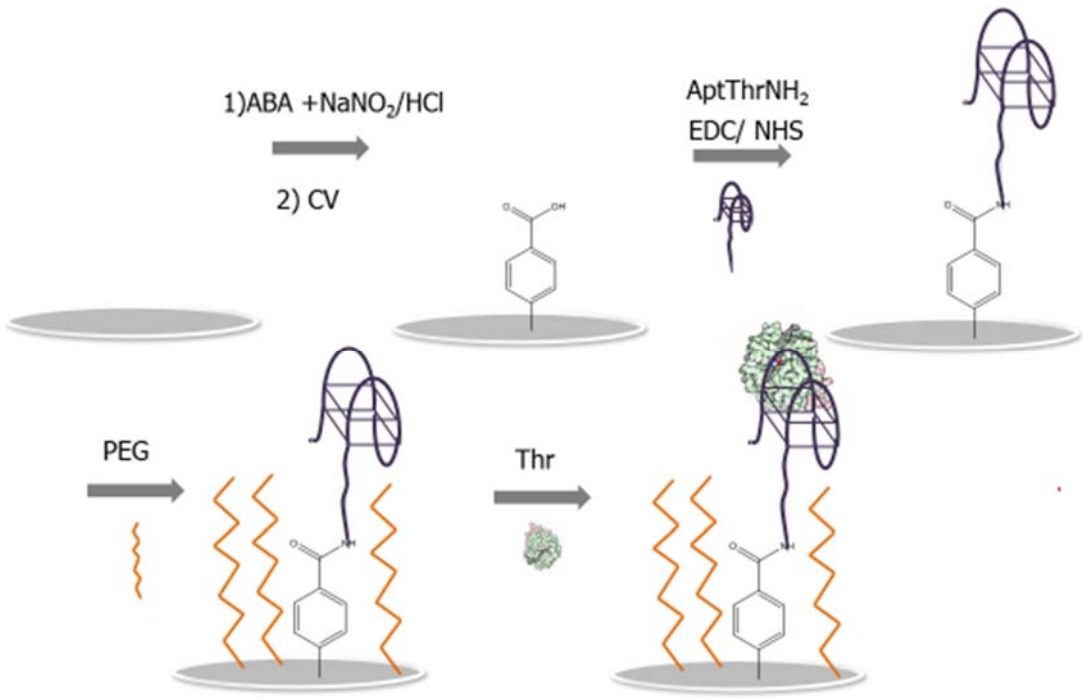

Figure 4.1.22. Scheme of the experimental protocol for the label-free aptasensor for thrombin detection based on covalent bond immobilization technique via electrochemical grafting.

-Optimization of the electrochemical grafting cycles

The optimum cycles of the electrochemical grafting method was determined in order to create a uniform layer of carboxyl-derivatized onto the electrode surface by observing changes in R_{ct} before and after the modification of the surface, Δ. As can be seen in Figure 4.1.23, Δ increased with the number of cycles until to reach a saturation value, thus the optimum cycles of the method was choosen as a 200 cycles.

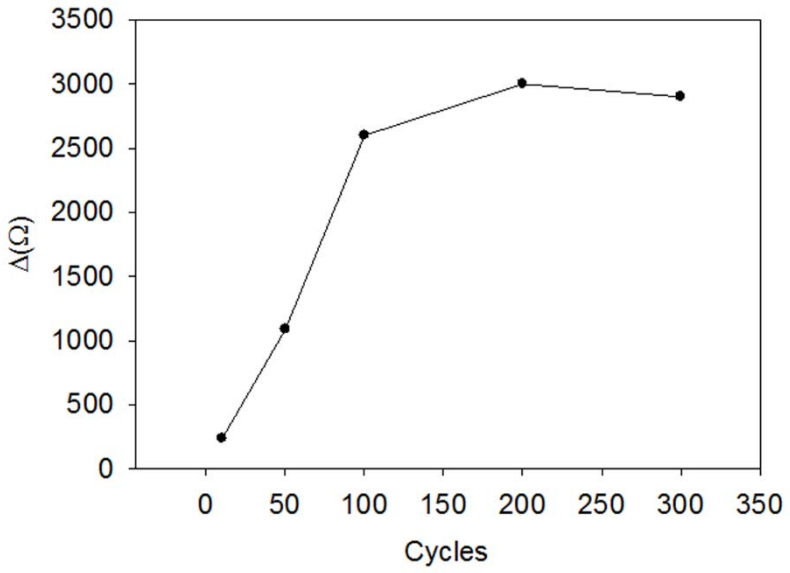

Figure 4.1.23. Optimization of the number of cycles for electrochemical grafting method.

-*Optimization of Aptamer and PEG concentrations*

To obtain an optimal impedance response of the aptasensor, the experimental concentrations of aptamer and PEG were optimized. As shown in Figure 4.1.24 and 4.1.25, both aptamer and PEG concentrations were obtained through its corresponding calibration curve. The optimal concentration values were chosen as 1.5 μM and 40 mM respectively, where the saturation values are reached.

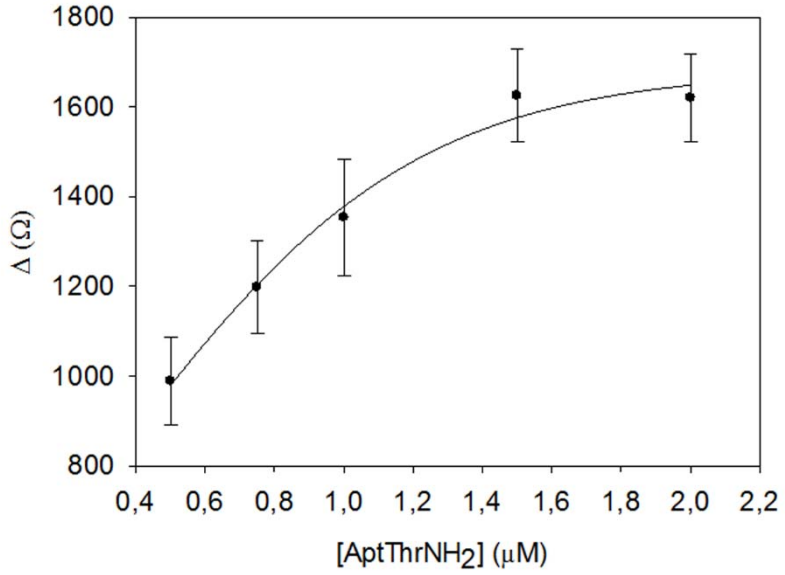

Figure 4.1.24. Optimization of the concentration of $ApThrNH_2$. Uncertainty values corresponding to replicated experiments (n=5).

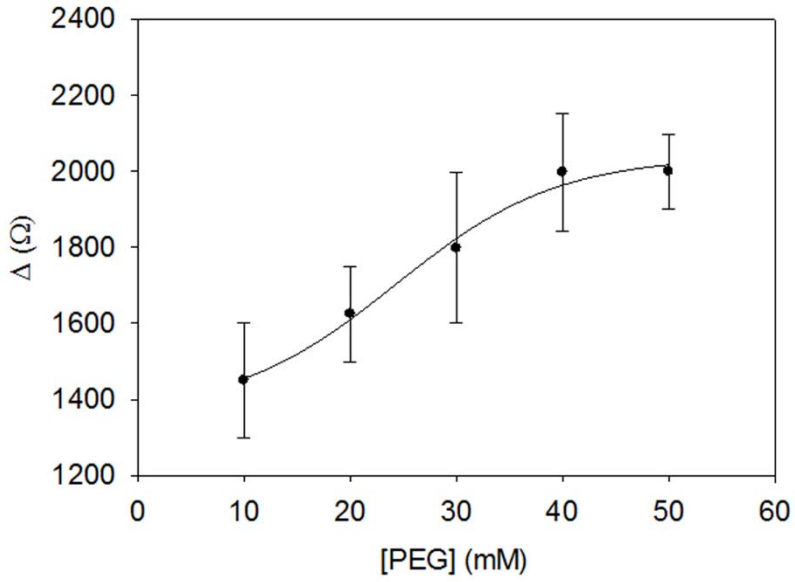

Figure 4.1.25. Optimization of the concentration of PEG. Uncertainty values corresponding to replicated experiments (n=5).

-Impedimetric response

The modification steps of the experimental procedure could be followed through EIS, as can be seen in Figure 4.1.26. After electrode surface modification via electrochemical grafting, the transfer-electron resistance showed a high increase due to the formation of anchor points on the electrode surface; then its decrease was observed due to the immobilization of AptThrNH$_2$ on the surface through the carbodiimide reaction, as a result of the decrease negative density of charge of the electrode surface. When the electrode was incubated with the target protein, a big increase in R_{ct} was noticed due to hindrance caused by the formation of a double layer.

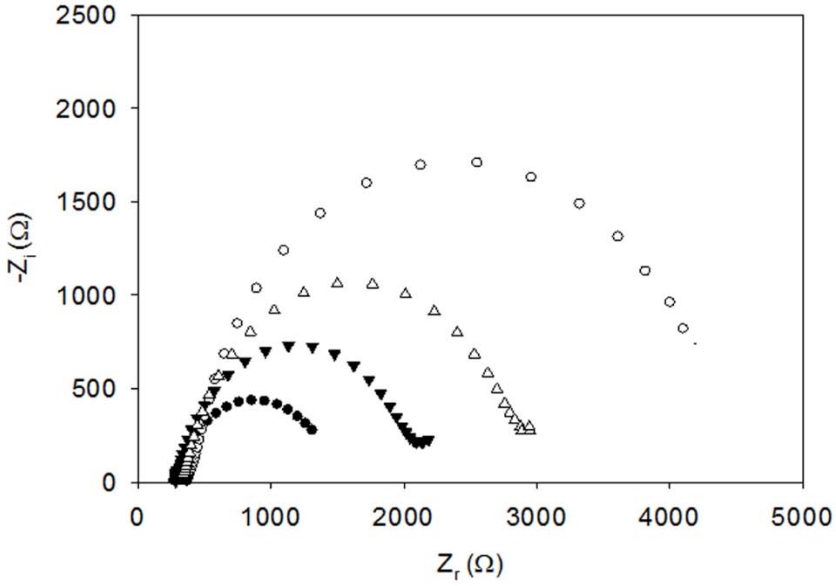

Figure 4.1.26. Nyquist Diagram of: (A) bare electrode (●), (B) electrochemical grafting (o), (C) AptThrNH$_2$ (▼) and (D) AptThrNH$_2$ –Thr (75pM) (Δ).

- Analytical performance of the aptasensor for detection of thrombin

The quantitative behavior of the fabricated aptasensor for thrombin was assessed by measuring the dependence of the Δ_{ratio} upon the concentration of thrombin under the optimized experimental conditions. Figure 4.1.25 shows the responses of the aptasensor against different concentrations of thrombin. It is obvious that the R_{ct} increases with an increase of the concentration of thrombin. The Δ_{ratio} was linear with the concentration of thrombin over the range of 0.2 to 100 pM. The regression equation was $\Delta_{ratio} = 1.007 + 8.756 \cdot 10^{9}$ [Thr] with a correlation coefficient of 0.994. Moreover, the detection limit for thrombin was estimated to be 7.3 pM and the relative standard derivation (R.S.D.) of five replicate determination of thrombin at 10 pM was 7.2%; suggesting excellent reproducibility of the proposed aptasensor.

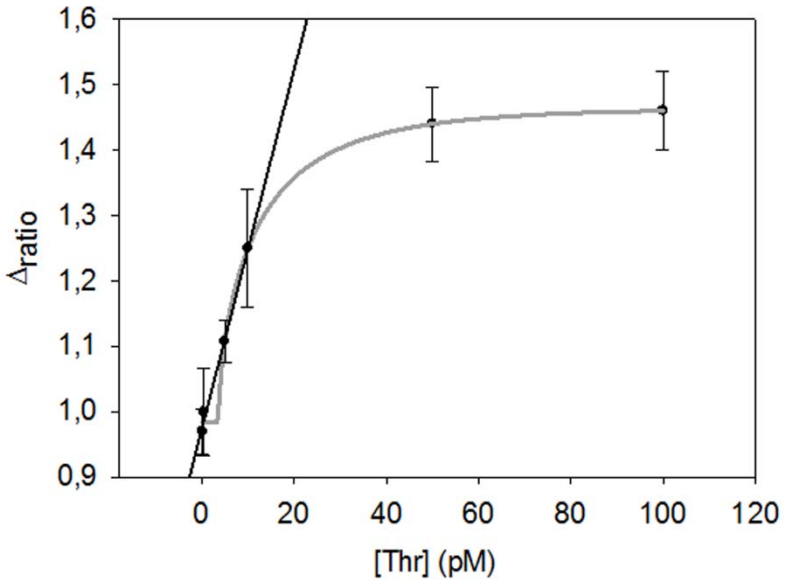

Figure 4.1.27. Calibration curve vs. thrombin concentration.

-Selectivity of the aptasensor

Table 4.1.4. Summary of calibration results for thrombin and other major proteins presents in serum.

PROTEIN	REGRESSION PLOT	SENSITIVITY (M^{-1})	DETECTION LIMIT	TYPICAL CONC. IN SERUM
Thr	Δ_{ratio} = 1.007 + $8.756 \cdot 10^9$ [Thr]	$8.756 \cdot 10^9$	7.3 pM	0
Fbr	Δ_{ratio} =-1.464 +$8.103 \cdot 10^5$ [Fbr]	$8.103 \cdot 10^5$	0.1 μM	6–12 μM
IgG	Δ_{ratio} =0.965 + $1.605 \cdot 10^4$ [IgG]	$1.605 \cdot 10^4$	14.9 μM	60–100 μM
BSA	No response	–	–	0.52-0.75 μM

In order to evaluate the specificity of the present detection system, the influence of other common proteins was also investigated. The results in Table 4.1.4 shows that the aptasensor exhibited the highest sensitivity for Thr, with its slope being four and five orders of magnitude greater than the slope for Fbr and IgG, respectively. In addition, no response was obtained when the aptasensors was evaluated with BSA. Consequently, these results are in agreement with the others thrombin aptasensors based on different immobilization techniques.

4.1.1.5. Comparison of four different immobilization techniques for thrombin detection

The goal of this part of the thesis was to study and compare the four different immobilization technique employed above, using GEC and AvGEC electrodes.

-Studies of electrodes reproducibilities

The reproducibility of polishing and of electrode construction was investigated by EIS. For both studies the impedimetric spectra of a bare electrode was recorded in PBS1 solution containing 0.01 M $K_3[Fe(CN)_6]/K_4[Fe(CN)_6]$.

The reproducibility of polishing was studied considering that the polishing procedure employed for the electrode surface renovation could influence the impedimetric measures. Moreover, the reproducibility of electrodes construction was also evaluated in order to verify the influence of the different handmade electrode on the impedimetric response.

In order to calculate the relative standard desviation (% RSD) of the results, the values of charge transfer resistance due to the reaction of the redox marker were used. Values of % RSD are shown in Table 4.1.5.

Table 4.1.5 Results obtained in studies of reproducibility using five different electrodes.

ELECTRODE	**%RSD** $_{\text{POLISHING}}$	**%RSD** $_{\text{CONSTRUCTION}}$
GECs	3.9	7.3
AvGECs	5.2	8.3

As indicated in the table, the % RSD due to the polishing procedure resulted less than the one attributable to the electrode construction. This could be due to the fact that the influence of surface renovation by polishing is less than the one due to the electrode construction. In the electrode construction several uncontrolled factors affect to the impedimetric results due to the fact that they are handmade.

In addition, GECs electrodes showed more reproducibility than AvGECs in both reproducibility values. This could mean that when avidin molecules are

incorporated into the composite paste, their distribution influence the reproducibility of the impedimetric results both for polishing and construction.

-Electrodes surface area characterization

After reproducibility studies, the effective surface area of GEC and AvGEC electrodes were evaluated. For that CV experiments using a known procedure in 5 mM $[Fe(CN)_6]^{3-}/[Fe(CN)_6]^{4-}$ solution in the potential range of -1.5 to 1.5 V were performed [37]. The reduction peak current (i_p) was determined by the Randles-Sevcik equation [4], following the procedure described [37].

$$i_p = (2.69 \cdot 10^5)\, n^{3/2}\, D^{1/2}\, C\, A\, \upsilon^{1/2} \qquad (4.1.1)$$

where n is the number of transferred electrons for the redox reaction (in this case 1), D is the difussion coefficient for ferrocyanide ($6.32 \cdot 10^{-6}$ cm^2 s^{-1}), C is its molar concentration, A is the effective surface area (cm^2), and υ is the scan rate (V s^{-1}).

From equation (4.1.1), a linear relationship exists between i_p and $\upsilon^{1/2}$, see Figure 4.1.28. By performing linear regression of i_p versus $\upsilon^{1/2}$, the slope k can be obtained, and one may express A as:

$$A = k / ((2.69 \cdot 10^5)\, n^{3/2}\, D^{1/2}\, C) \qquad (4.1.2)$$

A series of scan rates (υ = 0.02, 0.1, 0.2, 0.25, 0.35, 0.5 V^{s-1}) was then used and the corresponding i_p recorded, see Figure 4.1.29. Once k could be determined, A was calculated in straightforward manner.

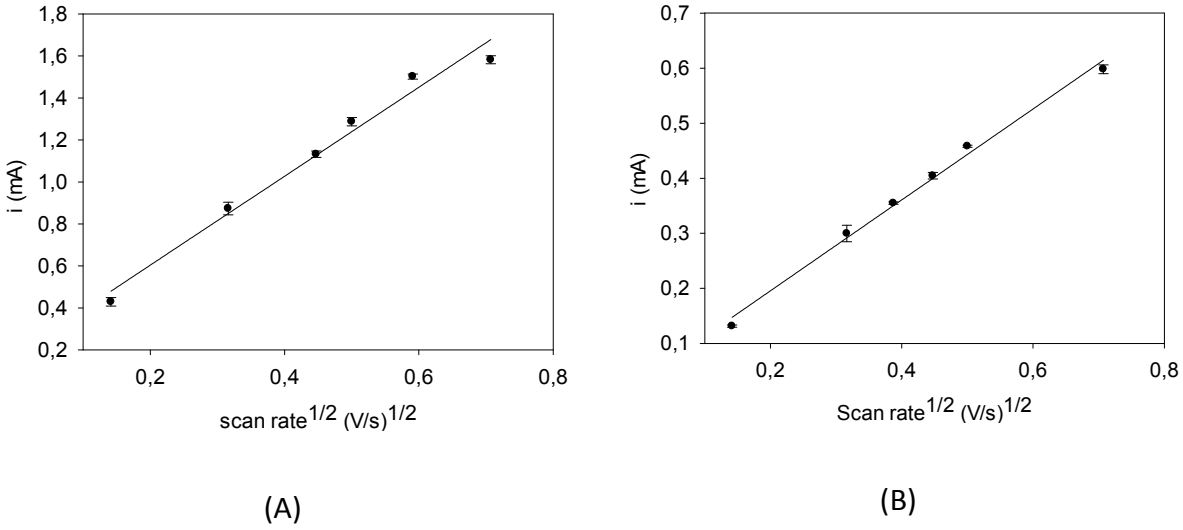

(A) (B)

Figure 4.1.28. Linear regression between the peak current (i_p) and the square root of the scan rate ($\upsilon^{1/2}$) for: (A) Av-GEC electrode and (B) GEC electrode .

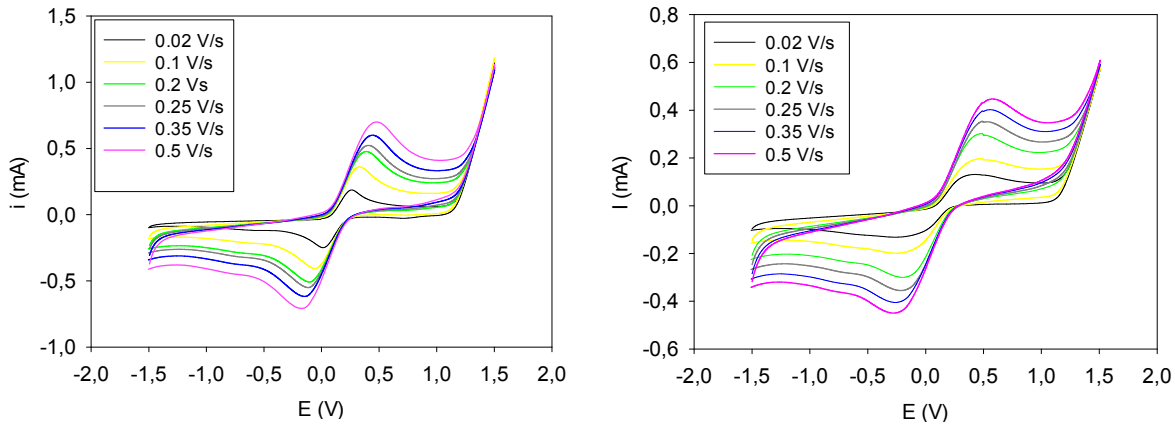

(A) (B)

Figure 4.1.29. Representative cyclic voltammograms in ferricyanide for a bare of: (A) AvGEC electrode and (B) GEC electrode at various scan rates (V/s).

The surface areas from GEC and AvGEC electrodes were 0.570 ± 0.08 cm^2 and 0.197 ± 0.05 cm^2 respectively, while they geometric area were 0.28 cm^2. The avidin protein present in the composite decreased the effective area due to the protein insulating nature, thus decreasing the effective surface area available for signal transduction. This observation is also in agreement with impedance characterization of bare electrodes, just the epoxy-graphite composite vs. those

modified with avidin, whereas the latter present increased impedance, in the form of larger R_{ct}.

-Surface coverage of aptamers onto the electrode surface

Another feature important to evaluate is the surface coverage of aptamers onto the electrode surfaces using different aptamer immobilization techniques. Thus, surface coverage values of each type of technique were obtained by a known CV method using a solution of $[Ru(NH_3)_6]^{3+}$ [15]. This complex binds to the phosphate backbone of aptamers through electrostatic interaction. Therefore, the redox charge of $[Ru(NH_3)_6]^{3+}$ is taken as the amounts of aptamers localized on electrode surface. The integration of the cathodic peak of the first scan at 0.5 V/s in $[Ru(NH_3)_6]^{3+}$gives the surface concentration of $[Ru(NH_3)_6]^{3+}$ (Γ_{Ru}) on aptamer-modified electrodes according to the equation:

$$\Gamma_{Ru} = \frac{Q}{nFA} \tag{4.1.3}$$

where n is the number of electrons in the redox reaction, F the Faraday constant (C/mol), and A the area (cm^2) of the working electrode.

The surface coverage of aptamers were calculated from Γ_{Ru} by using the following equation:

$$\Gamma_{aptamer} = \Gamma_{Ru} \frac{z}{m} N_a \tag{4.1.4}$$

where m is the number of nucleotides (phosphates) in the aptamer strand, N_a Avogadro's number and z the charge of the redox molecules.

Table 4.1.6. Aptamer surface density values of the different immobilization techniques used (Uncertainly values corresponds to triplicate experiments).

	$\Gamma(10^{12}$ Molecules/cm$^2)^*$		
ELECTRODE	**Bare electrode**	**AptThr**	**PEG**
GEC/physical adsorption	0.39 ± 0.23	3.25 ± 0.36	3.31 ± 0.32
AvGEC/avidin-biotin affinity	0.12 ± 0.01	6.46 ± 0.22	3.14 ± 0.51
GEC/Electrochemical Activation	0.32 ± 0.20	3.06 ± 0.31	8.60 ± 0.10
GEC/ Electrochemical Grafting	0.16 ± 0.01	7.62 ± 0.27	4.53 ± 0.33

$^*(\bar{x} \pm \frac{s \cdot t}{\sqrt{n}})$

The obtained results are shown in Table 4.1.6. As can be seen, electrochemical grafting technique provided a high value of surface coverage of aptamers when the aptamers were immobilizated onto the electrode surface via covalent bond. However, when the aptamer-modified electrodes were incubated with PEG, a decrease of the surface coverage was obtained. Thus, it could be due to the fact that PEG could replace some molecules of aptamer onto the electrode surface during the blocking step of the protocol. This decrease it also happened in the case of avidin-biotin affinity. Whilst in the cases of physical adsorption and electrochemical activation methods an increase of the surface coverage of aptamer values were achieved after incubating with PEG. This other phenomenon could be produced due to aptamers are not properly oriented and $[Ru(NH_3)_6]^{3+}$ could not easily interact with them. However, after incubating with PEG, $[Ru(NH_3)_6]^{3+}$ could interact with aptamer, and therefore a better distribution and/or conformation of aptamers can be deduced.

- Analytical performance of the different aptasensors for detection of thrombin

Table 4.1.7. Calibration curves results obtained with different AptThr immobilizations. % RSD values correspond to five replicate experiments at 75 pM thrombin concentration.

IMMOBILIZATION	SENSITIVITY (M^{-1})	REPRODUCIBILITY (RSD %)	LINEAR RANGE (pM)	LOD (pM)	CORRELATION COEFICIENT (r)
PHYSICAL ADSORPTION	$1.106 \cdot 10^{10}$	7.2	7.5-75	4.5	0.998
Av-Bio AFFINITY	$1.530 \cdot 10^{10}$	4.9	0.75-100	4.7	0.999
ELECTROCHEMICAL ACTIVATION	$1.206 \cdot 10^{10}$	8.3	2.5-100	10.5	0.996
ELECTROCHEMICAL GRAFTING	$8.756 \cdot 10^{9}$	7.2	0.2-10	7.3	0.994

All analytical results of each type of immobilization technique were compared. As we can see in Table 4.1.7, the highest sensitivity was attained using affinity immobilization due to the strong affinity of avidin with biotinylated AptThrBio1, therefore this method presents more efficiency on the biorecognition, rather than the covalent immobilization methods. Apart, its performance might be fine-tuned, if the amount of avidin on the AvGECs is optimized for each specific application. Moreover, the best reproducibility was achieved using the avidin modified biocomposite platform, this could be due to the surface presenting less heterogeneity among different electrodes compared to covalent bonding techniques. The response with highest linearity was obtained using the electrochemical grafting method, what suggests a proper interaction of the bonded aptamer but the broadest linear range corresponds to the affinity technique. Finally, the best detection limit corresponds to physical adsorption followed by affinity method. As inconvenient, it must be cited the added cost of the protein needed for the affinity method.

In order to judge the interest of the comparison done, the four immobilization protocols were compared with other label-free biosensors using aptamers for Thr detection. The label-free techniques considered were differential pulse voltammetry, potentiometry, and EIS.

Table 4.1.8. Comparison of the proposed Thr aptasensor with other recent reported label-free aptasensors in the literature.

TRANSDUCTION TECHNIQUE	PLATFORM	LOD	INTERFERENTS TESTED	RSD%	REF
DIFFERENTIAL PULSE VOTAMMETRY	Gold	10 nM	BSA, α-fetoprotein, carcinoembryonic antigen	-	[46]
DIFFERENTIAL PULSE VOLTAMMETRY	Gold	3 nM	Human serum	3	[45]
POTENTIOMETRY	FET	6.7 nM			[17]
EIS	Gold	80 pM	BSA	10	[28]
EIS	Gold recordable compact discs	5 nM	Human serum	1	[10]
EIS	MWCNT	105 pM	Human serum	7.5	[20]
EIS	Platinum/ poly(pyrrole-NTA)/Cu^{2+}	4.4 pM	BSA, lysozime, Immunoglobulin G	7.3	[43]
EIS	GEC/P.Adsoption AvGEC GEC/E.Activation GEC/E.Grafting	4.5 pM 4.7 pM 10.5 pM 7.3 pM	Fibrinogen, Immunoglobulin G, BSA	7.2 4.9 8.3 7.2	This work
EIS	Chemically modified graphene	10nM	Immunoglobulin G, BSA, Avidin	-	[26]

The details are shown in Table 4.1.8, where sensitivity info is presented as the LOD of each biosensor compared. Our proposed aptasensor is on the first range of lowest LOD and % RSD value, especially the avidin-biotin affinity method. These data demonstrate that our graphite-epoxy composite electrodes can be sensing platforms of choice for the development of aptasensors, in this case, for detecting Thr.

-Cross- Reactivity

Majoritary proteins in serum (BSA, Fbr and IgG) which may be present with Thr [36], were tested as potential interfering substances for the different aptasensors towards Thr compared in the study.

Table 4.1.9. Comparison among sensitivity values for interfering proteins in serum, obtained with different protocols for AptThr immobilization (Each sensitivity value obtain for calibration, of the single protein, n=4 in the linear range).

IMMOBILIZATION	**Thr SENSITIVITY (M^{-1})**	**Fbr SENSITIVITY (M^{-1})**	**IgG SENSITIVITY (M^{-1})**	**BSA SENSITIVITY (M^{-1})**
PHYSICAL ADSORTION	$1.10 \cdot 10^{10}$	$3.69 \cdot 10^{5}$	$2.38 \cdot 10^{4}$	--
Av-Bio AFFINITY	$1.53 \cdot 10^{10}$	$1.49 \cdot 10^{4}$	$1.08 \cdot 10^{5}$	--
ELECTROCHEMICAL ACTIVATION	$1.20 \cdot 10^{10}$	$3.02 \cdot 10^{5}$	$1.13 \cdot 10^{4}$	--
ELECTROCHEMICAL GRAFTING	$8.75 \cdot 10^{9}$	$8.10 \cdot 10^{5}$	$1.60 \cdot 10^{4}$	--

To evaluate the sensitivity of the aptasensor we compared the calibration plots for the different proteins, pure solution of single protein, by the different kinds of immobilization. Table 4.1.9, summarizes the parameters for each protein. The first thing one can see is that all types of immobilization showed the highest sensitivity for its target molecule, Thr, with its slope of response being five to six orders of magnitude greater than the slope for igG and also for Fbr.

Table 4.1.10. Comparison among EC_{50} values and % Cross-Response for interfering proteins in serum, obtained with different protocols for AptThr immobilization

IMMOBILIZATION	**EC_{50} (M)**		
	Thr	**Fbr**	**IgG**
PHYSICAL ADSORPTION	$4.40 \cdot 10^{-11}$	$2.30 \cdot 10^{-6}$	$3.40 \cdot 10^{-5}$
Av-Bio AFFINITY	$4.60 \cdot 10^{-11}$	$8.19 \cdot 10^{-6}$	$7.33 \cdot 10^{-5}$
ELECTROCHEMICAL ACTIVATION	$4.39 \cdot 10^{-11}$	$8.65 \cdot 10^{-6}$	$8.48 \cdot 10^{-5}$
ELECTROCHEMICAL GRAFTING	$2.28 \cdot 10^{-11}$	$8.93 \cdot 10^{-6}$	$5.00 \cdot 10^{-5}$
IMMOBILIZATION	**% CR**		
	Thr	**Fbr**	**IgG**
PHYSICAL ADSORPTION	100	$1.91 \cdot 10^{-3}$	$1.29 \cdot 10^{-4}$
Av-Bio AFFINITY	100	$5.62 \cdot 10^{-4}$	$6.28 \cdot 10^{-5}$
ELECTROCHEMICAL ACTIVATION	100	$5.08 \cdot 10^{-4}$	$5.17 \cdot 10^{-5}$
ELECTROCHEMICAL GRAFTING	100	$2.55 \cdot 10^{-4}$	$4.56 \cdot 10^{-5}$

In addition, EC_{50} values for each type of immobilizations and % Cross Response (% CR) for all interfering proteins were determined, see Table 4.1.10. % CR was calculated according to the following equation [30]:

$$\%CR = \frac{EC_{50\,Thr}}{EC_{50\,interfering\,protein}} \cdot 100 \qquad (4.1.5)$$

The EC_{50} value corresponds to the turn point of the calibration curve towards the interfering species and represents the concentration of protein that provides 50 % of the Δ_{ratio} saturation value. Thus, the lower is the EC_{50} value, the greater is the affinity (or the interference) of the considered protein. The lowest EC_{50} value obtained, $2.30 \cdot 10^{-11}$ M, corresponded to electrochemical grafting immobilization for thrombin protein, and the larger, $8.48 \cdot 10^{-5}$ M, to electrochemical activation immobilization for IgG. In overall, the % CR values,

which states the degree of response in comparison to primary analyte Thr, ranged from 0.0019 % to $6.28 \cdot 10^{-5}$ %; these are openly low relative values, where the largest % CR corresponded to Fbr in adsorption immobilization. These results clearly demonstrated that the aptasensors showed a much higher sensitivity to Thr than the potential interfering proteins, that when they exhibit some effect is due to the high level of concentration at which they are present in serum.

-Studies of stability

The stability of the label-free aptasensors based on the different aptamer immobilization techniques was also investigated. To do this, different electrodes modified with aptamers were prepared the same day and stored in the refrigerator at 4ºC. Every day the impedance response of an electrode modified with aptamers was evaluated.

Table 4.1.11. Comparison among stability values for the aptasensors based on different immobilization techniques.

IMMOBILIZATION	STABILITY (DAYS)
GEC/PHYSICAL ADSORPTION	1
AvGEC/AVIDIN-BIOTIN AFFINITY	7
GEC/ELECTROCHEMICAL ACTIVATION	-
GEC/ ELECTROCHEMICAL GRAFTING	8

As can be seen in Table 4.1.11, the developed aptasensors based on electrochemical grafting exhibited the higher stability compared with the other aptasensors, which could retain its impedance response after a storage of eight

days with a negligible loss of activity. It is not surprising, in fact the long term stability of this aptasensor may be expected due to the covalent interaction between the modified electrode surface and the aptamers. In addition, aptasensor based on avidin-biotin could retain its impedance response after 7 days, this could be due to that the strong interaction between AvGEC electrode surface and biotinylated aptamers is not as strong as covalent bond. Whereas in the aptasensor based on physical adsorption method the stability was one day, it could be attributable to the fact that the attachment of aptamers to the electrode surface is weak and they can be removed easily.

This feature of stability is very important from the practical point of view, once the aptamers are immobilized onto the electrode surfaces, they can be stored under appropriate conditions, employing them subsequently, when they are required for the construction and use of the aptasensor.

4.1.1.6. Avidin epoxy graphite composite electrode as platform for genosensing

In this part of this chapter, AvGEC electrodes were also evaluated as a platform for genosensing, in the same way that they was for aptasensing in Section 4.3.1.2. In this case, the genosensor was developed for the detection of *Escherichia Coli O104:H4* bacterium. This Bacterium was a Gram-negative bacterium notorious for the enterohaemorrhagic epidemic outbreak in Germany and other European countries in 2011. Early detection of this bacterium is important because its specific strain produces a Shiga toxin which inhibits protein synthesis and causes a hemolyticuremic syndrome [34]. The design strategy of the genosensor is illustrated in Figure 4.1.30.

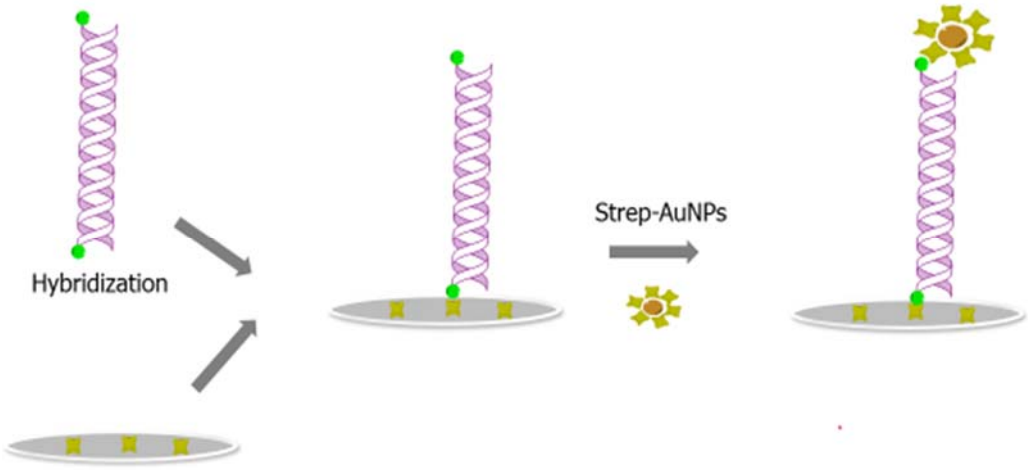

Figure 4.1.30. Scheme of experimental protocol for detection of *Escherichia Coli O104:14.*

-Optimization of amount of hybrid immobilized

In this study, the concentrations of DNA probe and target used were optimized in previous works [6, 8]. DNA probe and target assayed were 30 pmol in 160 µl of TSC1 buffer.

-Impedimetric response

After each step of the genosensing protocol, an EIS measurement was performed. As can be observed in Figure 4.1.31, when a DNA hybrid is immobilized on the sensor surface, an initial layer is formed and a negative charged interface is generated due to the presence of the negatively charged phosphate backbone of DNA. This fact produces a repulsion against the redox marker, also negatively charged, thus resulting in an inhibition of the electron transfer process and in an increment of the R_{ct} value. The addition of strep-AuNPs results in further increment of resistance value due to the hindrance caused by the formation of a double layer. In this way, the use of the EIS technique serves also as diagnostic that the biosensing surface was correctly prepared.

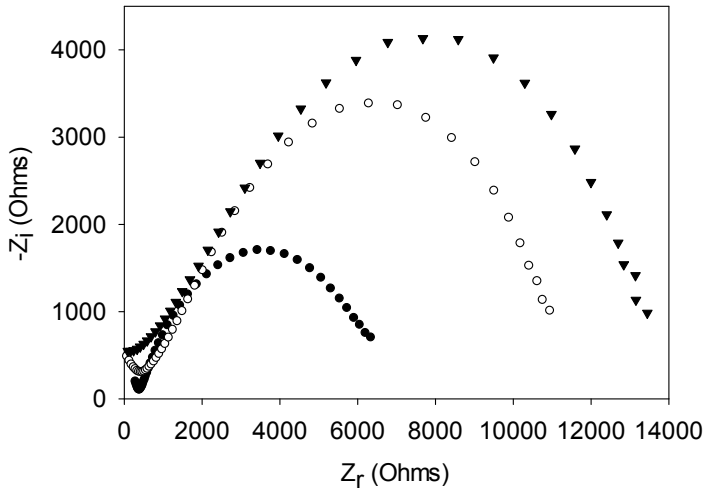

Figure 4.1.31. Nyquist Diagram for *E. Coli* detection.

-DNA testing

In this biosensing process, as explained before, the sequence followed for EIS measurement was: 1) Bare AvGEC electrode; 2) biotinylated hybrid modified AvGEC and 3) strep-AuNPs and biotinylated hybrid modified AvGEC. In this specific case, the hybridization was done taking place in solution because it has been observed to be more efficient [7]. In fact, given the DNA probe and target are both biotinylated, the immobilization into the surface of the electrode can be produced in two possible orientations, but both provide equivalent information as can be deduced from the comparable obtained RSD values. A non-complementary target sequence as well as the buffer solution alone was used as negative controls.

In Figure 4.1.32, results of experiments and negative controls were represented as the increment in R_{ct} between the bare electrode and the sample modified electrode (Δ). As it can be observed, the Δ increment corresponding to an experiment before amplification (bar (+), grey color) results almost double than Δ value corresponding to a negative control also before amplification (bar (-), grey color), highly significant if compared with the associated uncertainties, 7.5 % RSD for direct measurement and 3.1 % RSD for the amplified case. In addition, the further increment of the Δ value in the experiment after

amplification (bar (+), white color) results not significant in the case of negative control (bar (-), white color). The net signal amplification (positive test) was of 34 %.

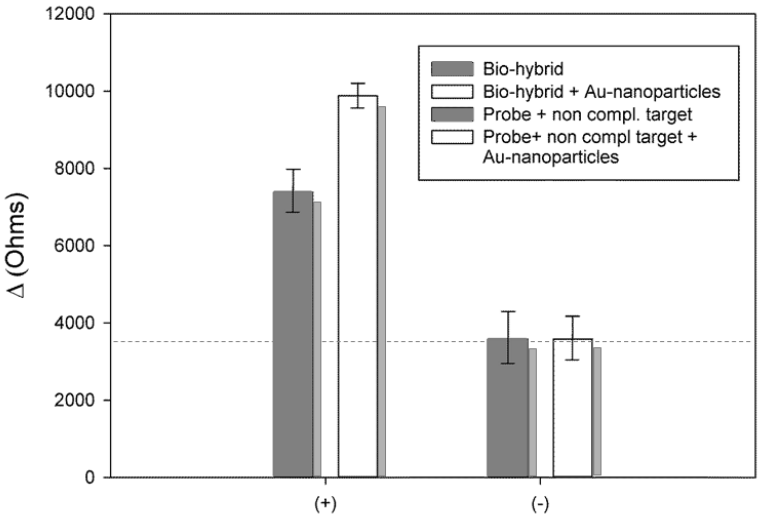

Figure 4.1.32. Comparison histogram between experiments and negative control (+) bars: experiments before (grey color) and after signal amplification with gold nanoparticles (white color); (-) bars: negative control before (grey color), after signal amplification with gold nanoparticles (white color). Indicated reproducibility corresponds to observed standard deviation of five replicated experiments.

A Student's t-test was performed to compare the results obtained in positive and negative experiments (both before and after signal amplification step). The difference between the mean values was highly significant in both cases. For the assay without amplification t_{calc} =67.97 > t_{tab}=2.13; for the assay with amplification t_{calc}=53.14 >t_{tab}=2.13, at the 95 % confidence level, 4 degrees of freedom. This confirms the significant difference between the signal obtained for the hybridization experiment with or without amplification and the one obtained for non-specific hybridization experiments with and without amplification.

- Scanning electron microscopy characterization

Enterohaemorragic *E.Coli* DNA biosensors were investigated by SEM after silver enhancement treatment. Silver enhancement treatment was employed in order to obtain an adequate size enlargement of strep-AuNPs present on sensor surface to allow their observation with SEM. This treatment was possible thanks to the use of biotinylated target, which allowed the coupling with extra elements on the free end. The images obtained are shown in Figure 4.1.33. Image on the left corresponds to the experiment where biotinylated complementary target was used during the hybridization step. In the figure, the strep-AuNPs distribution onto the electrode surface is quite homogeneous. This also implies a regular distribution of avidin molecules in the biocomposite and well-organized formation of the hybrid. Comparing this image with the one on the right, from a negative control, where a non-complementary target was employed in the hybridization, it is clear that the strep-AuNPs are bound to the positive test biotinylated DNA.

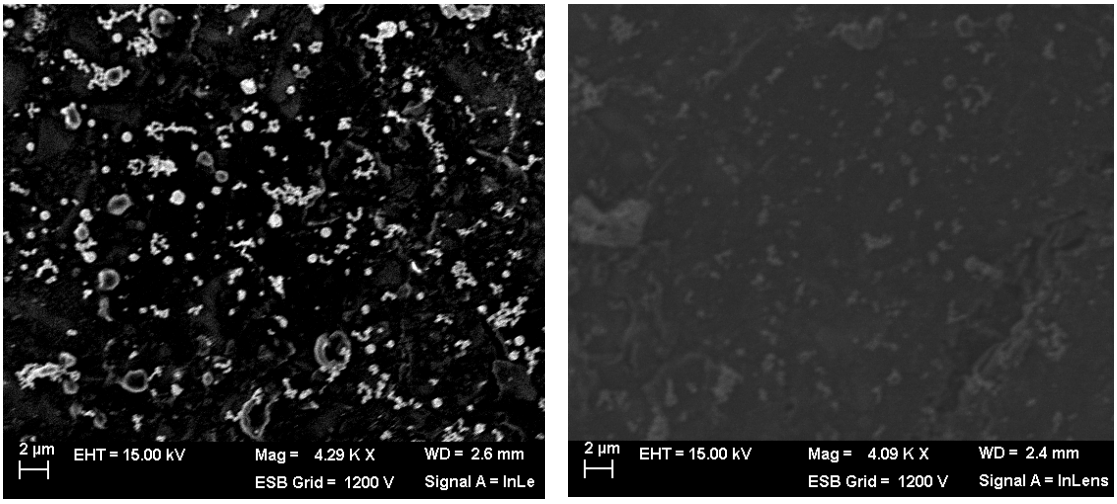

(A) (B)

Figure 4.1.33. SEM images of (A) experiment using biotinylated hybrid + strep-AuNPS + silver enhancement treatment (B) negative control using probe + non complementary target + strep-AuNPs + silver enhancement treatment.

As can be concluded from these results, AvGECs are excellent platforms for both biosensing variants, genosensing and aptasensing, providing high sensitivity. It is important to point out that the results are in agreement with previous studies in our research group [8, 24, 41].

4.1.2. Aptasensor for ultrasensitive detection of thrombin based on a sandwich protocol, gold nanoparticles and silver enhancement treatment

The use of aptamer sandwich protocol, streptavidin gold nanoparticles and silver enhancement treatment was proposed in this part of this study with the aim of amplifying the impedimetric signal obtained from the simple label-free aptasensor for Thr detection based on avidin-biotin affinity aptamer immobilization technique. The scheme of experimental protocol is represented in Figure 4.1.34.

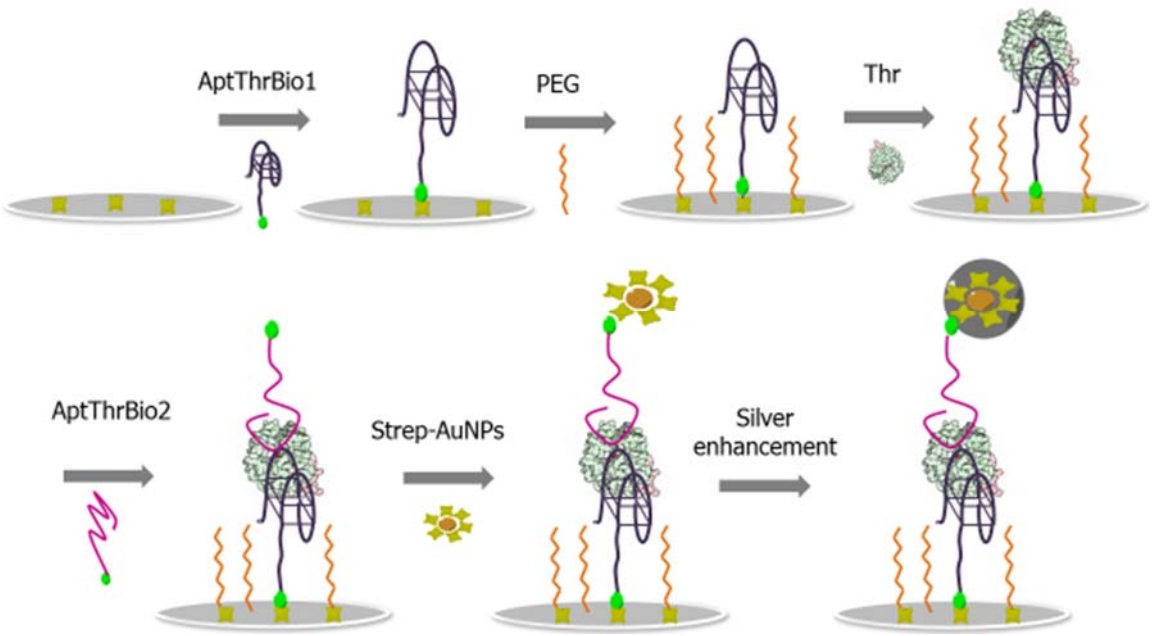

Figure 4.1.34. Scheme of the experimental protocol for the aptasensor for thrombin detection based on sandwich protocol, strep-AuNPS and silver enhancement treatment.

-Optimization of different concentrations

For the operation details of the aptasensor, the concentration of every reagent used was optimized. In detail AptThrBio1 and PEG were optimized in a previous work, see Section 4.1.1.2. As can be seen in Figure 4.1.35, the concentration of AptThrBio2 was optimized as the same way that the above reagents, by building its calibration curve. The optimal concentration was chosen as a 12 pmol in 160 µl of PBS1, and the strep-AuNPs were used just in excess to AptThrBio2.

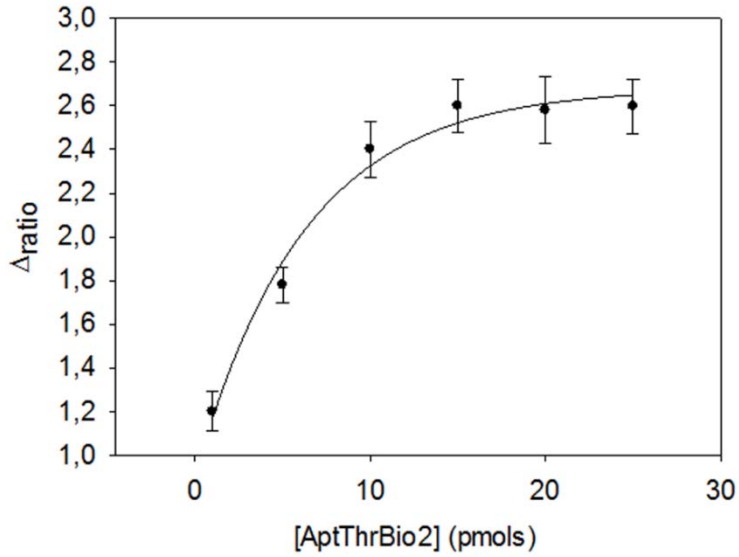

Figure 4.1.35. Optimization of the concentration of AptThrBio2. All experiments were performed with 50 pM of Thr in PBS solution and all EIS measurements were performed in PBS solution containing 0.01 M $K_3[Fe(CN)_6]/K_4[Fe(CN)_6]$. Uncertainty values corresponding to replicated experiments (n = 5).

-EIS measurements

In Figure 4.1.36, the EIS spectrum obtained for a biosensing experiment using aptamer sandwich protocol and silver enhancement amplification are shown. Impedance measurements were performed before modifying the electrode surface (bare AvGEC electrode), after modifying the electrode surface

with AptThrBio1, Thr, AptThrBio2 (sandwich formation), strep-AuNPs and finally, after silver deposition. As shown in this figure, R_{ct} increased after any modification of the electrode surface. This can be due to the increased difficulty of the redox reaction of $[Fe(CN)_6]^{3-/4-}$ to take place, due to the sensor surface alteration [21]. As mentioned above, two different factors may be taken into account to explain this: the electrostatic repulsion and the sterical hindrance. The former is more significant in the first step of protocol; when the AptThrBio1 is immobilized onto the electrode surface by avidin-biotin affinity, a first layer is formed, where negatively charged phosphate groups of aptamer skeleton are responsible of the electrostatic repulsion of the negatively charged redox marker, thus inhibiting the interfacial transfer process and resulting in R_{ct} increment. The addition of Thr and a second ApThrBio2 to form a sandwich results in a further increment of R_{ct} due to the increased quantity of negative charge and the hindrance caused by the formation of a double layer. In this work, strep-AuNPs and silver enhancement treatment were used with the aim of amplifying the EIS sandwich formation signal. After the addition of strep-AuNPs we can observe an increment of R_{ct} value because of the increased space resistance due to Au-streptavidin conjugates. Working at pH 7, streptavidin is slightly negatively charged (pI is around pH 5) and this fact also contributes to enhancement of impedance [38]. In the second amplification step, silver enhancement treatment [9, 19], a significant increment of R_{ct} value was also observed and attributable to the silver deposition on gold nanoparticles.

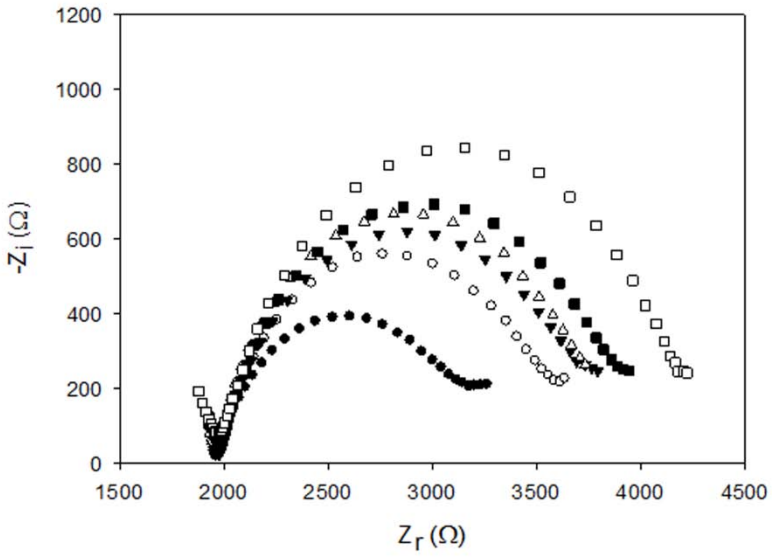

Figure 4.1.36. Nyquist diagrams for EIS measurements of: ● bare AvGEC electrode, ○ biotinylated aptamer of thrombin 1, ▼ biotinylated aptamer of thrombin and thrombin protein, Δ sandwich complex, ■ sandwich complex modified with strep-AuNPs, □ sandwich complex modified with strep-AuNPs and silver enhancement treatment. All experiments were performed in PBS solution and all EIS measurements were performed in PBS solution containing 0.01M $K_3[Fe(CN)_6]/K_4[Fe(CN)_6]$.

-CV characterization

Apart from EIS technique, CV is also an effective technique to investigate the changes of the electrode behavior after each step of the protocol. In CV, the change in peak current and peak to peak separation in voltammograms at different modification steps can be related to the electron transfer resistance. As shown in Figure 4.1.37, at the bare AvGEC electrodes, a pair of well-defined reversible redox peaks with high peak currents was observed. After immobilization of aptamer probe on the electrode surface, the peak current clearly decreased and the peak to peak potential separation increased, accounting for increased resistance to the charge transfer across aptamer probe attached on the electrode and reducing the effective surface area and available active sites for the electron transfer process. Then, after incubated with the target protein, the peak current decreased and the peak to peak potential separation

increased due to the sterical hindrance of the protein. When the electrode was incubated with the second biotinylated aptamer, AptThrBio2, the peak to peak potential separation increased due to the inhibition of the electron transfer resistance between the aptamer sandwich and the electrode surface. Moreover, when the electrode were modified with strep-AuNPs, a decrease in the peak current and an increase in the peak to peak separation was noticed due to the high sterical hindrance of the strep-AuNPs conjugates. Finally, the voltammetric peak response further decreased and peak potential separations increased when the silver enhancement treatment were carry out due to the deposition of the silver on the strep-AuNPs conjugates.

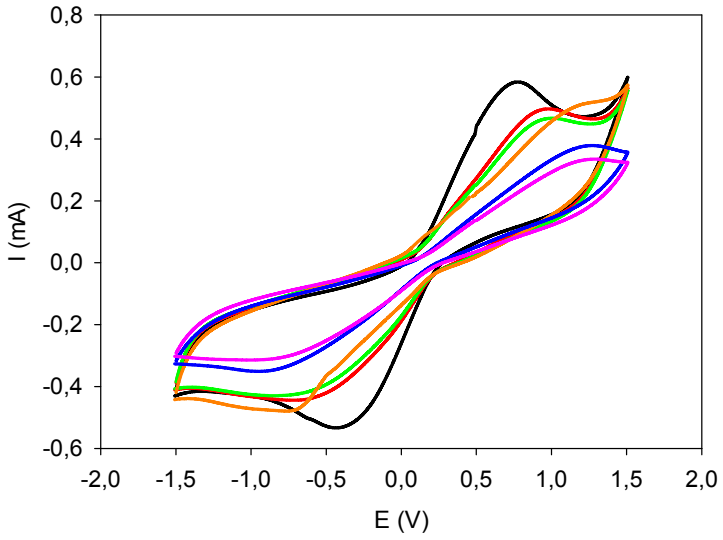

Figure 4.1.37. CV responses of all steps of the protocol: (black line) Bare AvGEC electrode, (red line) AvGEC electrode modified with AptThrBio1, (green line) AvGEC electrode modified with AptThrBio1 and Thr, (orange line) AvGEC electrode modified with aptamer sandwich, (blue line) AvGEC electrode modified with aptamer sandwich and strep-AuNPs, (pink line) AvGEC electrode modified with aptamer sandwich and strep-AuNPs and silver treatment. CV measurements were performed in PBS solution containing 0.01 M $K_3[Fe(CN)_6]/K_4[Fe(CN)_6]$ at scan rate of 0.05 V/s

The results were more and less consistent with the EIS measurements. However, EIS results presented more apparent differences for different modification steps, indicating better sensitivity compared to CV results.

-Confocal microscopy characterization

Aptamer sandwich formation was inspected by confocal microscopy after incubation with the strep-QDs. The images obtained are shown in Figure 4.2.38. The first image, Figure 4.1.38 (A), corresponds to the electrodes modified with aptamer sandwich formation and strep-QDs. The fluorescence points observed in this case are due to the presence of the complex formed between strep-QDs and the aptamer sandwich conjugated through the biotin-streptavidin affinity. The weak fluorescence observed in the second image, Figure 4.1.38 (B), corresponds to the negative control, which did not use biotinylated complementary aptamer. Comparison of the two images indicates that AptThrBio2 recognizes Thr and forms the expected sandwich conjugate.

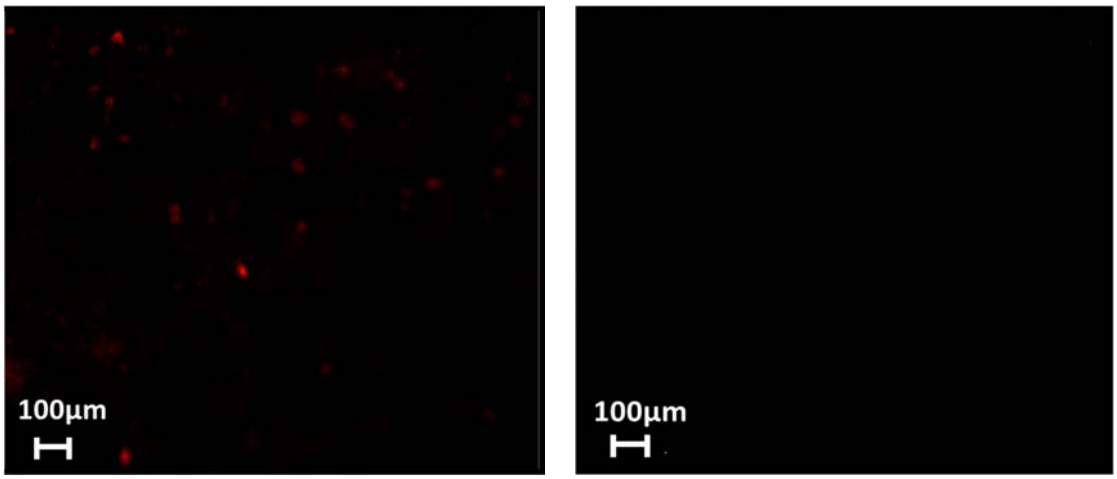

(A) (B)

Figure 4.1.38. Confocal images of: (A) positive control using biotinylated aptamer of thrombin 1 + thrombin + biotinylated aptamer of thrombin 2 + strep-QDs, (B) negative control using biotinylated aptamer of thrombin 1 + thrombin + biotinylated aptamer of cytocrome c + strep-QDs. Images were collected at 625 nm and with excitation wavelenght of 405nm.

-Scanning electron microscope characterization

Apart from amplifying the impedimeric response of the developed aptasensor, the silver enhancement treatment was used in order to visualize the presence and distribution of gold nanoparticles. These experiments also provided an image of the homogeneity and accessibility of the anchorage points supplied by the avidin entrapped in the biocomposite. SEM images are shown in Figure 4.1.39, illustrating a positive experiment with aptamer sandwich and strep-AuNPs. As it can be observed in the Figure 4.1.39 (A), the distribution of silver enhanced-gold nanoparticles is quite homogeneous. This also implies a regular distribution of avidin molecules in the biocomposite and well-organized formation of aptamer sandwich onto the electrode surface. Apart, the nanoparticles formed were monocrystalline; that is, thanks to the disposition of the streptavidin around of gold nanoparticles, the silver crystallized in specific directions. Comparing this experiment with the negative control that did not use the biotinylated complementary aptamer, Figure 4.1.39 (B), a surface without any nanoparticles can be observed demonstrating absence of non-specific signal.

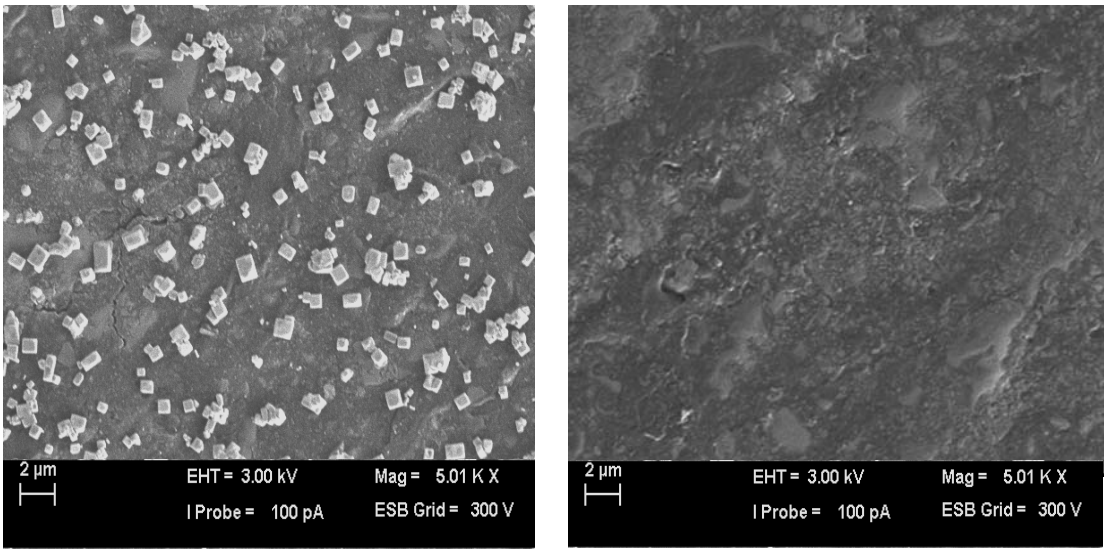

(A) (B)

Figure 4.1.39. SEM images of: (A) experiment using biotinylated aptamer of thrombin 1 + thrombin + biotinylated aptamer of thrombin 2 + strep-AuNPs + silver enhancement treatment, (B) experiment using biotinylated aptamer of thrombin 1 + Thr + biotinylated aptamer of cytochrome c + strep-AuNPs + silver enhancement treatment.

-Analytical performance of the aptasensor for detection of thrombin

After optimizing the concentrations involved in the construction of the aptasensor, calibrations curves of each step of the protocol were built. Figure 4.1.40 (A) shows calibration curves with increasing concentrations of Thr and Figure 4.1.40 (B), their respective regression curves in the linear range, at the different steps of the protocol: (1) AptThrBio1-Thr, (2) Sandwich formation between AptThrBio1, Thr and AptThrBio2, (3) aptamer sandwich modified with strep-AuNPs, and (4) aptamer sandwich modified with strep-AuNPs and silver enhancement treatment.

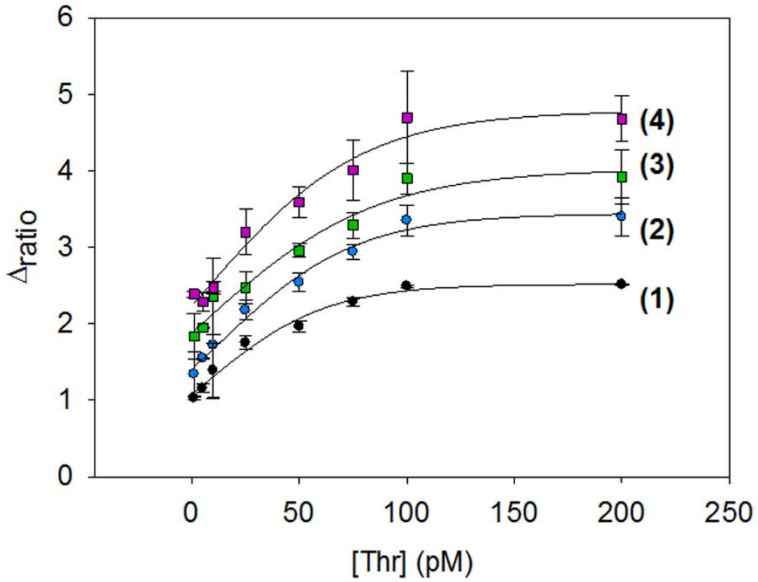

(A)

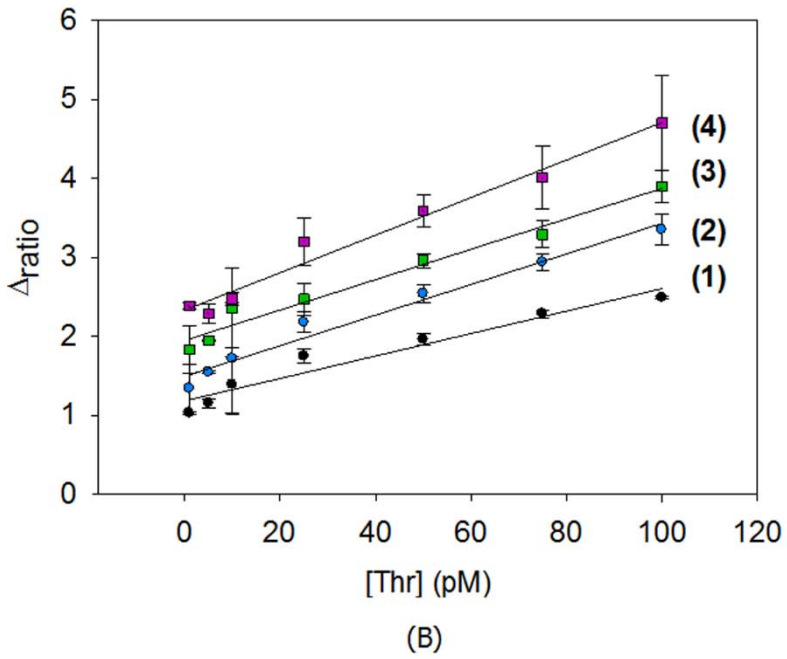

Figure 4.1.40. (A) Calibration curves and (B) Regression curves of: (1) (black circle) biotinylated aptamer of thrombin 1, (2) (blue circle) sandwich complex, (3) (green square) sandwich complex modified with strep-AuNPs, (4) (purple square) sandwich complex modified with strep-AuNPs and silver enhancement treatment. All experiments were performed in PBS solution and all EIS measurements were performed in PBS solution containing 0.01 M $K_3[Fe(CN)_6]/K_4[Fe(CN)_6]$. Uncertainty values corresponding to replicated experiments (n = 5).

In previous experience in our laboratory with silver enhancement related to DNA hybridization biosensing, it was not possible to obtain good impedimetric measurements following amplification treatment mainly because of degraded reproducibility [6]. In this case, although the reproducibility was not excellent, the calibration curve obtained showed a good % RSD. As can be seen in Figure 4.1.40 (A), all calibration curves increased until the value of 100 pM of Thr, this could be due to the fact that concentrations larger then 100 pM cause a saturation on the sensor surface. Moreover, a signal increment of up to 89 % between AptThrBio1-Thr (the simple biosensing) and sandwich formation with strep-AuNPs and silver enhancement treatment was observed.

Table 4.1.12. Summary of calibration results.

CALIBRATION CURVE	REGRESSION PLOT	DETECTION LIMIT	LINEAR RANGE	% RSD*	% AMPLIFICATION
AptThrBio1-Thr	Δ_{ratio}=1.042+0.0157[Thr]	4.7 pM	0.75-100 pM	2.2	-
Aptamer Sandwich	Δ_{ratio}=1.495+0.0194[Thr]	2.0 pM	0.75-100 pM	3.4	35
Aptamer sandwich/Strep-AuNPs	Δ_{ratio}=1.874+0.0201[Thr]	0.2 pM	0.2-100pM	5.2	57
Aptamer sandwich/strep-AuNPs/silv.enh	Δ_{ratio}=2.477+0.0219[Thr]	0.3 pM	0.2-100pM	9.9	89

* Corresponding to five replicate experiments at 75 pM thrombin.

As can be observed in Table 4.1.12, the use of silver enhancement treatment led to the highest sensitivity and signal amplification compared to the other calibration curves obtained. This confirms that the silver deposition on gold nanoparticles increases essentially the sterical hindrance, producing an increment of observed impedance. Despite a higher sensitivity, the detection limit obtained in this case, 0.3 pM, is slightly worse than the one obtained with only strep-AuNPs. This fact, caused by the deteriorated reproducibility, could be attributable to the increased number of process steps and associated increased potential errors. The best detection limit, approximately 0.2 pM, corresponded to the sandwich and strep-AuNPS calibration curve. This confirmed that the proposed methods show low detection limit and ultrahigh sensitivity for the detection of thrombin.

Table 4.1.13. Comparison of the proposed biosensor with other reported methodologies as thrombin detection.

ANALYTICAL TECHNIQUE	DETECTION LIMIT	REFERENCE
AMPEROMETRY	0.12 pM	[2]
POTENTIOMETRY	6.7 nM	[17]
VOLTAMMETRY	0.52 pM	[14]
DPV	7.82 aM	[50]
EIS	4.4 pM	[43]
EIS	0.1 pM	[13]
EIS AND CV	93 pM	[49]
EIS	0.2 pM	Our work
SPR	0.1 nM	[3]
ELECTROLUMINISCENCE	1.6 fM	[18]
ELECTROLUMINISCENCE	0.4 pM	[40]
ELECTROLUMINISCENCE	0.5 pM	[47]
SERS	0.16 pM	[42]
PET	13 pM	[48]
FRET	2.5 nM	[11]
FLUORESCENCE	1. 1 nM	[22]

When the proposed aptasensor was compared with other detection methodologies for thrombin detection, some interesting facts are inferred. The results are shown in Table 4.1.13, where sensitivity information is presented as the LOD of each biosensor compared. The lowest detection limit value among all the analytical techniques corresponded to [50], but this Thr biosensor used a double amplification strategy, with thiocyanuric acid and gold nanoparticle-labeled aptamer, and differential pulse voltammetry (DPV). Our proposed aptasensor is on the second range of lowest LOD in electrochemical techniques and impedance, thus demonstrating satisfactory results for the detection of thrombin in real samples, given that this level corresponds to physiological concentration levels. Moreover, the proposed aptasensor showed many advantages: it is stable for seven days, its surface is easily regenerable by polishing and the followed procedure was simple and easy.

-Selectivity of the aptasensor

To verify that the signal was dependent on the specific recognition, our protocol for thrombin detection was evaluated by challenging it with possible interfering proteins present in blood serum, comparing it to the simple biosensing, label-free detection alternative, as indicated Figure 4.1.41.

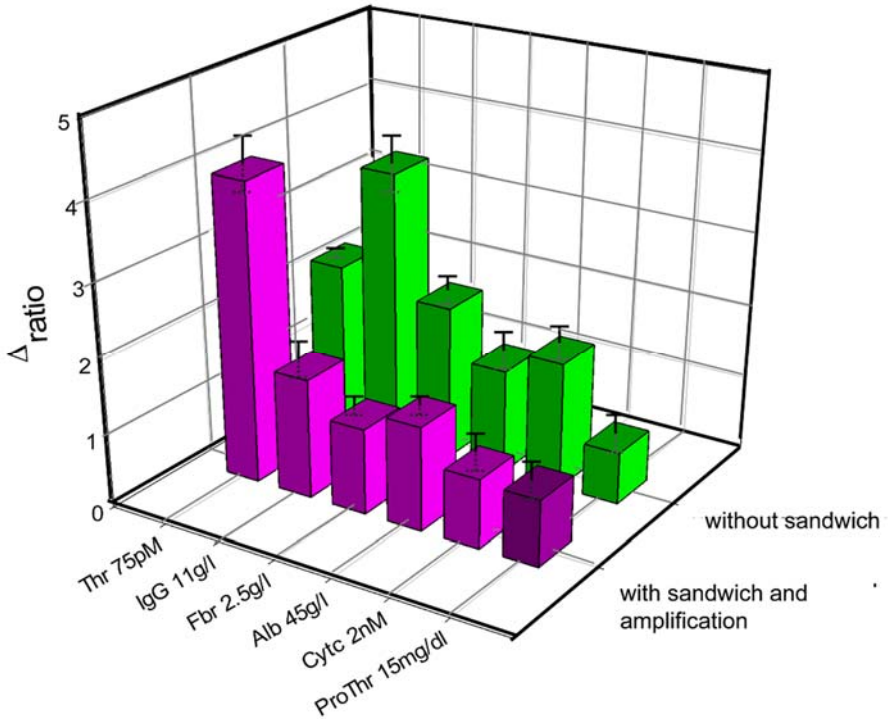

Figure 4.1.41. 3D bar chart of response towards different proteins present in serum, without the amplification protocol and with the sandwich/amplification protocol. Uncertainty values corresponding to replicated experiments (n = 5).

From this investigation, we found that the presence of interfering proteins such as BSA, Cyt *c*, Fbr, prothrombin (ProThr) and IgG, at serum concentration level exhibits negligible response compared with 75 pM Thr in the amplified sandwich protocol, even using concentrations four or five orders of magnitude higher than typical Thr concentration. The figure also demonstrates that the sandwich protocol displays as clear advantage, more than the signal

amplification, the marked decrease of interfering effects that are still noticeable in the simple biosensing scheme. These observations suggest that the sensing mechanism relies on specific recognition and that the aptasensor sandwich method is highly specific for the detection of Thr. Moreover, it is important to emphasize that prothrombin protein is the precursor of thrombin in the blood clotting process and this aptasensor is capable of distinguishing both proteins with high selectivity.

Apart of these proteins, ascorbic acid, uric acid and dopamine were also tested for interference because of their relatively high concentration in biological samples and low oxidation potentials. As can be seen in Figure 4.1.42, uric and ascorbic acid showed negligible responses compared with 75 pM Thr, tested at concentrations eight and six orders of magnitude higher than that of Thr. Dopamine exhibited certain low interfering signal (17 %) at typical serum concentration, but it should be considered that this compound is only present in serum during physical and emotional stress.

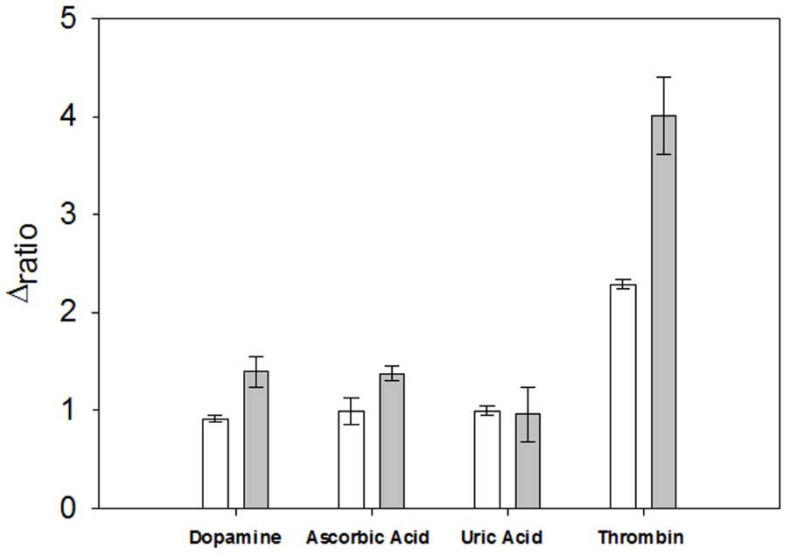

Figure 4.1.42. Bar chart of response towards non-proteic compounds present in serum and thrombin, without the amplification protocol (white bars) and with the sandwich/amplification protocol (grey bars). The concentrations were: 4.75 nM Dopamine, 80 µM Ascorbic Acid, 0.73 mM Uric Acid and 75 pM Thr. Uncertainty values corresponding to replicated experiments (n = 5).

-Spiked real samples

As it has been mentioned, the detection of thrombin in human blood is of great importance in clinical analysis, not only for the diagnosis of cardiovascular diseases also for its consideration as a tumor marker. Considering that, the aptasensor was evaluated with Thr spiked samples. Thus, human serum samples were diluted at 50 % with PBS1 and then different concentrations of thrombin were spiked into the diluted serum.

The recovery values were calculated using the following equation:

$$\%\, Recovery = (([Thr]found| - [Thr]_{blank})/[Thr]expected) \cdot 100 \qquad (4.2.6)$$

Table 4.1.14. Recovery studies performed in diluted human serum samples for applicability of the aptasensor (n=3).

[Thr] added (pM)	[Thr] found (pM)*	% RECOVERY	% RSD
75	72.2 ± 5.4	96.5	4.5
10	10.3 ± 1.0	102.7	7.6
5	4.5 ± 0.7	89.0	8.1

*$(\bar{x} \pm \frac{s \cdot t}{\sqrt{n}})$

As can be seen in table 4.1.14, the recovery values obtained were from 89 % to 102.7 % with RSD between 8.1 % and 4.5 %, demonstrating the excellent performance of the aptasensor and its suitability for the direct analysis of Thr in serum samples at the low pM level.

4.2. IMPEDIMETRIC APTASENSORS FOR CYTOCHROME C DETECTION

4.2. Impedimetric aptasensors for cytochrome *c* detection

As indicated in Chapter 1, the quantification of Cyt *c* is of great importance as a preclinical indicator of several diseases such as diabetes-specific microvascular diseases, Alzheimer's disease, Huntington's disease, muscular dystrophies, etc.

This chapter is focused on the development of impedimetric aptasensors for the detection of this protein. Firstly, a simple label-free aptasensor for Cyt *c* detection using a wet physical adsorption immobilization technique and the already described aptamer [12] was performed and evaluated. Afterwards, with the goal to amplify the impedimetric signal, a hybrid aptamer-antibody sandwich protocol using MWCNT screen printed electrodes was carried out.

4.2.1. Label-free aptasensor for cytochrome c detection based on aptamer physical adsorption immobilization technique

The same experiments performed using physical adsorption immobilization technique for Thr detection were reproduced using an aptamer of cytochrome c for Cyt *c* detection. The biosensing protocol is shown in Figure 4.2.1.

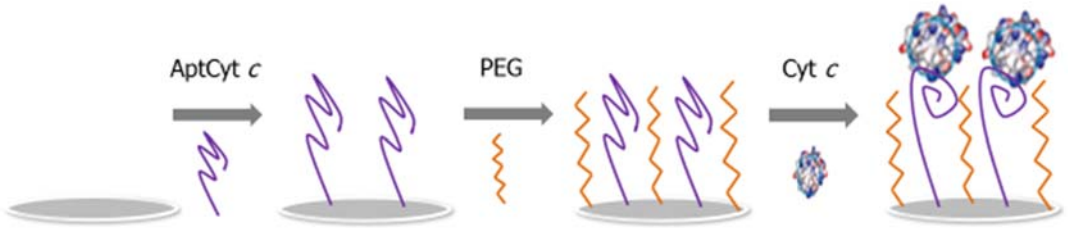

Figure 4.2.1. Scheme of the experimental protocol for the aptasensor for cytochrome c detection based on physical adsorption method.

-Optimization of aptamer and PEG concentrations

Important experimental concentrations including aptamer and PEG were optimized to obtain a highly sensitivity of the fabricated aptasensor by constructing its relative response curves.

The aptamer calibration curve was carried out by increasing amount of concentration of AptCyt *c* used in the from 1 to 2,5 μM. The different concentrations were evaluated by the changes in the Δ_p. As can be seen in the Figure 4.2.2, the Δ_p increased with the AptCyt *c* concentration until a saturation value. This is due to the physical adsorption of the aptamer onto the electrode surface, which followed a Langmuir isotherm; in it, the variation of R_{ct} increased

to reach a saturation value, chosen as the optimal concentration. The value selected for the aptasensor corresponded to a concentration of aptamer of 1.75 μM, as the compromise between the two extremes.

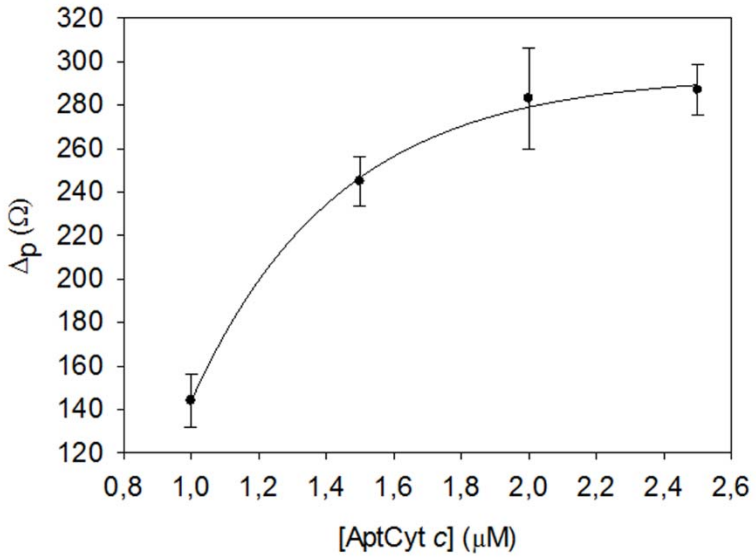

Figure 4.2.2. Optimization of the concentration of AptCyt *c* immobilized on each aptasensor. All experiments were performed in PBS solution and all EIS measurements were performed in PBS solution containing 0.01 M $K_3[Fe(CN)_6]/K_4[Fe(CN)_6]$. Uncertainty values corresponding to replicated experiments (n = 5).

The use of blocking agent (PEG) on the electrode surface was introduced to minimize the nonspecific adsorption of other species, which would alter the observed impedimetric signal. Apart, these other species can potentially interact or disturb the binding of the Cyt *c* on the AptCyt *c* in the further steps and thus must be avoided. For the optimization of the PEG concentration we proceeded as above. PEG concentrations were increased from 20 until 70 mM and the electrochemical characteristics of the electrode were determined. As it can be observed in Figure 4.2.3, the Δ_p increased up to a certain saturation value. The value selected as the optimal PEG concentration was 35 mM, corresponding to the intersection of the two extreme behaviours.

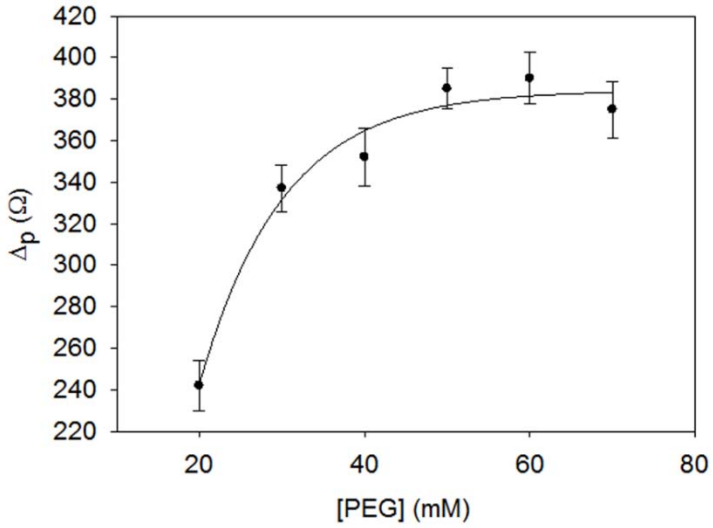

Figure 4.2.3. Optimization of the concentration of the blocking agent, PEG. All experiments were performed in PBS solution and all EIS measurements were performed in PBS solution containing 0.01 M $K_3[Fe(CN)_6]/K_4[Fe(CN)_6]$. Uncertainty values corresponding to replicated experiments (n = 5).

-Surface coverage of the electrode surface

Table 4.2.1. Quantification of surface coverage of all steps of the procedure (Uncertainly values correspond to triplicate experiments).

	Bare electrode	**AptCyt c**	**PEG**	**Cyt *c* (10^{-9} M)**
Γ(10^{11} MOLECULES/CM^2)	0.04 ± 0.20	3.33 ± 0.34	3.45 ± 0.33	1.76 ± 0.34

In order to obtain the surface coverage, the procedure described in Section 4.1.1.5 was also used [15]. This consisted in obtaining the CV responses of $[Ru(NH_3)_6]^{3+}$ on an epoxy-graphite composite electrode (bare electrode) with AptCyt *c*, after PEG treatment and after cytochrome c detection, see Figure 4.2.4. The results are shown in Table 4.2.1. The values clearly showed that the surface density is maintained before and after PEG treatment, consistent with the obtained results from the aptasensor for thrombin detection based on the same aptamer immobilization method.

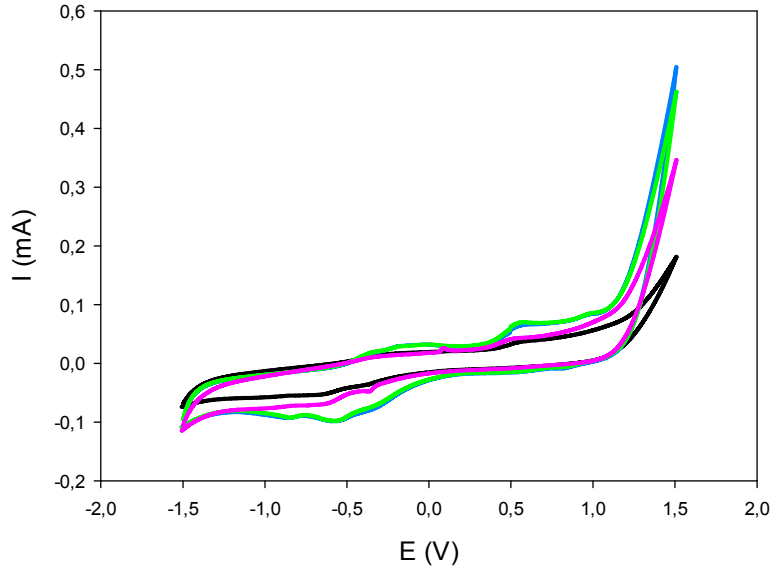

Figure 4.2.4. CV responses of: bare electrode (black line), electrode modified with AptCyt *c* 1.75μM (green line), electrode modified with 35 mM PEG (blue line), and electrode modified with 10^{-9} M Cyt *c* (pink line). All experiments were performed in 10 mM Tris buffer pH 7.4 containing 50 μM $[Ru(NH_3)_6]^{3+}$ at scan rate of 0.05 V/s

-Detection of Cyt c

The aptamer of Cyt c forms a linear single-strand oligonucleotide, in sequence that recognizes the protein by a specific folding. During this folding, weak interactions between the aptamer and protein of the host-guest type are created, leading to complex AptCyt *c*-Cyt *c*. One example of the obtained response after each biosensing step is shown in Figure 4.2.5. As can be seen in this figure, when the AptCyt *c* is immobilized onto the electrode surface, a R_{ct} increment was observed, due to the formation of a first layer, where negatively charged phosphate groups of aptamer skeleton are responsible of the electrical repulsion towards the negatively charged redox marker, thus inhibiting the interfacial transfer process. When the protein is added R_{ct} should decrease considering that the pI of the protein is 10-10.5 [39], and therefore it is positively charged, then favouring electrostatically the arrival of the redox marker to the

electrode. In contrast, according to the capacitance values calculated from the different experiments varying Cyt *c* concentration, the capacitance values are kept practically constant, 0.45±0.03 μF. The R_{ct} increase seems to be due, then, to the sterical factor dominating over the electrostatic factor.

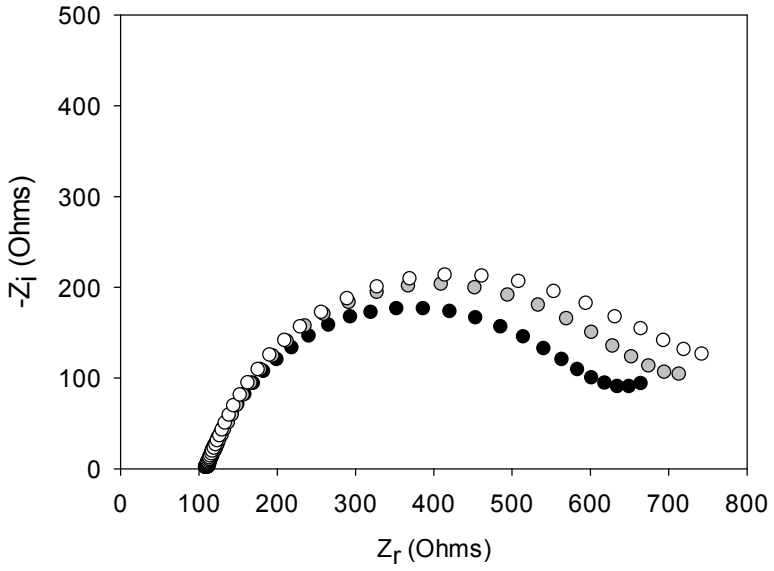

Figure 4.2.5. Nyquist diagrams for EIS measurements of: (black circles) bare GEC electrodes, (grey circles) AptCyt *c* modified electrodes and (white circles) AptCyt *c*-Cyt *c* modified electrodes. All experiments were performed in PBS solution and all EIS measurements were performed in PBS solution containing 0.01M $K_3[Fe(CN)_6]/K_4[Fe(CN)_6$

- Analytical performance of the aptasensor for detection of Cyt c

In order to obtain the sensitivity of the aptasensor a complete calibration curve, was built defined by using an increasing concentration of Cyt *c*. Figure 4.2.6, illustrates the increase of the impedimetric signal with increasing Cyt *c* concentration. Relative signal Δ_{ratio} were plotted for the different Cyt *c* concentration assays, as shown on Figure 4.2.7. As can be observed, a calibration curve was obtained which a logarithm trend, however for the range from 50 pM to 1 nM a linear trend was still observed. Moreover, a good linear relationship (r

= 0.993) between the relative analytical signal (Δ_{ratio}) and the Cyt *c* concentration in this range was obtained according to the equation: $\Delta_{ratio} = 1.13 + 5.24 \cdot 10^{8}$ [Cyt *c*] (M). The detection limit was estimated as three times the standard deviation of the intercept obtained from the linear regression, which was 63.2 pM. The reproducibility of the method showed a relative standard deviation (RSD) of 6.8 %, obtained from a series of 5 experiments carried out at a concentration of 500 pM Cyt *c*.

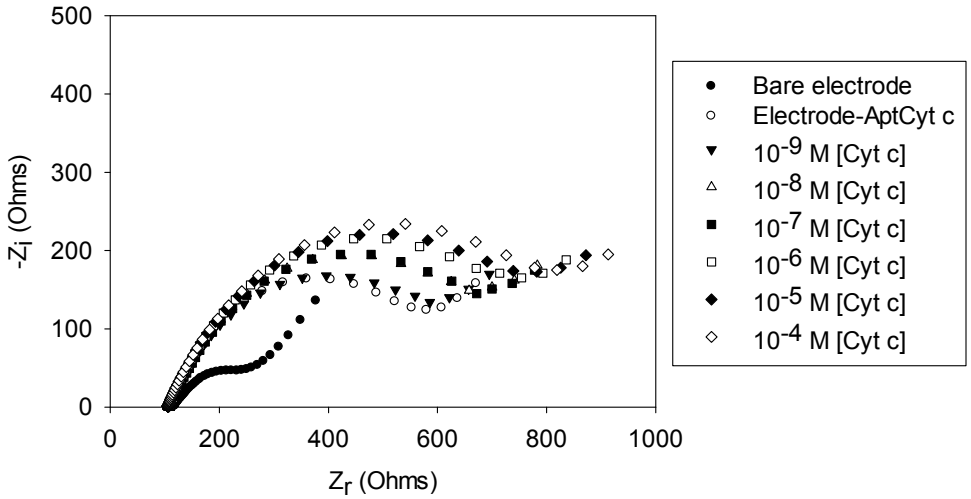

Figure 4.2.6. Nyquist diagrams for different concentrations of Cyt *c*. All experiments were performed in PBS solution and all EIS measurements were performed in PBS solution containing 0.01 M $K_3[Fe(CN)_6]/K_4[Fe(CN)_6]$.

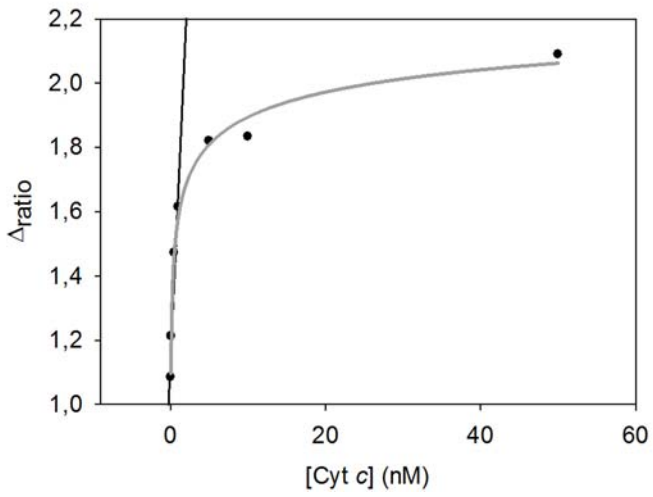

Figure 4.2.7. Calibration curve and regression plot, relative signal *vs.* Cyt c concentration. All experiments were performed in PBS solution and all EIS measurements were performed in PBS solution containing 0.01 M $K_3[Fe(CN)_6]/K_4[Fe(CN)_6]$.

-Selectivity of the aptasensor

Cyt *c* is present in blood serum, which can be described as a complex sample matrix containing hormones, lipids, blood cells and other proteins. To study the selectivity of the system, we evaluated the response of proteins present in serum such as Fbr, IgG and BSA. All proteins showed some degree of interference for Cyt *c*. For this reason, the calibration curves were built for the serum level concentration of each protein.

Table 4.2.2. Summary of calibration results for Cyt c and other major proteins presents in serum.

PROTEIN	REGRESSION PLOT	SENSITIVITY (M^{-1})	DETECTION LIMIT	TYPICAL CONC. IN SERUM
Cyt *c*	$\Delta_{ratio} = 1.130+5.236\cdot10^{8}$ [Cyt *c*]	$5.24\cdot10^{8}$	63.2 pM	2 nM
BSA	$\Delta_{ratio} = 0.672+8.377\cdot10^{3}$ [BSA]	$8.38\cdot10^{3}$	0.3 mM	0.52–0.75 mM
Fbr	$\Delta_{ratio} = -0.909+5.330\cdot10^{5}$ [Fbr]	$5.33\cdot10^{5}$	7.10 µM	6–12 µM
IgG	$\Delta_{ratio} =-0.618+4.435\cdot10^{4}$ [IgG]	$4.44\cdot10^{4}$	0.143 µM	60–100 µM

To evaluate the sensitivity of the aptasensor we compared the calibration plots for the different interferent proteins. Table 4.2.2 summarizes the parameters of the calibration curve of each protein and Cyt *c*, as well as their respective slopes and detection limits. The aptasensor showed the highest sensitivity for its target molecule, Cyt *c*, with its slope being three orders of magnitude greater than the slope for Fbr and four orders of magnitude more than that of IgG. Therefore, it was demonstrated that the aptasensor exhibited a much higher sensitivity to Cyt *c* than that to regarding potential interfering proteins, which displayed this effect greatly due to the high level of concentration in which they were assayed.

Table 4.2.3. Summary of EC_{50} and % Cross-response values of each interferent protein.

PROTEIN	EC_{50} (M)	% CROSS-RESPONSE
Cyt *c*	$6.68 \cdot 10^{-10}$	100
BSA	$6.06 \cdot 10^{-5}$	$1.01 \cdot 10^{-3}$
IgG	$3.63 \cdot 10^{-5}$	$1.84 \cdot 10^{-3}$
Fbr	$1.37 \cdot 10^{-6}$	0.05

(% CR = (EC_{50} cytochrome c/EC_{50} interferent)·100).

Apart of previous data, EC_{50} values for each protein and % Cross Response (% CR) for all interfering proteins were calculated, as summarized on Table 4.2.3. The lowest EC_{50} value obtained corresponded Cyt *c*, the target protein with a value of $6.68 \cdot 10^{-10}$ M, and the larger, $3.63 \cdot 10^{-5}$ M, to Fbr. The largest % CR value corresponded to Fbr, 0.05 %, and the lowest to BSA. Therefore, it was demonstrated that the aptasensor showed a much higher sensitivity to Cyt c, regarding potential interfering proteins, which displayed this effect due to the high level of concentration in which they are present in serum, and not in a secondary recognition by aptamer or antibody.

-Comparative study of the developed aptasensor with other biosensors.

Table 4.2.4. Comparison of the proposed Cyt *c* biosensor with other reported biosensing methods.

ANALYTICAL METHOD	DETECTION LIMIT	BIORECOGNITION ELEMENT	%RSD	INTERFERING PROTEINS	REFERENCE
EIS	63.2 pM	Aptamer	6.8	Albumin, Fbr, IgG	Our work
EIS	10 nM	Calixarens	10	BSA	[29]
CV	0.5 μM	Enzyme	2.8	Ascorbic and Uric acid	[33]
SWV	0.2 μM	Enzyme	-	Serum samples	[1]
FLUORESCENCE	44.4 pM	Aptamer	-	Serum samples	[23]
ICP-MS/ TEM	1.5 fM	Antibody	6.6	Serum samples	[25]

Additionally, the proposed aptasensor was compared with other detection methodologies for the direct Cyt *c* detection. The detailed results are shown in Table 4.2.4, where sensitivity info is presented as the LOD of each biosensor compared. The lowest detection limit value among all the analytical techniques corresponded to [25] , but this Cyt *c* biosensor used ICP-MS as the transduction technique. This methodology displays high sensitivity but is not simple, portable or easy to use. Our proposed aptasensor is on the second range of lowest LOD, thus demonstrating satisfactory results for the detection of Cyt *c* in real samples, given this level corresponds to concentration in human serum when apoptosis appears.

4.2.2. Aptamer-antibody sandwich assay for cytochrome c employing a MWCNT platform

A sensitive aptamer-antibody interaction based sandwich assay for Cytc *c* using electrochemical impedance were performed. Electrochemical grafting technique was employed in order to immobilize aminated aptamers onto multi-walled carbon nanotubes on the surface of a screen-printed electrodes via covalent bond. The experimental scheme is represented in Figure 4.2.8.

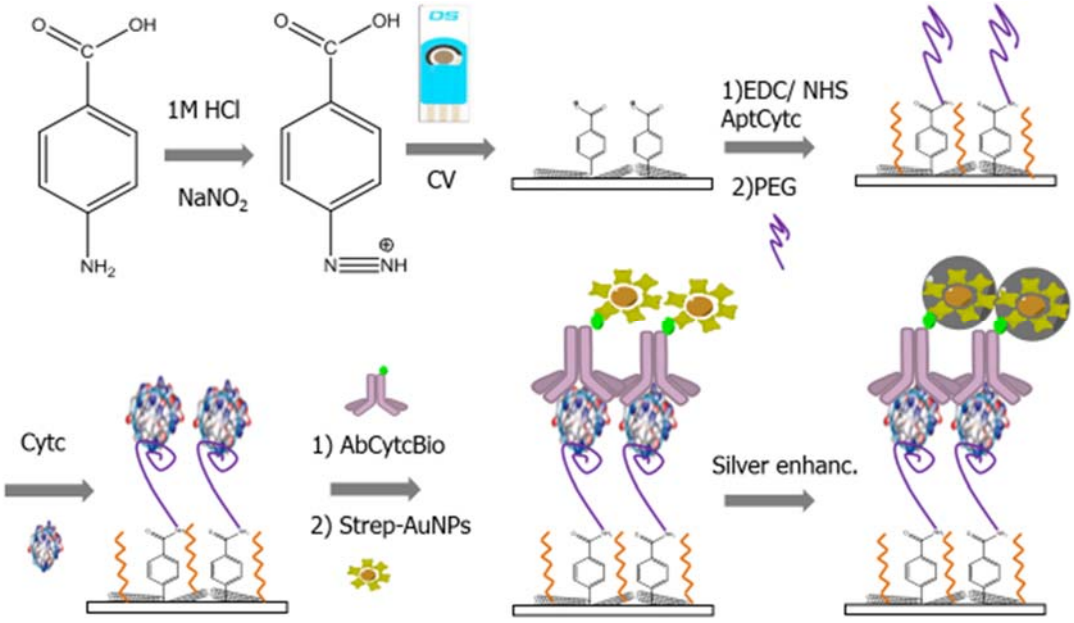

Figure 4.2.8. Scheme of the experimental protocol for the aptamer-antibody sandwich assay for cytochrome c employing a MWCNT platform.

-Optimization of the experimental concentrations involved in the aptamer-antibody sandwich assay response to Cyt c

All concentrations involved in the analytical performance of the aptasensor for detection of Cyt *c* were optimized.

AptCyt *c* and PEG concentrations were optimized by constructing their relative response curve. For this, increasing concentrations of AptCyt *c* NH_2 and PEG were used to determine the immobilization and surface blocking, respectively, evaluating the changes in the Δ_p. Figure 4.2.9 shows the curve of AptCyt *c* immobilization onto the electrode surface. It can be observed that the difference in resistance (Δ_p) increased up to a value. This is due to the physical adsorption of the aptamer onto the electrode surface, which followed a Langmuir isotherm. Embodied by the variation of R_{ct} which increases to reach a saturation value, the optimal concentration was chosen as initial value to reach it. This value corresponded to a concentration of aptamer of 1.5 µM. Concerning blocking agent, and as shown in Figure 4.2.10, a different behaviour was obtained. The optimal concentration of blocking agent was chosen as 30 mM because it was the concentration point where a small plateau was observed.

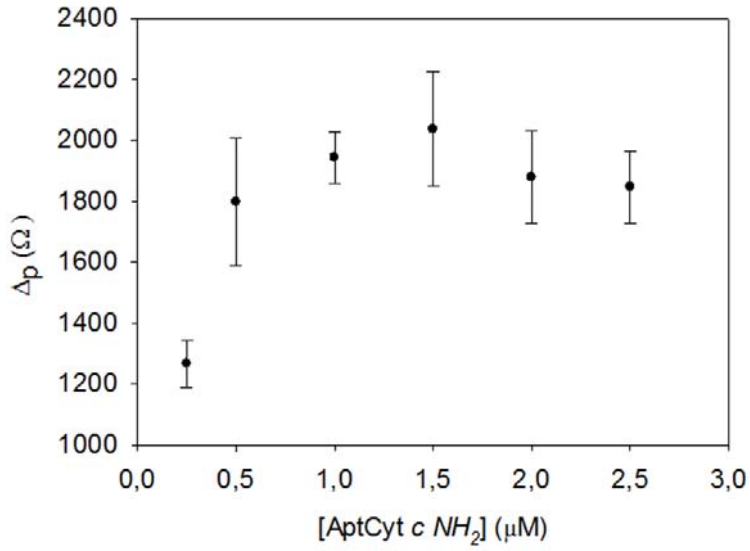

Figure. 4.2.9. Optimization of the amount of AptCyt *c* NH_2 immobilized on each electrode.

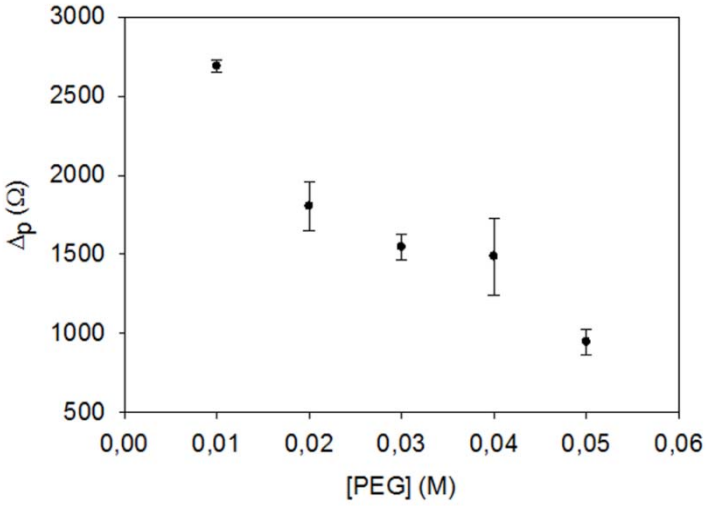

Figure 4.2.10.Optimization of the concentration of the blocking agent, PEG. Uncertainty values corresponding to replicated experiments (n=5).

Additionally, to obtain the optimal concentration of AbCyt *c* to be used in the biosensing protocol, its response was evaluated with increasing concentration of antibody. The optimal concentration was evaluated by the changes in the Δ_{ratio}. As can be seen in Figure 4.2.11, the highest signal response was obtain for 1/500 stock dilution and this concentration was chosen as an optimal value.

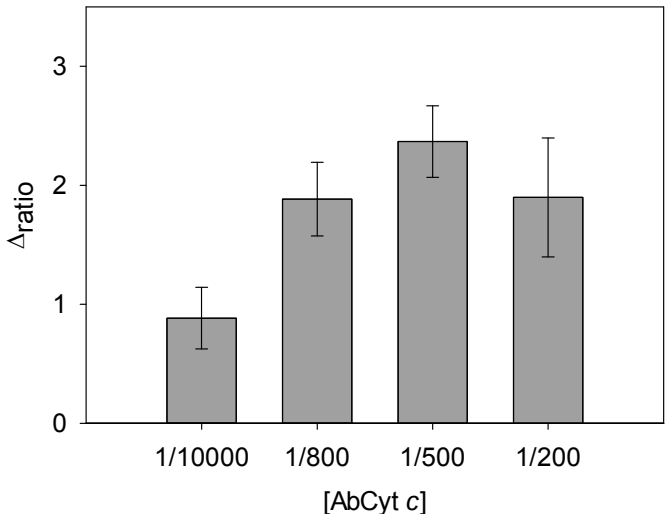

Figure 4.2.11. Optimization of the concentration of AbCyt *c.* All experiments were performed with 100 pM of Cyt *c* in PBS solution and all EIS measurements were performed in PBS solution containing 0.01 M $K_3[Fe(CN)_6]/K_4[Fe(CN)_6]$. Uncertainty values corresponding to replicated experiments (n = 5).

-Impedance response

To prove the feasibility of this aptasensing strategy, EIS measurements were performed to study the interface properties of different modified electrodes. Figure 4.2.12 (A) shows the Nyquist plots obtained by electrochemical impedance spectroscopy. As can be seen, modification of the MWCNT electrode with ABA gave rise to a large increase in the electron transfer resistance as a consequence of the electrostatic repulsion between the redox maker and the negatively charged carboxylate groups. Thereafter, surface-confined carboxyl groups were activated with EDC/NHS to form amide bonds with amino terminated aptamer. After aptamer incubation, the R_{ct} decreased in relation to the modification surface with ABA due to reduction of the negative charge density of the electrode surface, as can be observed in Figure 4.2.12 (B). Afterwards, the R_{ct} value diameter of the semicircle increased after each performed step. The addition of a target protein, Cyt *c*, and Cyt *c* Ab to form a complex AptCyt *c* NH_2– Cyt *c* and a sandwich respectively, resulted in a less marked increment of the resistance value due to the augmented quantity of negative charges and to the hindrance caused by the formation of a double layer. After the addition of strept-AuNPs we can observe a further increment of charge transfer resistance because of the increased hindrance due to the formed conjugates. In the second amplification step, the silver enhancement treatment [9, 19], a significant increment of R_{ct} value was also observed and attributable to the silver deposition on gold.

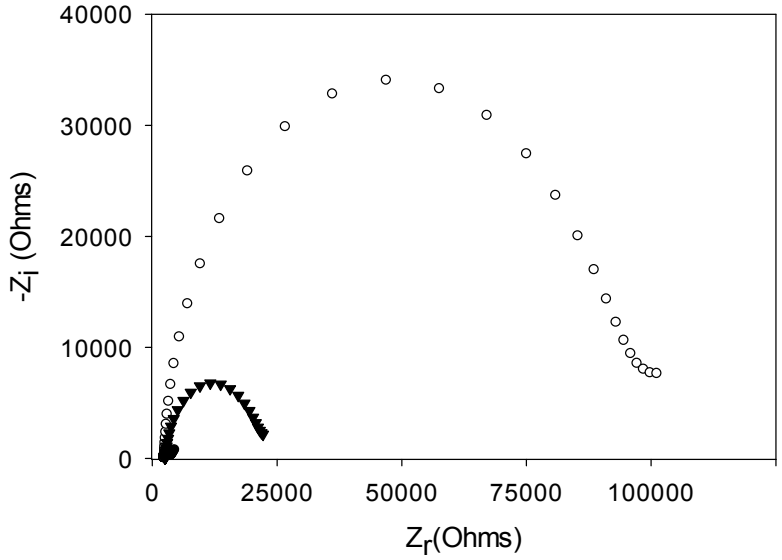

(A)

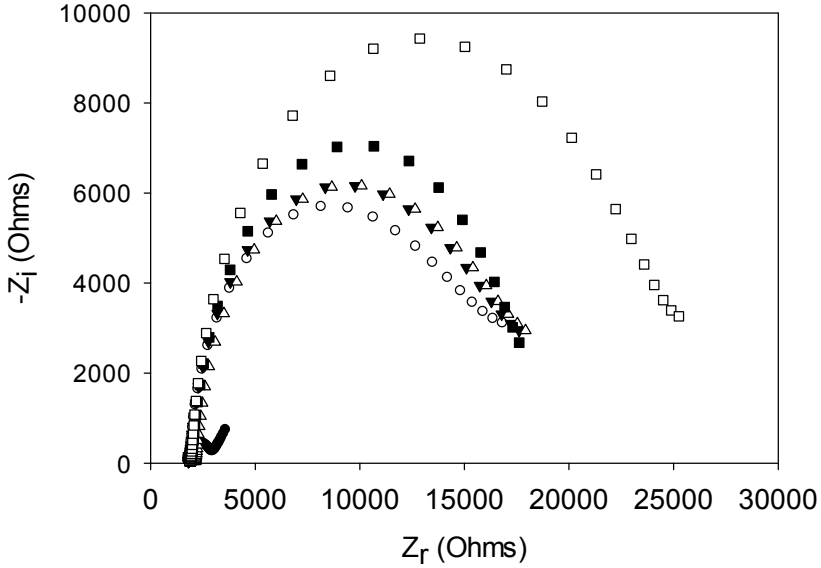

(B)

Figure 4.2.12. (A) Nyquist diagrams of: (●) Bare electrode, (○) Electrochemical grafting treatment and (▼) Aptamer immobilization. (B) Nyquist diagrams of: (●) Bare electrode, (○) aptamer immobilization, (▼) Aptamer with Cyt *c*, (Δ) sandwich complex with antibody, (■) sandwich complex modified with gold-nanoparticles and (□) sandwich complex modified with gold-nanoparticles and silver enhancement treatment. All experiments were performed in PBS solution and all EIS measurements were performed in PBS solution containing 0.01 M $K_3[Fe(CN)_6]$/ $K_4[Fe(CN)_6]$.

-Scanning electron microscope characterization

MWCNT-SPEs surfaces were investigated by SEM after the gold Enhancement treatment. $HAuCl_4$ was employed in order to achieve an adequate amplification of strept-AuNPs present on sensor surface to allow their direct observation by SEM. SEM images taken at an acceleration voltage of 3 kV are shown in Figure 4.2.13, illustrating a positive experiment with sandwich protocol and strep-AuNPs conjugation. As can be observed in Figure 4.2.13 (A), the distribution of gold enhanced-gold nanoparticles is quite homogeneous. This also implies a regular distribution of MWCNT and well-organized formation of sandwich complex onto the electrode surface. This high density distribution also demonstrates the proper functionality of the MWCNT platform and the immobilization of the biomolecule. Comparing this experiment with the negative control that did not use the biotinylated Cyt *c* Ab, Figure 4.2.13 (B), a surface with almost absent nanoparticles can be observed. The curious regular parallelepipedic shapes indicate the monocrystalline growth, and is specially seen for freshly purchased and prepared silver enhancements reagents.

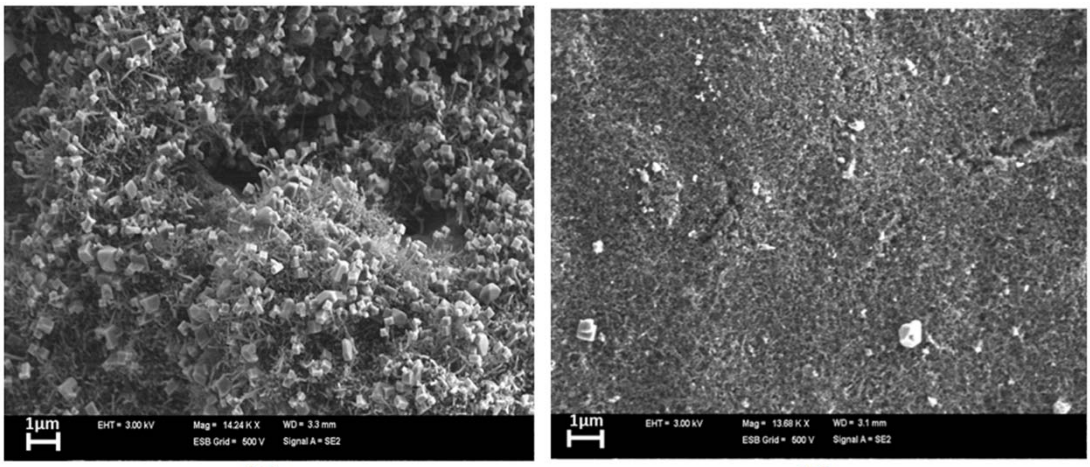

Figure 4.2.13. SEM images of (A) experiment using sanwich complex + strep-AuNPs+ gold enhancement treatment (B) negative control using AptCyt *c* NH_2 + Cyt *c* + non complementary aptamer + strep-AuNPs + gold enhancement treatment. All images were taken at an acceleration voltage of 3 kV and a resolution of 2 µm.

-Analytical performance of the aptamer-antibody sandwich assay for detection of Cyt c

Table 4.2.5. Summary of the different calibration curves considering different stages of the assay.

CALIBRATION CURVE	REGRESSION PLOT	AMPLIFICATION %	RSD *%
(1)AptCyt *c*/Cyt *c*	Δratio = 0.935 + 0.104· log[Cyt *c*]	-	2.3
(2)Sandwich complex	Δratio = 0.904 + 0.144· log[Cyt *c*]	5	3.2
(3)Sandwich/ strep-AuNPs	Δratio = 0.241 + 0.651·log[Cyt *c*]	35	5.9
(4) Sandwich/strep-AuNPs/Silver enhanc.	Δratio = -0.999 + 1.702·log[Cyt *c*]	108	6.8

*Corresponding to five replicated experiments at 75 pM.

After experimental concentration optimizations, the aptasensor was then used following the sandwich protocol, plus amplification employing the strep-AuNPs and silver enhancement treatment. Figure 4.2.14 shows calibration curves with increasing concentrations of Cyt *c* and their respective regression lines in the logaritmic scale, at the different steps of the protocol: (1) AptCyt *c* NH_2–Cyt *c*, (2) sandwich formation between AptCyt *c* NH_2, Cyt *c* and AbCyt *c* , (3) aptamer sandwich modified with strep-AuNPs, and (4) aptamer sandwich modified with strep-AuNPs and silver enhancement treatment. Although reproducibility was not ideal in all cases, the calibration curves obtained showed a good % RSD. As can be seen in Figure 4.2.14 (A), all calibration curves increased until the value of 100 pM of Cyt *c*, this could be due to the fact that concentrations larger than 100 pM caused a saturation on the sensor surface. As can be observed in Table 4.2.5, the use of silver enhancement treatment led to the highest sensitivity and signal amplification, resulting in 108 % increase compared to the simple biosensing scheme. This demonstrates that the silver deposition on gold nanoparticles,

basically increases the sterical hindrance, producing an increment of observed impedance, given this conductive silver is not wired to the electrode surface. Together with the higher sensitivity, the detection limit obtained in this case was 12 pM (calculated as the intersection with the horizontal reference line) and it is slightly improving the one obtained with only strep-AuNPs (15 pM). Without sandwich amplification, signal is of the same magnitude than associated errors, making the assay of impractical use. This results confirmed that the best method, showing a low detection limit and an ultrahigh sensitivity for the detection of Cyt *c* involves the sandwich and amplification protocol.

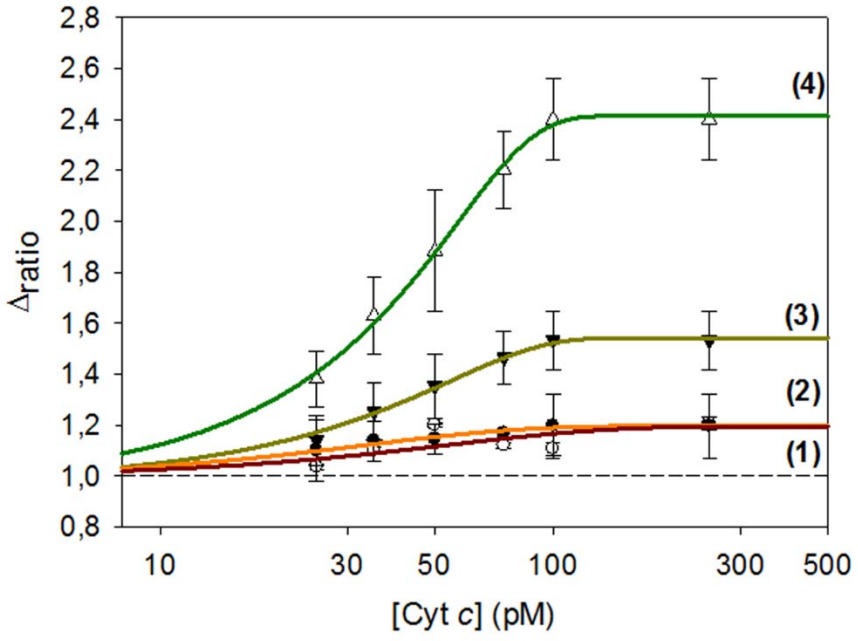

(A)

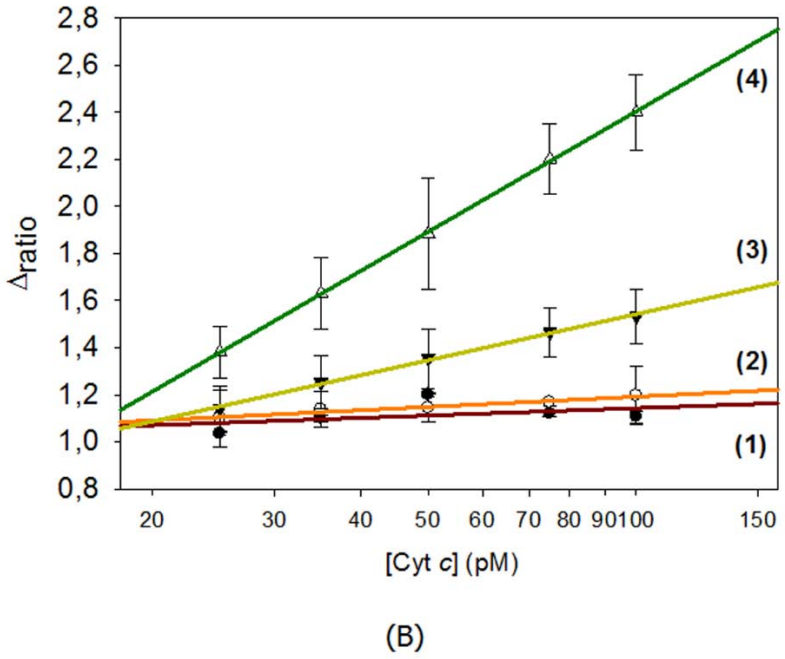

(B)

Figure 4.2.14. Calibration (A) and regression curves (B) of: (1) (black circle) AptCyt *c* NH_2 and Cyt *c*, (2) (white circle) sandwich complex, (3) (black triangle) sandwich complex modified with strep-AuNPs, (4) (white triangle) sandwich complex modified with strep-AuNPs and silver enhancement treatment. All experiments were performed in PBS solution and all EIS measurements were performed in PBS solution containing 0.01M $K_3[Fe(CN)_6]/K_4[Fe(CN)_6]$. Uncertainty values corresponding to replicated experiments (n =5).

-Selectivity of the aptamer-antibody sandwich assay

Control experiments were conducted to investigate the specificity of aptamer-antibody assay. In this work, majority serum proteins, such as human IgG, Fbr and BSA at serum physiological levels were tested to operate the proposed aptasensor instead of Cyt *c* under the same experimental conditions. As shown in Figure 4.2.15, the presence of interfering proteins at serum concentration level exhibits negligible response compared with 100 pM Cyt *c* in the amplified sandwich protocol, even at concentrations four or five orders of magnitude higher than typical Cyt *c* concentrations. Figure 4.2.15 also demonstrates that the sandwich protocol displays as clear advantage, more than

the signal amplification, the marked decrease of interfering effects that are still remarkable in the simple biosensing protocol. This is specially remarkable for IgG protein (human), which shows appreciable interference in the assay without amplification, although it becomes practically negligible with the sandwich variant.

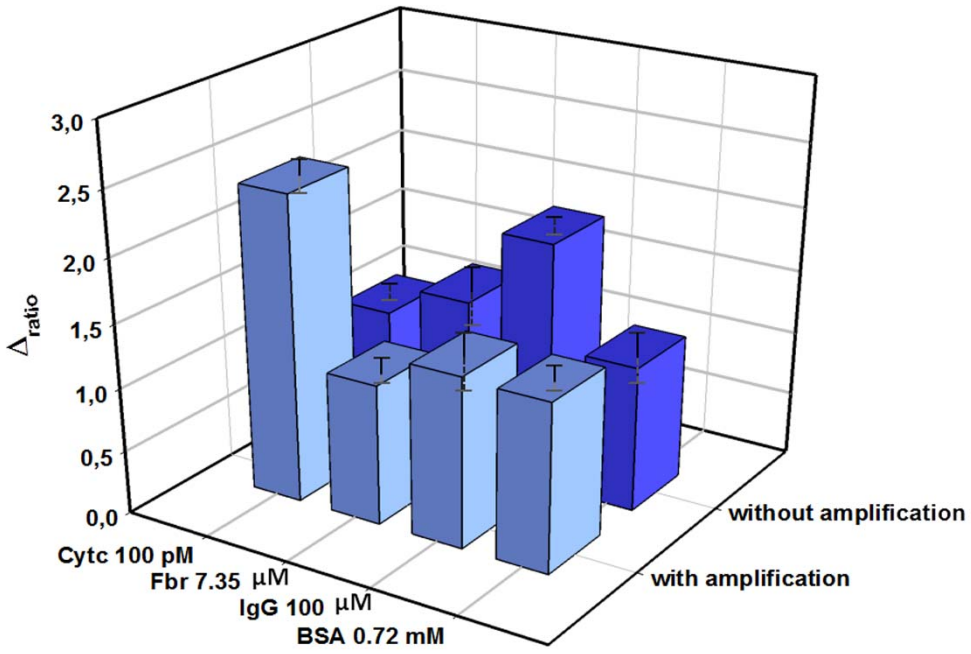

Figure 4.2.15. 3D bar chart of response towards different proteins present in serum, without the amplification protocol and with the sandwich/amplification protocol. Uncertainty values corresponding to replicated experiments (n = 5).

-Detection of Cyt c in spiked serum samples

Table 4.2.6. Recovery studies performed in spiked serum samples for applicability of biosensor.

[Cyt c] spiked (pM)	[Cyt c] found (pM)	% RECOVERY	% RSD*
90.0	97.1 ± 14.7	107.8	8.98
60.0	58.9 ± 9.0	98.3	9.07
30.0	28.4 ± 3.9	94.6	8.23

*Corresponding to triplicated experiments.

The applicability of the biosensor was tested by the analysis of spiked samples of human serum samples. For that purpose, human serum samples were spiked with three different concentrations of Cyt *c*. As shown in Table 4.2.6, the recoveries of spiked samples were between 94.6 % and 107.8 % when using this method, which showed a satisfactory result. In addition, a good reproducibility of the blanks was obtained, 5.5 % RSD. These findings imply that the developed methodology has a promising feature for the analytical application in complex biological samples.

-Comparative study of the developed aptamer-antibody assay with other biosensing methodologies.

Table 4.2.7. Comparison of the Cyt c biosensor with other reported biosensing methods.

ANALYTICAL METHOD	LOD	BIORECOGNITION ELEMENT	LINEAR RANGE	INTERFERENCE	REAL SAMPLES	REF
SPR	≥50 pM	Aptamer	80 pM-80 nM	x	√	[27]
FLUORESCENCE	266 pM	Aptamer	-	x	√	[23]
ICP-MS/TEM	1.5 fM	Antibody	0.1-20 nM	√	√	[25]
EIS	63.2 pM	Aptamer	50 pM-50 nM	√	x	[31]
EIS	12 pM	Aptamer-antibody	25-100 pM	√	√	Our work
CV	10 nM	Enzyme	10 nM - 500 µM	x	√	[32]
CV	0.5 µM	Enzyme	1-1000 µM	√	√	[33]

Once we had confirmed that our biosensor was able to detect Cyt *c* with excellent analytical performance also in real samples, its analytical features were compared to other detection methodologies for Cyt *c* detection, as described in the literature. Details are shown in Table 4.2.7, where sensitivity info is presented as the LOD of each biosensor compared. The lowest detection limit value among all the analytical techniques corresponded to ref [25], but this Cyt *c* biosensor used ICP-MS as the transduction technique. This methodology displays high sensitivity and selectivity but is not simple, portable or easy to use. However, our biosensor showed the second lowest LOD value and it was suitable for real samples, considering that the lowest level of Cyt *c* in serum samples is about 10 pM, and the concentration of this protein increase to nM range when apoptosis occurs.

Different basal levels for Cyt *c* in serum can be found in literature. The LOD of 63.2 pM achieved by label-free aptasensor was compared with 2 nM [5]. Value of 12 pM represents an enhancement of the previous LOD value, which it was obtained by considering around 10 pM as basal level [35]. Despite the use of different basal level values for the evaluation of the LODs in this PhD thesis, both developed values are suitable detection parameters for Cyt *c*, regarding the fact that when apoptosis occurs the level of Cyt *c* in serum increases until nM range [35].

4.3. References

[1] D. Ashe, T. Alleyne, E. Iwuoha, Serum cytochrome c detection using a cytochrome c oxidase biosensor, Biotechnology and Applied Biochemistry 46 (2007) 185-189.

[2] L. Bai, Y. Chai, R. Yuan, Y. Yuan, S. Xie, L. Jiang, Amperometric aptasensor for thrombin detection using enzyme-mediated direct electrochemistry and DNA-based signal amplification strategy, Biosensors and Bioelectronics 50 (2013) 325-330.

[3] Y. Bai, F. Feng, L. Zhao, C. Wang, H. Wang, M. Tian, J. Qin, Y. Duan, X. He, Aptamer/thrombin/aptamer-AuNPs sandwich enhanced surface plasmon resonance sensor for the detection of subnanomolar thrombin, Biosensors and Bioelectronics 47 (2013) 265-270.

[4] A.J. Bard, Faulkner, L. R., Electrochemical Methods: Fundamentals and Applications, Wiley, New York, 2000.

[5] Z. Ben-Ari, H. Schmilovotz-Weiss, A. Belinki, O. Pappo, J. Sulkes, M.G. Neuman, E. Kaganovsky, B. Kfir, R. Tur-Kaspa, T. Klein, Circulating soluble cytochrome c in liver disease as a marker of apoptosis, Journal of Internal Medicine 254 (2003) 168-175.

[6] A. Bonanni, M.J. Esplandiu, M. del Valle, Signal amplification for impedimetric genosensing using gold-streptavidin nanoparticles, Electrochimica Acta 53 (2008) 4022-4029.

[7] A. Bonanni, M.I. Pividori, S. Campoy, J. Barbé, M. del Valle, Impedimetric detection of double-tagged PCR products using novel amplification procedures based on gold nanoparticles and Protein G, Analyst 134 (2009) 602-608.

[8] A. Bonanni, M.I. Pividori, M. del Valle, Application of the avidin-biotin interaction to immobilize DNA in the development of electrochemical impedance genosensors, Analytical Bioanalytical Chemistry 389 (2007) 851-861.

[9] H. Cai, Y.Q. Wang, P.G. He, Y.H. Fang, Electrochemical detection of DNA hybridization based on silver-enhanced gold nanoparticle label, Analytical Chimica Acta 469 (2002) 165-172.

[10] G. Castillo, L. Trnkova, R. Hrdy, T. Hianik, Impedimetric Aptasensor for Thrombin Recognition Based on CD Support, Electroanalysis 24 (2012) 1079-1087.

[11] H. Chen, F. Yuan, S. Wang, J. Xu, Y. Zhang, L. Wang, Aptamer-based sensing for thrombin in red region via fluorescence resonant energy transfer between NaYF4: Yb,Er upconversion nanoparticles and gold nanorods, Biosensors and Bioelectronics 48 (2013) 19-25.

[12] D.J. Chinnapen, D. Sen, Hemin-stimulated docking of cytochrome c to a hemin-DNA aptamer complex, Biochemistry 41 (2002) 5202-5212.

[13] C. Deng, J. Chen, Z. Nie, M. Wang, X. Chu, X. Chen, X. Xiao, C. Lei, S. Yao, Impedimetric Aptasensor with Femtomolar Sensitivity Based on the Enlargement of Surface-Charged Gold Nanoparticles, Analytical Chemistry 81 (2008) 739-745.

[14] H. Fu, C. Ge, W. Cheng, C. Luo, D. Zhang, L. Yan, Y. He, G. Yi, A Hairpin Electrochemical Aptasensor for sensitive and specific detection of thrombin based on homogenous target recognition, Electroanalysis 25 (2013) 1223-1229.

[15] B. Ge, Y.C. Huang, D. Sen, H.Z. Yu, Electrochemical investigation of DNA-modified surfaces: From quantitation methods to experimental conditions, Journal of Electroanalytical Chemistry 602 (2007) 156-162.

[16] S.S. Ghosh, G.F. Musso, Covalent attachment of oligonucleotides to solid supports, Nucleic Acids Research 15 (1987) 5353-5372.

[17] T. Goda, Y. Miyahara, Label-free and reagent-less protein biosensing using aptamer-modified extended-gate field-effect transistors, Biosensors and Bioelectronics 45 (2013) 89-94.

[18] G. Gui, Y. Zhuo, Y.Q. Chai, N. Liao, M. Zhao, J. Han, Q. Zhu, R. Yuan, Y. Xiang, Supersandwich-type electrochemiluminescenct aptasensor based on Ru(phen)3 2+ functionalized hollow gold nanoparticles as signal-amplifying tags, Biosensors and Bioelectronics 47 (2013) 524-529.

[19] H. Hanaee, H. Ghourchian, A.A. Ziaee, Nanoparticle-based electrochemical detection of hepatitis B virus using stripping chronopotentiometry, Analytical Biochemistry 370 (2007) 195-200.

[20] P. Kara, A. de la Escosura-Muñiz, M. Maltez-da Costa, M. Guix, M. Ozsoz, A. Merkoçi, Aptamers based electrochemical biosensor for protein detection using carbon nanotubes platforms, Biosensors and Bioelectronics 26 (2010) 1715-1718.

[21] E. Katz, I. Willner, Probing Biomolecular Interactions at Conductive and Semiconductive Surfaces by Impedance Spectroscopy: Routes to Impedimetric Immunosensors, DNA-Sensors, and Enzyme Biosensors, Electroanalysis 15 (2003) 913-947.

[22] L. Kong, J. Xu, Y. Xu, Y. Xiang, R. Yuan, Y. Chai, A universal and label-free aptasensor for fluorescent detection of ATP and thrombin based on SYBR Green I dye, Biosensors and Bioelectronics 42 (2013) 193-197.

[23] I.P.M. Lau, E.K.S. Ngan, J.F.C. Loo, Y.K. Suen, H.P. Ho, S.K. Kong, Aptamer-based bio-barcode assay for the detection of cytochrome-c released from apoptotic cells, Biochemical and Biophysical Research Communications 395 (2010) 560-564.

[24] A. Lermo, S. Campoy, J. Barbé, S. Hernández, S. Alegret, M.I. Pividori, In situ DNA amplification with magnetic primers for the electrochemical detection of food pathogens, Biosensors and Bioelectronics 22 (2007) 2010-2017.

[25] J.M. Liu, X.P. Yan, Ultrasensitive, selective and simultaneous detection of cytochrome c and insulin based on immunoassay and aptamer-based bioassay in combination with

Au/Ag nanoparticle tagging and ICP-MS detection, Journal of Analytical Atomic Spectrometry 26 (2011) 1191-1197.

[26] A.H. Loo, A. Bonanni, A. Ambrosi, H.L. Poh, M. Pumera, Impedimetric immunoglobulin G immunosensor based on chemically modified graphenes, Nanoscale 4 (2012) 921-925.

[27] F.-C. Loo, S.-P. Ng, C.-M.L. Wu, S.K. Kong, An aptasensor using DNA aptamer and white light common-path SPR spectral interferometry to detect cytochrome-c for anti-cancer drug screening, Sensors and Actuators B: Chemical 198 (2014) 416-423.

[28] N. Meini, C. Farre, C. Chaix, R. Kherrat, S. Dzyadevych, N. Jaffrezic-Renault, A sensitive and selective thrombin impedimetric aptasensor based on tailored aptamers obtained by solid-phase synthesis, Sensors and Actuators, B: Chemical 166-167 (2012) 715-720.

[29] M.A. Mohsin, F.G. Banica, T. Oshima, T. Hianik, Electrochemical impedance spectroscopy for assessing the recognition of cytochrome c by immobilized calixarenes, Electroanalysis 23 (2011) 1229-1235.

[30] M. Moreno-Guzmán, I. Ojeda, R. Villalonga, A. González-Cortés, P. Yáñez-Sedeño, J.M. Pingarrón, Ultrasensitive detection of adrenocorticotropin hormone (ACTH) using disposable phenylboronic-modified electrochemical immunosensors, Biosensors and Bioelectronics 35 (2012) 82-86.

[31] C. Ocaña, E. Arcay, M. Del Valle, Label-free impedimetric aptasensor based on epoxy-graphite electrode for the recognition of cytochrome c, Sensors and Actuators, B: Chemical 191 (2014) 860-865.

[32] M. Pandiaraj, A.R. Benjamin, T. Madasamy, K. Vairamani, A. Arya, N.K. Sethy, K. Bhargava, C. Karunakaran, A cost-effective volume miniaturized and microcontroller based cytochrome c assay, Sensors and Actuators A: Physical 220 (2014) 290-297.

[33] M. Pandiaraj, T. Madasamy, P.N. Gollavilli, M. Balamurugan, S. Kotamraju, V.K. Rao, K. Bhargava, C. Karunakaran, Nanomaterial-based electrochemical biosensors for cytochrome c using cytochrome c reductase, Bioelectrochemistry 91 (2013) 1-7.

[34] C.R.H. Raetz, C. Whitfield, Lipopolysaccharide endotoxins, Annual Review of Biochemistry 71 (2002) 635-700.

[35] I. Sakaida, T. Kimura, T. Yamasaki, Y. Fukumoto, K. Watanabe, M. Aoyama, K. Okita, Cytochrome c is a possible new marker for fulminant hepatitis in humans, Journal of Gastroenterology 40 (2005) 179-185.

[36] W.H. Seegers, L. McCoy, R.K. Kipfer, G. Murano, Preparation and properties of thrombin, Archives of Biochemistry and Biophysics 128 (1968) 194.

[37] J. Shi, J.C. Claussen, E.S. McLamore, A. ul Haque, D. Jaroch, A.R. Diggs, P. Calvo-Marzal, J.L. Rickus, D.M. Porterfield, A comparative study of enzyme immobilization strategies for multi-walled carbon nanotube glucose biosensors, Nanotechnology 22 (2011) 355502.

[38] S. Sivasankar, S. Subramaniam, D. Leckband, Direct molecular level measurements of the electrostatic properties of a protein surface, Proceedings of the National Academy of Sciences 95 (1998) 12961-12966.

[39] A.B.P. Van Kuilenburg, A.C.F. Gorren, H.L. Dekker, P. Nieboer, B.F. Van Gelder, A.O. Muijsers, Presteady-state and steady-state kinetic properties of human cytochrome c oxidase, European Journal of Biochemistry 205 (1992) 1145-1154.

[40] X.Y. Wang, A. Gao, C.C. Lu, X.W. He, X.B. Yin, An electrochemiluminescence aptasensor for thrombin using graphene oxide to immobilize the aptamer and the intercalated Ru(phen)32+ probe, Biosensors and Bioelectronics 48 (2013) 120-125.

[41] E. Williams, M.I. Pividori, A. Merkoçi, R.J. Forster, S. Alegret, Rapid electrochemical genosensor assay using a streptavidin carbon-polymer biocomposite electrode, Biosensors and Bioelectronics 19 (2003) 165-175.

[42] Z. Wu, Y. Liu, X. Zhou, A. Shen, J. Hu, A "turn-off" SERS-based detection platform for ultrasensitive detection of thrombin based on enzymatic assays, Biosensors and Bioelectronics 44 (2013) 10-15.

[43] H. Xu, K. Gorgy, C. Gondran, A. Le Goff, N. Spinelli, C. Lopez, E. Defrancq, S. Cosnier, Label-free impedimetric thrombin sensor based on poly(pyrrole-nitrilotriacetic acid)-aptamer film, Biosensors and Bioelectronics 41 (2013) 90-95.

[44] S. Yamazaki, Z. Siroma, T. Ioroi, K. Tanimoto, K. Yasuda, Evaluation of the number of carboxyl groups on glassy carbon after modification by 3,4-dihydroxybenzylamine, Carbon 45 (2007) 256-262.

[45] F. Yan, F. Wang, Z. Chen, Aptamer-based electrochemical biosensor for label-free voltammetric detection of thrombin and adenosine, Sensors and Actuators B: Chemical 160 (2011) 1380-1385

.

[46] Z. Yan, Z. Han, H. Huang, H. Shen, X. Lu, Rational design of a thrombin electrochemical aptasensor by conjugating two DNA aptamers with G-quadruplex halves, Analytical Biochemistry 442 (2013) 237-240.

[47] X. Yang, A. Wang, J. Liu, A facile label-free electrochemiluminescence biosensor for target protein specific recognition based on the controlled-release delivery system, Talanta 114 (2013) 5-10.

[48] L. Zhang, P. Cui, B. Zhang, F. Gao, Aptamer-based turn-on detection of thrombin in biological fluids based on rfficient phosphorescence energy transfer from Mn-doped ZnS quantum dots to carbon nanodots, Chemistry - A European Journal 19 (2013) 9242-9250.

[49] Z. Zhang, L. Luo, L. Zhu, Y. Ding, D. Deng, Z. Wang, Aptamer-linked biosensor for thrombin based on AuNPs/thionine-graphene nanocomposite, Analyst 138 (2013) 5365-5370.

[50] J. Zheng, W. Feng, L. Lin, F. Zhang, G. Cheng, P. He, Y. Fang, A new amplification strategy for ultrasensitive electrochemical aptasensor with network-like thiocyanuric acid/gold nanoparticles, Biosensors and Bioelectronics 23 (2007) 341-347.

CHAPTER 5. CONCLUSIONS

5. Conclusions

5.1. General conclusions

The general conclusions of this work were:

1. The design and development of impedimetric aptasensors were achieved for the first time in our group, employing different electrodes such as GECs, AvGECs and MWCNT-SPEs, and different protocols for protein detection.

2. Electrochemical Impedance Spectroscopy has demonstrated to be a highly sensitive technique to monitor each step of the different aptasensing protocols, achieving good reproducibility values in all the cases.

3. The use of amplification strategy based on sandwich protocol with aptamer double or aptamer-antibody combinating were developed with success, and gold-nanoparticles and silver enhancement treatment allowed an improvement in impedimetric response, for both the sensitivity and the selectivity of the method.

4. The developed aptasensors based on sandwich protocol were successfully applied for the detection of their respective protein target in spiked serum samples.

5.2. Specific conclusions

In connection with the objectives, the conclusions of this PhD thesis can be divided into two main parts according to the different detected proteins.

A. Impedimetric aptasensors for thrombin detection:

A.1. Four different label-free aptasensors were performed based on different aptamer immobilization technique using GEC electrodes.

A.1.1. With the different methods reported: physical adsorption, avidin-biotin affinity, covalent bond via electrochemical activation and via electrochemical grafting, low detection limits (in the pM level), ample ranges of response for thrombin concentration (more than one decade) and low % RSD values were achieved. Among the four methods proposed, avidin-biotin affinity was the best overall method

displaying high affinity with a sensitivity value of 1.530 10^{10} M^{-1}, a linear range of 0.75–100 pM and a reproducibility of 4.9 % RSD. The lower detection limit attained was 4.5 pM by physical adsorption method, although the latter was also the one with poorer selectivity (highest % CR values).

Considering interfering effects produced by serum proteins, Fbr and IgG demonstrated some effect, which may restrict the utility of the aptasensors; still, given the high concentration values at which they interfere and the low % CR determined (lower than 0.001 %), these interfering effects may be tolerated.

Electrochemical grafting technique exhibited the higher stability compared with the other methodologies, which could retain its impedance response after a storage of eight days with a negligible loss of activity.

In addition, aptasensor based on physical adsorption technique could be regenerated by dissociating the AptThr-Thr complex.

A.1.2. AvGEC electrodes were also successfully used as a platforms for aptasensing and genosensing, achiving excellent results of sensitivity and reproducibility for both cases. The developed genosensor was performed for the detection of enterohaemorragic *Escherichia Coli O104:H4* bacterium.

A.2. An impedimetric aptasensor assay based on a sandwich protocol based on double aptamer sandwich protocol, strep-AuNPs and silver enhancement treatment was carried out.

The use of biotinylated aptamer permitted rapid formation of an easily detected conjugate with a strep-AuNPs and strep-QDs through a streptavidin-biotin interaction.

A.2.1. Signal amplification by using aptamer sandwich, strep-AuNPs and silver enhancement treatment led to a high sensitivity increase, obtaining a detection limit of 0.3 pM. Despite a higher sensitivity, this detection limit is slightly worse than the one obtained with only strep-AuNPs, 0.2 pM. This fact, caused by the deteriorated reproducibility, could be attributable to the increased number of process steps and associated increased potential errors. Besides, for a comparable amount of AptThrBio1-Thr, the signal resulted in 89% amplification, compared to results recorded with simple biosensing label-free assay.

In addition, a good linear range, 0.2 -100 pM, and a good reproducibility value, 9.9 % RSD, were obtained.

A.2.2. Furthermore, high selectivity with respect to different serum proteins and organic compounds at serum concentration level were also attained with this protocol. The results also demonstrated that the sandwich protocol displays a clear advantage, more than the signal amplification, the marked decrease of interfering effects that are still noticeable in the simple biosensing assay and are disappeared with the double recognition protocol.

A.2.3. The aptasensor was evaluated with thrombin spiked serum samples. Good recovery and reproducibility values were obtained, 89 % -102.7 % and 8.1 %-4.5 %, respectively, demonstrating the exceptional performance of the aptasensor and its suitability for the direct analysis of Thr in serum samples at the low pM level.

B. Impedimetric aptasensors for cytochrome c detection

B.1. A label-free aptasensor for Cyt c detection based on a wet physical adsorption immobilization technique using GEC electrodes were carried out.

B.1.1 The aptasensor showed a low detection limit, 63.2 pM, good range of Cyt *c* concentration, from 50 pM to 1 nM, high sensitivity, $5.24 \cdot 10^8$ M^{-1} and good reproducibility, 6.8 % RSD.

Moreover, the Cyt *c* detection process could be finished in 40 minutes and the stability of a prepared sensor was at least 24 hours.

B.1.2. The interference produced by serum proteins, such as IgG, Fbr and BSA, demonstrated some limitations in the operation of the aptasensor, although usable given the concentration excess at which they manifest.

B.2. An ultrasensitive impedance aptamer-antibody sandwich assay for Cyt c detection using MWCNT-SPEs was developed.

B.2.1 Thanks to the signal amplification with strep-AuNPs and silver deposition, it was possible to increase the sensitivity of the assay. Additionally, for a comparable amount of AptCyt *c* NH_2-Cyt *c*, the signal resulted in 108 % amplification, compared to results recorded with simple biosensing assay.

Furthermore, a good detection limit, 12 pM, good reproducibility, 6.8 % RSD, and acceptable linear range, 25-100 pM, were attained with this protocol.

B.2.2 High selectivity with respect to different serum proteins at serum concentration level were also achieved with this protocol thanks to the double recognition scheme utilized.

B.2.3 The suitability of the biosensor for measurements in real samples was checked by determining Cyt *c* in spiked human serum samples. Obtained recovery and reproducibility values in the range between 94.6 to 107.8 % and between 8.2 % to 9.1 % respectively, demonstrated a promising feature for the analytical application in complex biological samples.

5.3. Future perspectives

The results obtained during this PhD thesis open the door to interesting aptasensing field using EIS technique, not only in the detection of proteins, but also in small targets such as toxins, organic compounds, etc.

Additionally, the integration of new nanomaterials such as graphene, nanodiamonds, etc. with the composite conductive paste could improve the sensitivity of our GEC electrodes.

Since the great specialty of our research group is the development of electronic tongues, in a further work, cross response of some aptamers could be used to develop an aptamer electronic tongue using EIS technique.

PUBLICATIONS

Article 1. A reusable impedimetric aptasensor for detection of thrombin employing a graphite-epoxy composite electrode

C. Ocaña, M. Pacios and M. del Valle

Sensors, 2012, 12, 3037-3048.

Sensors **2012**, *12*, 3037-3048; doi:10.3390/s120303037

OPEN ACCESS

sensors

ISSN 1424-8220

www.mdpi.com/journal/sensors

Article

A Reusable Impedimetric Aptasensor for Detection of Thrombin Employing a Graphite-Epoxy Composite Electrode

Cristina Ocaña, Mercè Pacios and Manel del Valle *

Sensors and Biosensors Group, Department of Chemistry, Universitat Autònoma de Barcelona, Bellaterra 08193, Spain; E-Mails: cristina.ocana@uab.es (C.O.); merce.pacios@uab.es (M.P.)

* Author to whom correspondence should be addressed; E-Mail: manel.delvalle@uab.es; Tel.: +34-935-811-017; Fax: +34-935-812-477.

Received: 13 January 2012; in revised form: 15 February 2012 / Accepted: 23 February 2012 / Published: 6 March 2012

Abstract: Here, we report the application of a label-free electrochemical aptasensor based on a graphite-epoxy composite electrode for the detection of thrombin; in this work, aptamers were immobilized onto the electrodes surface using wet physical adsorption. The detection principle is based on the changes of the interfacial properties of the electrode; these were probed in the presence of the reversible redox couple $[Fe(CN)_6]^{3-}/[Fe(CN)_6]^{4-}$ using impedance measurements. The electrode surface was partially blocked due to formation of aptamer-thrombin complex, resulting in an increase of the interfacial electron-transfer resistance detected by Electrochemical Impedance Spectroscopy (EIS). The aptasensor showed a linear response for thrombin in the range of 7.5 pM to 75 pM and a detection limit of 4.5 pM. The aptasensor was regenerated by breaking the complex formed between the aptamer and thrombin using 2.0 M NaCl solution at 42 °C, showing its operation for different cycles. The interference response caused by main proteins in serum has been characterized.

Keywords: aptamer; thrombin; electrochemical impedance spectroscopy; labeless; adsorption

---

1. Introduction

Aptamers are artificial DNA or RNA oligonucleotides selected *in vitro* which have the ability to bind to proteins, small molecules or even whole cells, recognizing their target with affinities and specificities often matching or even exceeding those of antibodies [1]. Furthermore, the recognition process can be inverted and is stable in broad terms. Due to all these properties, aptamers can be used in a wide range of applications, such as therapeutics [2], molecular switches [3], drug development [4], affinity chromatography [5] and biosensors [6].

One of the most known and used aptamers is selective to thrombin, with the sequence 5'-GGTTGGTGTGGTTGG-3'. Thrombin is the last enzyme protease involved in the coagulation cascade, and converts fibrinogen to insoluble fibrin which forms the fibrin gel, both in physiological conditions and in a pathological thrombus [7]. Therefore, thrombin plays a central role in a number of cardiovascular diseases [8], and it is thought to regulate many processes such as inflammation and tissue repair at the blood vessel wall. Concentration levels of thrombin in blood are very low, and levels down to picomolar range are associated with disease; because of this, it is important to be able to assess this protein concentration at trace level, with high selectivity [9].

In previous years, there has been great interest in the development of aptasensors. Aptasensors are biosensors that use aptamers as the biorecognition element. Different transduction techniques such as optical [10], Atomic Force Microscope [11], electrochemical [12] and piezoelectric [13] variants have been reported. Recently, among the different electrochemical techniques available, the use of Electrochemical Impedance Spectroscopy (EIS) [14] has grown among studies [15,16]. EIS is rapidly developing as a reference technique for the investigation of bulk and interfacial electrical properties of any kind of solid or liquid material which is connected to or part of an appropriate electrochemical transducer. Impedance is a simple, high-sensitivity, low-cost and rapid transduction principle to follow biosensing events that take place at the surface of an electrode [17–19]. Moreover, apart from the detection of the recognition event when an immobilized molecule interacts with its target analyte, EIS can be used to monitor and validate the different sensing stages, including preparation of biosensor. Together with Surface Plasmon Resonance and the Quartz Crystal Microbalance, EIS is one of the typical transduction techniques that do not require labelled species for detection.

In the present communication, we report the application a label-free electrochemical aptasensor for the detection of thrombin using graphite-epoxy composite electrodes (GEC). This platform is of general use in our laboratories and has been already extensively studied and applied for amperometric, enzymatic, immuno- and genosensing assays [20,21]. The uneven surface of the graphite-epoxy electrode allows the immobilization of the aptamer onto its surface by simple wet physical adsorption. Afterwards, the electrode surface may be renewed after each experiment by polishing with abrasive paper. The transduction principle used is based on the change of electron-transfer resistance in the presence of the $[Fe(CN)_6]^{3-}/[Fe(CN)_6]^{4-}$ redox couple, which can be measured by EIS. The proposed aptasensor showed appropriate response behaviour values to determine thrombin in the picomolar range. Moreover, this proposed method has some advantages such as high sensitivity, simple instrumentation, low production cost, fast response, portability and what's more, the biosensor has been shown to be easily regenerated by wet procedures.

2. Experimental

2.1. Chemicals

Potassium ferricyanide $K_3[Fe(CN)_6]$, potassium ferrocyanide $K_4[Fe(CN)_6]$, potassium dihydrogen phosphate, sodium monophosphate and the target protein thrombin (Thr), were purchased from Sigma (St. Louis, MO, USA). Poly(ethylene glycol) (PEG), sodium chloride and potassium chloride were purchased from Fluka (Buchs, Switzerland). All reagents were analytical reagent grade. All-solid-state electrodes (GECs) were prepared using 50 μm particle size graphite powder (Merck, Darmstadt, Germany) and Epotek H77 resin and its corresponding hardener (both from Epoxy Technology, Billerica, MA, USA). The aptamer (AptThr) used in this study, with sequence 5'-GGTTGGTGTGGTTGG-3', was prepared by TIB-MOLBIOL (Berlin, Germany). All solutions were made up using MilliQ water from MilliQ System (Millipore, Billerica, MA, USA). The buffer employed was PBS (187 mM NaCl, 2.7 mM KCl, 8.1 mM $Na_2HPO_4{\cdot}2H_2O$, 1.76 mM KH_2PO_4, pH 7.0). Stock solutions of aptamer and thrombin were diluted with sterilized and deionised water, separated in fractions and stored at −20 °C until used.

2.2. Apparatus

AC impedance measurements were performed with an IM6e Impedance Measurement Unit (BAS-Zahner, Kronach, Germany) and Autolab PGStat 20 (Metrohm Autolab B.V, Utrecht, The Netherlands). Thales (BAS-Zahner) and Fra (Metrohm Autolab) software, respectively, were used for data acquisition and control of the experiments. A three electrode configuration was used to perform the impedance measurements: a platinum-ring auxiliary electrode (Crison 52–67 1, Barcelona, Spain), an Ag/AgCl reference electrode and the constructed GEC as the working electrode. Temperature-controlled incubations were done using an Eppendorf Thermomixer 5436.

2.3. Preparation of Working Electrodes

Graphite epoxy composite (GEC) electrodes used were prepared using a PVC tube body (6 mm i.d.) and a small copper disk soldered at the end of an electrical connector, as shown on Figure 1(a). The working surface is an epoxy-graphite conductive composite, formed by a mixture of graphite (20%) and epoxy resin (80%), deposited on the cavity of the plastic body [15,16]. The composite material was cured at 80 °C for 3 days. Before each use, the electrode surface was moistened with MilliQ water and then thoroughly smoothed with abrasive sandpaper and finally with alumina paper (polishing strips 301044-001, Orion) in order to obtain a reproducible electrochemical surface.

2.4. Procedure

The analytical procedure for biosensing consists of the immobilization of the aptamer onto the transducer surface using a wet physical adsorption procedure, followed by the recognition of the thrombin protein by the aptamer via incubation at room temperature. The scheme of the experimental procedure is represented in Figure 1(b), with the steps described in more detail below.

Figure 1. (**a**) Scheme of the manufacture of graphite-epoxy composite electrodes, (**b**) Steps of the biosensing procedure.

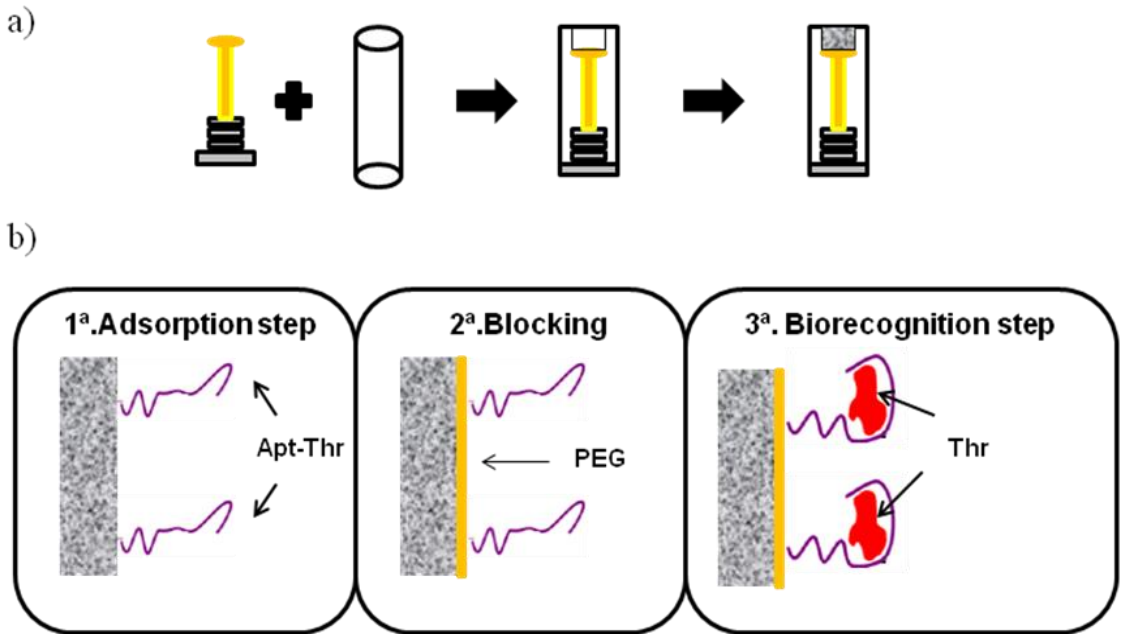

2.4.1. Aptamer Adsorption

First, 160 µL of aptamer solution in MilliQ water at the desired concentration was heated at 80–90 °C for 3 min to promote the loose conformation of the aptamer. Then, the solution was dipped in a bath of cold water and the electrode was immersed in it, where the adsorption took place at room temperature for 15 min with soft stirring. Finally, this was followed by two washing steps using PBS buffer solution for 10 min at room temperature, in order to remove unadsorbed aptamer.

2.4.2. Blocking

After aptamer immobilisation, the electrode was dipped in 160 µL of PEG 40 mM for 15 min at room temperature with soft stirring to minimize any possible nonspecific adsorption. This was followed by two washing steps using PBS buffer solution for 10 min.

2.4.3. Label-Free Detection of Thrombin

The last step is the recognition of thrombin by the immobilized aptamer. For this, the electrode was dipped in a solution with the desired concentration of thrombin. The incubation took place for 15 min at room temperature with soft stirring. After that, the biosensor was washed twice with PBS buffer solution for 10 min at room temperature to remove nonspecific adsorption of protein.

2.4.4. Regeneration of Aptasensor

Finally, to regenerate the aptasensor, the aptamer-thrombin complex must be broken. For this, the electrode was dipped in a 2 M NaCl, heated at 42 °C while stirring for 20 min. Afterwards, the electrode was washed twice with PBS buffer solution for 10 min.

2.5. Impedimetric Measurements

Impedimetric measurements were performed in 0.01 mM $[Fe(CN)_6]^{3-/4-}$ solution prepared in PBS at pH 7. The electrodes were dipped in this solution and a potential of +0.17 V (*vs.* Ag/AgCl) was applied. Frequency was scanned from 10 kHz to 50 mHz with a fixed AC amplitude of 10 mV. The impedance spectra were plotted in the form of complex plane diagrams (Nyquist plots, $-Z_{im}$ *vs.* Z_{re}) and fitted to a theoretical curve corresponding to the equivalent circuit with Z_{view} software (Scribner Associates Inc., USA). In the equivalent circuit shown in Figure 2, the parameter R_1 corresponds to the resistance of the solution, R_2 is the charge transfer resistance (also called R_{ct}) between the solution and the electrode surface, whilst CPE is associated with the double-layer capacitance (due to the interface between the electrode surface and the solution). The use of a constant phase element (CPE) instead of a capacitor is required to optimize the fit to the experimental data, and this is due to the nonideal nature of the electrode surface [14]. The parameters of interest in our case are the electron-transfer resistance (R_{ct}) and the chi-square (χ^2). The first one was used to monitor the electrode surface changes, while χ^2 was used to measure the goodness of fit of the model. In all cases the calculated values for each circuit were <0.2, much lower than the tabulated value for 50 degrees of freedom (67.505 at 95% confidence level). In order to compare the results obtained from the different electrodes used, and to obtain independent and reproducible results, relative signals are needed [16]. Thus, the Δ_{ratio} value was defined according to the following equations:

$$\Delta_{ratio} = \Delta_s / \Delta_p$$

$$\Delta_s = R_{ct\ (AptThr\text{-}Thr)} - R_{ct\ (electrode\text{-}buffer)}$$

$$\Delta_p = R_{ct\ (AptThr)} - R_{ct\ (electrode\text{-}buffer)}$$

where $R_{ct(AptThr\text{-}Thr)}$ was the electron transfer resistance value measured after incubation with the thrombin protein; $R_{ct\ (AptThr)}$ was the electron transfer resistance value measured after aptamer inmobilitation on the electrode, and $R_{ct\ (electrode\text{-}buffer)}$ was the electron transfer resistance of the blank electrode and buffer.

Figure 2. Equivalent circuit used for the data fitting. R_1 is the resistance of the solution, R_2 is the electron-transfer resistance and CPE, the capacitive contribution, in this case as a constant phase element.

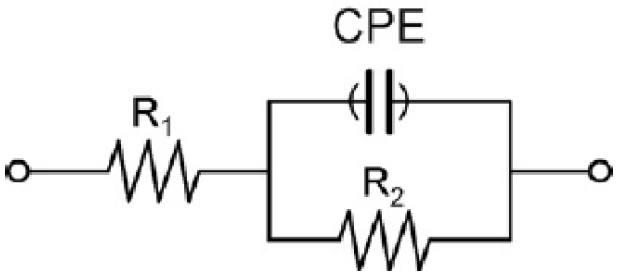

3. Results and Discussions

3.1. Optimization of Electrode Surface

First of all, the concentration of aptamer and PEG immobilized onto the electrode surface were optimized separately by building its response curves. For this, increasing concentrations of AptThr and PEG were used to carry out the immobilization, evaluating the changes in the Δ_p.

Figure 3 shows the curve of AptThr adsorption onto the electrode surface. It can be observed that the difference in resistance (Δ_p) increased up to a value. This is due to the physical adsorption of the aptamer onto the electrode surface, which followed a Langmuir isotherm; in it, the variation of R_{ct} increases to reach a saturation value, chosen as the optimal concentration. This value corresponded to a concentration of aptamer of 1 μM.

Figure 3. Optimization of the concentration of Apt-Thr. Uncertainty values corresponding to replicated experiments (n = 5).

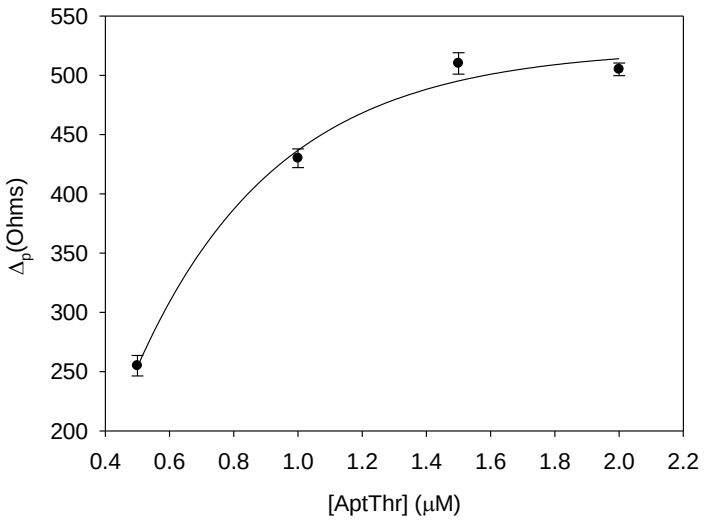

Figure 4. Optimization of the concentration of the blocking agent, PEG. Uncertainty values corresponding to replicated experiments (n = 5).

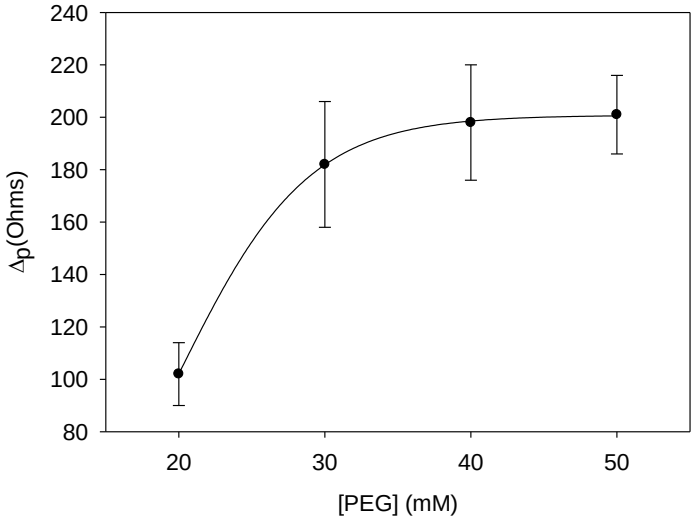

To minimize any possible nonspecific adsorption onto the electrode surface, polyethylene glycol (PEG) was used as the blocking agent. As shown in Figure 4, and like the previous case, there was an increase in resistance until the value of 40 mM of PEG where the saturation value is reached. Therefore, the optimal concentration of blocking agent was chosen as 40 mM.

3.2. Detection of Thrombin

With the optimized concentrations of aptamer and PEG and following the above experimental protocol for the detection of thrombin, the aptasensor response was initially evaluated. The aptamer of thrombin forms a single-strand oligonucleotide, a chain that recognizes the protein by a three-dimensional folding (quadriplex). During this folding, weak interactions between the aptamer and protein of the host-guest type are created, leading to complex AptThr-Thr [22]. One example of the obtained response after each biosensing step is shown in Figure 5. As can be seen, resistance R_{ct} between the electrode surface and the solution is increased. This fact is due to the effect on the kinetics of the electron transfer redox marker $[Fe(CN)_6]^{3-}/[Fe(CN)_6]^{4-}$ which is delayed at the interface of the electrode, mainly caused by steric hindrance and electrostatic repulsion presented by the complex formed.

Figure 5. Nyquist Diagram of: (**a**) Electrode-buffer ●, (**b**) Aptamer of thrombin (AptThr) ●, and (**c**) AptThr-Thr ○ 10 pM [Thr]. The arrow in each spectrum denotes the frequency (AC) of 10.9 Hz.

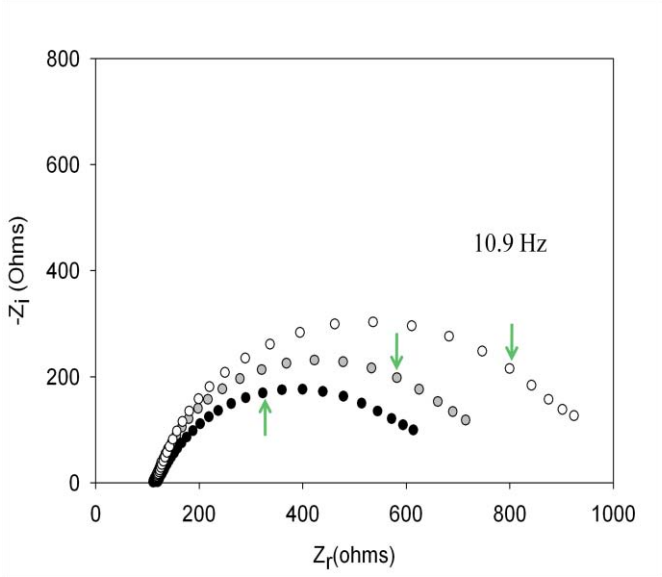

Performing new experiments with solutions containing different amount of thrombin, the calibration curve was built. Figure 6 shows the evolution of the Nyquist diagrams for the calibration of the aptasensor. There is a correct recognition of the protein by the aptamer; as by increasing thrombin concentration, the interfacial electron transfer resistance between the electrode surface and solution also increases, until reaching saturation. To evaluate the linear range and detection limit of the AptThr-Thr system, the calibration curve was built, representing the analytical signal expressed as Δ_{ratio} *vs.* the protein concentration (Figure 7). As can be seen, a sigmoidal trend is obtained, where the central area could be approximated to a straight line, with a linear range from 7.5 pM to 75 pM

for the protein. Moreover, a good linear relationship (r^2 = 0.9981) between the analytical signal (Δ_{ratio}) and the thrombin concentration in this range was obtained, according to the equation: Δ_{ratio} = 1.013 + 1.106 × 10^{10} [Thr]. The EC_{50} was estimated as 44 pM and the detection limit, calculated as three times the standard deviation of the intercept obtained from the linear regression, was 4.5 pM. The reproducibility of the method showed a relative standard deviation (RSD) of 7.2%, obtained from a series of 5 experiments carried out in a concentration of 75 pM Thr. These are satisfactory results for the detection of thrombin in real samples, given this level is exactly the concentration threshold when forming thrombus [9].

Figure 6. Nyquist diagrams for different concentrations of thrombin. ● Electrode-buffer, ○ AptThr, ▼ 1 × 10^{-12} M [Thr], Δ 2.5 × 10^{-12} M [Thr], ■ 5.5 × 10^{-12} M [Thr], □ 7.5 × 10^{-12} M [Thr], ◆ 1 × 10^{-11} M [Thr], ◊ 5 × 10^{-11} M [Thr], ▲ 7.5 × 10^{-11} M [Thr], ∇ 1 × 10^{-10} M [Thr]. The arrow in each spectrum denotes the frequency (AC) of 10.9 Hz.

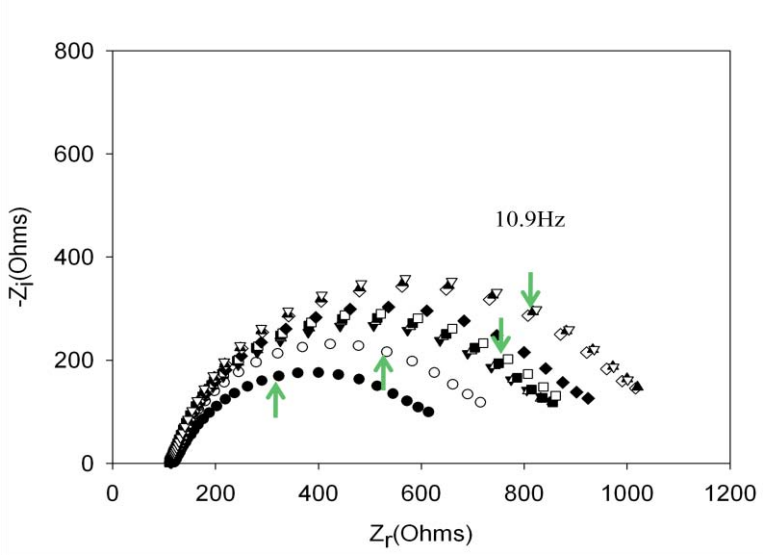

Figure 7. Calibration curve *vs.* thrombin concentration. ($\Delta_{ratio} = \Delta_s / \Delta_p$; $\Delta_s = R_{ct(\ AptThr\text{-}Thr)} - R_{ct\ (electrode\text{-}buffer)}$; $\Delta_p = R_{ct\ (AptThr)} - R_{ct(electrode\text{-}buffer)}$).

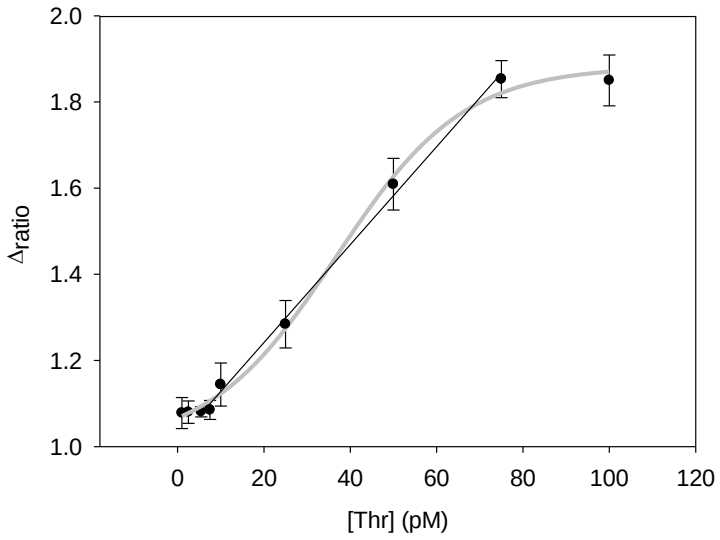

3.3. Selectivity of Aptasensor

Thrombin is present in blood serum, a complex sample matrix, with hormones, lipids, blood cells and other proteins [23]. To study the selectivity of the system, we evaluated the response of proteins typically present in serum such as fibrinogen, immunoglobulin G and albumin. In the first case, we tested albumin protein, which is found in serum at a level from 3,500 to 5,000 mg/dL [24], representing more than 60% of the total protein present. To perform the test, the highest concentration in serum was used, that is 5,000 mg /dL. When the aptamer was incubated with this protein, electron interfacial resistance did not increase, in this case it was observed a slight decrease. Afterwards, when the aptamer was incubated with thrombin, an increase in the resistance, and of expected magnitude, was observed. Therefore, it was proved that albumin was not recognized by the AptThr, and it did not interfere with aptamer-thrombin system.

In the second case, fibrinogen was evaluated as an interfering protein. Fibrinogen is a fibrillar protein involved in the blood clotting process. By the action of thrombin, fibrin is degraded and results in the formation of a clot [25]. This protein is present in human serum in a concentration range of 200 to 400 mg/dL [26]. It was observed that the electron interfacial resistance increased as a result of some type of recognition by the AptThr. Therefore, this protein could act as an interference for the system.

In the last case, generic immunoglobulin G (IgG) was used. IgG is a globular protein that is synthesized in response to the invasion of any bacteria, virus or fungi. It is present in human serum over a range of concentrations from 950 mg/dL to 1,550 mg/dL in serum, with a normal value of 1,250 mg/dL. IgG also acted as interferent, which is proved from the increase of the resistance R_{ct}. This increase, as it also happened in the case of fibrinogen, may be due to some biological interaction between the aptamer and these proteins, not yet described. In the last two cases, the addition of thrombin to the system increased the interfacial resistance between the electrode and the surface; this fact could be due to some phenomenon of partial displacement between thrombin and protein interferents that could take place.

Table 1. Summary of calibration results for thrombin and other major proteins presents in serum.

Protein	Regression Line	Sensitivity (M^{-1})	Detection limit	Typical conc. in serum
Thr	$\Delta_{ratio} = 1.013 + 1.106 \times 10^{10}$ [Thr]	1.106×10^{10}	4.5 pM	0
Fbr	$\Delta_{ratio} = 1.007 + 3.698 \times 10^{5}$ [Fbr]	3.698×10^{5}	2 μM	6–12 μM
IgG	$\Delta_{ratio} = 1.424 + 2.385 \times 10^{4}$ [IgG]	2.385×10^{4}	10 μM	60–100 μM
Albumin	No response	–	–	0.52–0.75 mM

To evaluate the sensitivity of the aptasensor we compared the calibration plots for the different proteins. Table 1 summarizes the parameters of the calibration curve of each protein and thrombin, as well as their respectives slopes and detection limits. The aptasensor showed the highest sensitivity for its target molecule, thrombin, with its slope being 6 orders of magnitude greater than the slope for IgG and five orders of magnitude more than the one for fibrinogen, as shown in Figure 8. Therefore, it was demostrated that the aptasensor showed a much higher sensitivity to Thr, regarding potential interfering proteins, which displayed this effect due to the high level of concentration in which they are present.

Figure 8. Response to proteins evaluated: IgG (●), Fbr (○) and Thr (▼).

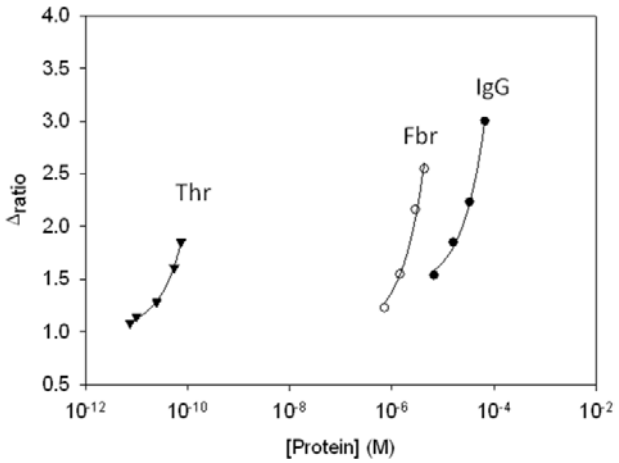

3.4. Regeneration of Aptasensor

Finally, it was possible to regenerate the aptasensor by dissociating the AptThr-Thr complex, formed by weak interactions. It was achieved by stirring the aptasensor in saline media and increasing the temperature (42 °C). In this way, to show regeneration, three sensing cycles were performed with a blank measure in between each. Thrombin was added to the media and an increase of R_{ct} due to complex formation AptThr-Thr was recorded. Then, by adding a saline buffer, increasing the temperature and stirring, the complex dissociated and resistance decreased to the baseline value of the correspondent (AptThr), and so on. Values were calculated as Δ_{ratio} on every step of the process and represented in the bar chart as shown in Figure 9. In the third incubation with Thr, Δ_{ratio} was increased more than in the other incubations, this was because it was incubated with a higher concentration. This type of regeneration may be an alternative to the polishing surface renewal, a typical feature of graphite-epoxy composite electrodes; an important advantage is that it regenerates the electrode surface without removing the immobilized aptamer on the electrode surface, which means that their use is largely facilitated and that cost of each analysis is reduced drastically.

Figure 9. Signals obtained for three consecutive processes of regeneration. [Thr] used: 7.5 pM (1 and 2), and 75 pM (3). Uncertainty values corresponding to replicated experiments (n = 3).

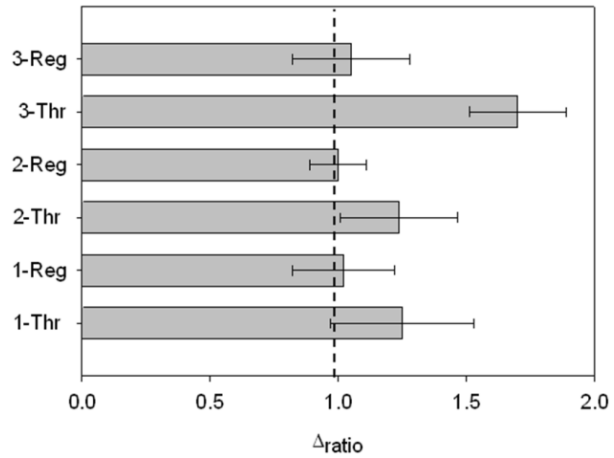

4. Conclusions

In conclusion, this work reports a simple, label-free and reusable aptasensor for detection of thrombin. The immobilized aptamer retained its bioactivity and could be used for recognition of the target substrate. The aptamer immobilization step or the recognition event modified the electron transfer kinetics of the redox probe at the electrode interface, which was examined by EIS.

The described aptasensor, based on physical adsorption of the aptamer, showed a low detection limit, good range of concentration for thrombin detection and high sensitivity. The interference produced by serum proteins, fibrinogen and immunoglobulin G, not described before, showed some limitations in the operation of the aptasensor, although usable given the concentration excess at which they manifest. In addition, the aptasensor can be regenerated by dissociating the complex formed between the aptamer and thrombin protein .This fact presents an alternative to polishing regeneration and reduces the cost of analysis.

Acknowledgements

Financial support for this work has been provided by the Ministry of Science and Innovation (MICINN, Madrid, Spain) through project CTQ2010-17099 and by the Catalonia program ICREA Academia. Cristina Ocaña thanks the support of Ministry of Science and Innovation (MICINN, Madrid, Spain) for the predoctoral grant.

References

1. Nimjee, S.M.; Rusconi, C.P.; Sullenger, B.A. Aptamers: An emerging class of therapeutics. *Annu. Rev. Med.* **2005**, *56*, 555-583.
2. Biesecker, G.; Dihel, L.; Enney, K.; Bendele, R.A. Derivation of RNA aptamer inhibitors of human complement C5. *Immunopharmacology* **1999**, *42*, 219-230.
3. Werstuck, G.; Green, M.R. Controlling gene expression in living cells through small molecule-RNA interactions. *Science* **1998**, *282*, 296-298.
4. Zhang, Y.; Hong, H.; Cai, W. Tumor-targeted drug delivery with Aptamers. *Curr. Med. Chem.* **2011**, *18*, 4185-4194.
5. Deng, Q.; German, I.; Buchanan, D.; Kennedy, R.T. Retention and separation of adenosine and analogues by affinity chromatography with an aptamer stationary phase. *Anal. Chem.* **2001**, *73*, 5415-5421.
6. Mir, M.; Vreeke, M.; Katakis, L., Different strategies to develop an electrochemical thrombin aptasensor. *Electrochem. Commun.* **2006**, *8*, 505-511.
7. Holland, C.A.; Henry, A.T.; Whinna, H.C.; Church, F.C. Effect of oligodeoxynucleotide thrombin aptamer on thrombin inhibition by heparin cofactor II and antithrombin. *FEBS Lett.* **2000**, *484*, 87-91.
8. Burgering, M.J.M.; Orbons, L.P.M.; van der Doelen, A.; Mulders, J.; Theunissen, H.J.M.; Grootenhuis, P.D.J.; Bode, W.; Huber, R.; Stubbs, M.T. The second Kunitz domain of human tissue factor pathway inhibitor: Cloning, structure determination and interaction with factor Xa. *J. Mol. Biol.* **1997**, *269*, 395-407.

9. Centi, S.; Tombelli, S.; Minunni, M.; Mascini, M. Aptamer-based detection of plasma proteins by an electrochemical assay coupled to magnetic beads. *Anal. Chem.* **2007**, *79*, 1466-1473.
10. Pavlov, V.; Xiao, Y.; Shlyahovsky, B.; Willner, I., Aptamer-functionalized Au nanoparticles for the amplified optical detection of thrombin. *J. Am. Chem. Soc.* **2004**, *126*, 11768-11769.
11. Basnar, B.; Elnathan, R.; Willner, I. Following aptamer-thrombin binding by force measurements. *Anal. Chem.* **2006**, *78*, 3638-3642.
12. Radi, A.E.; Sanchez, J.L.A.; Baldrich, E.; O'Sullivan, C.K. Reusable impedimetric aptasensor. *Anal. Chem.* **2005**, *77*, 6320-6323.
13. Pavlov, V.; Shlyahovsky, B.; Willner, I. Fluorescence detection of DNA by the catalytic activation of an Aptamer/Thrombin complex. *J. Am. Chem. Soc.* **2005**, *127*, 6522-6523.
14. Macdonald, J.R. Impedance Spectroscopy. In *Encyclopedia of Physical Science and Technology*, 3rd ed.; Robert, A.M., Ed.; Academic Press: New York, NY, USA, 2003; pp. 703-715.
15. Bonanni, A.; Pividori, M.; del Valle, M. Application of the avidin-biotin interaction to immobilize DNA in the development of electrochemical impedance genosensors. *Anal. Bioanal. Chem.* **2007**, *389*, 851-861.
16. Bonanni, A.; Esplandiu, M.J.; Pividori, M.I.; Alegret, S.; del Valle, M. Impedimetric genosensors for the detection of DNA hybridization. *Anal. Bioanal. Chem.* **2006**, *385*, 1195-1201.
17. Lisdat, F.; Schäfer, D. The use of electrochemical impedance spectroscopy for biosensing. *Anal. Bioanal. Chem.* **2008**, *391*, 1555-1567.
18. Patolsky, F.; Filanovsky, B.; Katz, E.; Willner, I. Photoswitchable antigen-antibody interactions studied by impedance spectroscopy. *J. Phys. Chem. B* **1998**, *102*, 10359-10367.
19. Loo, A.H.; Bonanni, A.; Pumera, M. Impedimetric thrombin aptasensor based on chemically modified graphenes. *Nanoscale* **2012**, *4*, 143-147.
20. Merkoçi, A.; Aldavert, .; ar n , S.; Alegret, S. New materials for electrochemical sensing V: Nanoparticles for DNA labeling. *TrAC Trends Anal. Chem.* **2005**, *24*, 341-349.
21. Pumera, M.; Aldavert, M.; Mills, C.; Merkoci, A.; Alegret, S. Direct voltammetric determination of gold nanoparticles using graphite-epoxy composite electrode. *Electrochim. Acta* **2005**, *50*, 3702-3707.
22. Fan, Y.; Wang, J.; Yang, S.; Yang, X.; Zhang, L.N.; Hua, Z.C.; Zhu, D.X. Molecular dynamics simulation of docking a novel hirudin-like anti-coagulant protein to thrombin. *Prog. Biochem. Biophys.* **2001**, *28*, 86-89.
23. Seegers, W.H.; McCoy, L.; Kipfer, R.K.; Murano, G. Preparation and properties of thrombin. *Arch. Biochem. Biophys.* **1968**, *128*, 194-201.
24. Tamion, F. Albumin in sepsis. *Ann. Fr. Anest. Reanim.* **2010**, *29*, 629-634.
25. Houssay, B.A.; Houssay, A.B.; Cingolani, H.E. *Fisiolog á humana de Bernardo A. Houssay*; El Ateneo: Buenos Aires, Argentina, 1988; Volume 6.
26. Blombäck, B.; Carlsson, K.; Fatah, K.; Hessel, B.; Procyk, R. Fibrin in human plasma: Gel architectures governed by rate and nature of fibrinogen activation. *Thromb. Res.* **1994**, *75*, 521-538.

© 2012 by the authors; licensee MDPI, Basel, Switzerland. This article is an open access article distributed under the terms and conditions of the Creative Commons Attribution license (http://creativecommons.org/licenses/by/3.0/).

Article 2. A comparison of four protocols for the immobilization of an aptamer on graphite-epoxy composite electrode

C. Ocaña and M. del Valle

Microchimica Acta, 2014, 181, 355-363.

Microchim Acta (2014) 181:355–363
DOI 10.1007/s00604-013-1126-0

ORIGINAL PAPER

A comparison of four protocols for the immobilization of an aptamer on graphite composite electrodes

Cristina Ocaña · Manel del Valle

Received: 24 July 2013 / Accepted: 27 October 2013 / Published online: 14 November 2013
© Springer-Verlag Wien 2013

Abstract We have performed a comparative study on four protocols for the immobilization of the thrombin aptamer on a graphite-epoxy composite electrode with the aim to identify the most practical method for designing the corresponding impedimetric aptasensor. The protocols included (a) physical adsorption, (b) avidin-biotin affinity interaction, (c) electrochemical activation and covalent bonding via amide groups, and (d) electrochemical grafting using 4-carboxybenzenediazonium coupling. The properties of the sensing surface were probed by electrochemical impedance measurements in the presence of the (ferri/ferro)hexacyanide redox couple. An increase in the interfacial charge transfer resistance (R_{ct}) was noted in all cases after the aptamer-thrombin interaction had occurred. The selectivity of the aptasensor over common serum proteins was also systematically investigated. Physical adsorption resulted in the lowest detection limit of the probe (4.5 pM), while avidin-biotin interaction resulted in highest selectivity and reproducibility exhibiting a 4.9 % relative standard deviation at pM thrombin concentration levels.

Keywords Aptamer · Thrombin · Electrochemical impedance spectroscopy · Immobilization · Label-free

Introduction

Cardiovascular diseases are leading cause of death worldwide. Every year more people die from these diseases than from any other causes [1]. In these diseases thrombin (Thr) plays a central role. Thr is the last protease enzyme involved in the coagulation cascade and converts fibrinogen to fibrin in blood coagulation [2]. The precursor of Thr is the inactive zymogen prothrombin. This protein is synthesized in the liver and secreted into blood circulation, and it is activated by vascular injury by limited proteolysis following upstream activation of the coagulation cascade. Thrombin activity is regulated by serum inhibitors and by its own action. With procoagulant and anticoagulant functions, it plays a central role in thrombosis and haemostasis, and it is an agonist for a number of cellular responses during inflammation and wound repair. Many diseases including stroke and myocardial infarction involve thrombosis [3]. Concentration levels of thrombin in blood are very low, while values down to picomolar range are associated with disease; consequently, it is important to assess this protein concentration at trace level and with high selectivity [4].

In the recent years, there has been great interest in the development of aptasensors. Aptasensors are essentially biosensors based on aptamers as recognition elements. Aptamers are artificial DNA or RNA oligonucleotides selected in vitro which have the ability to bind to proteins, small molecules or even whole cells; these molecules are capable of recognizing their targets with affinities and specificities often matching or even exceeding those of antibodies [5]. The first use of aptamers as biorecognition element in biosensors was reported in 1996, with an optical biosensor based on fluorescently labeled aptamers for Immunoglobulin G detection [6]. In 2005 the first electrochemical aptasensor was described, based on a sandwich format, where aptamers were labeled with glucose oxidase for the detection of Thr by amperometry [7]. Recently, among the different electrochemical techniques available, electrochemical impedance spectroscopy (EIS) has been increasingly used in biosensing studies [8–10]. EIS can be used as a tool for characterization of sensor platforms, and it can

Electronic supplementary material The online version of this article (doi:10.1007/s00604-013-1126-0) contains supplementary material, which is available to authorized users.

C. Ocaña · M. del Valle (✉)
Sensors and Biosensors Group, Department of Chemistry, Universitat Autònoma de Barcelona, Edifici Cn, 08193 Bellaterra, Barcelona, Spain
e-mail: manel.delvalle@uab.es

also be the transduction technique to observe biorecognition events [11, 12]. It is an effective method for probing interfacial properties of modified electrodes such as their capacitance, electron transfer resistance, blocking layers, etc. [13]. The important feature presented by EIS is that it does not require any labeled species (e.g. with fluorescent or enzyme tags) for the transduction; in this way, this detection technique can be used for designing label-free protocols thus avoiding more expensive and time-consuming procedures [14].

In this communication, we report a label-free electrochemical aptasensor for detection of Thr using graphite-epoxy composite electrodes (GEC), where different protocols for immobilization of the aptamer are evaluated and compared. GEC electrodes represent a platform for biosensing of general use in our laboratories and have been already extensively studied [15, 16]. The different immobilization protocols that have been studied in this work are: physical adsorption, avidin-biotin affinity, amido-link covalent bonding via electrochemical activation [17] and electrochemical grafting [18]. The transduction principle used is based on the change of electron-transfer resistance in the presence of the $[Fe(CN)_6]^{3-}/[Fe(CN)_6]^{4-}$ redox couple, which can be measured by EIS [19]. All different kinds of immobilization showed appropriate response behavior values to determine Thr in the picomolar range. The different procedures evaluated showed particular advantages, such as, high sensitivity, simple instrumentation, low production cost, fast response and portability.

Experimental

Reagents and solutions

Potassium ferricyanide $K_3[Fe(CN)_6]$, potassium ferrocyanide $K_4[Fe(CN)_6]$, potassium dihydrogen phosphate, sodium monophosphate, methanol, perchloric acid, hydrochloric acid, *N*-Hydroxysuccinimide, *N*-(3-Dimethylaminopropyl)-*N*′-ethylcarbodiimide hydrochloride, sodium nitrite, fibrinogen protein, immunoglobulin G from human serum, avidin from egg white, albumin from bovine serum (BSA) and the target protein thrombin (Thr), were purchased from Sigma (St. Louis, MO, USA, www.sigmaaldrich.com). Poly(ethylene glycol) 1.000 (PEG), sodium chloride and potassium chloride were purchased from Fluka (Buchs, Switzerland, www.sigmaaldrich.com). 4-aminobenzoic acid from Acros (Geel, Belgium, www.acros.com). All reagents were analytical reagent grade. All-solid-state electrodes (GECs) were prepared using 50 μm particle size graphite powder (Merck, Darmstadt, Germany, www.merck.com) and Epotek H77 resin and its corresponding hardener (both from Epoxy Technology, Billerica, MA, USA, www.epotek.com). All solutions were made up using MilliQ water from MilliQ System (Millipore, Billerica, MA, USA, www.millipore.com). The different modified aptamers (AptThr) [20] used in this study were prepared by TIB-MOLBIOL (Berlin, Germany, www.tib-molbiol.com). Their sequences and modifications are shown below:

AptThr: 5′-GGTTGGTGTGGTTGG-3′
NH_2-AptThr: 5′-NH_2- GGTTGGTGTGGTTGG-3′
Bio-AptThr: 5′-Bio- GGTTGGTGTGGTTGG-3′

Stock solutions of aptamer, thrombin and other proteins were diluted with sterilized and deionised water (to prevent any DNA cleavage), separated in fractions and stored at −20 °C until required. The buffer employed was PBS (187 mM NaCl, 2.7 mM KCl, 8.1 mM $Na_2HPO_4 \cdot 2H_2O$, 1.76 mM KH_2PO_4, pH 7.0). Stock solutions of aptamer and thrombin were diluted with sterilized and deionised water, separated in fractions and stored at −20 °C until use.

Electrode preparation procedures

Graphite-epoxy composite (GECs) electrodes used were prepared using a PVC tube body (6 mm i.d.) and a small copper disk soldered at the end of an electrical connector. The working surface is an epoxy-graphite conductive composite, formed by a mixture of graphite (20 %) and epoxy resin (80 %), deposited on the cavity of the plastic body [8]. The composite material was cured at 80 °C for 3 days. Before each use, the electrode surface was moistened with MilliQ water and then thoroughly smoothed with abrasive sandpaper and finally with alumina paper (polishing strips 301044–001, Orion) in order to obtain a reproducible electrochemical surface [21, 22].

Avidin modified graphite-epoxy composite electrodes (AvGECs) were prepared with the same protocol as that used to prepare the graphite epoxy composite. The composite is formed by 2 % lyophilized avidin, 18 % graphite and 80 % epoxy resin [9]. In this case, the composite material was cured at 40 °C for 1 week.

Protocol

The scheme of the experimental procedures is represented in Fig. 1, with specific steps described below. Before any immobilization, the aptamer solution was heated at 80–90 °C for 3 min to promote the loose conformation of the aptamer. Then, the solution was dipped in a bath of cold water to obtain the proper detecting conformation [23].

Aptamer immobilization

Physical adsorption After getting the proper aptamer conformation, the electrode was immersed in 160 μL of AptThr solution, where the adsorption took place at room temperature for 15 min with soft stirring. Finally, this step was followed by

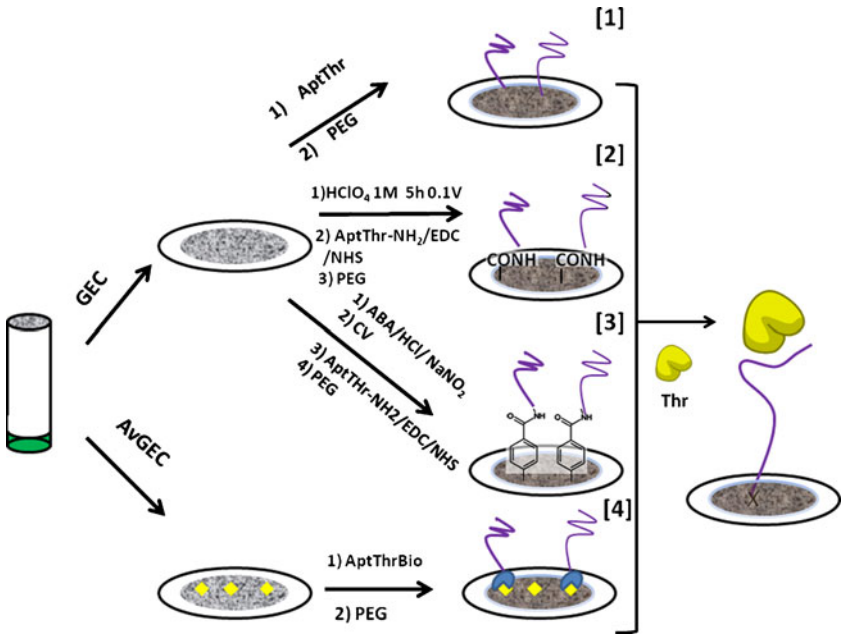

Fig. 1 Experimental scheme of the different immobilization techniques and biosensing steps. [1], Physical adsorption; [2], Electrochemical activation; [3], Electrochemical grafting; [4], Avidin-Biotin affinity

two washing steps using PBS buffer solution for 10 min at room temperature, in order to remove any unadsorbed aptamer [24].

Avidin-Biotin affinity The AvGEC electrode was dipped in 160 μL of biotinylated AptThr solution for 15 min at room temperature with soft stirring. This was followed by two washing steps using PBS buffer solution for 10 min.

Electrochemical activation + covalent immobilization First, carboxyl groups were electrochemically generated on the electrode surface, and next the aptamer was immobilized through amide bonding. To obtain an active surface with carboxyl groups, it was applied to the electrode a potential of +0.8 V versus reference electrode Ag/AgCl/KCl (sat.) in 1 M $HClO_4$ solution for 5 h [17]. After that, the electrode was immersed in 160 μL of aptamer in PBS solution with 1 mg of *N*-(3-dimethylaminopropyl)-*N′*-ethylcarbodiimide hydrochloride and 0.5 mg of *N*-hydroxysuccinimide for 24 h [23], with the goal of covalent immobilization of the amino-ended aptamer through the amide bond formation. This step was followed by two 10 min washing steps with PBS buffer solution.

Electrochemical grafting + covalent immobilization In this case, electrochemical grafting employing 4-aminobenzoic acid followed by aptamer immobilization through amide bonding was performed. Firstly, 30 mg of 4-aminobenzoic acid was dissolved in 3 mL of 1 M HCl and cooled with ice. Then, the diazonium salt was prepared by adding 570 μL of 2 mM $NaNO_2$ aqueous solution dropwise to the 4-aminobenzoic acid solution, with constant stirring. The electrode was immersed in this solution, and 200 successive voltammetric cycles ranging between 0.0 and −1.0 V (v = 200 mV s^{-1}) were performed [25], generating a carbon-carbon bond. The modified electrodes (benzoic acid modified carbon) were washed thoroughly with water and methanol and dried at room temperature. Finally, the electrodes were immersed in 160 μL of aptamer solution with 1 mg of *N*-(3-dimethylaminopropyl)-*N′*-ethylcarbodiimide hydrochloride and 0.5 mg of *N*-hydroxysuccinimide during 12 h, with the goal of covalent immobilization of the aptamer through the amide formation. This step was followed by two 10 min washing steps with PBS buffer solution [23].

Blocking step

After aptamer immobilization, the electrode was incubated in 160 μL of PEG 40 mM for 15 min at room temperature with soft stirring to minimize any possible nonspecific adsorption. This was followed by two washing steps using PBS buffer solution for 10 min.

Thrombin assay

The last step was the recognition of Thr by the immobilized AptThr. For this, the electrode was dipped in a solution with the desired concentration of Thr. The incubation took place for 15 min at room temperature. Then, the biosensor was washed twice with PBS buffer solution for 10 min at room temperature, and the EIS measurement performed.

Equipment

Impedance measurements were performed with an IM6e Impedance Measurement Unit (BAS-Zahner, Kronach Germany,

www.zahner.de) or an Autolab PGStat 20 (Metrohm Autolab B.V, Utrecht, The Netherlands, www.ecochemie.nl). Thales (BAS-Zahner) and FRA (Metrohm Autolab) software were used for data acquisition and control of the experiments, respectively. A three electrode configuration was used to perform the impedance measurements: a platinum-ring auxiliary electrode (Crison 52–67, Barcelona, Spain, www.crisoninstruments.com), a Ag/AgCl pseudo-reference electrode prepared in the laboratory and the constructed GEC as the working electrode. Temperature-controlled incubations were done using an Eppendorf Thermomixer 5436 (Hamburg, Germany, www.eppendorf.com).

EIS detection

Impedimetric measurements were performed in 0.01 M $[Fe(CN)_6]^{3-/4-}$ solution prepared in PBS at pH 7. The electrodes were dipped in this solution and a potential of +0.17 V (vs. Ag/AgCl) was applied. Frequency was scanned from 10 kHz to 50 mHz with a fixed AC amplitude of 10 mV. The obtained spectra were represented as Nyquist plots ($-Z_i$ vs. Z_r) in the complex plane and fitted to a theoretical curve corresponding to the equivalent circuit with Z_{view} software (Scribner Associates Inc., USA, www.scribner.com). The equivalent circuit was formed by one resistor/ capacitor element in series with a resistance. In the equivalent circuit, the resistance in series with the capacitor element, R_1, corresponds to the resistance of the solution, the resistance in parallel with the capacitor element, R_{ct}, is the charge transfer resistance between the solution and the electrode surface, while the capacitor element is the constant phase element (CPE) associated with the double-layer capacitance. The use of a CPE instead of a capacitor is required to optimize the fit to the experimental data, and this is due to the nonideal nature of the electrode surface. Any diffusional term was neglected as it was not the object of this study. The chi-square goodness-of-fit was calculated for each fitting and in all cases the calculated values for each circuit were <0.2, much lower than the tabulated value for 50 degrees of freedom (67.505 at 95 % confidence level).

Results and discussion

In the comparison of immobilization protocols, we observed the change of the charge transfer resistance (R_{ct}) between the solution and the electrode surface after each electrode modification, and after the Thr sensing. The charge transfer process monitored was that of the redox marker ($[Fe(CN)_6]^{3-/4-}$), as usual in electrochemical impedance studies. In it, any modification of the electrode surface, i.e. the aptamer immobilization, the PEG blocking or the biosensing event altered the electrochemical process of the redox marker [11, 26]. Thanks to these variations, it was possible to monitor each step of the biosensing, in this case by following the variation of R_{ct}.

In order to compare the results obtained from the different electrodes used, and to obtain independent and reproducible results, the relative signal was used, Δ_{ratio} [9]. Thus, the Δ_{ratio} value was defined according to the following equations:

$$\Delta_{ratio} = \Delta_s/\Delta_p \quad (1)$$

$$\Delta_s = R_{ct(AptThr\text{-}Thr)} - R_{ct(electrode\text{-}buffer)} \quad (2)$$

$$\Delta_p = R_{ct(AptThr)} - R_{ct(electrode\text{-}buffer)} \quad (3)$$

where $R_{ct\ (AptThr\text{-}Thr)}$ was the electron transfer resistance value measured after incubation with the thrombin protein; $R_{ct\ (AptThr)}$ was the electron transfer resistance value measured after aptamer inmobilization on the electrode, and $R_{ct\ (electrode\text{-}buffer)}$ was the electron transfer resistance of the blank electrode and buffer.

As can be seen in Fig. 2, the R_{ct} value, visualized as the diameter of the semicircle, increased after each biosensing step. This change was due to the inhibition of the electrochemical reaction of the redox marker at the electrode surface, caused by the presence of blocking layers. Two different factors should be taken into account to properly explain this effect: electrostatic repulsion and sterical hindrance [27]. When the AptThr is immobilized onto the electrode surface, an initial blocking layer is formed, where negatively charged phosphate groups of the AptThr skeleton are responsible for electrical repulsion towards the negatively charged redox marker, thus producing the increase of the R_{ct} value. The addition of target protein (Thr) resulted in the increment of the resistance value due to the sterical hindrance caused by the formation of the complex AptThr-Thr.

Detection of thrombin: comparison between different immobilization protocols

The goal of these experiments was to study and compare the best immobilization technique using a graphite-epoxy composite. All steps of these experiments have been optimized separately (data not shown). The obtained Thr calibration curves are represented in Fig. 3.

The first technique used was physical adsorption. This immobilization protocol is based on a direct adsorption of AptThr through weak, labile bonds with active substrate sites, in this case on a graphite-epoxy composite electrode. Adsorption is the simplest method to immobilize aptamers on electrodes. It does not require additional reagents or special nucleic acid modifications, thus resulting in a rapid, simple and low cost protocol for the aptamer immobilization [24].

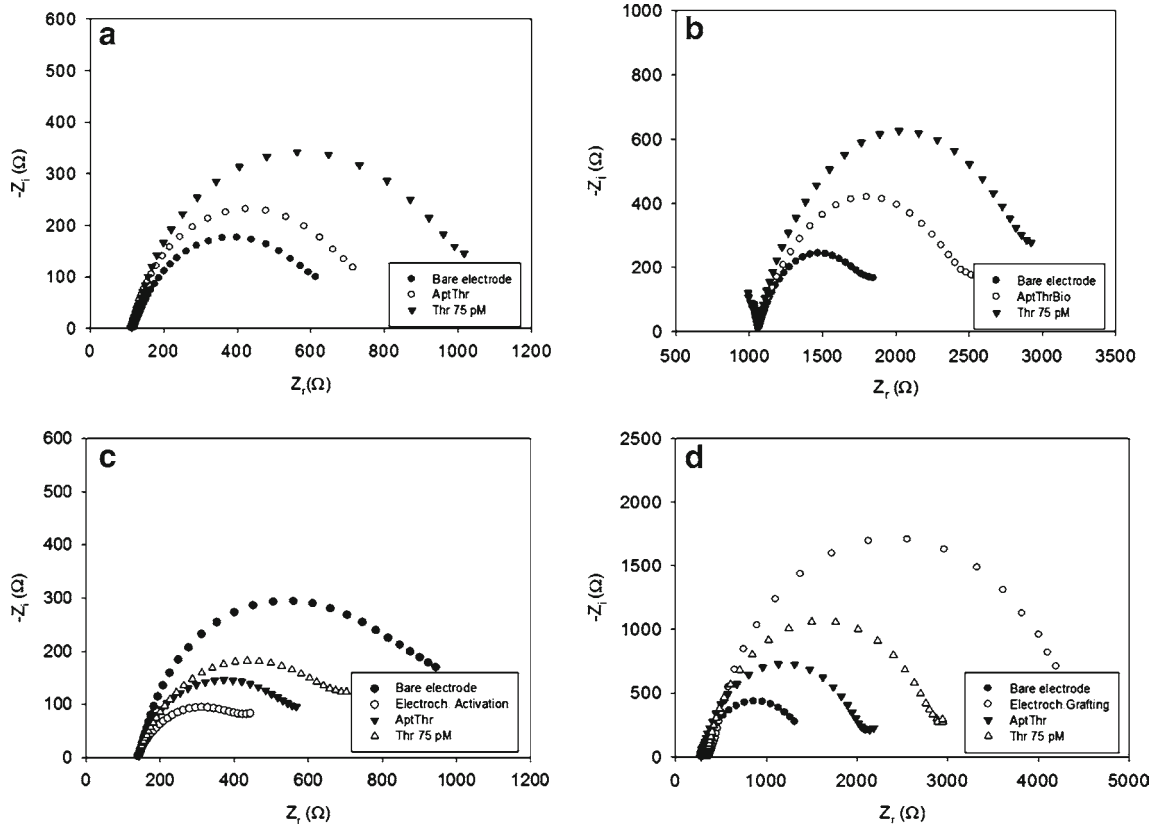

Fig. 2 Nyquist Diagram obtained for the Thrombin aptasensor prepared by: **a** physical adsorption, **b** avidin-biotin affinity, **c** covalent bonding via electrochemical activation and **d** covalent bonding via electrochemical grafting. All experiments were performed in PBS solution and all EIS measurements were performed in PBS solution containing 0.01 M $K_3[Fe(CN)_6]/K_4[Fe(CN)_6]$

This method presented high sensitivity and low detection limits, with a value for S/N=3 of 4.5 pM, see Fig. 3a.

The subsequent technique that was used to immobilize AptThr was through avidin-biotin interaction of the properly terminal-modified aptamer. The basis of this technique is the strong affinity, in this case, between avidin and biotin to form a complex (K_a=1 10^{15} M^{-1}) [28]. The stability of this interaction is nearly equal to that of a covalent bond. In fact, it can only be broken under very extreme conditions. As we can see in Fig. 3b, this method presented high sensitivity and a low detection limit, 4.7 pM for S/N=3.

Next, two different covalent bond immobilizations were used. These covalent bonds on the electrode surface can provide the benefits by structural flexibility and chemical stability, thus improving hybridization efficiency. The first technique used was through an electrochemical activation of the electrode surface and carboxyl moieties formation. For its operation, it needed application of a potential of +0.8 V vs Ag/AgCl to the carbon electrode surface for a duration of 5 h in perchloric acid 1 M. Due to the extreme conditions of the approach, the electrodes were surface-modified with carboxyl groups [17]. After that, this surface-confined carboxyl group were activated with *N*-(3-dimethylaminopropyl)-*N′*-ethylcarbodiimide hydrochloride / *N*-Hydroxysuccinimide to link amino groups of the properly terminated aptamers through the carbodiimide reaction [29]. The other covalent bond method used was electrochemical grafting [18]. This method consists of anchoring 4-aminobenzoic acid molecules to the electrode surface through diazonium salt reaction and C-C bond formation. The modification steps could be followed through EIS, see Fig. 2d. The electron-transfer resistance showed first a high increase due to the formation of anchor points on the electrode surface, in the form of benzoic acid functionalities; then a decrease in its value was observed due to the immobilization of the amino ended aptamer on the surface through the carbodiimide reaction, this decrease was a consequence of electrostatic repulsion. These two covalent immobilization methods presented narrower linear working ranges although the sensitivities were higher; these can be observed on the Fig. 3c and d. The highest net signal is obtained with the electrochemical activation approach.

All numerical results are represented in Table 1. The highest sensitivity was attained using affinity immobilization due to the strong affinity of avidin with biotinylated AptThr. This method presents more efficiency on the biorecognition than the covalent immobilization methods. In addition, its performance can be fine-tuned, by optimizing the amount of avidin on the AvGECs for each specific application. Also, the

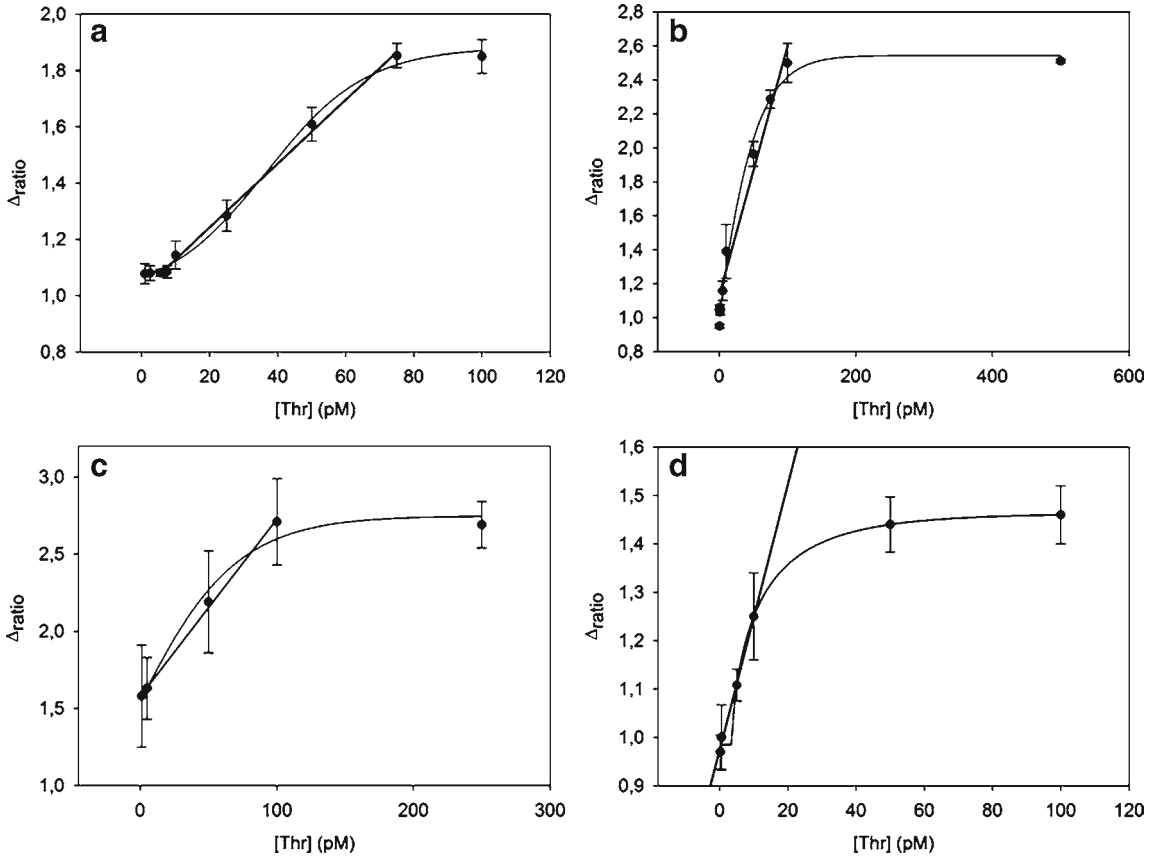

Fig. 3 Calibration curves and regression lines for the four immobilization procedures tested: **a** physical adsorption, **b** avidin-biotin affinity, **c** electrochemical activation and **d** electrochemical grafting. Uncertainly values correspond to five replicate experiments

best reproducibility was achieved using the avidin-modified biocomposite platform, probably due to the surface presenting less heterogeneity among different electrodes compared to electrodes prepared using covalent bonding techniques. The response with highest linearity was obtained using the electrochemical grafting method, what suggests a proper interaction of the bonded aptamer but the broadest linear range corresponds to the affinity process. Largest impedimetric signal (Δ_{ratio}) is observed for the electrochemically activated-amide bond immobilization, probably this is the configuration with best space orientation, optimal proximity of ligand to electrode and favorable steric effects. Finally, the lowest detection limit was yielded by the physical adsorption followed by the affinity method. Probably the high sensitivity can be attributable to the correct orientation of the receptor, while the reduced linear working range could be defined by the amount of recognition sites present on the electrode surface.

Apart of these response features, an important asset for the electrochemical grafting is that immobilization can be electrically addressed; this feature can be of high significance if preparing assays of aptamer biosensors for multiplex formats.

In order to judge the interest of the comparison done, the four immobilization protocols were compared with other label-free biosensors using aptamers for Thr detection. The label-free techniques considered were differential pulse voltammetry, potentiometry, and EIS. The details are shown in Table 2, where sensitivity info is presented as the LOD of each

Table 1 Calibration curves results obtained with different AptThr immobilizations. % RSD values correspond to five replicate experiments at 75 pM thrombin concentration

Immobilization	Sensitivity (M^{-1})	Reproducibility (RSD %)	Linear range (pM)	LOD (pM)	Correlation coeficient (r)
Physical adsorption	$1.106\ 10^{10}$	7.2	7.5–75	4.5	0.998
Av-Bio affinity	$1.530\ 10^{10}$	4.9	0.75–100	4.7	0.999
Electrochemical activation	$1.206\ 10^{10}$	8.3	2.5–100	10.5	0.996
Electrochemical grafting	$8.756\ 10^{9}$	7.2	0.2–10	7.3	0.994

Table 2 Comparison of the proposed Thr aptasensor with other recent reported label-free aptasensors in the literature

Transduction technique	Platform	LOD	Interferents tested	RSD%	Ref
Differential pulse votammetry	Gold	10 nM	BSA, α-fetoprotein, carcinoembryonic antigen	–	[33]
Differential pulse voltammetry	gold	3 nM	Human serum	3	[34]
Potentiometry	FET	6.7 nM			[35]
EIS	Gold	80 pM	BSA	10	[36]
EIS	Gold recordable compact discs	5 nM	Human serum	1	[37]
EIS	MWCNT	105 pM	Human serum	7.5	[38]
EIS	Platinum/ poly(pyrrole-NTA)/Cu^{2+}	4.4 pM	BSA, lysozime, Immunoglobulin G	7.3	[39]
EIS	GEC/Physical Adsorption	4.5 pM	Fibrinogen, Immunoglobulin G, BSA	7.2	This work
EIS	AvGEC	4.7 pM	Fibrinogen, Immunoglobulin G, BSA	4.9	This work
EIS	GEC/Electrochem. Activation	10.5 pM	Fibrinogen, Immunoglobulin G, BSA	8.3	This work
EIS	GEC/Electrochem. Grafting	7.3 pM	Fibrinogen, Immunoglobulin G, BSA	7.2	This work
EIS	Chemically modified graphene	10 nM	Immunoglobulin G, BSA, Avidin	–	[40]

biosensor compared. Our proposed aptasensor is on the first range of lowest LOD and % RSD value, specially the avidin-biotin affinity method. These data demonstrate that our graphite-epoxy composite electrodes can be sensing platforms of choice for the development of aptasensors, in this case, for detecting thrombin.

Cross-reactivity

Majoritary proteins in serum (BSA, Fibrinogen and Immunoglobulin G) which may accompany Thr [30], were tested as potential interfering substances for the different aptasensors towards Thr compared in the study, see the different EIS spectra on the Supplementary Information.

The first protein studied was BSA. BSA is found in serum at a level from 3,500 to 5,000 mg·dL^{-1}, representing more than 60 % of the total protein present. To perform the test, the highest concentration in serum was used, 5,000 mg dL^{-1} [31]. When the aptamer was incubated with this protein, the electron interfacial resistance did not increase, and instead, in this case a slight decrease was observed. Therefore, it was proven that albumin was not recognized by the AptThr, and it did not interfere with AptThr-Thr system, regardless of the immobilization method used.

Next, the protein studied was Fibrinogen. Fibrinogen is a fibrous protein involved in the blood clotting process. By the action of thrombin, fibrin is degraded and results in the formation of a clot. This protein is present in human serum in a concentration range of 200 to 400 mg dL^{-1} [32]. It was observed that the electron interfacial resistance increased as

Table 3 Comparison among sensitivity values for interfering proteins in serum, obtained with different protocols for AptThr immobilization (Each sensitivity value obtain for calibration, of the single protein, $n=4$ in the linear range)

Immobilization	Thr sensitivity (M^{-1})	Fibrinogen sensitivity (M^{-1})	Immunoglobulin G sensitivity (M^{-1})	BSA sensitivity (M^{-1})
Physical adsorption	$1.106\ 10^{10}$	$3.698\ 10^{5}$	$2.385\ 10^{4}$	–
Av-Bio affinity	$1.530\ 10^{10}$	$1.499\ 10^{4}$	$1.082\ 10^{5}$	–
Electrochemical activation	$1.206\ 10^{10}$	$3.022\ 10^{5}$	$1.132\ 10^{4}$	–
Electrochemical grafting	$8.756\ 10^{9}$	$8.103\ 10^{5}$	$1.605\ 10^{4}$	–

Table 4 Comparison among EC_{50} values and % Cross-Response for interfering proteins in serum, obtained with different protocols for AptThr immobilization. (% CR=100 (EC_{50} Thr/ EC_{50} interfering protein)

Immobilization	Thr	EC_{50} (M) fibrinogen	Immunoglobulin G
Physical adsorption	$4.400\ 10^{-11}$	$2.300\ 10^{-6}$	$3.400\ 10^{-5}$
Av-Bio affinity	$4.600\ 10^{-11}$	$8.190\ 10^{-6}$	$7.330\ 10^{-5}$
Electrochemical activation	$4.390\ 10^{-11}$	$8.650\ 10^{-6}$	$8.480\ 10^{-5}$
Electrochemical grafting	$2.280\ 10^{-11}$	$8.930\ 10^{-6}$	$5.000\ 10^{-5}$
Immobilization	**Thr**	**%CR fibrinogen**	**Immunoglobulin G**
Physical adsorption	100	$1.910\ 10^{-3}$	$1.290\ 10^{-4}$
Av-Bio affinity	100	$5.620\ 10^{-4}$	$6.275\ 10^{-5}$
Electrochemical activation	100	$5.080\ 10^{-4}$	$5.170\ 10^{-5}$
Electrochemical grafting	100	$2.550\ 10^{-4}$	$4.560\ 10^{-5}$

a result of some type of recognition by the AptThr. Therefore, this protein could act as interference for the system.

Lastly, the protein studied was Immunoglobulin G. Immunoglobulin G is a globular protein synthesized by the immune system in response to the invasion of any bacteria, virus or fungi. It is present in human serum over a range of concentrations from 950 mg dL^{-1} to 1,550 mg dL^{-1} in serum, with a reference value of 1,250 mg dL^{-1}. Immunoglobulin G also acted as an interferent, which is proven by the increase in the resistance R_{ct} value. This behavior, which was also exhibited by the aptasensor towards fibrinogen, may be due to some biological interaction between the aptamer and these proteins. These interactions are not yet fully described in the literature.

To evaluate the sensitivity of the aptasensor we compared the calibration plots for the different proteins, pure solution of single protein, by the different kinds of immobilization. Table 3, summarizes the parameters for each protein. The first thing one can see is that all types of immobilization showed the highest sensitivity for its target molecule, Thr, with its slope of response being five to six orders of magnitude greater than the slope for immunoglobulin G and also for fibrinogen. In addition, EC_{50} values for each type of immobilizations and % Cross Response (% CR) for all interfering proteins were calculated, Table 4 [25]. The EC_{50} value corresponds to the inflection point of the calibration curve towards the interfering species and represents the concentration of protein that provides 50 % of the Δ_{ratio} saturation value. Thus, the lower is the EC_{50} value, the greater is the affinity (or the interference) of the considered protein. The lowest EC_{50} value obtained, 2.30 10^{-11} M, corresponded to electrochemical grafting immobilization for thrombin protein, and the larger, 8.480 10^{-5} M, to electrochemical activation immobilization for immunoglobulin G. In overall, the % CR values, which states the degree of response in comparison to primary analyte thrombin, ranged from 1.910 10^{-3} to 6.275 10^{-5} %; these are openly low relative values, where the largest % CR corresponded to fibrinogen in adsorption immobilization. Therefore, it was demonstrated that the aptasensor showed a much higher sensitivity to Thr, regarding potential interfering proteins, that when they display some effect is due to the high level of concentration at which they are present in serum. Given all recognition events are due to the same aptamer used, the differences in interfering effects are attributable to incomplete blocking by PEG in some of the four protocols or to better immobilization orientation of the aptamer for biosensing. The latter is probably the case in the covalent immobilization (showing the lowest % CR) or some displacement effect in the case of physical adsorption.

Conclusions

In this paper, we have presented the use of aptasensors for the detection of thrombin based on graphite-epoxy composite electrodes. Results obtained with four kinds of AptThr immobilization (physical adsorption, avidin-biotin affinity, covalent bonding via electrochemical activation and covalent bonding via electrochemical grafting) were compared.

With the different methods reported, low detection limits (in the pM level), ample ranges of response for thrombin concentration (more than one decade) and low % RSD values were achieved. Among the four methods proposed, avidin-biotin affinity was the best overall method displaying high affinity with a sensitivity value of 1.530 10^{10} M^{-1}, a linear range of 0.75–100 pM and a reproducibility of 4.9 % RSD. However, it is an expensive method, as it needs the incorporation of the expensive avidin on the biocomposite. The lower detection limit attained was 4.5 pM by physical adsorption method, although the latter was also the one with poorer selectivity (highest % CR values). Considering interfering effects produced by serum proteins, fibrinogen and immunoglobulin G demonstrated some effect, which may restrict the utility of the aptasensor; still, given the high concentration values at which they interfere and the low % CR determined (lower than 0.001 %), these interfering effects may be tolerated. In the case a maximum accuracy is sought, a double recognition sandwich scheme, or an amplification scheme might be the solution.

Acknowledgments Financial support for this work has been provided by *Spanish Ministry of Science and Innovation*, (MICINN, Madrid) Through project CTQ2010-17099 and by *the Catalonia program ICREA Academia*. Cristina Ocaña thanks the support of *Ministry of Science and Innovation* (MICINN, Madrid, Spain) for the predoctoral grant.

References

1. Mendis S, Puska P, Norrving B (2011) Global Atlas on cardiovascular disease prevention and control. World Health Organization, Geneva
2. Holland CA, Henry AT, Whinna HC, Church FC (2000) Effect of oligodeoxynucleotide thrombin aptamer on thrombin inhibition by heparin cofactor II and antithrombin. FEBS Lett 484:87–91
3. Thiagarajan P, Narayanan AS (2009) Thrombin. John Whilley & Sons, Chichester
4. Centi S, Tombelli S, Minunni M, Mascini M (2007) Aptamer-based detection of plasma proteins by an electrochemical assay coupled to magnetic beads. Anal Chem 79:1466–1473
5. Nimjee SM, Rusconi CP, Sullenger BA (2005) Aptamers: an emerging class of therapeutics. Annu Rev Med 56:555–583
6. Davis KA, Abrams B, Lin Y, Jayasena SD (1996) Use of a high affinity DNA ligand in flow cytometry. Nucleic Acids Res 24:702–706
7. Tombelli S, Minunni M, Mascini M (2005) Piezoelectric biosensors: strategies for coupling nucleic acids to piezoelectric devices. Methods 37:48–56
8. Bonanni A, Esplandiu MJ, Pividori MI, Alegret S, del Valle M (2006) Impedimetric genosensors for the detection of DNA hybridization. Anal Bioanal Chem 385:1195–1201
9. Bonanni A, Pividori MI, del Valle M (2007) Application of the avidin-biotin interaction to immobilize DNA in the development of

electrochemical impedance genosensors. Anal Bioanal Chem 389: 851–861
10. Radi A, Acero Sánchez JL, Baldrich E, O'Sullivan CK (2005) Reusable impedimetric aptasensor. Anal Chem 77:6320–6323
11. Berggren C, Bjarnason B, Johansson G (2001) Capacitive biosensors. Electroanalysis 13:173–180
12. Lisdat F, Schafer D (2008) The use of electrochemical impedance spectroscopy for biosensing. Anal Bioanal Chem 391:1555–1567
13. Bardea A, Patolsky F, Dagan A, Willner I (1999) Sensing and amplification of oligonucleotide-DNA interactions by means of impedance spectroscopy: a route to a Tay-Sachs sensor. Chem Comm 1:21–22
14. Randviir EP, Banks CE (2013) Electrochemical impedance spectroscopy: an overview of bioanalytical applications. Anal Methods 5: 1098–1115
15. Merkoci A, Aldavert M, Marin S, Alegret S (2005) New materials for electrochemical sensing V: nanoparticles for DNA labeling. Trac-Trends Anal Chem 24:341–349
16. Pumera M, Aldavert M, Mills C, Merkoci A, Alegret S (2005) Direct voltammetric determination of gold nanoparticles using graphite-epoxy composite electrode. Electrochim Acta 50:3702–3707
17. Yamazaki S, Siroma Z, Ioroi T, Tanimoto K, Yasuda K (2007) Evaluation of the number of carboxyl groups on glassy carbon after modification by 3,4-dihydroxybenzylamine. Carbon 45:256–262
18. Belanger D, Pinson J (2011) Electrografting: a powerful method for surface modification. Chem Soc Rev 40:3995–4048
19. Bonanni A, del Valle M (2010) Use of nanomaterials for impedimetric DNA sensors: a review. Anal Chim Acta 678:7–17
20. Griffin LC, Tidmarsh GF, Bock LC, Toole JJ, Leung LLK (1993) In vivo anticoagulant properties of a novel nucleotide-based thrombin inhibitor and demonstration of regional anticoagulation in extracorporeal circuits. Blood 81:3271–3276
21. Lermo A, Campoy S, Barbé J, Hernández S, Alegret S, Pividori MI (2007) In situ DNA amplification with magnetic primers for the electrochemical detection of food pathogens. Biosens Bioelectron 22:2010–2017
22. Williams E, Pividori MI, Merkoçi A, Forster RJ, Alegret S (2003) Rapid electrochemical genosensor assay using a streptavidin carbon-polymer biocomposite electrode. Biosens Bioelectron 19:165–175
23. Pacios M, Martin-Fernandez I, Borrissé X, Valle Md, Bartrolí J, Lora-Tamayo E, Godignon P, Perez-Murano F, Esplandiu MJ (2012) Real time protein recognition in a liquid-gated carbon nanotube field-effect transistor modified with aptamers. Nanoscale 4:5917–5923
24. Ocaña C, Pacios M, del Valle M (2012) A reusable impedimetric aptasensor for detection of thrombin employing a graphite-epoxy composite electrode. Sensors 12:3037–3048
25. Moreno-Guzmán M, Ojeda I, Villalonga R, González-Cortés A, Yáñez-Sedeño P, Pingarrón JM (2012) Ultrasensitive detection of adrenocorticotropin hormone (ACTH) using disposable phenylboronic-modified electrochemical immunosensors. Biosens Bioelectron 35:82–86
26. Katz E, Willner I (2003) Probing biomolecular interactions at conductive and semiconductive surfaces by impedance spectroscopy: routes to impedimetric immunosensors, DNA-sensors, and enzyme biosensors. Electroanalysis 15:913–947
27. Bonanni A, Esplandiu MJ, del Valle M (2008) Signal amplification for impedimetric genosensing using gold-streptavidin nanoparticles. Electrochim Acta 53:4022–4029
28. Green NM (1963) Avidin 1. Use of 14C biotin for kinetics studies and for assay. Biochem J 89:585
29. Ghosh SS, Musso GF (1987) Covalent attachment of oligonucleotides to solid supports. Nucleic Acids Res 15:5353–5372
30. Seegers WH, McCoy L, Kipfer RK, Murano G (1968) Preparation and properties of thrombin. Arch Biochem Biophys 128:194
31. Tamion F (2010) Albumin in sepsis. Ann Fr Anesth Reanim 29:629–634
32. Blomback B, Carlsson K, Fatah K, Hessel B, Procyk R (1994) Fibrin in human plasma-Gel architectures governed by rate and nature of fibrinogen activation. Thromb Res 75:501–502
33. Yan Z, Han Z, Huang H, Shen H, Lu X (2013) Rational design of a thrombin electrochemical aptasensor by conjugating two DNA aptamers with G-quadruplex halves. Anal Biochem 442:237–240
34. Yan F, Wang F, Chen Z (2011) Aptamer-based electrochemical biosensor for label-free voltammetric detection of thrombin and adenosine. Sensors Actuators B Chem 160:1380–1385
35. Goda T, Miyahara Y (2013) Label-free and reagent-less protein biosensing using aptamer-modified extended-gate field-effect transistors. Biosens Bioelectron 45:89–94
36. Meini N, Farre C, Chaix C, Kherrat R, Dzyadevych S, Jaffrezic-Renault N (2012) A sensitive and selective thrombin impedimetric aptasensor based on tailored aptamers obtained by solid-phase synthesis. Sensors Actuators B Chem 166–167:715–720
37. Castillo G, Trnkova L, Hrdy R, Hianik T (2012) Impedimetric aptasensor for thrombin recognition based on CD support. Electroanalysis 24:1079–1087
38. Kara P, de la Escosura-Muñiz A, Maltez-da Costa M, Guix M, Ozsoz M, Merkoçi A (2010) Aptamers based electrochemical biosensor for protein detection using carbon nanotubes platforms. Biosens Bioelectron 26:1715–1718
39. Xu H, Gorgy K, Gondran C, Le Goff A, Spinelli N, Lopez C, Defrancq E, Cosnier S (2013) Label-free impedimetric thrombin sensor based on poly(pyrrole-nitrilotriacetic acid)-aptamer film. Biosens Bioelectron 41:90–95
40. Loo AH, Bonanni A, Ambrosi A, Poh HL, Pumera M (2012) Impedimetric immunoglobulin G immunosensor based on chemically modified graphenes. Nanoscale 4:921–925

Article 3. Avidin epoxy-graphite composite electrodes as platforms for genosensing and aptasensing

C. Ocaña, C. Figueras and M. del Valle

Journal of Nanoscience and Nanotechnology, 2014, 14, 1-9.

Article

Journal of
Nanoscience and Nanotechnology
Vol. 14, 1–9, 2014
www.aspbs.com/jnn

AMERICAN SCIENTIFIC PUBLISHERS
Copyright © 2014 American Scientific Publishers
All rights reserved
Printed in the United States of America

Avidin Epoxy-Graphite Composite Electrodes as Platforms for Genosensing and Aptasensing

Cristina Ocaña, Cristina Figueras, and Manel del Valle*

Sensors and Biosensors Group, Department of Chemistry, Universitat Autònoma de Barcelona, Edifici Cn, 08193 Bellaterra, Barcelona, Spain

This work presents two examples of biosensors that employ DNA as the recognition element. The transduction technique chosen is electrochemical impedance spectroscopy, which makes labeless detection possible. In the first case, a DNA probe was used to hybridize and detect a complementary DNA target; this principle may be used to construct biosensors to confirm a microbial, vegetal or animal species. The working example shown is the detection of enterohaemorragic *Escherichia Coli* O104:H4 bacteria, blamed of an epidemic outbreak in vegetables in Germany in 2011. As a second example, a specific DNA aptamer, able to interact with proteins, is used to develop a biosensor to detect thrombin, an important protein mediating in blood coagulation. Following the current trend in the field, these DNA biosensors have been prepared with help of nanocomponents in order to improve or to confirm and visualize the detection capabilities.

Keywords: Biosensor, DNA Sensing, Aptamer, Thrombin, Electrochemical Impedance Spectroscopy.

1. INTRODUCTION

DNA biosensor (or genosensor) technologies are rapidly being developed as alternatives to the classical gene assay, due to several advantages such as rapid analysis, low cost, simplicity and the possibility of miniaturization. Genosensors are devices that combine, as a biological recognition agent, single-strand DNA with a transducer. The selectivity of this device is due to the former, whilst its sensitivity is provided by the latter.[1] Genosensors make use of the hybridization event to detect a target DNA sequence.[2] The determination of nucleic acid sequences from humans, animals, bacteria and viruses could serve as starting point to solve different problems: investigation of food and water contamination caused by microorganisms, detection of genetic disorders or bioterrorism threats, tissue matching, forensic applications, etc. Inside the genosensor field, recently has appeared a new class: aptasensors. Aptasensors are biosensors that use aptamers as the biorecognition element. Aptamers are artificial DNA or RNA oligonucleotides selected *in vitro* which possess properties comparable to those of protein monoclonal antibodies, and thus are clear alternatives to already established antibody-based diagnostic or biotechnological products. This class of nucleic acids are able to fold into complex three dimensional shapes,[3,4] thus forming binding pockets and clefts for the specific recognition and tight binding of any given molecular target,[5] from metal ions and small molecules to large proteins and higher order protein complexes. They can be considered as a substitute for antibodies in certain therapeutic and diagnostic application cases. Due to all these properties, aptamers may be used in a wide range of applications, such as therapeutics,[6] molecular switches, drug development, affinity chromatography[7] and biosensors.[8] One well known and often used aptamer is selective to the thrombin protein. Thrombin is the last enzyme protease involved in the coagulation cascade, and converts fibrinogen to insoluble fibrin which forms the fibrin gel, both in physiological conditions and in the pathological thrombus.[9] Therefore, thrombin plays a central role in a number of cardiovascular diseases,[10] and it is known for regulating many processes such as inflammation and tissue repair at the blood vessel wall. Concentration levels of thrombin in blood are very low, and levels as low as picomolar are associated with disease; because of this, it is important to assess this protein concentration at trace level,[11] with high selectivity.

*Author to whom correspondence should be addressed.

Escherichia Coli O104:H4 is a Gram-negative bacterium notorious for the enterohaemorrhagic epidemic outbreak in Germany and other European countries in 2011. Early detection of this bacterium is important because its specific strain produces a Shiga toxin which inhibits protein synthesis and causes a hemolytic-uremic syndrome.[12] A viable analytical method to detect this bacterium is by finding specific fragments of its DNA.[13]

Among the different types of genosensors or aptasensors, and depending on the technique employed for the transduction, three main classes may be distinguished: optical,[14] piezoeletric,[15] and electrochemical.[16] Lately, among the different electrochemical techniques available, the use of Electrochemical Impedance Spectroscopy (EIS) is receiving an increasing amount of attention.[17] EIS is a characterization technique that provides electrical information in the frequency domain. Due to its ability for probing the interfacial properties at the electrode surface, lately EIS has been used for the sensitive observation of bio-recognition events.[18, 19] Other important features presented by EIS are: it does not require any special reagent for the analysis, it is capable of label-free detection and it is a cost-efficient technique. For all these reasons, EIS is becoming an attractive electrochemical tool for numerous applications such as: immunosensing,[20] genosensing,[21] enzyme activity determination,[22] studies of corrosion[23] and surface phenomena.[24] Using this technique, each spectrum obtained can be associated with an equivalent electrical circuit which represents the experimental electrochemical system.[17] Each electrical element in the circuit is directly correlated to a simple process such as electron transfer resistance, diffusion, double layer formation or capacitance change.

In recent years, the use of nanoscale materials for electrochemical biosensing has seen an explosive growth. A wide variety of nanoscale materials are now available such as carbon nanotubes, nanostructured silicon, gold nanoparticles, quantum dots, etc. The great interest in nanomaterials has been driven by their outstanding physicochemical properties.[25, 26] Within biosensing, some of these are: high surface area, non toxicity, biocompatibility, charge-sensitive conductance (in biosensing) and integration with bioelectronic devices.[27] This is especially true when the target molecules are in the same order of dimension as the utilized nanocomponents, (in this case with DNA and aptamers). These nanostructured materials-based electrochemical DNA devices may in that case present a number of key features, including high sensitivity, high selectivity and fast response time.

In this work, we focus on the comparison of two nanostructured biosensors based on an avidin bulk-modified graphite-epoxy composite electrode. The first case employed the specific DNA target corresponding to enterohaemorrhagic *Escherichia Coli* O104:H4 as the biorecognition element; the second case employed a specific aptamer to detect thrombin. In the DNA detection, gold nanoparticles were used to amplify the impedance signal. Biorecognition elements, DNA and aptamer previously biotinylated, were immobilized onto avidin modified electrodes, thus taking advantage of the strong interaction between avidin and biotin. This strong interaction (affinity constant $K_a = 10^{15}$) has been studied by several authors for the immobilization of several types of biomolecules.[28, 29] The presence of avidin molecules as anchorage points on the conductive composite electrodes, allows an easy immobilization of biotin modified DNA or aptamer molecules onto the electrode surface. Avidin graphite-epoxy composite electrodes (Av-GEC) have been previously studied and used by our research group in specific applications such as immunosensing[30] and genosensing.[31, 32]

2. MATERIALS AND METHODS

2.1. Chemicals

Potassium ferricyanide $K_3[Fe(CN)_6]$, potassium ferrocyanide $K_4[Fe(CN)_6]$, potassium dihydrogen phosphate, sodium monophosphate, avidin, trisodium citrate, disodium hydrogen phoshate bihydrate, potassium phosphate monobasic, streptavidin-gold nanoparticles, strep-AuNPs (Ref. S9059) and the target protein thrombin (Thr), were purchased from Sigma (St. Louis, MO, USA). Poly(ethylene glycol) (PEG), sodium chloride and potassium chloride were purchased from Fluka (Buchs, Switzerland). All reagents were analytical reagent grade. All-solid-state electrodes (Av-GEC) were prepared using 50 μm particle size graphite powder (Merck, Darmstadt, Germany), Epotek H77 resin and its corresponding hardener (both from Epoxy Technology, Billerica, MA, USA) and avidin. LI Silver Enhancement Kit was obtained from Nanoprobes (Yaphank, NY). The aptamer (AptThr) used in this study was prepared by TIB-MOLBIOL (Berlin, Germany). Other oligonucleotides used in the study were prepared by Sigma (St. Louis, MO, USA). *E.Coli* O104:H4 genome was specially sequenced shortly after the outbreak of haemolytic endemic syndrome in Germany in 2011.[33] Their sequences and modifications are were as follow:

- AptThr:
  5′-Bio-TTTGGGTTGGTGTGGTTGG-3′
- *E.Coli* O104:H4 Probe:
  5′-Bio-CCTCACTCTGAACTGGGGGCGAATC-3′
- *E.Coli* O104:H4 Target:
  5′-Bio-GATTCGCCCCCAGTTCAGAGTGAGG-3′
- Non complementary target
  5′-GTACCAGCCCTTGTGATACAGCGGG-3′.

All solutions were made up using MilliQ water from MilliQ System (Millipore, Billerica, MA, USA). The buffers employed were: PBS (187 mM NaCl, 2.7 mM KCl, 8.1 mM $Na_2HPO_4 \cdot 2H_2O$, 1.76 mM KH_2PO_4, pH

7.0), TSC 1 (0.75 M NaCl, 0.075 M trisodium citrate, pH 7.0), TSC 2 (0.30 M NaCl, 0.030 M, trisodium citrate, pH 7.0). Stock solutions of aptamer, thrombin and oligonucleotides were diluted with sterilized MilliQ water, separated in fractions and stored at − 20 °C until used.

2.2. Equipment

AC impedance measurements were performed with an Autolab PGStat 20 (Metrohm Autolab B.V, Utrecht, The Netherlands). FRA (Metrohm Autolab) software was used for data acquisition and control of the experiments. A three-electrode cell was used to perform the impedance measurements. The cell comprised an Ag/AgCl reference electrode, a platinum ring electrode (Crison 52-67-1, Barcelona, Spain), and the constructed avidin modified biocomposite (Av-GEC) working electrodes. Temperature-controlled incubations were done by using an Eppendorf Thermomixer 5436.

2.3. Preparation of Working Electrodes

All solid-state working electrodes were prepared using a PVC tube body and a small copper disk soldered to the end of an electrical connector. The conductive part of the Av-GEC was an avidin-epoxy–graphite conductive paste, formed from graphite (18%), epoxy resin (80%) and avidin (2%), which was deposited into the cavity in the plastic body, filling it. The biocomposite material was cured at 40 °C for one week.

Before each use, the surface electrode was wetted with MilliQ water and then thoroughly smoothed with abrasive paper followed by alumina paper (polishing strips 301044-001, Orion, Boston, MA, USA) to expose fresh avidin protein as anchorage site. The reproducibility of the construction and polishing processes for the biosensors have been reported previously.[34]

2.4. Procedures

Two different procedures were employed in this work, the general protocol is represented in Figure 1. The first one, shown in Figure 2, is used for DNA testing, and the second procedure is used for protein detection, in this case thrombin, shown in Figure 3. All experimental procedures are described in more detail below.

2.4.1. DNA Testing

The first step of the protocol was DNA hybrid formation in a solution containing the biotinylated probe and its complementary target. 30 pmol of biotinylated DNA probe and 30 pmol of its complementary target in TSC1 buffer were mixed in an Eppendorf tube; hybridization took place in a thermomixer at 42 °C for 30 min with soft stirring. After that, an avidin-modified electrode was dipped into an Eppendorf containing the biotinylated hybrid. The tube with the sensor was gently shaken for 20 min at 42 °C. The previously formed biotinylated hybrid became immobilized onto the electrode surface due to the high affinity between the avidin exposed on the electrode surface and the biotin moiety on the biotinylated hybrid. This was followed by two washing steps with TSC 2 at 42 °C for 10 min.

In order to amplify the signal, strep-AuNPS and silver enhancement was used. GEC electrodes modified with biotinylated hybrid were incubated in an Eppendorf tube containing a solution of strep-AuNPs, 1:100 stock solution, in PBS buffer. The tube was then incubated at 42 °C with soft stirring for 20 min. This step was followed by two gentle washing steps in PBS buffer for 10 min at 42 °C.

Then, 20 μl of solution obtained by the combination of equal volumes of silver enhancer and initiator were deposited onto the electrode surface, and left for 7 minutes to react. The electrodes were then washed with MilliQ water in order to stop the reaction. The negative control consisted of a non-biotinylated complementary target.

2.4.2. Protein Detection

The first step consisted of immobilization of the aptamer onto the electrode surface. An aliquot of 160 μL of biotinylated aptamer solution in MilliQ water (at the desired concentration) was heated to 80–90 °C for 3 min to promote the loose conformation of the aptamer. Then, the solution was dipped in a bath of cold water and the electrode was immersed in it, at which point the adsorption took place at room temperature for 15 min with soft stirring. This was followed by two washing steps using PBS buffer solution for 10 min at room temperature, in order to remove any unfixed aptamer.

Subsequently, the electrode was dipped into 160 μL of 40 mM PEG for 15 min at room temperature with soft stirring to minimize any possible nonspecific adsorption. This was followed by two washing steps using PBS buffer solution for 10 min.

The last step was the recognition of thrombin by the immobilized aptamer. Therefore, the electrode was dipped in a solution with the desired concentration of thrombin. Incubation took place for 15 min at room temperature with soft stirring. Afterwards, the biosensor was washed twice with PBS buffer solution for 10 min.

All incubations took place at a controlled temperature in the thermomixer, with a stirring speed of 600 rpm.

2.4.3. EIS Measurements

Impedance measurements were recorded between 50 kHz and 0.05 Hz, at a sinusoidal voltage perturbation of 10 mV amplitude and a sampling rate of 10 points per decade above 66 Hz, and five points per decade at the lower range. All experiments were carried out at an applied potential of 0.17 V (vs. Ag/AgCl reference electrode) in a PBS buffer solution containing 5 mM $K_3[Fe(CN)_6]/K_4[Fe(CN)_6]$ (1:1)

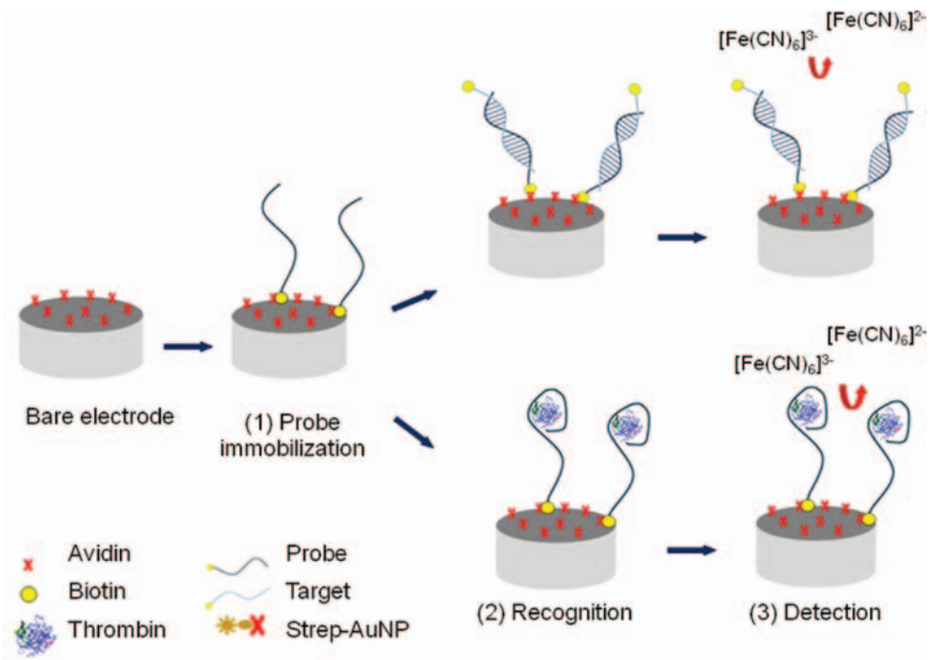

Figure 1. General scheme protocols involved in the operation of hybridization DNA biosensor for genes (top), and aptamer biosensor for proteins (bottom).

mixture, used as a redox marker. The impedance spectra were plotted in the form of imaginary vs. real complex plane diagrams (Nyquist plots, $-Z_i$ vs. Z_r) and fitted to a theoretical curve corresponding to the equivalent circuit with Zview software (Scribner Associates Inc., USA). The obtained spectra were fitted to a Randle's equivalent circuit, shown in Figure 4; in this, the parameter R_1 corresponds to the resistance of the solution, R_2 is the charge transfer resistance (also called R_{ct}) between the solution and the electrode surface, whilst CPE is associated with the double-layer capacitance. For all performed fittings, the chi-square goodness-of-fit test was thoroughly checked to verify calculations. In all cases, calculated values for each circuit were <0.2, much lower than the tabulated value for 50 degrees of freedom (67.505 at 95% confidence level). In our experiments, we focused on the

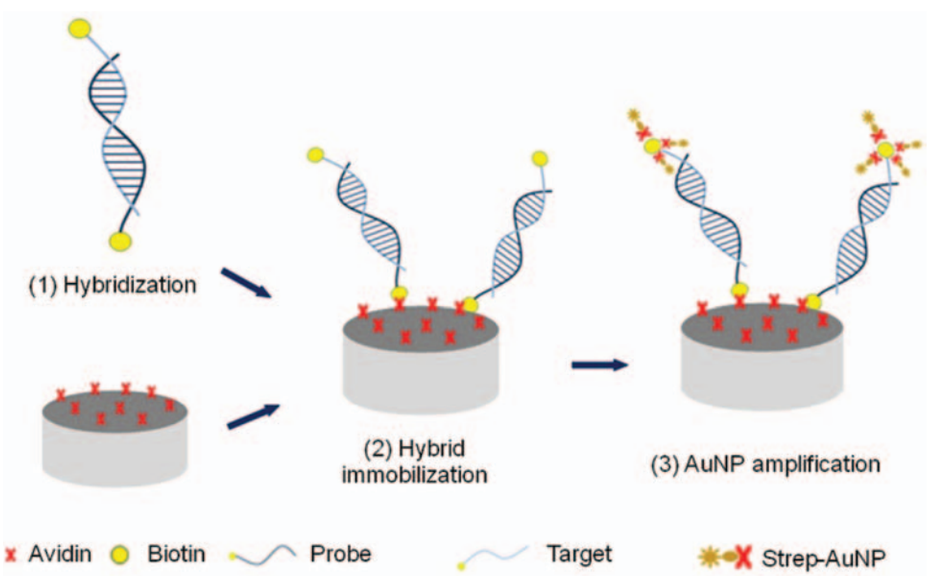

Figure 2. Scheme of the steps followed in an EIS genosensing experiment.

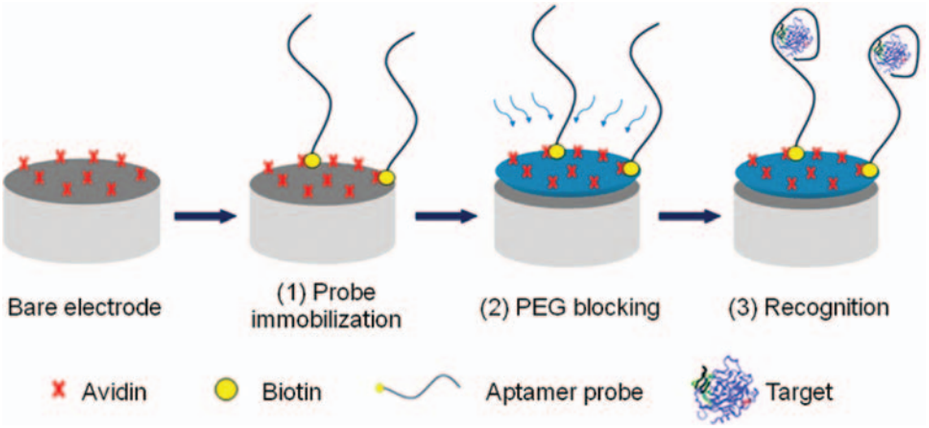

Figure 3. Scheme of the steps followed in an EIS protein detection using an aptamer sensor.

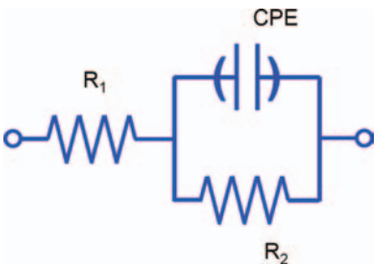

Figure 4. Equivalent circuit used for the data fitting.

charge transfer resistance (R_{ct}), which was used to monitor the electrode surface changes. Two different ways to express R_{ct} variation in normalized scale were chosen according to the different protocols: Δ and Δ_{ratio}.[35] Their formulae are as follows:

$$\Delta = R_{ct(hybrid\ or\ amplification)} - R_{ct(electrode\text{-}buffer)}$$

$$\Delta_{ratio} = \Delta_s/\Delta_p$$

with:

$$\Delta_s = R_{ct(AptThr\text{-}Thr)} - R_{ct(electrode\text{-}buffer)}$$

$$\Delta_p = R_{ct(AptThr)} - R_{ct(electrode\text{-}buffer)}$$

In the formulae Δ_p corresponds to R_{ct} variation after aptamer immobilization, whilst Δ_s represents R_{ct} variation after the last step of biorecognition and Δ corresponds to the step of DNA biosensing (i.e., hybridization or signal amplification step).

3. RESULTS AND DISCUSSION

3.1. Impedimetric Response

Figure 5 shows the different Nyquist plots obtained in a whole experiment of *E.Coli* DNA and Thrombin biosensing. After each step of the protocol, an EIS measurement was performed. As can be observed in Figures 5(a) and (b), the R_{ct} value diameter of the semicircle increased after each step was performed. This corresponds to the augmented difficulty of the redox reaction of $[Fe(CN)_6]^{3-/4-}$ to take place at the electrode surface, due to the sensor surface alteration.[36] When a DNA hybrid or aptamer is immobilized onto the sensor surface, an initial layer is formed and a negatively charged interface is generated due to the presence of the negatively charged phosphate backbone of DNA. This circumstance repels the redox marker, also with negative charge, thus resulting in the inhibition of the electron transfer process and in an increment of the R_{ct} value. The addition of strep-AuNPs in the first case, and protein thrombin in the second case, results in a further increment of the resistance value due to the hindrance caused by the formation of a double layer. In this way, the use of the EIS technique serves also as confirmation that the biosensing surface was correctly prepared.

3.2. Optimization of Amount of Receptor Immobilized

In the case of *E.Coli* DNA detection, the concentrations of the DNA probe and target were similar to those in previous works:[37,38] The DNA target assayed was 30 pmol, previously found to be the saturation value.

EIS measurements with different concentrations of aptamer and PEG were carried out in order to optimize the aptamer and PEG concentration to be used in the protocol. Figure 6 shows the curve of AptThr fixation onto the electrode surface. In this graph, superposition of two behaviors can be noted. First, the avidin-biotin interaction is detected, with an approximately steady value of Δ_p 3 KΩ. After this, an uniform increase for higher aptamer concentrations can also be observed, which corresponds to simple non-specific adsorption on exposed surface sites. The behavior exhibited by the first follows the Langmuir isotherm, displayed as an increase of R_{ct} until a saturation value, which was then chosen as the optimal concentration. This value corresponds to a 1.5 μM aptamer concentration. To minimize any possible nonspecific adsorption onto the

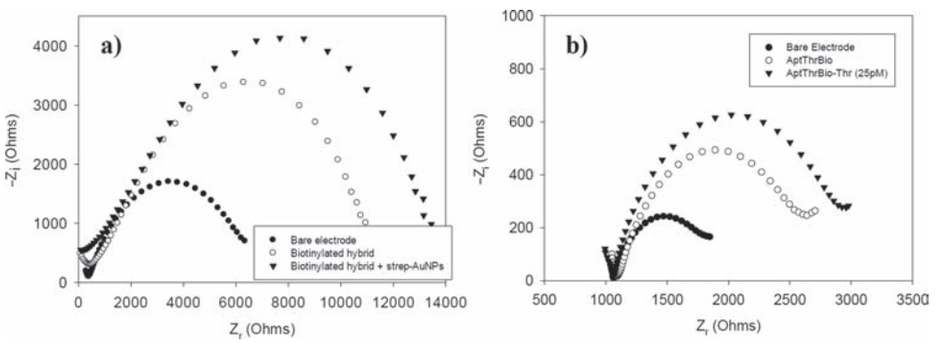

Figure 5. Nyquist Diagram for: (a) *E. Coli* detection and (b) Thrombin detection.

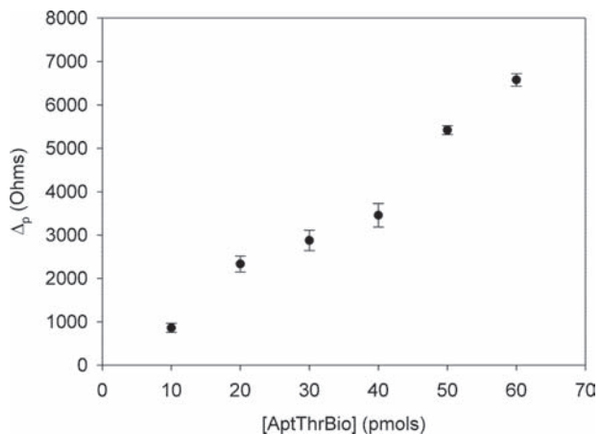

Figure 6. Optimization of the concentration of biotinylated aptamer for thrombin Apt-Thr. Uncertainty values corresponding to replicated experiments ($n = 5$).

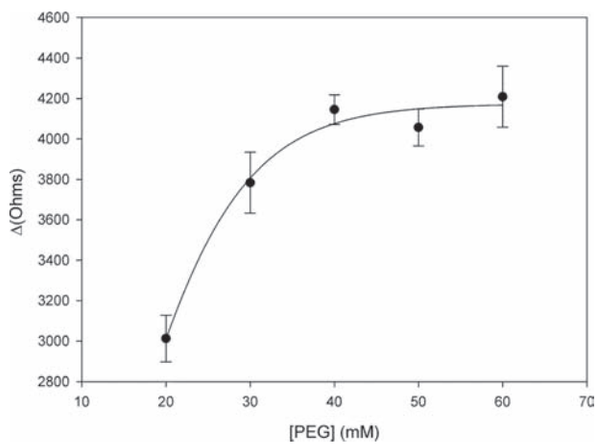

Figure 7. Optimization of the concentration of the blocking agent, PEG. Uncertainty values corresponding to replicated experiments ($n = 5$).

electrode surface, polyethylene glycol (PEG) was used as a blocking agent following aptamer fixation. Figure 7 shows the curve of PEG concentration on the electrode surface and, like in the previous case, there is an increase in resistance until a value of 40 mM of PEG where the saturation value is reached. Therefore, the optimal concentration of blocking agent was chosen as 40 mM.

3.3. Detection

After the subsequent optimization of concentrations of the DNA probe or thrombin aptamer, the biosensing process was performed.

3.3.1. DNA Testing

In this case, as explained before, the sequence followed for EIS measurement was: (1) Bare Av-GEC electrode; (2) biotinylated hybrid modified Av-GEC. In this specific case, the hybridization took place in solution because a previously observed increased efficiency.[13] In fact, given the DNA probe and target are both biotinylated, the immobilization into the surface of the electrode can be produced in two possible orientations, but both provide equivalent information as can be deduced from the comparable obtained RSD values. A non-complementary target sequence, as well as the buffer solution alone, were used as negative controls.

In Figure 8, results of experiments and negative controls are represented as the increment in R_{ct} between the bare electrode and the sample modified electrode (Δ). As can be observed, the Δ increment corresponding to an experiment before amplification (bar (+), grey color) results in almost doubling the Δ value corresponding to a negative control. Also before amplification, (bar (−), grey color), these values are highly significant if compared with the associated uncertainties, given as 7.5% RSD for direct measurement and 3.1% RSD for the amplified case. In addition, further increment of the Δ value in the experiment after amplification (bar (+), white color) does not result in a significant change in the case of negative control (bar (−), white color). The net signal amplification (positive test) was of 34%. A rapid estimation of the detection limit was 5.4 pmols.

A Student's *t*-test was performed to compare the results obtained in the positive and negative experiments (both before and after signal amplification step). The difference between the mean values was highly significant in both cases. For the assay without amplification

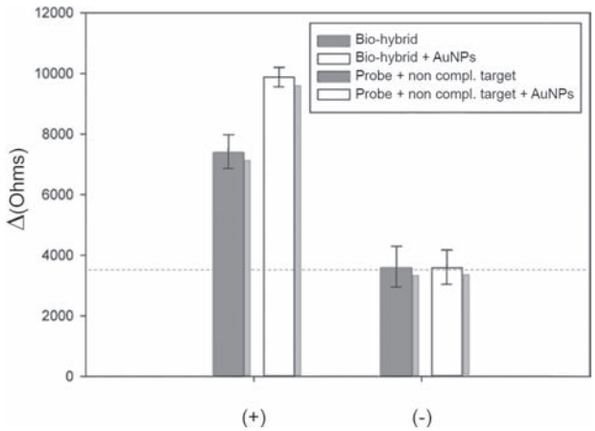

Figure 8. Comparison histogram between experiments and negative control (+) bars: experiments before (grey color) and after signal amplification with gold nanoparticles (white color); (−) bars: negative control before (grey color), after signal amplification with gold nanoparticles (white color). Indicated reproducibility corresponds to observed standard deviation of five replicated experiments.

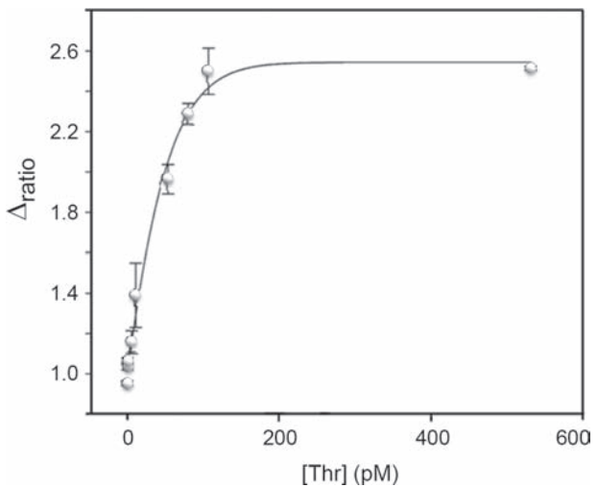

Figure 9. Calibration curve versus thrombin concentration. ($\Delta_{ratio} = \Delta s/\Delta p$; $\Delta s = R_{ct(AptThrBio\text{-}Thr)} - R_{ct(bare\ electrode)}$; $\Delta p = R_{ct(AptThrBio)} - R_{ct(bare\ electrode)}$).

$t_{calc} = 67.97 > t_{tab} = 2.13$; for the assay with amplification $t_{calc} = 53.14 > t_{tab} = 2.13$, at the 95% confidence level and 4 degrees of freedom. Finally, this confirms the significant difference between the signal obtained for the hybridization experiment, with or without amplification and that obtained for non-specific hybridization experiments with, and without amplification.

3.3.2. Protein Detection

The association of the protein (in this case thrombin) with the aptamer resulted in the switch of the surface charge. This provided a positive charge interface that led to a decrease in electron transfer resistance due to the electrostatic attraction of the redox marker. Detected changes in the interfacial electron-transfer resistances at various protein concentrations enabled quantitative analysis of thrombin protein. Figure 9 shows the calibration curve, representing relative signal, Δ_{ratio}, versus the concentration of thrombin. As can be observed, a saturation curve is obtained, where the initial step can be approximated to a straight line, with a linear range from 0.75 pM to 100 pM for the protein. Moreover, a good linear relationship ($r^2 = 0.9921$) between the analytical signal (Δ_{ratio}) and the thrombin concentration in this range was obtained, according to the equation: $\Delta_{ratio} = 1.053 + 1.530 \cdot 10^{10}$ [Thr]. The detection limit, calculated as three times the standard deviation of the intercept obtained from the linear regression, was 4.7 pM. The reproducibility of the method showed a relative standard deviation (RSD) of 4.9%, obtained from a series of 5 experiments carried out in a concentration of 75 pM Thr. These are satisfactory results for the detection of thrombin in real samples, since this level is exactly the concentration threshold for the formation of thrombus.

To study the selectivity of this system, we evaluated the response of proteins typically present in serum such as fibrinogen, immunoglobulin G and albumin. Table I summarizes the parameters of the calibration curve for each protein as well as thrombin, in addition to their respective slopes and detection limits. The aptasensor showed the highest sensitivity for its target molecule, thrombin, with its slope being five orders of magnitude greater than the slope for IgG, and six orders of magnitude larger than the one for fibrinogen. Thus, it was demonstrated that the aptasensor exhibited a much higher sensitivity to Thr, regarding potential interfering proteins, which displayed this effect due to the high level of concentration in which they may be present in serum.

3.3.3. Scanning Electron Microscopy

E.Coli DNA biosensors were investigated via SEM after the silver enhancement treatment (an acceleration voltage of 15 kV and a resolution of 2 μm were used to take the different images). Silver enhancement treatment was employed in order to obtain an adequate size enlargement of strep-AuNPs present on sensor surface to allow their observation with SEM. This treatment was made possible with the use of the biotinylated target, which allowed the coupling with extra elements to the free end. Images obtained are shown in Figure 10. Image on the left corresponds to the experiment where the biotinylated complementary target was used during the hybridization step. In the figure, the strep-AuNPs distribution onto the electrode surface is quite homogeneous. This also implies a regular distribution of avidin molecules in the biocomposite and a well-organized formation of the hybrid. Comparing this image with the one on the right, from a negative control, where a non-complementary target was employed in the hybridization, it is clear that the

Table I. Summary of calibration results for thrombin and other major proteins presents in serum.

Protein	Regression line	Sensitivity (M^{-1})	Detection limit	Typical conc. in serum
Thrombin	$\Delta_{ratio} = 1.053 + 1.530 \cdot 10^{10}$ [Thr]	$1.530 \cdot 10^{10}$	4.7 pM	0
Fibrinogen	$\Delta_{ratio} = 0.9857 + 1.499 \cdot 10^{4}$ [Fbr]	$1.499 \cdot 10^{4}$	1.6 μM	6–12 μM
Immunoglobulin G	$\Delta_{ratio} = 0.6942 + 1.082 \cdot 10^{5}$ [IgG]	$1.082 \cdot 10^{5}$	7.9 μM	60–100 μM
Albumin	No response	–	–	0.52–0.75 μM

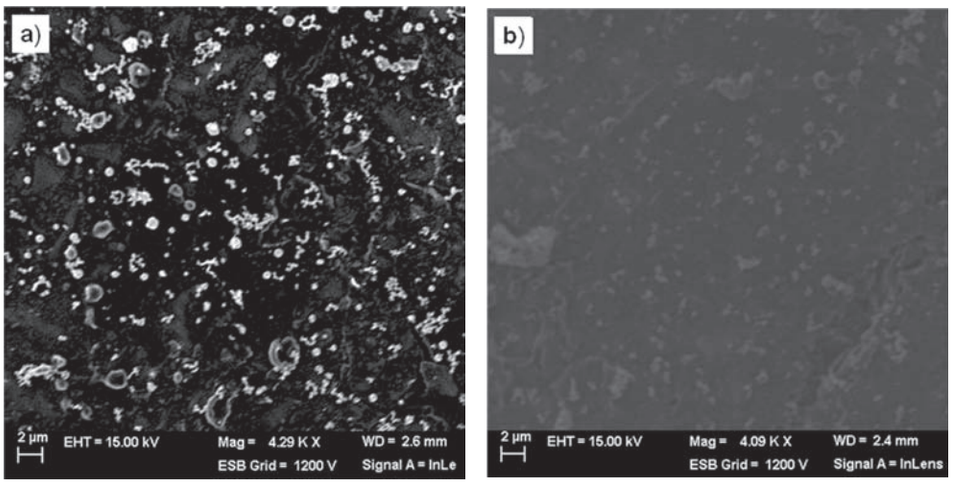

Figure 10. SEM images of (a) experiment using biotinylated hybrid + strep-AuNPS + silver enhancement treatment (b) negative control using probe + non complementary target + strep-AuNPs + silver enhancement treatment. All images were taken at an acceleration voltage of 15 kV and a resolution of 2 μm.

strep-AuNPs are bound to the positive test biotinylated DNA.

4. CONCLUSIONS

This work reports on an Av-GEC based biosensor platform for two different detection strategies: the DNA hybrid and protein detection using electrochemical impedance spectroscopy. This electrochemical technique has demonstrated itself as being a very sensitive technique for the monitoring of biorecognition events such as the hybridization event discussed as well as protein detection. The two strategies were performed and compared in order to improve the Av-GEC performance. The first strategy was used for the rapid and sensitive detection of *Escherichia Coli* O104:H4, and the second strategy was used for thrombin detection employing an aptamer as the biorecognition element. These two systems presented high sensitivity and reproducibility; accordingly, these methods could represent a valid alternative to more conventional gene assays or immunoassay techniques. The applicability of the avidin-modified surface is then demonstrated for the two different biosensing variants. Signal amplification of the biotinylated hybrid by strep-AuNPs was demonstrated with a nanomaterial such as gold nanoparticles. In this case, net amplification of the signal can be approximately 34%, thereby improving sensitivity. In addition, the observation of the electrode surface by SEM after silver enhancement treatment confirmed the homogeneity of the Av-GEC bioplatform used, and thus permitted direct visualization of the biosensor performance.

Acknowledgments: Financial support for this work has been provided by the Ministry of Science and Innovation (MICINN, Madrid, Spain) through project CTQ2010-17099 and by the Catalonia program ICREA Academia. Cristina Ocaña thanks for the support to Ministry of Science and Innovation (MICINN, Madrid, Spain) for the predoctoral grant.

References and Notes

1. K. M. Millan, A. J. Spurmanis, and S. R. Mikkelsen, *Electroanalysis* 4, 929 (**1992**).
2. M. Yang, M. E. McGovern, and M. Thompson, *Anal. Chim. Acta* 346, 259 (**1997**).
3. D. J. Patel and A. K. Suri, *Reviews in Molecular Biotechnology* 74, 39 (**2000**).
4. D. J. D. Patel, *Curr. Opin. Chem. Biol.* 1, 32 (**1997**).
5. M. Famulok and A. Jenne, *Curr. Opin. Chem. Biol.* 2, 320 (**1998**).
6. L. Gold, B. Polisky, O. Uhlenbeck, and M. Yarus, *Annu. Rev. Biochem.* 64, 763 (**1995**).
7. R. B. Kotia, L. Li, and L. B. McGown, *Anal. Chem.* 72, 827 (**2000**).
8. G. A. Evtugyn, V. B. Kostyleva, A. V. Porfireva, M. A. Savelieva, V. G. Evtugyn, R. R. Sitdikov, I. I. Stoikov, I. S. Antipin, and T. Hianik, *Talanta* 102, 156 (**2012**).
9. C. A. Holland, A. T. Henry, H. C. Whinna, and F. C. Church, *FEBS Lett.* 484, 87 (**2000**).

10. M. J. M. Burgering, L. P. M. Orbons, A. vanderDoelen, J. Mulders, H. J. M. Theunissen, P. D. J. Grootenhuis, W. Bode, R. Huber, and M. T. Stubbs, *J. Mol. Biol.* 269, 395 **(1997)**.
11. S. Centi, S. Tombelli, M. Minunni, and M. Mascini, *Anal. Chem.* 79, 1466 **(2007)**.
12. C. R. H. Raetz and C. Whitfield, *Annu. Rev. Biochem.* 71, 635 **(2002)**.
13. A. Bonanni, M. I. Pividori, S. Campoy, J. Barbé, and M. d el Valle, *Analyst* 134, 602 **(2009)**.
14. M. Lee and D. R. Walt, *Anal. Biochem.* 282, 142 **(2000)**.
15. B. R. Srijanto, C. P. Cheney, D. L. Hedden, A. C. Gehl, P. B. Crilly, M. A. Huestis, and T. L. Ferrell, *Sens. Lett.* 10, 850 **(2012)**.
16. A. Radi, J. L. Acero Sánchez, E. Baldrich, and C. K. O'Sullivan, *Anal. Chem.* 77, 6320 **(2005)**.
17. J. R. McDonald, Impedance Spectroscopy, Wiley, New York **(1987)**.
18. A. Bonanni and M. del Valle, *Anal. Chim. Acta* 678, 7 **(2010)**.
19. A. Bardea, F. Patolsky, A. Dagan, and I. Willner, *Chem. Commun.* 21 **(1999)**.
20. A. H. Loo, A. Bonanni, A. Ambrosi, H. L. Poh, and M. Pumera, *Nanoscale* 4, 921 **(2012)**.
21. A. Bonanni, M. J. Esplandiu, and M. del Valle, *Biosens. Bioelectron.* 26, 1245 **(2010)**.
22. Y. Li, L. Syed, J. Liu, D. H. Hua, and J. Li, *Anal. Chim. Acta* 744, 45 **(2012)**.
23. F. Blin, P. Koutsoukos, P. Klepetsianis, and M. Forsyth, *Electrochim. Acta* 52, 6212 **(2007)**.
24. Y.-M. Liao, Z.-D. Feng, and Z.-L. Chen, *Journal of Dentistry* 35, 425 **(2007)**.
25. J. Wang, *Analyst* 130, 421 **(2005)**.
26. A. Merkoci, M. Aldavert, S. Marin, and S. Alegret, *Trac-Trends Anal. Chem.* 24, 341 **(2005)**.
27. I. I. Suni, *TrAC Trends in Analytical Chemistry* 27, 604 **(2008)**.
28. S. Tombelli, M. Minunni, A. Santucci, M. M. Spiriti, and M. Mascini, *Talanta* 68, 806 **(2006)**.
29. M. B. Gonzalez-Garcia, C. Fernandez-Sanchez, and A. Costa-Garcia, *Biosens. Bioelectron.* 15, 315 **(2000)**.
30. A. Ambrosi, M. T. Castaneda, A. J. Killard, M. R. Smyth, S. Alegret, and A. Merkoci, *Anal. Chem.* 79, 5232 **(2007)**.
31. A. Lermo, S. Campoy, J. Barbé, S. Hernández, S. Alegret, and M. I. Pividori, *Biosens. Bioelectron.* 22, 2010 **(2007)**.
32. S. Alegret, *Analyst* 121, 1751 **(1996)**.
33. J. Kim, K. Oh, S. Jeon, S. Cho, D. Lee, S. Hong, S. Cho, M. Park, D. Jeon, and S. Kim, *Emerging Infectious Diseases* 17, 1755 **(2011)**.
34. E. Williams, M. I. Pividori, A. Merkoçi, R. J. Forster, and S. Alegret, *Biosens. Bioelectron.* 19, 165 **(2003)**.
35. A. Bonanni, M. J. Esplandiu, M. I. Pividori, S. Alegret, and M. del Valle, *Anal. Bioanal. Chem.* 385, 1195 **(2006)**.
36. E. Katz and I. Willner, *Electroanalysis* 15, 913 **(2003)**.
37. A. Bonanni, M. J. Esplandiu, and M. del Valle, *Electrochim. Acta* 53, 4022 **(2008)**.
38. A. Bonanni, M. I. Pividori, and M. del Valle, *Anal. Bioanal. Chem.* 389, 851 **(2007)**.

Received: 30 April 2013. Accepted: 30 May 2013.

Article 4. Label-free impedimetric aptasensor based on epoxy-graphite electrode for the recognition of cytochrome c

C. Ocaña, E. Arcay and M. del Valle

Sensors and Actuators:B, 2014, 191, 860-865.

Provided for non-commercial research and education use.
Not for reproduction, distribution or commercial use.

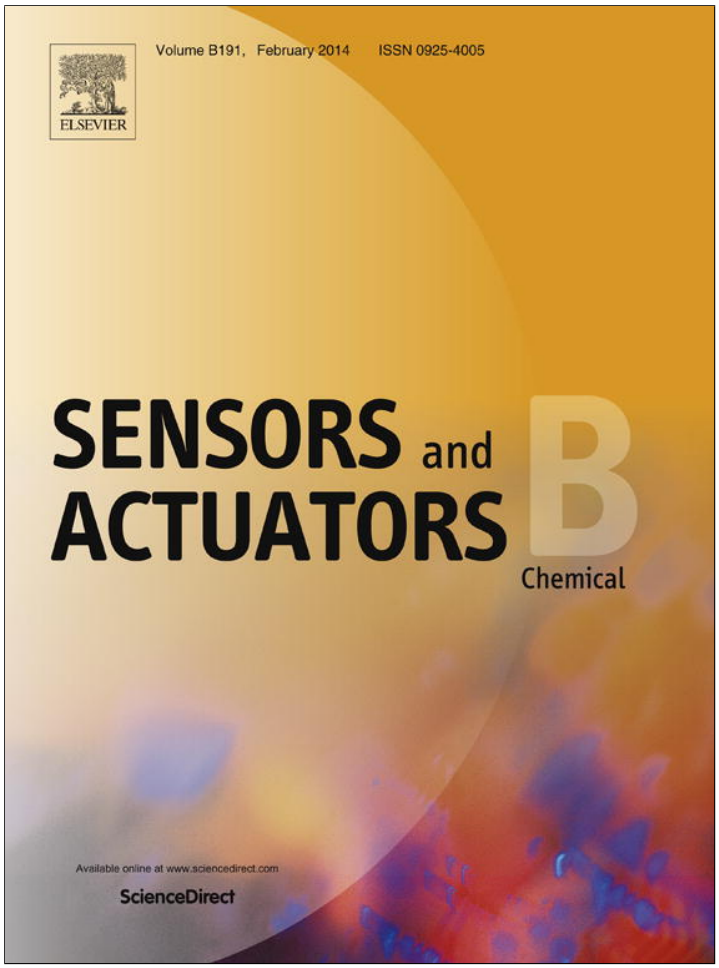

This article appeared in a journal published by Elsevier. The attached copy is furnished to the author for internal non-commercial research and education use, including for instruction at the authors institution and sharing with colleagues.

Other uses, including reproduction and distribution, or selling or licensing copies, or posting to personal, institutional or third party websites are prohibited.

In most cases authors are permitted to post their version of the article (e.g. in Word or Tex form) to their personal website or institutional repository. Authors requiring further information regarding Elsevier's archiving and manuscript policies are encouraged to visit:

http://www.elsevier.com/authorsrights

Author's personal copy

Sensors and Actuators B 191 (2014) 860–865

Contents lists available at ScienceDirect

Sensors and Actuators B: Chemical

journal homepage: www.elsevier.com/locate/snb

Label-free impedimetric aptasensor based on epoxy-graphite electrode for the recognition of cytochrome *c*

Cristina Ocaña, Evelien Arcay, Manel del Valle*

Sensors and Biosensors Group, Department of ChemistryUniversitat Autonoma de Barcelona, Bellaterra, Barcelona 08193, Spain

ARTICLE INFO

Article history:
Received 16 July 2013
Received in revised form
30 September 2013
Accepted 9 October 2013
Available online 25 October 2013

Keywords:
Cytochrome *c*
Aptasensor
Impedance
Aptamer
Label free

ABSTRACT

In this work, we present a label -free impedimetric aptasensor for the recognition of cytochrome *c* (Cyt *c*) at a pM concentration level based on an epoxy-graphite composite electrode. The technique employed for the detection of the protein Cyt *c* is electrochemical impedance spectroscopy (EIS). Detection occurs when the protein interacts with the immobilized aptamer on the aptasensor. The aptamer immobilization technique is based on its wet physical adsorption onto the electrode surface, which assures a simple, ready-to-use preparation of the biosensing platform. The work first optimizes concentration of immobilized aptamer, followed by blocking agent to avoid non specific interactions, and finally performs the label-free detection of Cyt *c*. The amount of protein is quantified by the observed increase of the electron-transfer resistance, determined employing EIS and the $[Fe(CN)_6]^{3-,4-}$ redox marker. Results demonstrate that the aptasensor has a good detection range for Cyt *c* between 50 pM and 50 nM, as well as a high sensitivity with a low detection limit of 63.2 pM, well below levels of this protein in serum. Cross response of the developed aptamer biosensor versus potential interfering proteins also present in human serum has been fully characterized.

© 2013 Elsevier B.V. All rights reserved.

1. Introduction

Cytochrome *c* (Cyt *c*) is primarily known as an electron-carrying mitochondrial protein. The transition of Cyt *c* between the ferrous and ferric states within the cell makes it an efficient biological electron-transporter whereas it plays a vital role in cellular oxidations in both plants and animals. It is generally regarded as a universal catalyst of respiration, forming an essential electron-bridge between the respirable substrates and oxygen. This protein has been identified as an important mediator in apoptotic pathways. The release of mitochondrial Cyt *c* into the cytoplasm stimulates apoptosis, therefore it is used as an indicator of the apoptotic process in the cell [1]. For this reason, it is important to evaluate its concentration. Normal non-pathological level of this protein in human serum is around 2 nM [2].

In recent years, there has been great interest in the development of aptasensors [3]. Aptasensors are biosensors that use aptamers as the biorecognition element. Aptamers are artificial DNA or RNA oligonucleotides selected *in vitro* which have the ability to bind to proteins, small molecules or even whole cells, recognizing their target with high affinity and specificity, often matching or even exceeding those of antibodies [4]. Furthermore, because of a marked reversibility, the recognition process can be reverted and is stable in broad terms, an important advantage in front of immunosensors. Among described cases in the literature, there are two different configurations of aptamers: linear and molecular beacon. Aptamers with a linear configuration maintain, in certain physicochemical conditions, a typical 3D shape conformation with a specific binding site for the target molecule. Obviously recognition employs host-guest principles [5]. On the other hand, aptamers with a molecular beacon configuration initially form a loop that changes conformation following binding to the analyte of interest [6]. Aptamers can be used in a wide range of applications, such as therapeutics [7], molecular switches, drug development, affinity chromatography [8] or biosensors [9].

In biosensor field, different transduction techniques can be used; optical [10], atomic force microscope [11], surface plasmon resonance [12], electrochemical [13] and piezoelectric [14] aptasensors have been described. In the last years, among the different electrochemical techniques reported, the use of electrochemical impedance spectroscopy (EIS) has grown among these studies [15]. EIS is a characterization technique that is based on applying an AC potential to an electrochemical cell and measuring the current that crosses through the cell [16]. It is very sensitive to changes of the interfacial properties of modified electrodes upon biorecognition events taking place at the electrode surfaces [17,18]. Other important features presented by EIS are that it does not require any special reagent for the analysis, has the capacity for

* Corresponding author. Tel.: +34 93 5813235; fax: +34 93 5812477.
E-mail addresses: manel.delvalle@uab.cat, manel.delvalle@uab.es (M. del Valle).

0925-4005/$ – see front matter © 2013 Elsevier B.V. All rights reserved.
http://dx.doi.org/10.1016/j.snb.2013.10.040

Author's personal copy

label-free detection and is a cost-efficient technique. For all these reasons, EIS is becoming a popular electrochemical tool for numerous applications such as immuno [18], genosensing [19], enzyme activities [20] or studies of corrosion [21] or surface phenomena [22].

In this communication, we report a label-free impedimetric aptasensor for the recognition of Cyt c. The transducer employed consists of a graphite-epoxy composite (GEC) electrode, of general use in our laboratories which has already been extensively studied and applied to amperometric, enzymatic, immuno and genosensing [23–25] assays. The uneven porous surface of the GEC electrode allows the immobilization of aptamers on its surface by simple wet physical adsorption. This surface can be renewed after each experiment by simply polishing with different abrasive papers and reused after the assay with a wet thermal treatment [3]. This type of sensor has been already used for impedimetric detection of DNA hybridization [26] and very recently for the first aptasensor [3]. The transduction principle used is based on the change of electron transfer resistance in the presence of the $K_3[Fe(CN)_6]/K_4[Fe(CN)_6]$ redox marker, which can be measured by EIS [16]. The proposed aptasensor showed appropriate response behaviour values to determine Cyt *c* in the picomolar range.

2. Experimental

2.1. Chemicals

Potassium dihydrogen phosphate, potassium ferricyanide $K_3[Fe(CN)_6]$, potassium ferrocyanide $K_4[Fe(CN)_6]$, hexaammineruthenium(III) chloride $[Ru(NH_3)_6]Cl_3$, sodium monophosphate and the target protein cytochrome *c* (Cyt *c*), were purchased from Sigma (St. Louis, MO, USA). Poly(ethylene glycol) 1.000 (PEG), tris(hydroxymethyl)aminomethane (Tris), sodium chloride and potassium chloride were purchased from Fluka (Buchs, Switzerland). All solid-state electrodes (GECs) were prepared using 50 μm particle size graphite powder (Merck, Darmstadt, Germany) and Epotek H77 resin and its corresponding hardener (both from Epoxy Technology, Billerica, MA, USA). All reagents were analytical reagent grade. The aptamer (AptCyt*c*) used in this study [2], with sequence 5′-AGTGTGAAATATCTAAACTAAATGTGGAGGGTGGGACGGGAAGAA-GTTTATTTTTCACACT-3′, was prepared by TIB-MOLBIOL (Berlin, Germany). Stock solutions of aptamer and Cyt *c* were diluted with sterilized and deionised water, separated in fractions and stored at −20 °C until used.

All solutions were prepared using Milli*Q* water from MilliQ System (Millipore, Billerica, MA, USA). The buffer employed was PBS (187 mM NaCl, 2.7 mM KCl, 8.1 mM $Na_2HPO_4{\cdot}2H_2O$, 1.76 mM KH_2PO_4, pH 7.0).

2.2. Apparatus

AC impedance measurements and Cyclic Voltammetry were performed in an Autolab PGStat 20 (Metrohm Autolab B.V, Utrecht, The Netherlands). FRA and GPES (Metrohm Autolab) software were used for data acquisition and control of the experiments. A three electrode configuration was used to perform the impedance measurements: a platinum-ring auxiliary electrode (Crison 52-67, Barcelona, Spain), an Ag/AgCl reference electrode and the constructed GEC as the working electrode (with a geometric area of 28.27 mm^2). Temperature-controlled incubations were done using an Eppendorf Thermomixer 5436.

2.3. Preparation of working electrodes

The electrodes were prepared using a PVC tube body (6 mm i.d.) and a small copper disk soldered to the end of an electrical connector. The working surface is an epoxy-graphite conductive composite, formed by a mixture of graphite (20%) and epoxy resin (80%), deposited in the cavity of the plastic body [25]. The composite material was cured at 80 °C for 3 days. Before each use, the electrode surface was moistened with MilliQ water, then thoroughly smoothed with abrasive sandpaper and finally with alumina paper (polishing strips 301044-001, Orion) in order to obtain a reproducible electrochemical surface.

2.4. Procedure

The analytical procedure for biosensing consists of the immobilization of the aptamer onto the transducer surface using a wet physical adsorption procedure, the blocking to minimize non specific adsorption and the recognition of the protein by the aptamer. The scheme of the experimental procedure is represented in Fig. 1, with the steps described in more detail below.

The first step consisted of aptamer immobilization onto the electrode surface.160 μL of aptamer solution in MilliQ water at the desired concentration was heated at 80–90 °C for 3 min to promote the loose conformation of the aptamer. Then, the solution was dipped in a bath of cold water and the electrode was immersed in it, where the adsorption took place for 15 min. This was followed by two washing steps using PBS buffer solution for 10 min, in order to remove any unadsorbed aptamer.

After that, to minimize any possible nonspecific adsorption, the electrode was dipped in 160 μL of PEG 35 mM for 15 min. This was followed by two washing steps using PBS buffer solution for 10 min.

The last step is the recognition of Cyt *c* by the immobilized aptamer. For this, the electrode was dipped in a solution with the desired concentration of Cyt *c*. The incubation took place for 15 min. Then, the biosensor was washed twice with PBS buffer solution for 10 min.

2.5. Cyclic voltammetry measurements

Cyclic Voltammetry (CV) experiments to determine the redox potential of the redox pair $K_3[Fe(CN)_6]/K_4[Fe(CN)_6]$ were carried out at room temperature in PBS buffer containing 0.01 M $K_3[Fe(CN)_6]/K_4[Fe(CN)_6]$ in the voltage range of −1.5 V to 1.5 V at a scan rate of 0.5 V/s. CV measurements to obtain surface density of AptCyt*c* were performed at room temperature in 10 mM Tris buffer (pH 7.4) containing 50 μM $[Ru(NH_3)_6]Cl_3$, in the voltage range of −1.5 V to 1.5 V, at scan rate 0.05 V/s. In these CV, the cathodic peak of the first scan was integrated to determine the AptCyt*c* surface density on GEC electrodes.

2.6. Impedimetric measurements

Impedance experiments were carried out at an applied potencial of 0.17 V (vs. Ag/AgCl reference electrode) obtained from the redox potential of $[Fe(CN)_6]^{3-}/[Fe(CN)_6]^{4-}$ by CV (see Appendices A and B), with a range of frequency of 50 kHz–0.05 Hz, an AC amplitude of 10 mV and a sampling rate of 10 points per decade above 66 Hz and 5 points per decade at the lower range. All measurements were performed in PBS buffer containing 0.01 M $K_3[Fe(CN)_6]/K_4[Fe(CN)_6]$ (1:1) mixture, used as a redox marker. In all cases impedance data were recorded in the following order after each electrode successive modification: (1) bare electrode; (2) immobilization step; (3) Blocking step; (4) Biorecognition. The impedance spectra were

Author's personal copy

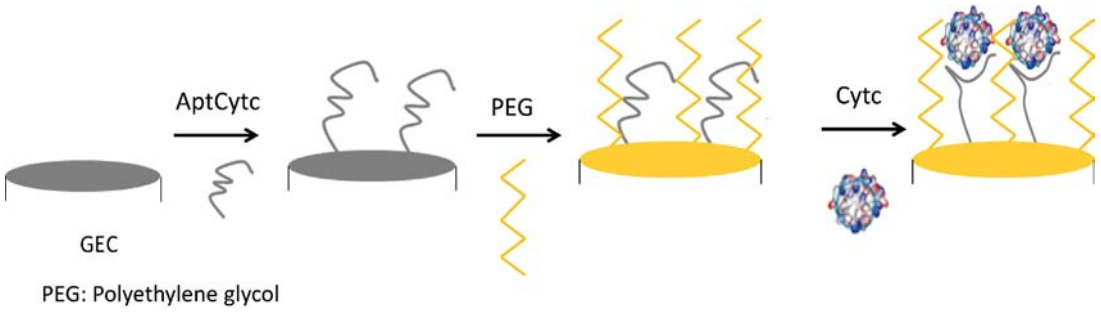

Fig. 1. Schematic representation of electrochemical aptasensor for the detection of Cyt *c* based on a graphite-epoxy composite.

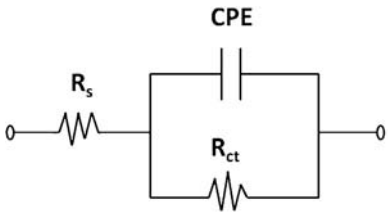

Fig. 2. Equivalent circuit used for the data fitting. R_s is the resistance of the solution, R_{ct} is the electron-transfer resistance and CPE, the capacitive contribution, in this case as a constant phase element.

plotted in the form of complex plane diagrams (Nyquist plots, $-Z_i$ *vs.* Z_r) and fitted to a theoretical curve corresponding to the equivalent circuit with Z_{view} software (Scribner Associates Inc., USA). The equivalent circuit, shown in Fig. 2, was formed by one resistor/capacitor element in series with a resistance. The parameter R_s corresponds to the resistance of the solution, R_{ct} is the charge transfer resistance between the solution and the electrode surface, whilst constant phase element (CPE) is associated with the double-layer capacitance (attributable to the interface between the electrode surface and the solution). For all performed fittings, the chi-square goodness-of-fit test was thoroughly checked to verify calculations. In all cases, calculated values for each circuit remained in the range of 0.0003–0.15 much lower than the tabulated value for 50 degrees of freedom (67.505 at 95% confidence level). In this work, we focused on the variation of change in resistance transfer (R_{ct}). In order to compare the results obtained from the different electrodes used, and to obtain independent and reproducible results, relative and normalized signals were needed [16]. Thus, the Δ_{ratio} value was defined according to the following equations:

$$\Delta_{ratio} = \frac{\Delta_s}{\Delta_p}$$

$$\Delta_s = R_{ct(AptCytc-Cytc)} - R_{ct(electrode-buffer)}$$

$$\Delta_p = R_{ct(AptCytc)} - R_{ct(electrode-buffer)}$$

where $R_{ct(AptCytc\text{-}Cytc)}$ was the electron transfer resistance value measured after incubation with the Cyt *c* protein, $R_{ct\ (AptCytc)}$ was the electron transfer resistance value measured after aptamer inmobilitation on the electrode and $R_{ct\ (electrode\text{-}buffer)}$ was the electron transfer resistance of the blank electrode and buffer.

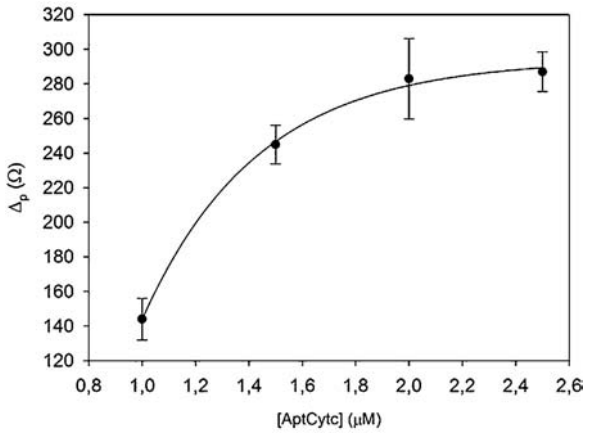

Fig. 3. Optimization of the concentration of AptCyt*c* immobilized on each aptasensor. All experiments were performed in PBS solution and all EIS measurements were performed in PBS solution containing 0.01 M $K_3[Fe(CN)_6]/K_4[Fe(CN)_6]$. Uncertainty values corresponding to replicated experiments ($n = 5$).

3. Results and discussion

3.1. Optimization of aptamer and PEG concentrations

The first step of the experiment was the optimization of the experimental concentrations of aptamer immobilized on the electrode and poly(ethylene glycol) (PEG) on the electrode surface by constructing its relative response curves.

The calibration curve was carried out by increasing amount of concentration of AptCyt*c* used from 1 to 2.5 μM. The different concentrations were evaluated by the changes in the Δ_p. As can be seen in Fig. 3, the Δ_p increased with the AptCyt*c* concentration until a saturation value. This is due to the physical adsorption of the aptamer onto the electrode surface, which followed a Langmuir isotherm; in it, the variation of R_{ct} increased to reach a saturation value, chosen as the optimal concentration. The value relected for the aptasensor corresponded to a concentration of aptamer of 1.75 μM, as the compromise between the two extremes.

The use of blocking agent (PEG) on the electrode surface was introduced to minimize the non specific adsorption of other species, which would alter the observed impedimetric signal. Apart, these other species can potentially interact or disturb the binding of the Cyt *c* on the AptCyt*c* in the further steps and thus must be avoided. For the optimization of the PEG concentration we proceeded as

Table 1
Quantification of surface coverage of all steps of the procedure.

	Bare electrode	AptCyt*c*	PEG	Cyt *c* (10^{-9} M)
Γ (10^{11} molecules/cm^2)	0.04 ± 0.20	3.33 ± 0.34	3.45 ± 0.33	1.76 ± 0.34

Author's personal copy

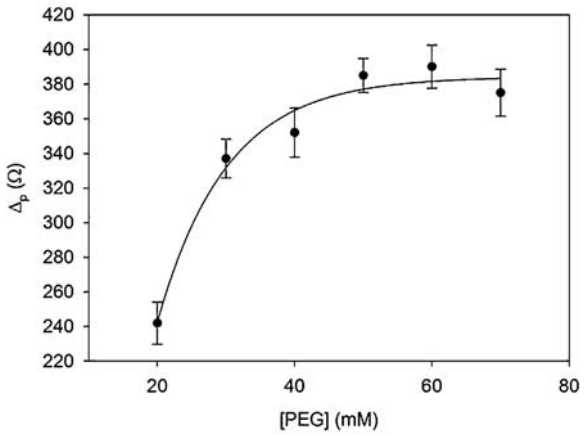

Fig. 4. Optimization of the concentration of the blocking agent, PEG. All experiments were performed in PBS solution and all EIS measurements were performed in PBS solution containing 0.01 M $K_3[Fe(CN)_6]/K_4[Fe(CN)_6]$. Uncertainty values corresponding to replicated experiments ($n = 5$).

above. PEG concentrations were increased from 20 to 70 mM and the electrochemical characteristics of the electrode were determined. As it can be observed in Fig. 4, the Δ_p increased up to a certain saturation value. The value selected as the optimal PEG concentration was 35 mM, corresponding to the intersection of the two extreme behaviours.

In order to obtain the surface coverage, a known procedure was used [27]. This consisted in obtaining the CV responses of $[Ru(NH_3)_6]^{6+}$ on an epoxy-graphite composite electrode (electrode-buffer) with AptCyt*c*, after PEG treatment and after cytochrome *c* detection (see Appendices A and B). The results are shown in Table 1. The values clearly show that the surface density is maintained before and after PEG treatment.

3.2. Detection of Cyt c

The aptamer of Cyt *c* forms a linear single-strand oligonucleotide, in sequence that recognizes the protein by a specific folding. During this folding, weak interactions between the aptamer and protein of the host-guest type are created, leading to complex AptCyt*c*-Cyt*c*. One example of the obtained response after each biosensing step is shown in Fig. 5. As can be seen in this figure, R_{ct} increased after any modification of the electrode surface.

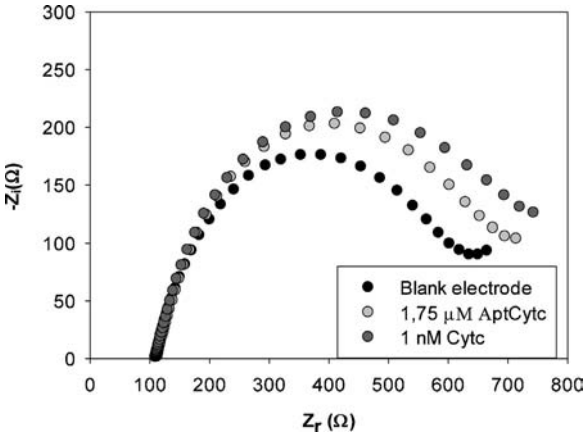

Fig. 5. Nyquist diagrams for EIS measurements of: (black circles) bare GEC electrodes, (grey circles) AptCyt*c* modified electrodes and (dark grey circles) AptCyt*c*–Cyt *c* modified electrodes. All experiments were performed in PBS solution and all EIS measurements were performed in PBS solution containing 0.01 M $K_3[Fe(CN)_6]/K_4[Fe(CN)_6]$.

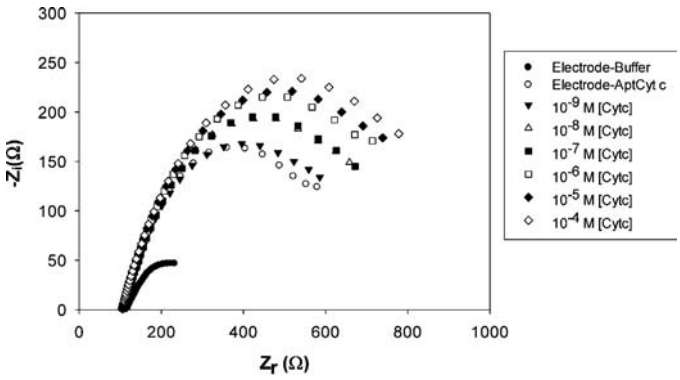

Fig. 6. Nyquist diagrams for different concentrations of Cyt *c*. All experiments were performed in PBS solution and all EIS measurements were performed in PBS solution containing 0.01 M $K_3[Fe(CN)_6]/K_4[Fe(CN)_6]$.

This can be due to the increased difficulty of the redox reaction of $[Fe(CN)_6]^{3-/4-}$ to take place, due to the sensor surface alteration [28]. Two different factors may be taken into account to explain that: the electrostatic effect and the sterical hindrance. The electrostatic repulsion is more significant in the first step of protocol; when the AptCyt*c* is immobilized onto the electrode surface, a first layer is formed, where negatively charged phosphate groups of aptamer skeleton are responsible of the electrical repulsion towards the negatively charged redox marker, thus inhibiting the interfacial transfer process and resulting in R_{ct} increment. When the protein is added R_{ct} should decrease considering that the pI of the protein is 10–10.5 [29], and therefore it is positively charged, then favouring electrostatically the arrival of the redox marker to the electrode. In contrast, according to the capacitance values calculated from the different experiments varying Cytc concentration, the capacitance values are kept practically constant, 0.45 ± 0.03 μF. The R_{ct} increase seems to be due, then, to the sterical factor dominating over the electrostatic factor.

3.3. Sensitivity of aptasensor

In order to obtain the sensitivity of the aptasensor a complete calibration curve, was built defined by using an increasing concentration of Cyt *c*. Fig. 6, illustrates the increasing impedimetric signal with increasing Cyt *c* concentration. Relative signal Δ_{ratio} were plotted for the different Cyt *c* concentration assays, as shown in Fig. 7. As it can be observed, a logarithmic relationship was obtained, with a linear range from 50 pM to 50 nM

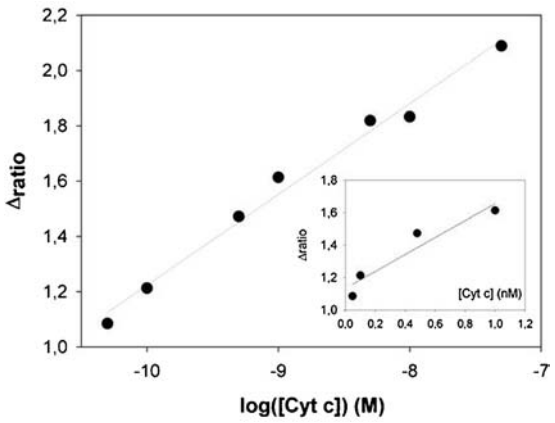

Fig. 7. Calibration curve, relative signal *vs.* Cyt *c* concentration. All experiments were performed in PBS solution and all EIS measurements were performed in PBS solution containing 0.01 M $K_3[Fe(CN)_6]/K_4[Fe(CN)_6]$.

Author's personal copy

Table 2
Comparison of the proposed Cyt *c* biosensor with other reported biosensing methods.

Analytical method	Detection limit	Biorecognition element	%RSD	Interfering proteins	Reference
EIS	63.2 pM	Aptamer	6.8	Albumin, Fbr, IgG	Our work
EIS	10 nM	Calixarens	10	BSA	[31]
CV	0.5 μM	Enzyme	2.8	Ascorbic and Uric acid	[32]
SQR-CV	0.2 μM	Enzyme	-	Serum samples	[33]
Fluorescence	44.4 pM	Aptamer	-	Serum samples	[34]
ICP-MS/TEM	1.5 fM	Antibody	6.6	Serum samples	[30]

Table 3
Summary of calibration results for Cyt *c* and other major proteins presents in serum.

Protein	Regression line	Sensitivity (M^{-1})	Detection limit	Typical conc. in serum
Cyt *c*	$\Delta_{ratio} = 1.130 + 5.236 \times 10^8$ [Cyt *c*]	5.24×10^8	63.2 pM	2 nM
Albumin	$\Delta_{ratio} = 0.672 + 8.377 \times 10^3$ [Alb]	8.38×10^3	0.300 mM	0.52–0.75 mM
Fbr	$\Delta_{ratio} = -0.909 + 5.3301 \times 10^5$ [Fbr]	5.33×10^5	7.10 μM	6–12 μM
IgG	$\Delta_{ratio} = -0.6181 + 4.435 \times 10^4$ [IgG]	4.44×10^4	0.143 μM	60–100 μM

for the protein. Moreover, a good linear relationship ($r = 0.993$) between the relative analytical signal (Δ_{ratio}) and the Cyt *c* concentration in this range was obtained according to the equation: $\Delta_{ratio} = 1.13 + 5.24 \times 10^8$ [Cyt *c*] (M). The detection limit was estimated as three times the standard deviation of the intercept obtained from the linear regression, which was 63.2 pM. The reproducibility of the method showed a relative standard deviation (RSD) of 6.8%, obtained from a series of 5 experiments carried out at a concentration of 500 pM Cyt *c*. Additionally, the proposed aptasensor was compared with other detection methodologies for the direct Cyt *c* detection. The detailed results are shown in Table 2, where sensitivity info is presented as the LOD of each biosensor compared. The lowest detection limit value among all the analytical techniques corresponded to [30], but this Cyt *c* biosensor used ICP–MS as the transduction technique. This methodology displays high sensitivity but is not simple, portable or easy to use. Our proposed aptasensor is on the second range of lowest LOD, thus demonstrating satisfactory results for the detection of Cyt *c* in real samples, given this level corresponds to concentration in human serum.

3.4. Selectivity of the aptasensor

Cyt *c* is present in blood serum, which can be described as a complex sample matrix containing hormones, lipids, blood cells and other proteins. To study the selectivity of the system, we evaluated the response of proteins present in serum such as fibrinogen, immunoglobulin G and albumin. All proteins showed some degree of interference for Cyt *c*. For this reason, the calibration curves were built for the serum level concentration of each protein.

To evaluate the sensitivity of the aptasensor we compared the calibration plots for the different interferent proteins. Table 3 summarizes the parameters of the calibration curve of each protein and Cyt *c*, as well as their respective slopes and detection limits. The aptasensor showed the highest sensitivity for its target molecule, Cyt *c*, with its slope being three orders of magnitude greater than the slope for fibrinogen, five orders of magnitude greater than albumin and four orders of magnitude more than that of IgG. Therefore, it was demonstrated that the aptasensor exhibited a much higher sensitivity to Cyt *c* than that to regarding potential interfering proteins, which displayed this effect greatly due to the high level of concentration in which they were assayed.

Apart of previous data, EC_{50} values for each protein and % cross response (% CR) for all interfering proteins were calculated, as summarized in Table 4. The lowest EC_{50} value obtained corresponded Cyt *c*, the target protein with a value of 6.68×10^{-10} M, and the larger, 3.63×10^{-5} M, to Fbr. The largest % CR value corresponded to Fbr, 0.05%, and the lowest to Alb. Therefore, it was demonstrated that the aptasensor showed a much higher sensitivity to Cyt *c*, regarding potential interfering proteins, which displayed this effect due to the high level of concentration in which they are present in serum, and not in a secondary recognition by aptamer.

Table 4
Summary of EC_{50} and %Cross-response values of each interferent protein.

Protein	EC_{50} (M)	% Cross-response
Cyt *c*	6.68×10^{-10}	100
Albumin	6.06×10^{-5}	1.01×10^{-3}
Immunoglobulin G	3.63×10^{-5}	1.84×10^{-3}
Fibrinogen	1.37×10^{-6}	0.05

(%CR = (EC_{50} cytochrome *c*/EC_{50} interferent)100).

4. Conclusions

This comunication reported a simple label-free impedimetric aptasensor for the recognition of Cyt *c* at picomolar concentration level based on GEC electrodes. EIS technique has demonstrated itself as being a very sensitive technique for monitoring the biosensing event and confirmation of steps performed for building the aptasensor. The uneven surface of GEC allowed AptCyt*c* to be absorbed by a simple wet adsorption procedure. The simple preparation and the possibility of renewing the surface by polishing with abrasive paper make it suitable for repeated use. From the results, it can be concluded that the aptasensor showed a low detection limit, 63.2 pM, good range of concentration for Cyt *c* detection, from 50 nM to 50 pM, and high sensitivity, 5.24×10^8 M^{-1}. In addition, running an EIS assay is simple and quick - the Cyt *c* detection process can be finished in 40 min and the stability of a prepared sensor is at least 24 h. The interference produced by serum proteins, such as fibrinogen, immunoglobulin G and albumin, demonstrated some limitations in the operation of the aptasensor, although usable given the concentration excess at which they manifest.

Acknowledgments

Financial support for this work has been provided by the Ministry of Science and Innovation (MICINN, Madrid, Spain) through project CTQ2010-17099 and by the Catalonia program ICREA Academia. Cristina Ocaña thanks the support of Ministry of Science and Innovation (MICINN, Madrid, Spain) for the predoctoral grant.

Appendix A. Supplementary data

Supplementary data associated with this article can be found, in the online version, at http://dx.doi.org/10.1016/j.snb.2013.10.040.

Author's personal copy

References

[1] L.-L. Gao, Paris chinensis dioscin induces G2/M cell cycle arrest and apoptosis in human gastric cancer SGC-7901 cells, World J. Gastroenterol. 17 (2011) 6.
[2] Q. Zhao, X.-F. Li, X.C. Le, Aptamer-modified monolithic capillary chromatography for protein separation and detection, Anal. Chem. 80 (2008) 3915–3920.
[3] C. Ocaña, M. Pacios, M. del Valle, A reusable impedimetric aptasensor for detection of thrombin employing a graphite-epoxy composite electrode, Sensors 12 (2012) 3037–3048.
[4] S.M. Nimjee, C.P. Rusconi, B.A. Sullenger, Aptamers an emerging class of therapeutics, Annu. Rev. Med. 56 (2005) 555–583.
[5] E. Luzi, M. Minunni, S. Tombelli, M. Mascini, New trends in affinity sensing: aptamers for ligand binding, TrAC Trends in Anal. Chem. 22 (2003) 810–818.
[6] S.D. Jayasena, Aptamers An emerging class of molecules that rival antibodies in diagnostics, Clin. Chem. 45 (1999) 22.
[7] G. Biesecker, L. Dihel, K. Enney, R.A. Bendele, Derivation of RNA aptamer inhibitors of human complement C5, Immunopharmacology 42 (1999) 219–230.
[8] R.B. Kotia, L. Li, L.B. McGown, Separation of nontarget compounds by DNA aptamers, Anal. Chem. 72 (2000) 827–831.
[9] G.A. Evtugyn, V.B. Kostyleva, A.V. Porfireva, M.A. Savelieva, V.G. Evtugyn, R.R. Sitdikov, et al., Label-free aptasensor for thrombin determination based on the nanostructured phenazine mediator, Talanta 102 (2012) 156–163.
[10] M. Lee, D.R. Walt, A fiber-optic microarray biosensor using aptamers as receptors, Anal. Biochem. 282 (2000) 142–146.
[11] B. Basnar, R. Elnathan, I. Willner, Following aptamer-thrombin binding by force measurements, Anal. Chem. 78 (2006) 3638–3642.
[12] A. Vasilescu, S. Gaspar, I. Mihai, A. Tache, S.C. Litescu, Development of a label-free aptasensor for monitoring the self-association of lysozyme, Analyst 138 (2013) 3530–3537.
[13] A. Radi, J.L. Acero Sánchez, E. Baldrich, C.K. O'Sullivan, Reusable impedimetric aptasensor, Anal. Chem. 77 (2005) 6320–6323.
[14] B.R. Srijanto, C.P. Cheney, D.L. Hedden, A.C. Gehl, P.B. Crilly, M.A. Huestis, et al., Piezoresistive microcantilevers-based cocaine biosensors, Sens. Lett. 10 (2012) 850–855.
[15] J.R. McDonald, Impedance Spectroscopy, John Wiley, New York, 1987.
[16] A. Bonanni, M. del Valle, Use of nanomaterials for impedimetric DNA sensors: a review, Anal. Chim Acta. 678 (2010) 7–17.
[17] A Bardea, F. Patolsky, A. Dagan, I. Willner, Sensing and amplification of oligonucleotide–DNA interactions by means of impedance spectroscopy: a route to a tay-sachs sensor, Chem. Commun. 7 (1999), 21-2.
[18] A.H. Loo, A. Bonanni, A. Ambrosi, H.L. Poh, M. Pumera, Impedimetric immunoglobulin G immunosensor based on chemically modified graphenes, Nanoscale 4 (2012) 921–925.
[19] A. Bonanni, M.J. Esplandiu, M. del Valle, Impedimetric genosensing of DNA polymorphism correlated to cystic fibrosis: a comparison among different protocols and electrode surfaces, Biosens. Bioelectron. 26 (2010) 1245–1251.
[20] Y. Li, L. Syed, J. Liu, D.H. Hua, J. Li, Label-free electrochemical impedance detection of kinase and phosphatase activities using carbon nanofiber nanoelectrode arrays, Anal. Chim. Acta. 744 (2012) 45–53.
[21] F. Blin, P. Koutsoukos, P. Klepetsianis, M. Forsyth, The corrosion inhibition mechanism of new rare earth cinnamate compounds—electrochemical studies, Electrochim. Acta. 52 (2007) 6212–6220.
[22] Y.-M. Liao, Z.-D. Feng, Z.-L. Chen, In situ tracing the process of human enamel demineralization by electrochemical impedance spectroscopy (EIS), J. Dentis. 35 (2007) 425–430.
[23] A. Merkoci, M. Aldavert, S. Marin, S. Alegret, New materials for electrochemical sensing V: nanoparticles for DNA labeling, Trac—Trends Anal. Chem. 24 (2005) 341–349.
[24] M. Pumera, M. Aldavert, C. Mills, A. Merkoci, S. Alegret, Direct voltammetric determination of gold nanoparticles using graphite-epoxy composite electrode, Electrochim. Acta. 50 (2005) 3702–3707.
[25] A. Bonanni, M.J. Esplandiu, M.I. Pividori, S. Alegret, M. del Valle, Impedimetric genosensors for the detection of DNA hybridization, Anal. Bioanal. Chem. 385 (2006) 1195–1201.
[26] A. Bonanni, M.J. Esplandiu, M. del Valle, Signal amplification for impedimetric genosensing using gold-streptavidin nanoparticles, Electrochim. Acta. 53 (2008) 4022–4029.
[27] B. Ge, Y.C. Huang, D. Sen, H.Z. Yu, Electrochemical investigation of DNA-modified surfaces: from quantitation methods to experimental conditions, J. Electroanal. Chem. 602 (2007) 156–162.
[28] E. Katz, I. Willner, Probing biomolecular interactions at conductive and semiconductive surfaces by impedance spectroscopy: routes to impedimetric immunosensors, DNA-sensors, and enzyme biosensors, Electroanalysis 15 (2003) 913–947.
[29] A.B.P Van Kuilenburg, A.C.F. Gorren, H.L. Dekker, P. Nieboer, B.F. Van Gelder, A.O. Muijsers, Presteady-state and steady-state kinetic properties of human cytochrome *c* oxidase, Eur. J. Biochem. 205 (1992) 1145–1154.
[30] J.M. Liu, X.P. Yan, Ultrasensitive, selective and simultaneous detection of cytochrome *c* and insulin based on immunoassay and aptamer-based bioassay in combination with Au/Ag nanoparticle tagging and ICP-MS detection, J. Anal. At. Spectrom. 26 (2011) 1191–1197.
[31] M.A. Mohsin, F.G. Banica, T. Oshima, T. Hianik, Electrochemical impedance spectroscopy for assessing the recognition of cytochrome *c* by immobilized calixarenes, Electroanalysis 23 (2011) 1229–1235.
[32] M. Pandiaraj, T. Madasamy, P.N. Gollavilli, M. Balamurugan, S. Kotamraju, V.K. Rao, et al., Nanomaterial-based electrochemical biosensors for cytochrome *c* using cytochrome *c* reductase, Bioelectrochemistry 91 (2013) 1–7.
[33] D. Ashe, T. Alleyne, E. Iwuoha, Serum cytochrome *c* detection using a cytochrome *c* oxidase biosensor, Biotechnol. Appl. Biochem. 46 (2007) 185–189.
[34] I.P.M Lau, E.K.S. Ngan, J.F.C. Loo, Y.K. Suen, H.P. Ho, S.K. Kong, Aptamer-based bio-barcode assay for the detection of cytochrome-*c* released from apoptotic cells, Biochem. Biophys. Res. Commun. 395 (2010) 560–564.

Biographies

Manel del Valle received his Ph.D. in Chemistry in 1992 from the Universtitat Autònoma de Barcelona, Spain, where he got a position of associate professor in analytical chemistry. He is a member of the Sensors & Biosensors Group where he is a specialist for instrumentation and electrochemical sensors. He has initiated there the research lines of sensor arrays and electronic tongues. Other interests of his work are the use of impedance measurements for sensor development, biosensors and the design of automated flow systems.

Evelien Arcay got her M.Sc. in Chemical Engineering from Antwerpen University in Belgium in 2012. Also in 2012 she did a research stay at the group of Sensors and Biosensors at the Autonomous University of Barcelona where she worked on impedimetric aptamer biosensors.

Cristina Ocaña obtained her B.Sc. and M.Sc. in chemistry from the Universitat Autònoma de Barcelona, Spain, in 2011 and 2012, respectively. She is currently a Ph.D. student at the Universitat Autònoma de Barcelona, Spain. Her research interests include the development of DNA and aptamer biosensors using the impedance spectroscopy technique.

Article 5. Signal amplification for thrombin impedimetric aptasensor: sandwich protocol and use of gold-streptavidin nanoparticles

C. Ocaña and M. del Valle

Biosensors and Bioelectronics, 2012, 14, 408-414.

Provided for non-commercial research and education use.
Not for reproduction, distribution or commercial use.

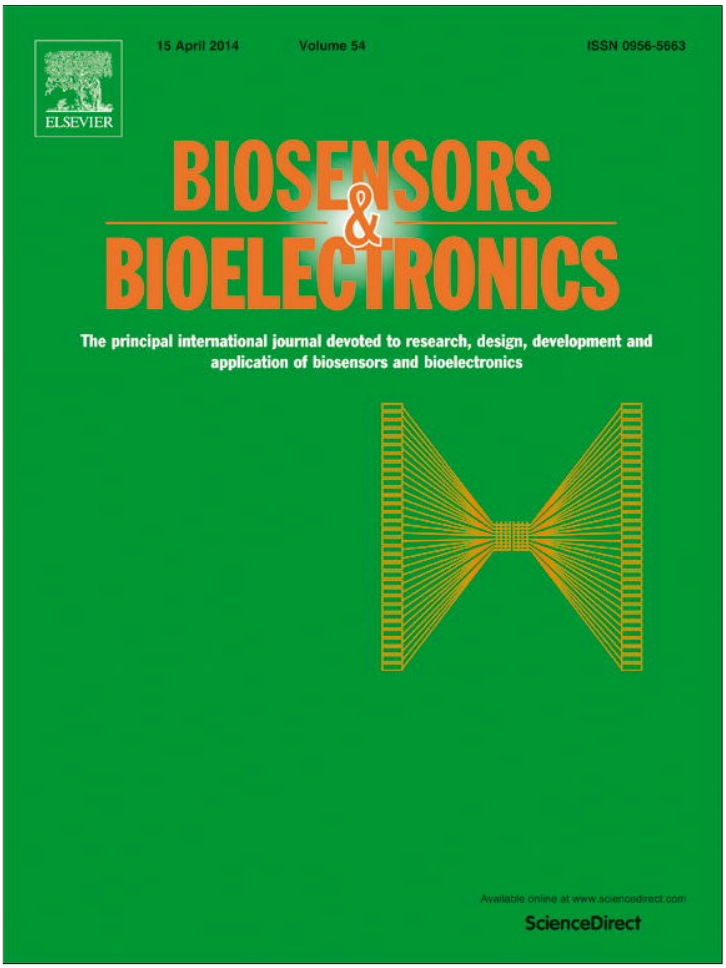

This article appeared in a journal published by Elsevier. The attached copy is furnished to the author for internal non-commercial research and education use, including for instruction at the authors institution and sharing with colleagues.

Other uses, including reproduction and distribution, or selling or licensing copies, or posting to personal, institutional or third party websites are prohibited.

In most cases authors are permitted to post their version of the article (e.g. in Word or Tex form) to their personal website or institutional repository. Authors requiring further information regarding Elsevier's archiving and manuscript policies are encouraged to visit:

http://www.elsevier.com/authorsrights

Author's personal copy

Biosensors and Bioelectronics 54 (2014) 408–414

Contents lists available at ScienceDirect

Biosensors and Bioelectronics

journal homepage: www.elsevier.com/locate/bios

Signal amplification for thrombin impedimetric aptasensor: Sandwich protocol and use of gold-streptavidin nanoparticles ☆

Cristina Ocaña, Manel del Valle *

Sensors and Biosensors Group, Department of Chemistry, Universitat Autonoma de Barcelona, 08193 Bellaterra, Spain

ARTICLE INFO

Article history:
Received 26 July 2013
Received in revised form
4 October 2013
Accepted 21 October 2013
Available online 7 November 2013

Keywords:
Impedance
Nanoparticles
Aptamer
Biosensor
Thrombin
Quantum dots

ABSTRACT

In this work, we report a highly specific amplification strategy demonstrated for the ultrasensitive biosensing of thrombin with the use of gold-streptavidin nanoparticles (strep-AuNPs) and silver reduction enhancement. The biotinylated aptamer of thrombin was immobilized onto an avidin-graphite epoxy composite (AvGEC) electrode surface by affinity interaction between biotin and avidin; electrochemical impedance measurements were performed in a solution containing the redox marker ferrocyanide/ferricyanide. The change in interfacial charge transfer resistance (R_{ct}) experimented by the redox marker, was recorded to confirm aptamer complex formation with target protein, thrombin (Thr), in a label-free first stage. A biotinylated second thrombin aptamer, with complementary recognition properties was then used in a sandwich approach. The addition of strep-AuNPs and silver enhancement treatment led to a further increment of R_{ct} thus obtaining significant signal amplification. The AptThrBio1-Thr-AptThrBio2 sandwich formation was inspected by confocal microcopy after incubation with streptavidin quantum dots. In order to visualize the presence of gold nanoparticles, the same silver enhancement treatment was applied to electrodes already modified with the nanoparticle-sandwich conjugate, allowing direct observation by scanning electron microscopy (SEM). Results showed high sensitivity and selectivity for thrombin detection, with an improvement from ca. 4.7 pM in a simple assay to 0.3 pM in the amplified reported scheme.

© 2013 Elsevier B.V. All rights reserved.

1. Introduction

Aptamers are synthetic nucleic acids (DNA or RNA) which selectively bind to low-molecular-weight organic or inorganic substrates or to macromolecules such as proteins (Jayasena, 1999). The affinity constant of aptamers toward their substrates lies in the micromolar to nanomolar range, comparable to the binding constants of antibodies to antigens (Jenison et al., 1994). The interest in aptamers as specific binding agents originates from the relative ease of their preparation by an evolutionary selection procedure that eliminates the need for sophisticated design of the receptor units. Not surprisingly, aptamers have found growing interest as active separation materials in chromatography (Kotia et al., 2000), and electrophoresis (Clark and Remcho, 2002), as therapeutic (Biesecker et al., 1999; Hicke et al., 2001) or diagnostic agents, and as active materials for biosensing (Evtugyn et al., 2012). The use of aptamers for biosensing is particulary interesting, as aptamers could substitute antibodies in bioanalytical sensing given they reveal obvious advantages over immunosensors. The aptamer of thrombin is the most known and utilized aptamer. Thrombin is the last enzyme protease involved in the coagulation cascade, and converts fibrinogen to insoluble fibrin which forms the fibrin gel, both in physiological conditions and in a pathological thrombus (Holland et al., 2000). Therefore, thrombin plays a central role in a number of cardiovascular diseases (Burgering et al., 1997), and is thought to regulate many processes such as inflammation and tissue repair at the blood vessel wall. Concentration levels of thrombin in blood are very low, and levels down to the picomolar range are associated with disease; because of this, it is important to assess its concentration at trace level (Centi et al., 2007).

In recent years, there has been large interest in the development of aptasensors. Aptasensors are biosensors that use aptamers as the biorecognition element. This type of biosensors can be classified, depending on the technique employed for transduction, into optical (Lee and Walt, 2000), piezoelectric (Srijanto et al., 2012) and electrochemical types (Ocaña et al., 2012; Radi et al., 2005). Electrochemical aptasensors make use of electrochemical transduction for biosensing. Recently, among the different electrochemical techniques available, electrochemical impedance spectroscopy (EIS) (McDonald, 1987), has been used in numerous studies, also for protein detection (Lisdat and Schafer, 2008; Radi et al., 2005). This technique is very sensitive to changes in the

☆This work was presented as Poster P126 at the 3rd International Conference on Bio-Sensing Technology 2013 (BITE 2013), held in Sitges (Barcelona) on 12–15 May 2013.

* Corresponding author. Tel.: +34 935813235; fax: +34 935812477.
E-mail addresses: manel.delvalle@uab.cat, manel.delvalle@uab.es (M. del Valle).

0956-5663/$ - see front matter © 2013 Elsevier B.V. All rights reserved.
http://dx.doi.org/10.1016/j.bios.2013.10.068

Author's personal copy

interfacial properties of the modified electrodes caused by biorecognition events at the electrode surface (Bardea et al., 1999; Loo et al., 2012). For this reason, EIS is becoming an attractive electrochemical technique for numerous applications such as immunosensing (Loo et al., 2012), genosensing (Bonanni et al., 2010), enzyme activity determinations (Li et al., 2012), studies of corrosion (Blin et al., 2007) or other surface phenomena (Liao et al., 2007).

Gold nanoparticles have been widely used in biosensing for tagging purposes and also for amplification thanks to their excellent properties, such as high biocompatibility, distinctive size-related electronic and optical behavior, high electrical conductivity and high catalytic activity. In recent years, several protocols using gold nanoparticles-assisted electrochemical aptamer biosensing were developed with the aim of enhancing the electrochemical response (Deng et al., 2008; Zheng et al., 2007).

In this work, we report a highly specific amplification strategy demonstrated for the ultrasensitive detection of thrombin with the use of streptavidin gold nanoparticles and silver enhancement treatment. The transducer employed consisted of an avidin graphite-epoxy composite electrode (AvGEC), of general use in our laboratories and already extensively studied and applied to amperometric, enzymatic, immuno and genosensing assays (Bonanni et al., 2006; Merkoci et al., 2005; Pumera et al., 2005). The uneven surface of the avidin graphite-epoxy electrode allows the immobilization of biotinylated aptamer of thrombin (AptThrBio1) on its surface by affinity interaction between biotin and avidin. The change of interfacial charge transfer resistance (R_{ct}) experimented by the redox marker was recorded to confirm the aptamer sandwich formation with target protein, thrombin (Thr). Then, a biotinylated second thrombin aptamer (AptThrBio2), with complementary recognition properties to those used in the previous approach was employed to form the sandwich. The addition of strep-AuNPs and silver enhancement treatment led to a further increment of R_{ct} and the subsequent achievement of significant signal amplification, high sensitivity and improvement of selectivity.

2. Experimental

2.1. Chemicals

Potassium dihydrogen phosphate, potassium ferricyanide $K_3[Fe(CN)_6]$, potassium ferrocyanide $K_4[Fe(CN)_6]$, sodium monophosphate, streptavidin gold nanoparticles, 655 nm streptavidin quantum dots (strep-QDs), avidin and the target protein thrombin (Thr), were purchased from Sigma (St. Louis, MO, USA). Poly (ethylene glycol) 1000 (PEG), sodium chloride and potassium chloride were purchased from Fluka (Buchs, Switzerland). LI silver enhancement kit was obtained from Nanoprobes (Yaphank, New York). All-solid-state electrodes (AvGECs) were prepared using 50 μm particle size graphite powder (Merck, Darmstadt, Germany), Epotek H77 resin and its corresponding hardener (both from Epoxy Technology, Billerica, MA, USA), and avidin. All reagents were analytical reagent grade. Aptamers used in this study were purchased from TIB-MOLBIOL (Berlin, Germany). Stock solutions of aptamers were diluted with sterilized and deionised water, separated into fractions and stored at −20 °C until required. Their base sequences were:

- AptThrBio1: 5′-GGTTGGTGTGGTTGG-Biotin-3′,
- AptThrBio2: 5′-Biotin-AGTCCGTGGTAGGGCAGGTT GGGGTGACT-3′ and
- AptCytc: 5′-Biotin-AGTGTGAAATATCTAAAC TAAATGTGGAGGGTGGGACGGGAAGAAGTTTATTTTTCACACT-3′.

All solutions were made up using MilliQ water from MilliQ System (Millipore, Billerica, MA, USA). The buffers employed were: PBS (187 mM NaCl, 2.7 mM KCl, 8.1 mM $Na_2HPO_4 \cdot 2H_2O$, 1.76 mM KH_2PO_4, and pH 7.0) and 10 nM PBS without NaCl and KCl.

2.2. Apparatus

AC impedance measurements and cyclic voltammetry were performed with the aid of an Autolab PGStat 20 (Metrohm Autolab B.V, Utrecht, The Netherlands). FRA and GPES (Metrohm Autolab) software were used for data acquisition and control of the experiments. A three electrode configuration was used to perform the impedance and cyclic voltammetry measurements: a platinum-ring auxiliary electrode (Crison 52-67 1, Barcelona, Spain), a Ag/AgCl reference electrode and the constructed AvGEC as the working electrode (with a geometric area of 0.28 cm^2). Temperature-controlled incubations were done using an Eppendorf Thermomixer 5436. A scanning electron microscope (SEM) (Merlin, Zeiss, Germany) and a confocal microscope (SP5, Leica, Solms, Germany) were used to visualize the silver enhanced strep-AuNPs and strep-QDs respectively on the electrode surface.

2.3. Construction of working electrodes

The electrodes were prepared using a PVC tube body (6 mm i.d.) and a small copper disk soldered to the end of an electrical connector. The conductive part of AvGECs was an avidin epoxy graphite conductive paste, formed from graphite (18%), avidin (2%) and epoxy resin (80%), which was deposited into the cavity in the plastic body, filling it, as shown Fig. 1(a) (Bonanni et al., 2007). The composite material was cured in an oven at 40 °C for 7 days. Before each use, the electrode surface was moistened with MilliQ

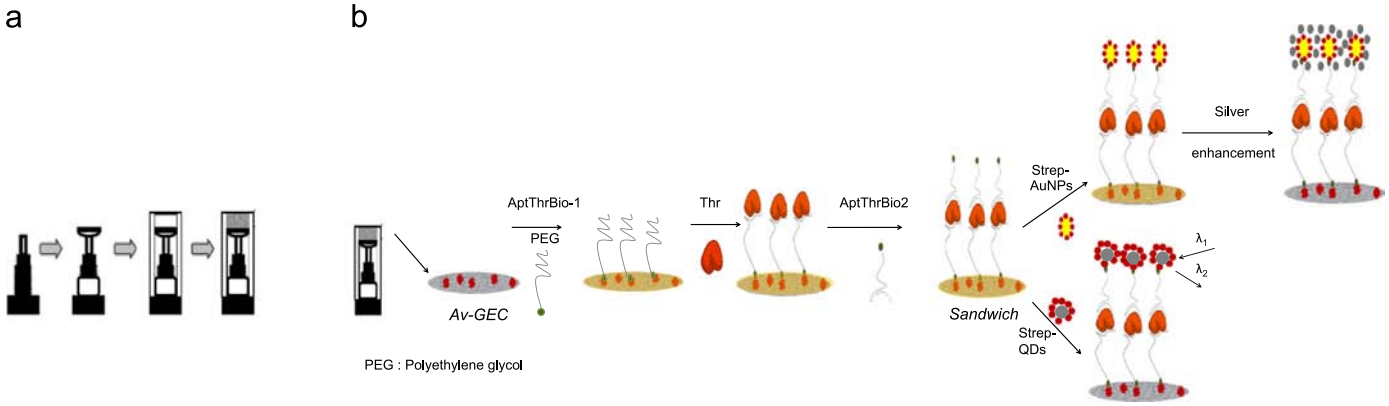

Fig. 1. (a) Scheme of construction of avidin graphite-epoxy composite electrodes and (b) scheme of the biosensing procedure.

Author's personal copy

water and then thoroughly smoothed with abrasive sandpaper and finally with alumina paper (polishing strips 301044-001, Orion) in order to obtain a reproducible electrochemical surface (Lermo et al., 2007; Williams et al., 2003).

2.4. Protein capture and amplification protocol

The scheme of experimental protocol for thrombin analysis, described in detail below, is represented in Fig. 1(b).

2.4.1. Aptamer immobilization

The first step consists of aptamer AptThrBio1 immobilization on the electrode surface. A volume of 160 μL of MilliQ water containing 35 pmol of aptamer solution was heated to 80–90 °C for 3 min to promote the loose conformation of the aptamer. Then, the solution was dipped in a bath of cold water and the electrode was immersed in it, where the avidin–biotin affinity interaction took place for 15 min at the electrode surface. This was followed by two washing steps using PBS buffer solution for 10 min, in order to remove any unadsorbed aptamer.

2.4.2. Blocking step

To minimize any possible nonspecific adsorption, the electrodes were dipped in 160 μL of PEG 40 mM. This was followed by two washing steps using PBS buffer solution for 10 min.

2.4.3. Thrombin detection

The electrodes were dipped in a solution with the desired concentration of Thr. The incubation took place for 15 min. Then, the biosensors were washed twice with PBS buffer solution for 10 min.

2.4.4. Sandwich formation

In order to achieve the aptamer sandwich formation, the electrodes were dipped in 160 μL of PBS solution containing 12 pmol of AptThrBio2. The incubation took place for 15 min. This was followed by two washing steps using PBS buffer solution for 10 min.

2.5. Amplification

Two different variants were used, with employ of quantum dots, just for visualizing the sandwich formed, and with employ of strep-AuNPs for impedimetric signal amplification.

2.5.1. Addition of strep-QDs

Av-GEC electrodes modified with the biotin end aptamer sandwich were incubated in a solution of 40 nM of strep-QDs for 20 min at 25 °C with stirring. Then the electrodes were washed twice with 10 mM PBS buffer. Negative controls were performed for the strep-QDs addition step either using AptCytc as second aptamer.

2.5.2. Addition of strep-AuNPs

Av-GEC electrodes modified with the sandwich complex were incubated in 160 μL of strep-AuNPs, from a 1/100 dilution of the stock solution in PBS buffer. The tube was incubated at 25 °C with gentle stirring for 20 min. This step was followed by two gentle washing steps in PBS buffer for 10 min at 25 °C. Negative controls were performed for the strep-AuNPs addition step using AptCytc as aptamer without affinity.

2.5.3. Silver enhancement of strep-AuNPs

Twenty microliters of a solution obtained by the combination of 10 μL of enhancer and 10 μL of initiator were deposited onto the electrode surface and left for 7 min to facilitate the reaction. Silver enhancement occurs during the catalytic reduction of silver from one solution (e.g. the enhancer) by another (e.g. the initiator) in the presence of gold particles. The reduction reaction causes silver to build up on the surface of the gold nanoparticles. After this catalytic silver reduction, the electrodes were thoroughly washed with deionized water to stop the reaction. The silver enhancing solution was prepared immediately before each use. For silver enhancement treatment, the negative control used was a non-biotinylated AptCytc as aptamer without affinity.

Different selectivity experiments carried out were performed with the same protocol unless were specified.

All incubations were carried out at controlled temperature in the thermomixer.

2.6. Impedimetric detection

Impedance experiments were carried out at an applied potential of 0.17 V (vs. Ag/AgCl reference electrode), with a range of frequency of 50 KHz–0.05 Hz, an AC amplitude of 10 mV and a sampling rate of 10 points per decade above 66 Hz and 5 points per decade at the lower range. All measurements were performed in PBS buffer containing 0.01 M $K_3[Fe(CN)_6]/K_4[Fe(CN)_6]$ (1:1) mixture, used as a redox marker. The impedance spectra were plotted in the form of complex plane diagrams (Nyquist plots, $-Z_i$ vs. Z_r) and fitted to a theoretical curve corresponding to the equivalent circuit with Z_{view} software (Scribner Associates Inc., USA). The equivalent circuit was formed by one resistor/capacitor element in series with a resistance. In it, the resistance in series with the capacitor element, R_1, corresponds to the resistance of the solution, the resistance in parallel with the capacitor element, R_{ct}, is the charge transfer resistance between the solution and the electrode surface, whilst the capacitor element is the constant phase element (CPE) associated with the double-layer capacitance. The use of a CPE instead of a capacitor is required to optimize the fit to the experimental data, and this is due to the nonideal nature of the electrode surface. For all performed fittings, the chi-square goodness-of-fit test was thoroughly checked to verify calculations. In all cases, calculated values for each circuit remained in the range of 0.0003–0.15 much lower than the tabulated value for 50 degrees of freedom (67.505 at 95% confidence level). In this work, we focused on the variation of charge resistance transfer (R_{ct}), as indicator of changes on the electrode surface. In order to compare the results obtained from the different electrodes used, and to obtain independent and reproducible results, a relative transformation of signals was needed (Bonanni et al., 2006). Thus, the Δ_{ratio} value was defined according to the following equations:

$$\Delta_{ratio} = \Delta_s / \Delta_p$$

$$\Delta_s = R_{ct\ (AptThrBio1\text{-}Thr/AptThrBio2/strep\text{-}AuNPs/silver\ enhancement)} - R_{ct\ (electrode\text{–}buffer)}$$

$$\Delta_p = R_{ct\ (AptThrBio1)} - R_{ct\ (electrode\text{–}buffer)}$$

where $R_{ct\ (AptThrBio1\text{-}Thr/AptThrBio2/strep\text{-}AuNPs/silver\ enhancement)}$ was the electron transfer resistance value measured after aptamer sandwich formation; $R_{ct\ (AptThrBio1)}$ was the electron transfer resistance value measured after aptamer immobilization on the electrode, and $R_{ct\ (electrode\text{–}buffer)}$ was the electron transfer resistance of the blank electrode and buffer.

3. Results

3.1. Electrode surface area characterization

Effective surface area was characterized by CV using a known procedure (Shi et al., 2011). CVs for bare electrodes in ferricyanide

Author's personal copy

followed expected trends, and a plot of peak current vs. the square root of scan rate was linear, (see Supplementary information, Fig. S2). Using the Randles–Sevcik equation (Bard and Faulkner, 2000), the effective surface area of AvGEC was $0.197 \pm 0.05\ cm^2$, while its geometric area was $0.28\ cm^2$. The avidin protein present in the composite decreased the effective area due to the protein insulating nature, thus decreasing the effective surface area available for signal transduction. This observation is also in agreement with impedance characterization of bare electrodes, just the epoxy-graphite composite vs. those modified with avidin, whereas the latter present increased impedance, in the form of larger R_{ct}.

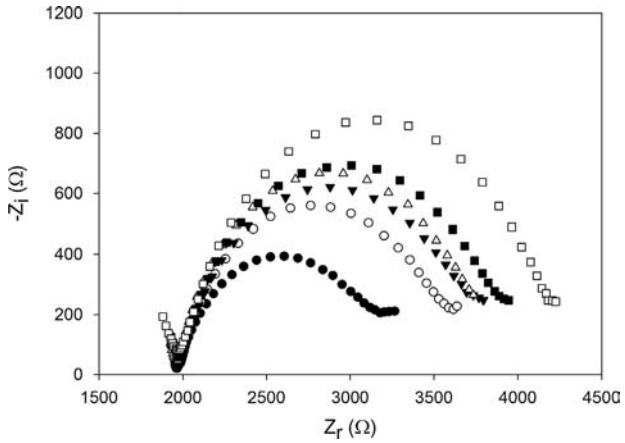

Fig. 2. Nyquist diagrams for EIS measurements of: •, bare AvGEC electrode; ○, biotinylated aptamer of thrombin 1; ▾, biotinylated aptamer of thrombin and thrombin protein; Δ, sandwich complex; ■, sandwich complex modified with strep-AuNPs; and □, sandwich complex modified with strep-AuNPs and silver enhancement treatment. All experiments were performed in PBS solution and all EIS measurements were performed in PBS solution containing 0.01 M $K_3[Fe(CN)_6]$/$K_4[Fe(CN)_6]$.

3.2. EIS characterization

For the operation details of the proposed aptasensor, the amounts used of AptThrBio1 and PEG were optimized in a previous work (Ocaña et al., in press); the AptThrBio2 amount used was optimized by building its titer curve (see Supplementary information, Fig. S1), and the strep-AuNPs were used just in excess to AptThrBio2.

In Fig. 2, the EIS spectrum obtained for a biosensing experiment using aptamer sandwich protocol and silver enhancement amplification are shown. Impedance measurements were performed before modifying the electrode surface (bare Av-GEC electrode), after modifying the electrode surface with AptThrBio1, Thr, AptThrBio2 (sandwich formation), strep-AuNPs and finally, after silver deposition. As shown in this figure, R_{ct} increased after any modification of the electrode surface. This can be due to the increased difficulty of the redox reaction of $[Fe(CN)_6]^{3-/4-}$ to take place, due to the sensor surface alteration (Katz and Willner, 2003). Two different factors may be taken into account to explain this: the electrostatic repulsion and the sterical hindrance. The former is more significant in the first step of protocol; when the AptThrBio1 is immobilized onto the electrode surface by avidin–biotin affinity, a first layer is formed, where negatively charged phosphate groups of aptamer skeleton are responsible of the electrostatic repulsion of the negatively charged redox marker, thus inhibiting the interfacial transfer process and resulting in R_{ct} increment. The addition of Thr and a second ApThrBio2 to form a

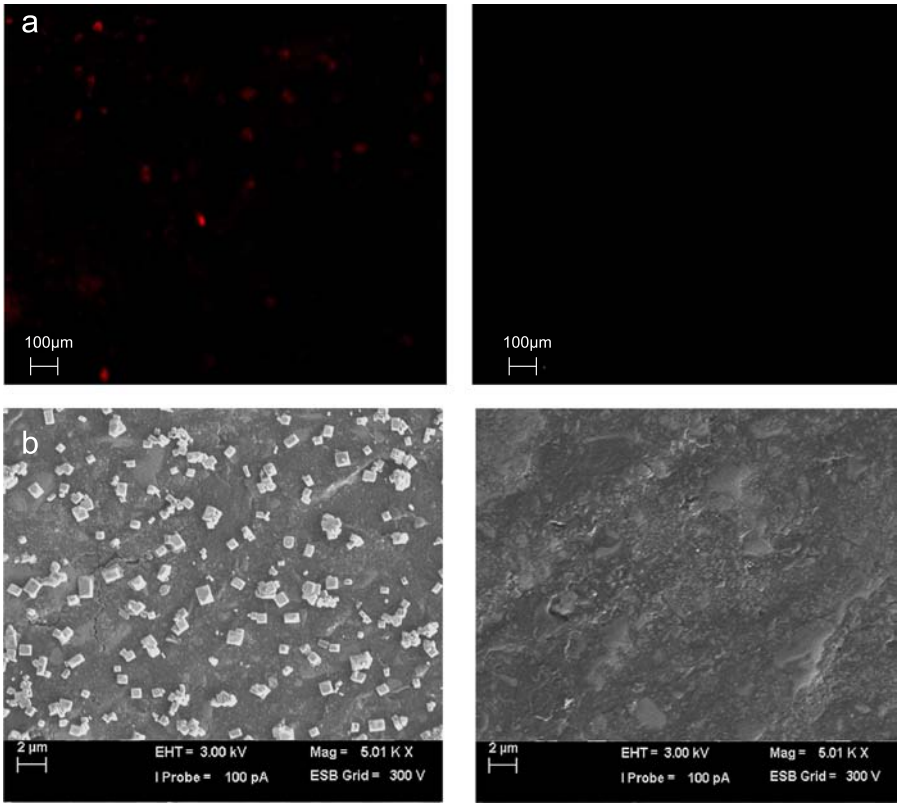

Fig. 3. (a) Confocal images of: (left) positive control using biotinylated aptamer of thrombin 1+thrombin+biotinylated aptamer of thrombin 2+strep-QDs and (right) negative control using biotinylated aptamer of thrombin 1+thrombin+biotinylated aptamer of cytochrome c+strep-QDs. (b) SEM images of: (left) experiment using biotinylated aptamer of thrombin 1+thrombin+biotinylated aptamer of thrombin 2+strep-AuNPs+silver enhancement treatment and (right) negative control using biotinylated aptamer of thrombin 1+thrombin+biotinylated aptamer of cytochrome c+strep-AuNPs+silver enhancement treatment. SEM images were taken at a acceleration voltage of 3 KV and a resolution of 2 µm and confocal images were collected at 625 nm and with excitation wavelength of 405 nm.

Author's personal copy

sandwich results in a further increment of R_{ct} due to the increased quantity of negative charge and the hindrance caused by the formation of a double layer. In this work, strep-AuNPs and silver enhancement treatment were used with the aim of amplifying the EIS sandwich formation signal. After the addition of strep-AuNPs we can observe an increment of R_{ct} value because of the increased space resistance due to Au-streptavidin conjugates. Working at pH 7, streptavidin is slightly negatively charged (pI is around pH 5) and this fact also contributes to enhancement of impedance (Sivasankar et al., 1998). In the second amplification step, silver enhancement treatment (Cai et al., 2002; Hanaee et al., 2007), a significant increment of R_{ct} value was also observed and attributable to the silver deposition on gold.

3.3. Confocal microscopy characterization

Aptamer sandwich formation was inspected by confocal microscopy after incubation with the strep-QDs. The images obtained are shown in Fig. 3(a). The first image (Fig. 3(a), left) corresponds to the electrodes modified with aptamer sandwich formation and strep-QDs. The fluorescence points observed in this case are due to the presence of the complex formed between strep-QDs and the aptamer sandwich conjugated through the biotin–streptavidin affinity. The weak fluorescence observed in the second image (Fig. 3(a) right) corresponds to the negative control, which did not use biotinylated complementary aptamer. Comparison of the two images indicates that AptThrBio2 recognizes Thr and forms the expected sandwich conjugate.

3.4. Scanning electron microscope characterization

In order to visualize the presence and distribution of gold nanoparticles, the silver enhancement treatment was used. These experiments also provided an image of the homogeneity and accessibility of the anchorage points supplied by the avidin entrapped in the biocomposite. SEM images taken at an acceleration voltage of 3 kV are shown in Fig. 3(b) left, illustrating a positive experiment with aptamer sandwich and strep-AuNPs. As it can be observed in Fig. 3(b) left, the distribution of silver enhanced-gold nanoparticles is quite homogeneous. This also implies a regular distribution of avidin molecules in the biocomposite and well-organized formation of aptamer sandwich onto the electrode surface. Apart, the nanoparticles formed were monocrystalline; that is, thanks to the disposition of the streptavidin around of gold nanoparticles, the silver crystallized in specific directions. Comparing this experiment with the negative control that did not use the biotinylated complementary aptamer, Fig. 3(b) right, a surface without nanoparticles can be observed.

3.5. Analytical performance of the aptasensor for detection of thrombin

Taking the already established reaction conditions for AptThrBio1, AptThrBio2 and PEG, the proposed aptasensor was then used following the sandwich protocol, plus amplification employing the strep-AuNPs and silver enhancement treatment. Fig. 4(a) shows calibration curves with increasing concentrations of Thr and Fig. 4 (b), their respective regression curves in the linear range, at the different steps of the protocol: (1) AptThrBio1-Thr, (2) sandwich formation between AptThrBio1, Thr and AptThrBio2, (3) aptamer sandwich modified with strep-AuNPs, and (4) aptamer sandwich modified with strep-AuNPs and silver enhancement treatment. In our previous experience with silver enhancement, related to DNA hybridization biosensing, it was not possible to obtain good impedimetric measurements following amplification treatment (Bonanni et al., 2008). In this case, although the reproducibility was not excellent, the calibration curve obtained showed a good RSD. As can be seen in Fig. 4(a), all calibration curves increased until the value of 100 pM of Thr, this could be due to the fact that concentrations larger than 100 pM cause a saturation on the sensor surface. Moreover, a signal increment of up to 89% between AptThrBio1-Thr (the simple biosensing) and sandwich formation with strep-AuNPs and silver enhancement treatment was observed. As can be observed in Table 1, the use of silver enhancement treatment led to the highest sensitivity and signal amplification compared to the other calibration curves obtained. This confirms that the silver deposition on gold nanoparticles increases essentially the sterical hindrance, producing an increment of observed impedance. Despite a higher sensitivity, the detection limit obtained in this case, 0.3 pM, is slightly worse than the one obtained with only strep-AuNPs. This fact, caused by the deteriorated reproducibility, could be attributable to the increased number of process steps and associated increased potential errors. The best detection limit, approximately 0.2 pM, corresponded to the sandwich and strep-AuNPS calibration curve. This confirmed that the proposed methods may reach a low detection limit and ultrahigh sensitivity for the detection of thrombin.

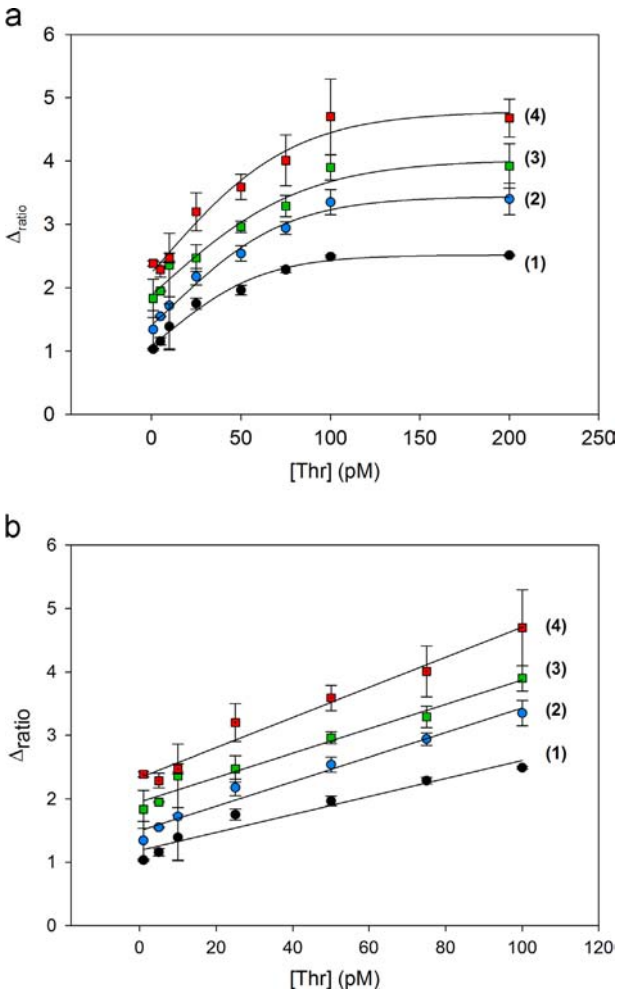

Fig. 4. (a) Calibration curves and (b) linear portions of: (1, black circle) biotinylated aptamer of thrombin 1, (2, blue circle) sandwich complex, (3, green square) sandwich complex modified with strep-AuNPs, and (4, red square) sandwich complex modified with strep-AuNPs and silver enhancement treatment. All experiments were performed in PBS solution and all EIS measurements were performed in PBS solution containing 0.01 M $K_3[Fe(CN)_6]/K_4[Fe(CN)_6]$. Uncertainty values corresponding to replicated experiments ($n=5$). (For interpretation of the references to color in this figure legend, the reader is referred to the web version of this article.)

Author's personal copy

Table 1
Summary of calibration results.

Calibration curve	*Regression curve*	*Detection limit* (pM)	*Linear range* (pM)	*% RSD*[a]	*% Amplification*
AptThrBio1-Thr	$\Delta_{ratio} = 1.042 + 0.0157[Thr]$	4.7	0.75–100	2.2	–
Aptamer sandwich	$\Delta_{ratio} = 1.495 + 0.0194[Thr]$	2	0.75–100	3.4	35
Aptamer sandwich/strep-AuNPs	$\Delta_{ratio} = 1.874 + 0.0201[Thr]$	0.2	0.1–100	5.2	57
Aptamer sandwich/strep-AuNPs/silv.enh	$\Delta_{ratio} = 2.477 + 0.0219[Thr]$	0.3	0.1–100	9.9	89

[a] Corresponding to five replicate experiments at 75 pM thrombin.

Table 2
Comparison of proposed biosensor with other reported methodologies for thrombin detection.

Analytical technique	Detection limit	Reference
Amperometry	0.12 pM	Bai et al. (2013)
Potentiometry	6.7 nM	Goda and Miyahara (2013)
Voltammetry	0.52 pM	Fu et al. (2013)
DPV	7.82 aM	Zheng et al. (2007)
EIS	4.4 pM	Xu et al. (2013)
EIS	0.1 pM	Deng et al. (2008)
EIS and CV	93 pM	Zhang et al. (2013)
EIS	0.2 pM	Our work
SPR	0.1 nM	Bai et al. (2013)
Electroluminiscence	1.6 fM	Gui et al. (2013)
Electroluminiscence	0.4 pM	Wang et al. (2013)
Electroluminiscence	0.5 pM	Yang et al. (2013)
SERS	0.16 pM	Wu et al. (2013)
PET	13 pM	Zhang et al. (2013)
FRET	2.5 nM	Chen et al. (2013)
Fluorescence	1.1 nM	Kong et al. (2013)

When the proposed aptasensor was compared with other detection methodologies for thrombin detection, some interesting facts are inferred. The results are shown in Table 2, where sensitivity information is presented as the LOD of each biosensor compared. The lowest detection limit value among all the analytical techniques corresponded to (Zheng et al., 2007), but this Thr biosensor used a double amplification strategy, with thiocyanuric acid and gold nanoparticle-labeled aptamer, and differential pulse voltammetry (DPV). Our proposed aptasensor is on the second range of lowest LOD in electrochemical techniques and impedance, thus demonstrating satisfactory results for the detection of thrombin in real samples, given that this level corresponds to physiological concentration. Moreover, the proposed aptasensor showed many advantages: it is stable for 7 days, its surface is easily regenerable by polishing and the followed procedure was simple and easy.

3.6. Selectivity of the aptasensor

To verify that the signal was dependent on the specific recognition, our protocol for thrombin detection was evaluated by challenging it with possible interfering proteins present in blood serum, comparing it to the simple biosensing, label-free detection alternative, see Fig. 5. From this investigation, we found that the presence of interfering proteins such as albumin, cytochrome c, fibrinogen, prothrombin and immunoglobulin G, at serum concentration level exhibits negligible response compared with 75 pM Thr in the amplified sandwich protocol, even at concentrations four or five orders of magnitude higher than typical Thr concentration. The figure also demonstrates that the sandwich protocol displays a clear advantage, more than the signal amplification, the marked decrease of interfering effects that are still noticeable in the simple biosensing scheme. These observations suggest that the sensing mechanism relies on specific recognition and that the aptasensor sandwich method is highly specific for the

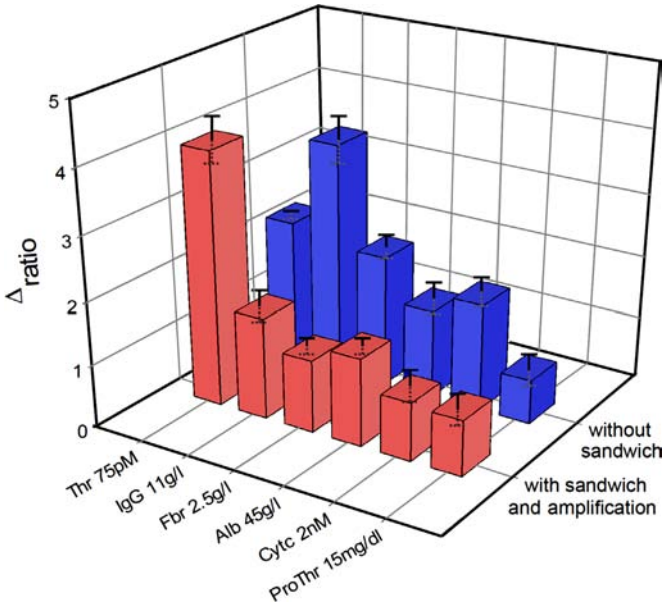

Fig. 5. 3D bar chart of response towards different proteins present in serum, without the amplification protocol and with the sandwich/amplification protocol. Uncertainty values corresponding to replicated experiments ($n=5$).

detection of Thr. Moreover, it is important to emphasize that prothrombin protein is the precursor of thrombin in the blood clotting process and this aptasensor is capable of distinguishing both proteins with high selectivity.

Apart of these proteins, other common compounds present in blood were also tested for interference (see Supplementary information Fig. S3). Uric and ascorbic acid showed negligible responses compared with 75 pM Thr, tested at concentrations eight and six orders of magnitude higher than that of Thr. Dopamine exhibited certain low interfering signal (17%) at typical serum concentration, but it should be considered that this compound is only present in serum during physical and emotional stress.

4. Conclusions

In this work, the impedimetric signal amplification for the detection of thrombin was proposed using an aptamer sandwich formation with strep-AuNPs and silver enhancement treatment. The use of strep-AuNPs and strep-QDs permitted rapid formation of an easily detected conjugate with a biotinylated aptamer sandwich through a streptavidin–biotin interaction. Thanks to the signal amplification with strep-AuNPs and silver deposition, it was possible to increase the sensitivity of the method. Besides, for a comparable amount of AptThrBio1-Thr, the signal resulted in 89% amplification, compared to results recorded with simple biosensing AptThrBio1-Thr. Moreover, the limit of detection obtained was 0.3 pM. A good linear range, 0.1–100 pM, and high

Author's personal copy

selectivity with respect to different serum proteins and organic compounds at serum concentration level were also attained with this protocol. The silver enhancement treatment also permitted to visualize the gold nanoparticles on the electrode surface with SEM. This allowed confirming the proposed steps of the protocol and a homogeneous distribution of biosensing sites on the electrodes. We believe that this method could be extended for the determination of other proteins in serum and that it results promising for clinical application.

Acknowledgments

Financial support for this work has been provided by Spanish Ministry of Science and Innovation, (MICINN, Madrid) through Project CTQ2010-17099 and by the Catalonia program ICREA Academia. Cristina Ocaña thanks the support of Ministry of Science and Innovation (MICINN, Madrid, Spain) for the predoctoral grant.

Appendix A. Supporting information

Supplementary data associated with this article can be found in the online version at http://dx.doi.org/10.1016/j.bios.2013.10.068.

References

Bai, L., Chai, Y., Yuan, R., Yuan, Y., Xie, S., Jiang, L., 2013. Biosens. Bioelectron. 50, 325–330.
Bai, Y., Feng, F., Zhao, L., Wang, C., Wang, H., Tian, M., Qin, J., Duan, Y., He, X., 2013. Biosens. Bioelectron. 47, 265–270.
Bard, A.J., Faulkner, L.R., 2000. Electrochemical Methods: Fundamentals and Applications. Wiley, New York.
Bardea, A., Patolsky, F., Dagan, A., Willner, I., 1999. Chem. Commun. 1, 21–22.
Biesecker, G., Dihel, L., Enney, K., Bendele, R.A., 1999. Immunopharmacology 42 (1–3), 219–230.
Blin, F., Koutsoukos, P., Klepetsianis, P., Forsyth, M., 2007. Electrochim. Acta 52 (21), 6212–6220.
Bonanni, A., Esplandiu, M.J., del Valle, M., 2008. Electrochim. Acta 53 (11), 4022–4029.
Bonanni, A., Esplandiu, M.J., del Valle, M., 2010. Biosens. Bioelectron. 26 (4), 1245–1251.
Bonanni, A., Esplandiu, M.J., Pividori, M.I., Alegret, S., del Valle, M., 2006. Anal. Bioanal. Chem. 385 (7), 1195–1201.
Bonanni, A., Pividori, M.I., del Valle, M., 2007. Anal. Bioanal. Chem. 389 (3), 851–861.
Burgering, M.J.M., Orbons, L.P.M., vanderDoelen, A., Mulders, J., Theunissen, H.J.M., Grootenhuis, P.D.J., Bode, W., Huber, R., Stubbs, M.T., 1997. J. Mol. Biol. 269 (3), 395–407.
Cai, H., Wang, Y.Q., He, P.G., Fang, Y.H., 2002. Anal. Chim. Acta 469 (2), 165–172.
Centi, S., Tombelli, S., Minunni, M., Mascini, M., 2007. Anal. Chem. 79 (4), 1466–1473.
Clark, S.L., Remcho, V.T., 2002. Electrophoresis 23 (9), 1335–1340.
Chen, H., Yuan, F., Wang, S., Xu, J., Zhang, Y., Wang, L., 2013. Biosens. Bioelectron. 48, 19–25.
Deng, C., Chen, J., Nie, Z., Wang, M., Chu, X., Chen, X., Xiao, X., Lei, C., Yao, S., 2008. Anal. Chem. 81 (2), 739–745.
Evtugyn, G.A., Kostyleva, V.B., Porfireva, A.V., Savelieva, M.A., Evtugyn, V.G., Sitdikov, R.R., Stoikov, I.I., Antipin, I.S., Hianik, T., 2012. Talanta 102, 156–163.
Fu, H., Ge, C., Cheng, W., Luo, C., Zhang, D., Yan, L., He, Y., Yi, G., 2013. Electroanalysis 25 (5), 1223–1229.
Goda, T., Miyahara, Y., 2013. Biosens. Bioelectron. 45 (1), 89–94.
Gui, G., Zhuo, Y., Chai, Y.Q., Liao, N., Zhao, M., Han, J., Zhu, Q., Yuan, R., Xiang, Y., 2013. Biosens. Bioelectron. 47, 524–529.
Hanaee, H., Ghourchian, H., Ziaee, A.A., 2007. Anal. Biochem. 370 (2), 195–200.
Hicke, B.J., Marion, C., Chang, Y.F., Gould, T., Lynott, C.K., Parma, D., Schmidt, P.G., Warren, S., 2001. J. Biol. Chem. 276 (52), 48644–48654.
Holland, C.A., Henry, A.T., Whinna, H.C., Church, F.C., 2000. FEBS Lett. 484 (2), 87–91.
Jayasena, S.D., 1999. Clin. Chem. 45 (9), 22.
Jenison, R.D., Gill, S.C., Pardi, A., Polisky, B., 1994. Science 263 (5152), 1425–1429.
Katz, E., Willner, I., 2003. Electroanalysis 15 (11), 913–947.
Kong, L., Xu, J., Xu, Y., Xiang, Y., Yuan, R., Chai, Y., 2013. Biosens. Bioelectron. 42 (1), 193–197.
Kotia, R.B., Li, L., McGown, L.B., 2000. Anal. Chem. 72 (4), 827–831.
Lee, M., Walt, D.R., 2000. Anal. Biochem. 282 (1), 142–146.
Lermo, A., Campoy, S., Barbé, J., Hernández, S., Alegret, S., Pividori, M.I., 2007. Biosens. Bioelectron. 22 (9–10), 2010–2017.
Li, Y., Syed, L., Liu, J., Hua, D.H., Li, J., 2012. Anal. Chim. Acta 744, 45–53.
Liao, Y.-M., Feng, Z.-D., Chen, Z.-L., 2007. J. Dent. 35 (5), 425–430.
Lisdat, F., Schafer, D., 2008. Anal. Bioanal. Chem. 391 (5), 1555–1567.
Loo, A.H., Bonanni, A., Ambrosi, A., Poh, H.L., Pumera, M., 2012. Nanoscale 4 (3), 921–925.
McDonald, J.R., 1987. Impedance Spectroscopy. John Wiley, New York.
Merkoci, A., Aldavert, M., Marin, S., Alegret, S., 2005. Trac-Trends Anal. Chem. 24 (4), 341–349.
Ocaña, C., Figueras, C., del Valle, M., 2013. J. Nanosc. Nanotechnol (in press).
Ocaña, C., Pacios, M., del Valle, M., 2012. Sensors 12 (3), 3037–3048.
Pumera, M., Aldavert, M., Mills, C., Merkoci, A., Alegret, S., 2005. Electrochim. Acta 50 (18), 3702–3707.
Radi, A., Acero Sánchez, J.L., Baldrich, E., O'Sullivan, C.K., 2005. Anal. Chem. 77 (19), 6320–6323.
Shi, J., Claussen, J.C., McLamore, E.S., ul Haque, A., Jaroch, D., Diggs, A.R., Calvo-Marzal, P., Rickus, J.L., Porterfield, D.M., 2011. Nanotechnology 22 (35), 355502.
Sivasankar, S., Subramaniam, S., Leckband, D., 1998. Proc. Natl. Acad. Sci. 95 (22), 12961–12966.
Srijanto, B.R., Cheney, C.P., Hedden, D.L., Gehl, A.C., Crilly, P.B., Huestis, M.A., Ferrell, T.L., 2012. Sens. Lett. 10 (3–4), 850–855.
Wang, X.Y., Gao, A., Lu, C.C., He, X.W., Yin, X.B., 2013. Biosens. Bioelectron. 48, 120–125.
Williams, E., Pividori, M.I., Merkoçi, A., Forster, R.J., Alegret, S., 2003. Biosens. Bioelectron. 19 (3), 165–175.
Wu, Z., Liu, Y., Zhou, X., Shen, A., Hu, J., 2013. Biosens. Bioelectron. 44 (1), 10–15.
Xu, H., Gorgy, K., Gondran, C., Le Goff, A., Spinelli, N., Lopez, C., Defrancq, E., Cosnier, S., 2013. Biosens. Bioelectron. 41, 90–95.
Yang, X., Wang, A., Liu, J., 2013. Talanta 114, 5–10.
Zhang, L., Cui, P., Zhang, B., Gao, F., 2013. Chem. Eur. J. 19 (28), 9242–9250.
Zhang, Z., Luo, L., Zhu, L., Ding, Y., Deng, D., Wang, Z., 2013. Analyst 138 (18), 5365–5370.
Zheng, J., Feng, W., Lin, L., Zhang, F., Cheng, G., He, P., Fang, Y., 2007. Biosens. Bioelectron. 23 (3), 341–347.

Article 6. Aptamer-antibody assay for cytochrome c detection employing a MWCNT platforma and the electrochemical impedance spectroscopy

C. Ocaña, S. Lukic and M. del Valle

Microchimica Acta, (submitted).

Aptamer-antibody sandwich assay for cytochrome c employing a MWCNT platform and the electrochemical impedance technique

Cristina Ocaña[1], Sonja Lukic[2] and Manel del Valle[1*]

[1]*Sensors and Biosensors Group, Department of Chemistry, Universitat Autònoma de Barcelona, Edifici Cn, 08193 Bellaterra, Barcelona, SPAIN*
[2]*Institute of Analytical Chemistry, Chemo- and Biosensors, University of Regensburg, 93053 Regensburg, GERMANY*

Abstract

We report on a sensitive aptamer-antibody interaction-based assay for cytochrome c (Cyt *c*) using electrochemical impedance. 4-amino benzoic acid is used for the oriented immobilization of aminated aptamers onto multi-walled carbon nanotubes on the surface of a screen-printed electrode via electrochemical grafting. Impedance was measured in a solution containing the redox marker ferro/ferricyanide. The change in interfacial charge transfer resistance (Rct) experienced by the redox marker was recorded to confirm the formation of a complex between aptamer and the target (Cyt *c*). A biotinylated antibody against cytochrome c (Cyt *c* Ab) was then used in a sandwich type of assay. The addition of streptavidin conjugated to gold nanoparticles and signal enhancement by treatment with silver led to a further increase in Rct. Under optimized conditions, a detection limit as low as 12 pM was obtained. Cross-reactivity against other serum proteins (including fibrinogen, BSA and immunoglobulin G) demonstrated improved selectivity.

Keywords: Aptamer, sandwich, cytochrome c, SEM, gold-nanoparticles Electrochemical Impedance Spectroscopy.

Running title: Aptamer-antibody sandwich assay for Cyt *c* detection using EIS

* E-mail: manel.delvalle@uab.cat; tel: +34 93 5813235; fax: +34 93 5812477

Introduction

Cytochrome c (Cyt *c*) is a heme containing metalloprotein located in the intermembrane space of mitochondria. It plays a central role in electron transport chain and it is also an intermediate in apoptosis. When mitochondria are injured under pathological conditions, Cyt *c* is released into the cytosol of the cell. This translocation of Cyt *c* from mitochondria to cytosol is a decisive event in the activation of intracellular signaling; it results in a cascade of caspase activation and leads to programmed cell death (apoptosis). For this reason, the quantification of Cyt *c* may be of great importance in clinical diagnostics and therapeutic research [1].

Aptamers are oligonucleotides (DNA or RNA) that possess properties comparable to those of protein monoclonal antibodies, and thus are clear alternatives to well established antibody-based diagnostic or other biotechnological tasks for research [2,3], therapy [4,5] and diagnostics [6,7]. This kind of functional nucleic acids can fold into complex three-dimensional shapes, thus forming binding pockets and cavities able for specific recognition. Therefore, aptamers are able to obtain a high affinity binding of any given molecular target, from metal ions and small chemicals structures to large proteins and higher order proteins complexes, even whole cells, viruses or parasites [8]. Aptamers are generated by an in vitro selection process called SELEX (Systematic Evolution of Ligands by Exponential Enrichment), which was first reported in 1990 [9,10]. This method has permitted the identification of unique DNA/RNA fragments, from large sets of random sequence oligomers (DNA or RNA libraries), which may bind to a specific target molecule with very high specificity and affinity [11]. Due to their numerous advantages versus antibodies, aptamers have been increasingly used in biosensing in the recent years [12-17].

Among the different electrochemical techniques available, electrochemical impedance spectroscopy (EIS) [18] has been used in numerous studies [19-21]. This technique is very sensitive to changes in the interfacial properties of the modified electrodes caused by biorecognition events at the electrode surface [22,23]. For this reason, EIS is becoming an attractive electrochemical technique for numerous applications such as immunosensing [24], enzyme activity determination [25], genosensing [26,27], studies of corrosion [28] and other surface phenomena [29].

Signal amplification based on bifunctional nanomaterials is attracting significant attention due to the need for ultrasensitive bioassays. Among nanomaterials, gold nanoparticles have been widely used thanks to their excellent properties, such as high biocompatibility, distinctive size-related electronic and optical behavior, high electrical conductivity and high catalytic activity [30]. For example, Deng et al. [31] used AuNPs stabilized with sodium dodecylsulfate to amplify the impedimetric signal for the detection of thrombin, Zheng et al. [32] used network-like thiocyanuric acid/gold nanoparticles to amplify the signal for the detection of thrombin, etc.

In this work, we report a sensitive impedimetric aptamer-antibody sandwich assay for Cyt *c* detection using a highly specific amplification strategy with the use of streptavidin gold nanoparticles and silver enhancement treatment. The employed transducer consisted of a multi-walled carbon nanotube (MWCNT) screen-printed electrode which surface allowed the immobilization of aptamer binding cytochrome c (AptCyt *c*) by covalent bond via prior electrochemical grafting. As a transducer material, MWCNTs are used for promoting electron-transfer between the electroactive species and electrode and provide a novel method for fabricating biosensors. The change of interfacial charge transfer resistance (Rct) experimented by the redox marker, was recorded to confirm the aptamer complex formation with target protein, cytochrome c (Cyt *c*). After that, a biotinylated anti-cytochrome c antibody (Cyt *c* Ab) is used to form the sandwich. The addition of strep-AuNPs and silver enhancement treatment led to a further increment of Rct and the subsequent achievement of significant signal amplification, high sensitivity and improvement of selectivity.

Experimental

Reagents and solutions

Potassium dihydrogen phosphate, potassium ferricyanide $K_3[Fe(CN)_6]$, potassium ferrocyanide $K_4[Fe(CN)_6]$, sodium monophosphate, 4-aminobenzoic acid (ABA), sodium nitrite, *N*-(3-dimethylaminopropyl)-*N*′-ethylcarbodiimide hydrochloride (EDC), gold (III) chloride solution ($HAuCl_4$), *N*-hydroxysuccinimide (NHS), streptavidin gold nanoparticles, fibrinogen, immunoglobulin G and the target protein cytochrome c (Cyt *c*), were all purchased from Sigma (St. Louis, MO, USA, www.sigmaaldrich.com). Poly(ethylene glycol) 1000 (PEG), sodium chloride,

hydroxylamine hydrochloride ($NH_2OH{\cdot}HCl$) and potassium chloride were purchased from Fluka (Buchs, Switzerland). Polyclonal biotinylated anti-cytochrome *c* antibody (Cyt *c* Ab) was purchased from BioLegend (San Diego, California, www.biolegend.com). LIS silver enhancement kit was obtained from Nanoprobes (Yaphank, New York, www.nanoprobes.com). All reagents were analytical reagent grade. The aptamer used in this study was synthetized by TIB-MOLBIOL (Berlin, Germany, www.tib-molbiol.de). Stock solutions of aptamers were diluted with sterilized and deionised water, separated into fractions and stored at −20 °C until required. Aptamer solutions were prepared in phosphate buffer pH 7 from stock solutions. A well-known aptamer for thrombin (AptThr) was used for negative control purposes. Base sequences of both aptamers were the following:

AptCyt *c*: 5'–NH_2–AGTGT GAAAT ATCTA AACTA AATGT GGAGG GTGGG ACGGG AAGAA GTTTA TTTTC ACACT–3'

AptThr: 5'–AGTCC GTGGT AGGGC AGGTT GGGGT GACT–Biotin–3'

All solutions were prepared using MilliQ water from MilliQ System (Millipore, Billerica, MA, USA, www.emdmillipore.com). The buffers employed were: phosphate buffer (187 mM NaCl, 2.7 mM KCl, 8.1 mM $Na_2HPO_4{\cdot}2H_2O$, 1.76 mM KH_2PO_4, pH 7.0) and triethylammonium bicarbonate (0.6 M).

Biosensing Protocol

The steps of the experimental protocol for Cyt *c* analysis, described in detail below, are represented in Figure 1.

<FIGURE 1>

Aptamer immobilization

MWCNT screen-printed electrodes were modified with aminobenzoic acid by means of a one step procedure. Firstly, 30 mg of ABA were dissolved in 3 mL of 1 M HCl and ice-cooled. Then, the diazonium salt was prepared by adding 570 µL of 2 mM $NaNO_2$ aqueous solution dropwise to the 4-aminobenzoic acid solution, with constant stirring. The electrode was immersed in this solution, and 10 successive voltammetric

cycles ranging between 0.0 and -1.0 V (v=200 mV·s^{-1}) were performed [24], generating a carbon-carbon bond and eliminating the azonium group. The modified electrodes (benzoic acid modified) were washed thoroughly with water and methanol and dried at room temperature. Finally, 60 µL of aptamer solution (together with 1 mg of EDC and 0.5 mg of NHS) was placed on the modified electrode and left to react for 12 h, with the goal of covalent immobilization of the aminated aptamer through the amide formation. This step was followed by two 10 min washing steps with phosphate buffer.

Blocking step

To minimize any possible nonspecific adsorption of secondary species, 60 µL of PEG were dropped onto the electrodes and left to incubate during 15 min. This was followed by two washing steps using phosphate buffer for 10 min.

Cytochrome c detection

60 µL of a solution with the desired concentration of Cyt *c* were dropped onto the electrodes. The incubation took place for 15 min. Then, the biosensors were washed twice with phosphate buffer for 10 min.

Sandwich formation

In order to achieve the aptamer–antibody sandwich formation, electrodes were dropped 60 µL of Cyt *c* Ab, from a 1/500 dilution of the stock solution in phosphate buffer. The incubation took place for 15 min. This was followed by two washing steps using phosphate buffer for 10 min.

Addition of strep-AuNPs

60 µL of strep-AuNPs, from a 1/100 dilution of the stock solution in phosphate buffer were dropped onto the electrodes [33]. This step was followed by two gentle washing steps in phosphate buffer for 10 min at 25ºC. In order to obtain a negative control, for the strep-AuNPs addition step, an aptamer without affinity (Apt Thr) was used instead of Apt Cyt *c*

Silver enhancement of strep-AuNPs

20 µl of a solution obtained by the combination of 10 µL of enhancer and 10 µL of initiator (commercial solutions) were deposited onto the electrode surface and left for

7 minutes to facilitate the reaction [33]. After the catalytic silver reduction, the electrodes were thoroughly washed with deionized water to stop the reaction. The silver enhancing solution was prepared immediately before each use. For silver enhancement treatment, the negative control used was a biotinylated AptThr as a ptamer without affinity.

Gold enhancement of strep-AuNPs

The MWCNT screen-printed electrodes modified with sandwich and strep-AuNPs were immersed in a solution containing a mixture of 0.01% $HAuCl_4$ and 0.4 mM $NH_2OH{\cdot}HCl$ (pH 6.0) for 2 min at 25ºC, rinsed, and then treated for 2 additional min. In order to prevent the non-specific background of fine gold particles, the electrodes were rinsed with a solution of 0.6 M triethylammonium bicarbonate buffer after each amplification. Solutions for amplification were freshly prepared in a lightproof container before each use.

Different selectivity experiments were carried out to verify selectivity characteristics of the assay with potentially interfering proteins instead of Cyt *c*.

Spiked samples preparation

Cytochrome c serum samples were prepared by adding three different concentrations of Cyt *c* to undiluted serum samples. All experimental conditions were the same as for the target detection.

Equipment

AC impedance measurements were performed using an Autolab PGStat 20 (Metrohm Autolab B.V, Utrecht, The Netherlands, www.metrohm-autolab.com). FRA software (Metrohm Autolab) was used for data acquisition and control of the experiments. A three electrode configuration was used to perform the impedance measurements: a platinum-ring auxiliary electrode (Crison 52–67 1, Barcelona, Spain), a Ag/AgCl reference electrode and the MWCNT-screen printed electrode as the working electrode (Dropsens, Oviedo, Spain, www.dropsens.es). A scanning electron

microscope (SEM) (Merlin, Zeiss, Germany, www.zeiss.com) was used to visualize gold enhanced strep-AuNPs on the electrode surface.

EIS detection

Impedance experiments were performed at an applied potential of 0.17 V (vs. Ag/AgCl reference electrode), with a range of frequency of 50 kHz – 0.05 Hz, an AC amplitude of 10 mV and a sampling rate of 10 points per decade above 66 Hz and 5 points per decade at the lower range. All measurements were performed in phosphate buffer containing 0.01 M $K_3[Fe(CN)_6]/K_4[Fe(CN)_6]$ (1:1) mixture, used as a redox marker. The impedance spectra were plotted in the form of complex plane diagrams (Nyquist plots, $-Z_{im}$ *vs.* Z_{re}) and fitted to a theoretical curve corresponding to the equivalent circuit with Z_{view} software (Scribner Associates Inc., USA). The equivalent circuit was formed by one resistor/capacitor element in series with a resistance; the Warburg term was circumvented as the diffusion processes were not relevant in this study. For all performed fittings, the chi-square goodness-of-fit test was thoroughly checked to verify the calculations. In all cases, calculated values for each circuit remained in the range of 0.0003 – 0.15, which was much lower than the tabulated value for 50 degrees of freedom (67.505 at 95 % confidence level). The most important parameter in this work is the electron transfer resistance (R_{ct}), which reflects the resistance to charge transfer between the redox probe and the electrode surface. In order to compare the results obtained from the different electrodes used, and to obtain independent and reproducible results, a relative transformation of signals was needed [34]. Thus, the Δ_{ratio} value was defined according to the following equations:

$$\Delta_{ratio} = \Delta_s / \Delta_p \quad (1)$$

$$\Delta_s = Rct_{(AptCyt\ c/Cyt\ c/Cyt\ c\ Ab/strep\text{-}AuNPs/silver\ enhancement)} - Rct_{(electrode\text{-}buffer)} \quad (2)$$

$$\Delta_p = Rct_{(AptCyt\ c)} - Rct_{(electrode\text{-}buffer)} \quad (3)$$

Where $Rct_{(AptCyt\ c/Cyt\ c/Cyt\ c\ Ab/strep\text{-}AuNPs/silver\ enhancement)}$ was the electron transfer resistance value measured after sandwich formation and silver treatment; $Rct_{(AptCyt\ c)}$ was the electron transfer resistance value measured after aptamer immobilization on the electrode, and $Rct_{(electrode\text{-}buffer)}$ was the electron transfer resistance of the blank electrode in buffer.

Results and Discussion

The fundamentals of the developed assay are illustrated in Figure 1. Firstly, MWCNT screen-printed electrodes were modified with amino benzoic acid. Briefly, diazotation of ABA was performed with sodium nitrite in hydrochloride acid, the resulting 4-carboxybenzenediazonium ion solution was dropped onto the MWCNT electrode surface and the potential was cycled as described in Experimental Section. Figure 2a) shows the Nyquist plots obtained by electrochemical impedance spectroscopy. As can be seen, modification of the MWCNT electrode with ABA gave rise to a large increase in the electron transfer resistance as a consequence of the electrostatic repulsion between the redox maker and the negatively charged carboxylate groups. Thereafter, surface-confined carboxyl groups were activated with EDC/NHS to form amide bonds with amino terminated aptamer. After aptamer incubation, the R_{ct} decreased in relation to the modification surface with ABA due to reduction of the negative charge density of the electrode surface, as can be observed in Figure 2b). Afterwards, the Rct value diameter of the semicircle increased after each performed step. The addition of a target protein, Cyt *c*, and Cyt *c* Ab to form a complex AptCyt *c*–Cyt *c* and a sandwich respectively, resulted in a less marked increment of the resistance value due to the augmented quantity of negative charges and to the hindrance caused by the formation of a double layer. After the addition of strept-AuNPs we can observe a further increment of charge transfer resistance because of the increased hindrance due to the formed conjugates. In the second amplification step, the silver enhancement treatment [35,36], a significant increment of Rct value was also observed and attributable to the silver deposition on gold.

<FIGURE 2>

Optimization of the experimental concentrations involved in the aptamer-antibody sandwich assay response to Cyt *c*

All concentrations involved in the analytical performance of the aptansensor for detection of Cytc were optimized by constructing its relative response curve. For this, increasing concentrations of AptCyt *c* and PEG were used to determine the

immobilization and surface blocking, respectively, evaluating the changes in the Δp. Figure 3a) shows the curve of AptCyt *c* immobilization onto the electrode surface. It can be observed that the difference in resistance (Δp) increased up to a value. This is due to the physical adsorption of the aptamer onto the electrode surface, which followed a Langmuir isotherm. Embodied by the variation of R_{ct} which increases to reach a saturation value, the optimal concentration was chosen as initial value to reach it. This value corresponded to a concentration of aptamer of 1.5 μM. Concerning blocking agent, and as shown in Figure 3b), a different behavior was obtained. The optimal concentration of blocking agent was chosen as 30 mM because it was the concentration point where a small plateau was observed.

<FIGURE 3>

In addition, in order to obtain the optimal concentration of Cyt *c* Ab to be used in the biosensing protocol, response was evaluated with increasing concentration of antibody. The optimal concentration was chosen as maximum Δ_{ratio} value, 1/500 stock dilution, Figure S1 (Supplementary Information).

Scanning electron microscope examination

Screen-printed MWCNT electrode surfaces were investigated by SEM after the gold enhancement treatment. $HAuCl_4$ was employed in order to achieve an adequate amplification of strept-AuNPs present on sensor surface to allow their direct observation by SEM. SEM images taken at an acceleration voltage of 3 kV are shown in Figure 4, illustrating a positive experiment with sandwich protocol and strep-AuNPs conjugation. As can be observed in Figure 4a), the distribution of gold enhanced-gold nanoparticles is quite homogeneous. This also implies a regular distribution of MWCNT and well-organized formation of sandwich complex ont o the electrode surface. This high density distribution also demonstrates the proper functionality of the MWCNT platform and the immobilization of the biomolecule. Comparing this experiment with the negative control that did not use the biotinylated Cyt *c* Ab, Figure 4b), a surface with almost absent nanoparticles can be observed.

<FIGURE 4>

Analytical performance of the aptamer-antibody sandwich assay for detection of Cyt *c*

After experimental concentration optimizations, the aptasensor was then used following the sandwich protocol, plus amplification employing the strep-AuNPs and silver enhancement treatment. Figure 5 shows calibration curves with increasing concentrations of Cyt *c* and their respective regression lines in the logaritmic scale, at the different steps of the protocol: (1) AptCyt *c*–Cyt *c*, (2) sandwich formation between AptCyt *c*, Cyt *c* and Cyt *c* Ab, (3) aptamer sandwich modified with strep-AuNPs, and (4) aptamer sandwich modified with strep-AuNPs and silver enhancement treatment. Although reproducibility was not ideal in all cases, the calibration curves obtained showed a good RSD. As can be seen in Figure S2 (Supplementary Information), all calibration curves increased until the value of 100 pM of Cyt *c*, this could be due to the fact that concentrations larger than 100 pM caused a saturation on the sensor surface. As can be observed in Table 1, the use of silver enhancement treatment led to the highest sensitivity and signal amplification, resulting in 108 % increase compared to the simple biosensing scheme. This demonstrates that the silver deposition on gold nanoparticles, basically increases the sterical hindrance, producing an increment of observed impedance, given this conductive silver is not wired to the electrode surface. Together with the higher sensitivity, the detection limit obtained in this case was 12 pM (calculated as the intersection with the horizontal reference line) and it is slightly improving the one obtained with only strep-AuNPs (15 pM). Without sandwich amplification, signal is of the same magnitude than associated errors, making the assay of impractical use. This results confirmed that the best method, showing a low detection limit and an ultrahigh sensitivity for the detection of Cyt *c* involves the sandwich and amplification protocol.

<FIGURE 5>

<TABLE 1>

Selectivity of the aptamer-antibody sandwich assay

Control experiments were conducted to investigate the specificity of aptamer-antibody assay. In this work, majority serum proteins, such as human IgG, fibrinogen and albumin at serum physiological levels were tested to operate the aptasensor instead of Cyt *c* under the same experimental conditions. As can be seen in Figure 6, the presence of interfering proteins such as albumin, fibrinogen and immunoglobulin G, at serum concentration level exhibits negligible response compared with 100 pM Cyt *c* in the amplified sandwich protocol, even at concentrations four or five orders of magnitude higher than typical Cyt *c* concentrations. Figure 6 also demonstrates that the sandwich protocol displays as clear advantage, more than the signal amplification, the marked decrease of interfering effects that are still remarkable in the simple biosensing protocol. This is especially remarkable for IgG protein (human), which shows appreciable interference in the assay without amplification, although it becomes practically negligible with the sandwich variant.

<FIGURE 6>

Detection of Cyt *c* in spiked serum samples

<TABLE 2>

The applicability of the biosensor was tested by the analysis of spiked samples of human serum samples. For that purpose, human serum samples were spiked with three different concentrations of Cyt *c*. As shown in Table 2, the recoveries of spiked samples were between 94.6 % and 107.8·% when using this method, which showed a satisfactory result. In addition, a good reproducibility of the blanks was obtained, 5.54% RSD. These findings imply that the developed methodology has a promising feature for the analytical application in complex biological samples.

<TABLE 3>

Once we had confirmed that our biosensor was able to detect Cyt *c* with excellent analytical performance also in real samples, its analytical features were

compared to other detection methodologies for Cyt *c* detection, as described in the literature. Details are shown in Table 3, where sensitivity info is presented as the LOD of each biosensor compared. The lowest detection limit value among all the analytical techniques corresponded to ref [39], but this Cyt *c* biosensor used ICP-MS as the transduction technique. This methodology displays high sensitivity but is not simple, portable or easy to use. However, our biosensor showed the second lowest LOD value and it was suitable for real samples, considering that the lowest level of Cyt *c* in serum samples is about 10 pM [43].

Conclusions

An ultrasensitive aptamer-antibody sandwich assay for cytochrome c detection using electrochemical impedance technique was reported. Due to the signal amplification with strep-AuNPs and silver deposition, it was possible to increase the sensitivity of the assay. Additionally, for a comparable amount of AptCyt *c*–Cyt *c*, the signal resulted in 108% amplification, compared to results recorded with simple biosensing AptCyt *c*–Cyt *c*. Furthermore, the limit of detection obtained was 12 pM. An acceptable linear range, between 25-100 pM, and high selectivity with respect to different serum proteins at serum concentration level were also achieved with this protocol thanks to the double recognition scheme utilized. Finally, the suitability of the biosensor for measurement in real samples was checked by determining Cyt *c* in human serum samples. Obtained recovery values in the range 94.6–107.8%, demonstrated a promising feature for the analytical application in complex biological samples.

Acknowledgments

This research was partly supported by the Research Executive Agency (REA) of the European Union under Grant Agreement number PITN-GA-2010-264772 (ITN CHEBANA), by the Ministry of Science and Innovation (MCINN, Madrid, Spain) through the project CTQ2013-41577-P and by the Catalonia program ICREA Academia. Cristina Ocaña thanks the support of Ministry of Science and Innovation (MICINN, Madrid, Spain) for the predoctoral grant.

References

1. Alleyne T, Joseph J, Sampson V (2001) Cytochrome-c detection: A diagnostic marker for myocardial infarction. Applied Biochemistry and Biotechnology 90 (2):97-105.

2. Clark SL, Remcho VT (2002) Aptamers as analytical reagents. Electrophoresis 23 (9):1335-1340.

3. Radi A, Acero Sánchez JL, Baldrich E, O'Sullivan CK (2005) Reusable Impedimetric Aptasensor. Anal Chem 77 (19):6320-6323.

4. Biesecker G, Dihel L, Enney K, Bendele RA (1999) Derivation of RNA aptamer inhibitors of human complement C5. Immunopharmacology 42 (1-3):219-230.

5. Hicke BJ, Marion C, Chang YF, Gould T, Lynott CK, Parma D, Schmidt PG, Warren S (2001) Tenascin-C aptamers are generated using tumor cells and purified protein. J Biol Chem 276 (52):48644-48654.

6. Cox JC, Ellington AD (2001) Automated selection of anti-protein aptamers. Bioorganic & medicinal chemistry 9 (10):2525-2531

7. Cai H, Lee TM-H, Hsing IM (2006) Label-free protein recognition using an aptamer-based impedance measurement assay. Sensors and Actuators B: Chemical 114 (1):433-437.

8. Jayasena SD (1999) Aptamers: an emerging class of molecules that rival antibodies in diagnostics. Clin Chem 45 (9):1628-1650

9. Ellington AD, Szostak JW (1990) In vitro selection of RNA molecules that bind specific ligands. Nature 346 (6287):818-822

10. Tuerk C, Gold L (1990) Systemic evolution of ligands by exponential enrichment: RNA ligands to bacteriophage T4 DNA polymerase. Science 249 (4968):505-510

11. Tombelli S, Minunni M, Mascini M (2005) Analytical applications of aptamers. Biosens Bioelectron 20 (12):2424-2434

12. Zhang L, Cui P, Zhang B, Gao F (2013) Aptamer-based turn-on detection of thrombin in biological fluids based on rfficient phosphorescence energy transfer from Mn-doped ZnS quantum dots to carbon nanodots. Chemistry - A European Journal 19 (28):9242-9250

13. Chang M, Kwon M, Kim S, Yunn NO, Kim D, Ryu SH, Lee JB (2014) Aptamer-based single-molecule imaging of insulin receptors in living cells. Journal of Biomedical Optics 19 (5)

14. Loo AH, Bonanni A, Pumera M (2012) Impedimetric thrombin aptasensor based on chemically modified graphenes. Nanoscale 4 (1):143-147

15. Ho MY, D'Souza N, Migliorato P (2012) Electrochemical Aptamer-Based Sandwich Assays for the Detection of Explosives. Anal Chem 84 (10):4245-4247.

16. Lei P, Tang H, Ding S, Ding X, Zhu D, Shen B, Chang Q, Yan Y (2015) Determination of the invA gene of Salmonella using surface plasmon resonance along with streptavidin aptamer amplification. Michrochim. Acta (182):289-296.

17. Shen B, Li J, Cheng W, Yan Y, Tang R, Li Y, Ju H, Ding S (2015) Electrochemical aptasensor for highly sensitive determination of cocaine using a supramolecular aptamer and rolling circle amplification. Microchim. Acta (182):361-367.

18. McDonald JR (1987) Impedance Spectroscopy. John Wiley, New York

19. Bonanni A, Ambrosi A, Pumera M (2012) On Oxygen-Containing Groups in Chemically Modified Graphenes. Chem-Eur J 18 (15):4541-4548.

20. Bonanni A, Ambrosi A, Pumera M (2012) Nucleic Acid Functionalized Graphene for Biosensing. Chem-Eur J 18 (6):1668-1673.

21. Ocaña C, del Valle M (2014) A comparison of four protocols for the immobilization of an aptamer on graphite composite electrode, Microchim. Acta (181):355-363.

22. Bardea A, Patolsky F, Dagan A, Willner I (1999) Sensing and amplification of oligonucleotide-DNA interactions by means of impedance spectroscopy: a route to a Tay-Sachs sensor. Chem Comm (1):21-22.

23. Loo A H, Bonanni A, Ambrosi A, Poh H L, Pumera M (2012) Impedimetric immunoglobulin G immunosensor based on chemically modified graphenes. Nanoscale 4 (3):921-925.

24. Moreno-Guzmán M, Ojeda I, Villalonga R, González-Cortés A, Yáñez-Sedeño P, Pingarrón JM (2012) Ultrasensitive detection of adrenocorticotropin hormone (ACTH) using disposable phenylboronic-modified electrochemical immunosensors. Biosens Bioelectron 35 (1):82-86.

25. Zhang Y, Li Y, Wu W, Jiang Y, Hu B (2014) Chitosan coated on the layers' glucose oxidase immobilized on cysteamine/Au electrode for use as glucose biosensor. Biosens Bioelectron 60:271-276

26. Bonanni A, Esplandiu MJ, del Valle M (2010) Impedimetric genosensing of DNA polymorphism correlated to cystic fibrosis: A comparison among different protocols and electrode surfaces. Biosens Bioelectron 26 (4):1245-1251.

27. Bonanni A, Pumera M, Miyahara Y (2010) Rapid, Sensitive, and Label-Free Impedimetric Detection of a Single-Nucleotide Polymorphism Correlated to Kidney Disease. Anal Chem 82 (9):3772-3779.

28. Blin F, Koutsoukos P, Klepetsianis P, Forsyth M (2007) The corrosion inhibition mechanism of new rare earth cinnamate compounds — Electrochemical studies. Electrochim Acta 52 (21):6212-6220.

29. Liao Y-M, Feng Z-D, Chen Z-L (2007) In situ tracing the process of human enamel demineralization by electrochemical impedance spectroscopy (EIS). Journal of Dentistry 35 (5):425-430.

30. Bonanni A, del Valle M (2010) Use of nanomaterials for impedimetric DNA sensors: A review. Anal Chim Acta 678 (1):7-17.

31. Deng C, Chen J, Nie Z, Wang M, Chu X, Chen X, Xiao X, Lei C, Yao S (2008) Impedimetric Aptasensor with Femtomolar Sensitivity Based on the Enlargement of Surface-Charged Gold Nanoparticles. Anal Chem 81 (2):739-745.

32. Zheng J, Feng W, Lin L, Zhang F, Cheng G, He P, Fang Y (2007) A new amplification strategy for ultrasensitive electrochemical aptasensor with network-like thiocyanuric acid/gold nanoparticles. Biosens Bioelectron 23 (3):341-347.

33. Bonanni A, Esplandiu MJ, del Valle M (2008) Signal amplification for impedimetric genosensing using gold-streptavidin nanoparticles. Electrochim Acta 53 (11):4022-4029.

34. Bonanni A, Esplandiu MJ, Pividori MI, Alegret S, del Valle M (2006) Impedimetric genosensors for the detection of DNA hybridization. Anal Bioanal Chem 385 (7):1195-1201.

35. Cai H, Wang YQ, He PG, Fang YH (2002) Electrochemical detection of DNA hybridization based on silver-enhanced gold nanoparticle label. Anal Chim Acta 469 (2):165-172.

36. Hanaee H, Ghourchian H, Ziaee AA (2007) Nanoparticle-based electrochemical detection of hepatitis B virus using stripping chronopotentiometry. Anal Biochem 370 (2):195-200.

37. Loo FC, Ng SP, Wu C-ML, Kong SK (2014) An aptasensor using DNA aptamer and white light common-path SPR spectral interferometry to detect cytochrome-c for anti-cancer drug screening. Sensorsand Actuators B: Chemical (198):416-423.

38. Lau IPM, Ngan EKS, Loo JFC, Suen YK, Ho HP, Kong SK (2010) Aptamer-based bio-barcode assay for the detection of cytochrome-c released from apoptotic cells. Biochemical and Biophysical Research Communications (395):560-564.

39. Liu JM, Yan XP (2011) Ultrasensitive, selective and simultaneous detection of cytochrome c and insulin based on immunoassay and aptamer-based bioassay in combination with Au/Ag nanoparticle tagging and ICP-MS detection. Journal of Analytical Atomic Spectrometry (26):1191-1197.

40. Ocaña C, Arcay E, Del Valle M (2014) Label-free impedimetric aptasensor based on epoxy-graphite electrode for the recognition of cytochrome c. Sensors and Actuators, B: Chemical (191):860-865.

41. Pandiaraj M, Benjamin AR, Madasamy T, Vairamani K, Arya A, Sethy NK (2014) A cost-effective volume miniaturized and microcontroller based cytochrome c assay. Sensors and Actuators A: Physical (220):290-297.

42. Pandiaraj M, Madasamy T, Gollavilli PN, Balamurugan M, Kotamraju S, Rao (2013) Nanomaterial-based electrochemical biosensors for cytochrome c using cytochrome c reductase. Bioelectrochemistry (91):1-7.

43. Sakaida I, Kimura T, Yamasaki T, Fukumoto Y, Watanabe K, Aoyama M, Okita K (2005) Cytochrome c is a possible new marker for fulminant hepatitis in humans. Journal of Gastroenterology 40 (2):179-185.

FIGURE CAPTIONS

Fig.1. Scheme of the experimental protocol.

Fig.2. a) Nyquist diagrams of: (●) Bare electrode, (○) Electrochemical grafting treatment and (▼) Aptamer immobilization. b) Nyquist diagrams of: (●) Bare electrode, (○) aptamer immobilization, (▼) Aptamer with Cyt *c*, (Δ) sandwich complex with antibody, (■) sandwich complex modified with gold-nanoparticles and (□) sandwich complex modified with gold-nanoparticles and silver enhancement treatment. All experiments were performed in phosphate buffer and all EIS measurements were performed in PBS solution containing 0.01 M K3[Fe(CN)6]/ K4[Fe(CN)6].

Fig. 3. a) Optimization of the amount of cytochrome c aptamer AptCyt *c* immobilized on each electrode. b) Optimization of the concentration of the blocking agent, PEG. Uncertainty values corresponding to replicated experiments (n=5).

Fig.4. SEM images of (a) experiment using sandwich complex + strep-AuNPS+ gold enhancement treatment (b) negative control using AptCyt *c*+ Cyt *c* + non complementary aptamer + strep-AuNPs + gold enhancement treatment. All images were taken at an acceleration voltage of 3kV and a resolution of 2 µm.

Fig.5. Calibration and regression curves of: (1) (black circle) AptCyt *c* and Cyt *c*, (2) (white circle) sandwich complex, (3) (black triangle) sandwich complex modified with strep-AuNPs, (4) (white triangle) sandwich complex modified with strep-AuNPs and silver enhancement treatment. All experiments were performed in PBS solution and all EIS measurements were performed in phosphate buffer containing 0.01M $K_3[Fe(CN)_6]/K_4[Fe(CN)_6]$. Uncertainty values corresponding to replicated experiments (n = 5).

Fig.6. Comparison graph of responses towards different proteins present in serum, with simple biosensing scheme (white bar) and with the sandwich/amplification protocol (grey bar). The concentrations of the proteins were: 100 pM Cyt *c*, 7.35 µM Fbr, 100 µM IgG and 0.72 mM BSA. Uncertainty values corresponding to replicated experiments (n =5).

Table 1. Summary of the different calibration curves considering different stages of the assay.

Calibration curve	Regression curve	Amplification %	RSD*%
(1)AptCytc/Cytc	Δratio = 0.935 + 0.104· log[Cytc]	-	2.3
(2)Sandwich complex	Δratio = 0.904 + 0.144· log[Cytc]	5	3.2
(3)Sandwich/ strep-AuNPs	Δratio = 0.241 + 0.651·log[Cytc]	35	5.9
(4) Sandwich/strep-AuNPs/Silver enhanc.	Δratio = -0.999 + 1.702·log[Cytc]	108	6.8

*Corresponding to five replicated experiments at 75 pM.

Table 2 . R ecovery st udies p erformed i n sp iked ser um samples f or ap plicability o f biosensor (n = 3).

Samples	[Cyt *c*] spiked (pM)	% Recovery	% RSD
Sample 1	90.0	107.8	8.98
Sample 2	60.0	98.3	9.07
Sample 3	30.0	94.6	8.23

Table 3. Comparison of the Cyt c biosensor with other reported biosensing methods.

Analytical method	LOD	Biorecognition element	Linear range	Interference	Real Sampes	Reference
SPR	≥50 pM	aptamer	80 pM-80 nM	x	√	[37]
Fluorescence	266 pM	aptamer	-	x	√	[38]
ICP-MS/TEM	1.5 fM	antibody	0.1-20 nM	√	√	[39]
EIS	63.2 pM	Aptamer	50 pM-50 nM	√	x	[40]
EIS	11.8 pM	Aptamer-antibody	25-100 pM	√	√	Our work
CV	10 nM	Enzyme	10 nM - 500 µM	x	√	[41]
CV	0.5 µM	Enzyme	1-1000 µM	√	√	[42]

Figure 1

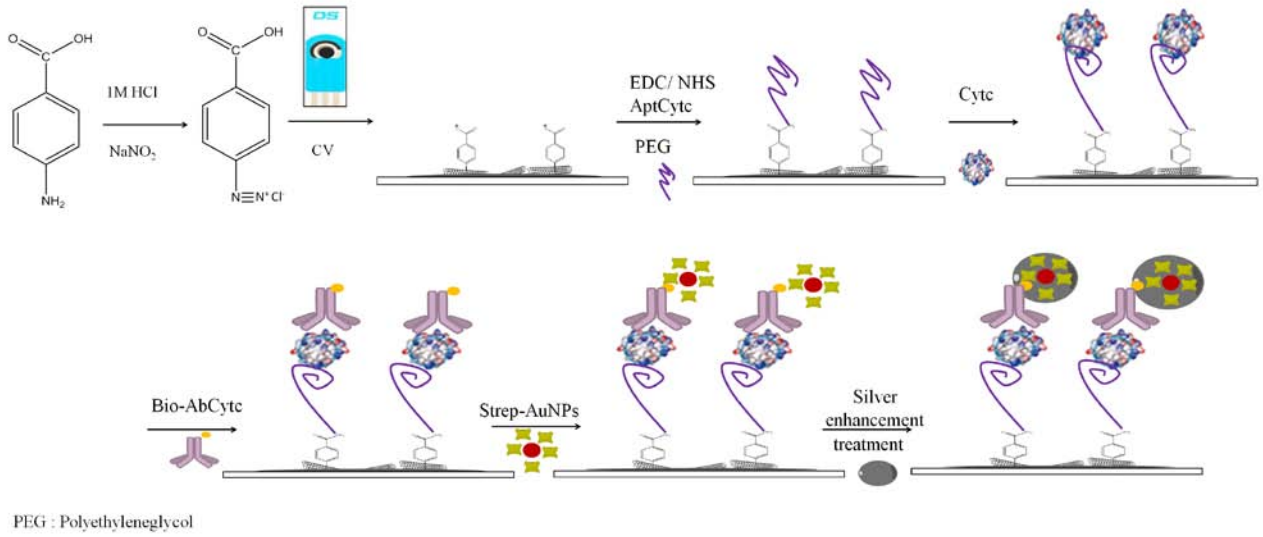

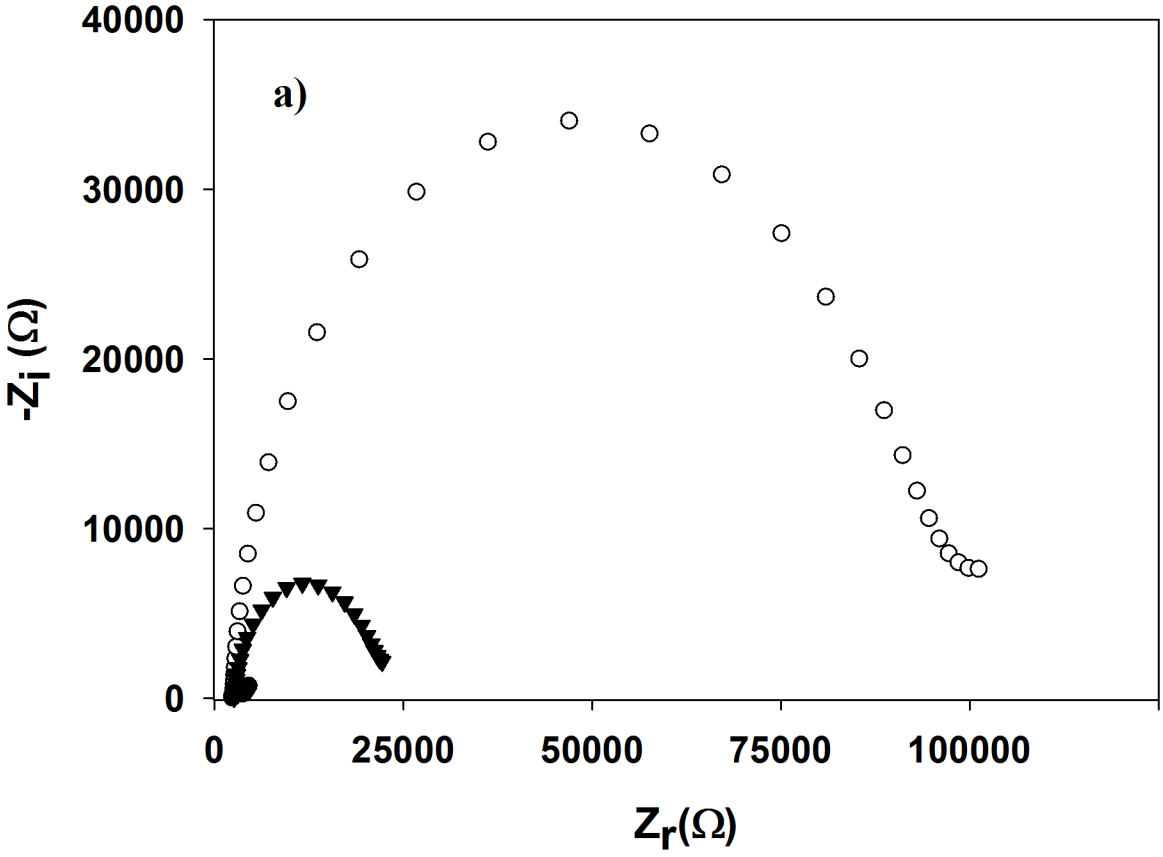
a)
40000
30000
20000
10000
0
-Zi (Ω)
0
25000
50000
75000
100000
Zr(Ω)

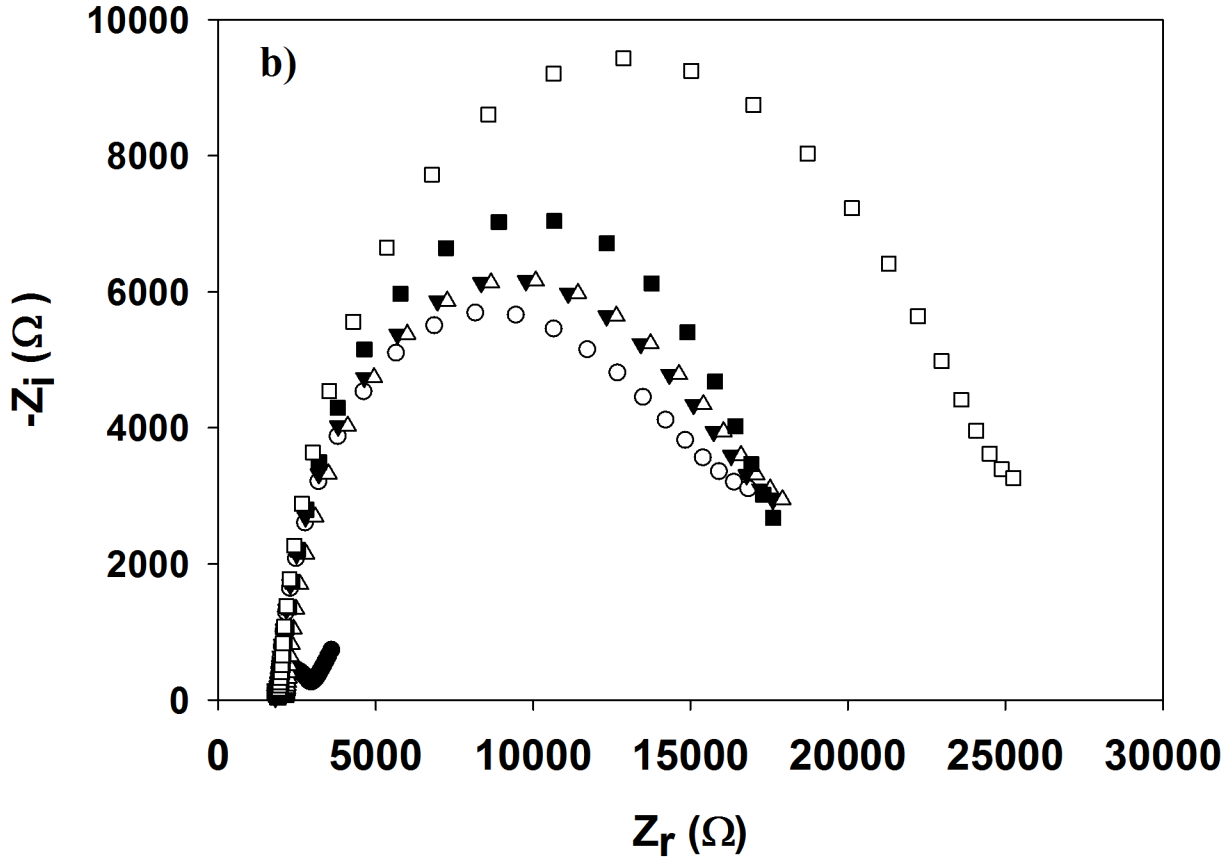
b)
10000
8000
6000
4000
2000
0
-Zi (Ω)
0
5000
10000
15000
20000
25000
30000
Zr (Ω)

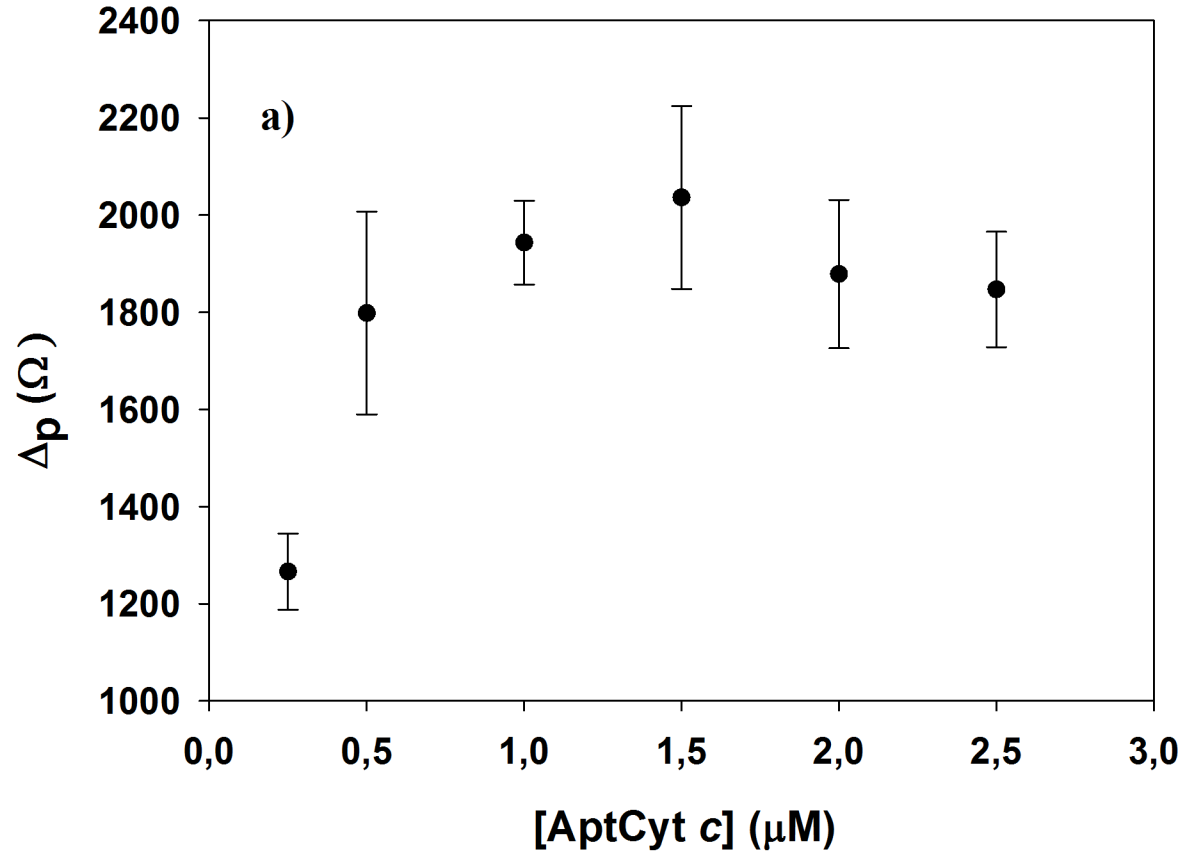
a)
2400
2200
2000
1800
1600
1400
1200
1000
Δp (Ω)
0,0
0,5
1,0
1,5
2,0
2,5
3,0
[AptCyt c] (μM)

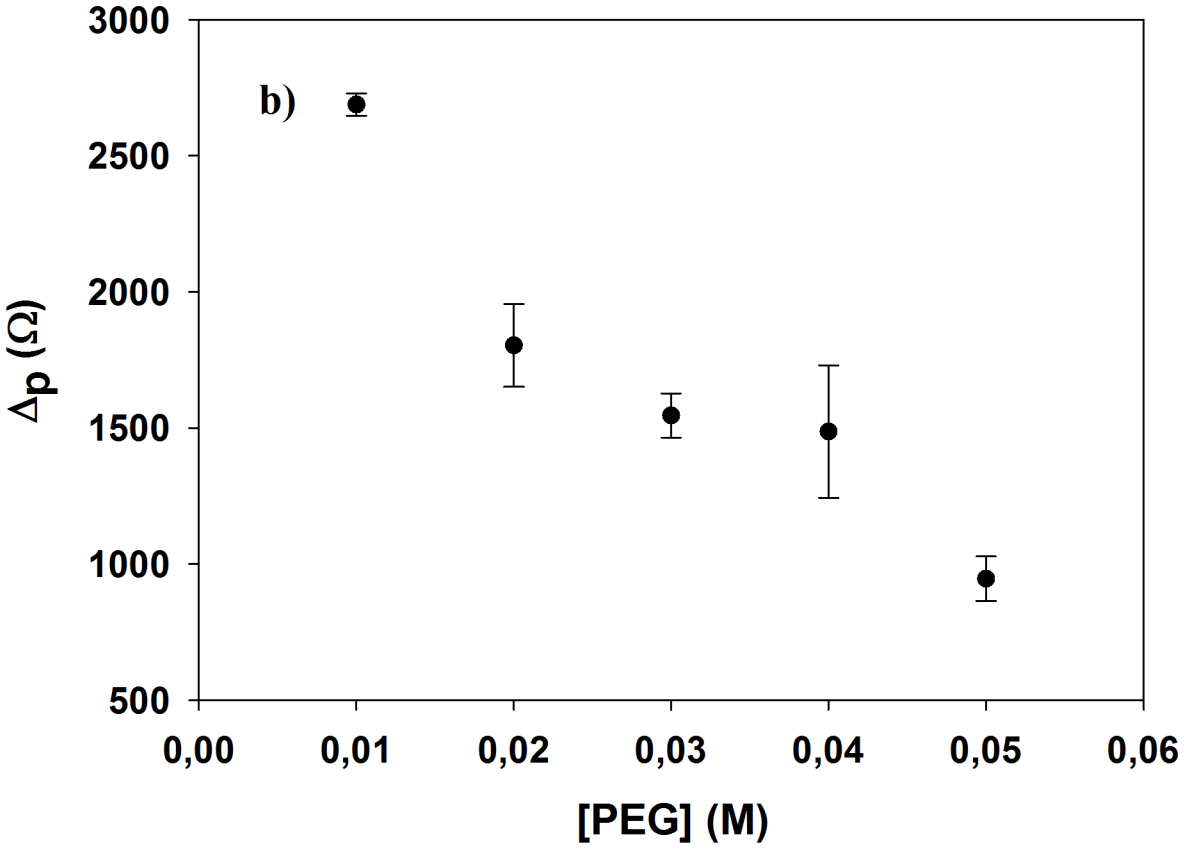
b)
3000
2500
2000
1500
1000
500
Δp (Ω)
0,00
0,01
0,02
0,03
0,04
0,05
0,06
[PEG] (M)

Figure 4

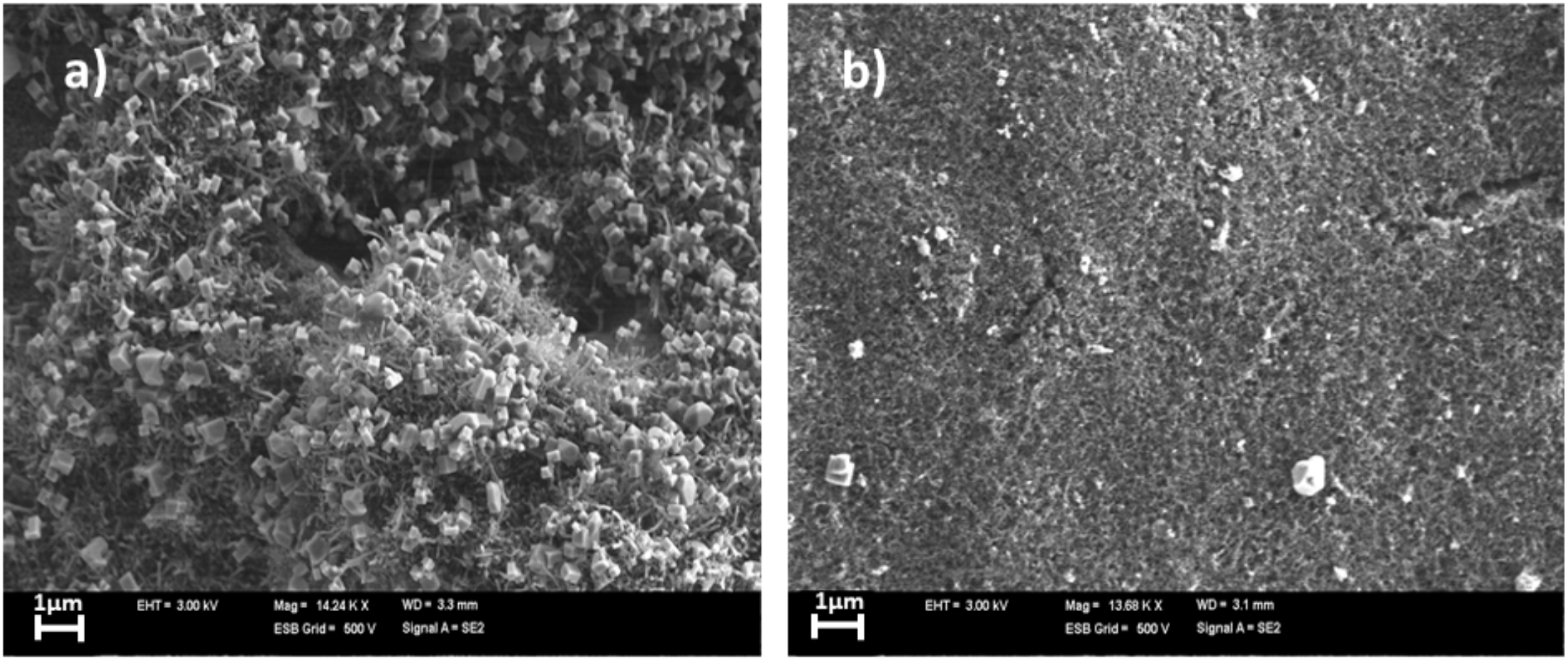
a)
1µm
EHT = 3.00 kV
Mag = 14.24 K X
WD = 3.3 mm
ESB Grid = 500 V
Signal A = SE2
b)
1µm
EHT = 3.00 kV
Mag = 13.68 K X
WD = 3.1 mm
ESB Grid = 500 V
Signal A = SE2

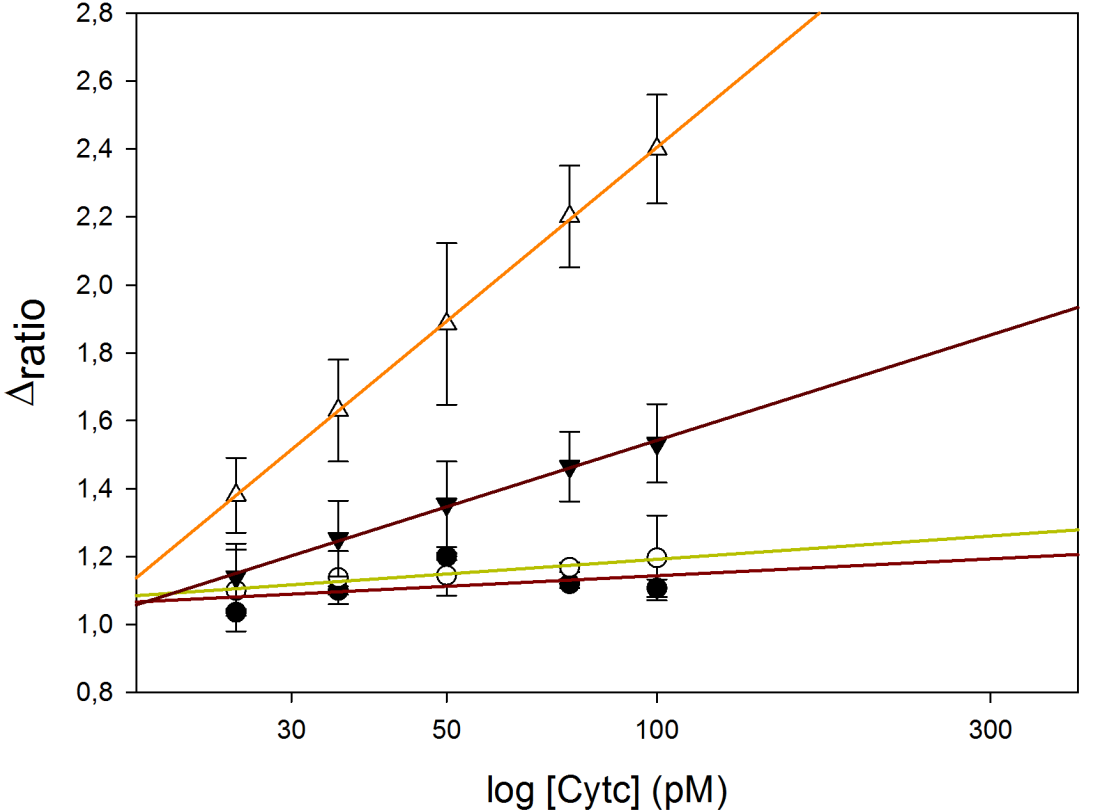
2,8
2,6
2,4
2,2
2,0
1,8
1,6
1,4
1,2
1,0
0,8
Δratio
30
50
100
300
log [Cytc] (pM)

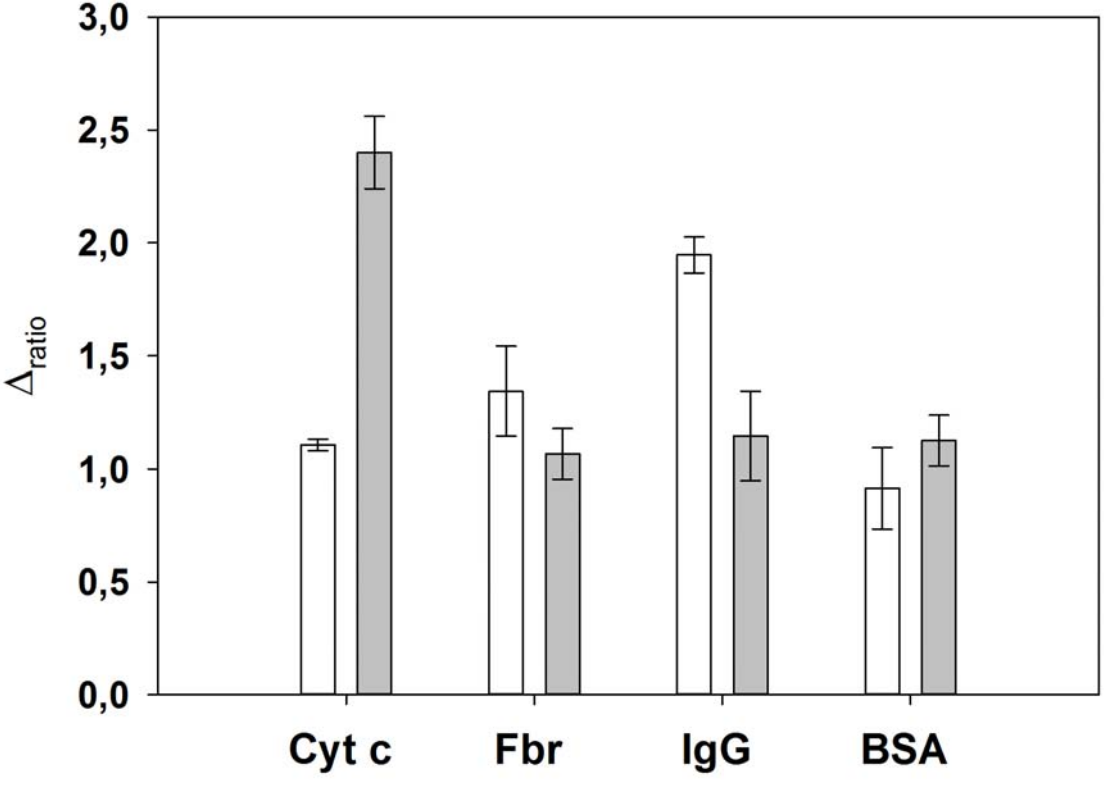
3,0
2,5
2,0
1,5
1,0
0,5
0,0
Δratio
Cyt c
Fbr
IgG
BSA

ANNEX

Article 7. Label-free selective impedimetric detection of Cu^{2+} ions using catalytic DNA

C. Ocaña, N. Malashikina, M. del Valle and V. Pavlov

Analyst, 2013, 138, 1995-1999.

Analyst

RSC Publishing

PAPER

View Article Online
View Journal | View Issue

Label-free selective impedimetric detection of Cu^{2+} ions using catalytic DNA

Cite this: *Analyst*, 2013, **138**, 1995

Cristina Ocaña,[a] Natalia Malashikhina,[b] Manel del Valle*[a] and Valeri Pavlov*[b]

Received 29th November 2012
Accepted 4th February 2013

DOI: 10.1039/c3an36778a

www.rsc.org/analyst

Copper is an essential element for regulation of many biological processes, however, in excess it is considered to be toxic for human health. This metal is frequently accompanied by other elements such as cadmium, nickel and lead. Thus, developing a selective and simple method for determination of copper in a matrix containing other heavy metal ions is of great importance. In this work, a novel selective method for copper detection was developed using electrodes modified with the DNAzyme capturing Cu^{2+} ions. The DNAzyme reconstituted with copper catalyzes oxidation of ascorbic acid leading to the build-up and adsorption of oxidation products on the electrode surface and produces changes in the interfacial properties of the electrode. The increase in the interfacial electron-transfer resistance is probed with electrochemical impedance spectroscopy (EIS) in the presence of the reversible redox couple $[Fe(CN)_6]^{3-}/[Fe(CN)_6]^{4-}$ as a marker. The DNAzyme based biosensor combines excellent selectivity against other heavy metal ions with sufficient sensitivity to Cu^{2+} in the range of 6.5–40 μM.

Published on 04 February 2013 on http://pubs.rsc.org | doi:10.1039/C3AN36778A
Downloaded on 13 March 2013

Introduction

Copper is a redox-active nutrient required in a number of electron transfer processes of many biological reactions.[1] However, at elevated concentrations it has been considered to be toxic for human health. Short-term exposure to an excess of copper can cause gastrointestinal disturbance, while long-term exposure causes liver or kidney damage, neurodegenerative diseases, *etc.*[2] The World Health Organization (WHO) as well as the U.S. Environmental Protection Agency (EPA) have set the limit of copper in drinking water to be 2 mg L^{-1} (32 μM) and 1.3 ppm (20 μM) respectively.[3] Therefore, the development of a sensitive, selective, comparatively inexpensive and portable sensor for Cu^{2+} ion detection is of great importance.

Various analytical methods for the detection of copper ions such as atomic absorption/emission spectroscopy,[4,5] inductively coupled plasma mass spectroscopy (ICP-MS),[6,7] and capillary electrophoresis[8] provide reliable and accurate results, but require expensive and sophisticated instrumentation and complicated sample pretreatment. Many electrochemical sensors such as ion-selective electrodes,[9–12] and voltammetric[13,14] and electrochemiluminescence sensors[15,16] are simple and relatively inexpensive, however, they suffer from low reproducibility and have high detection limits and low selectivity. Metal-selective fluorescent chemosensors have attracted intense attention during the past few decades, however, they need complicated organic synthesis and surface modifications; they require expensive instruments as well.[17–20]

Recently DNAzyme-based assays have attracted considerable interest for the detection of various analytes, including heavy metal ions. DNAzymes (deoxyribozymes, catalytic DNAs, DNA enzymes) are DNA molecules that exhibit different catalytic activities such as RNA cleavage, ligation, phosphorylation and porphyrin metallation.[21] DNAzymes cleaving RNA in the presence of different divalent ion metals have been reported.[22–26] Considering a DNAzyme a promising platform for an application in biosensing various attempts were made for the detection of target DNA,[27,28] or ion metals such as lead,[29] uranyl ions,[30] and mercury.[31] So far, only a few DNAzyme based sensors for copper ions have been reported.[32–34] The design of these DNAzyme probes involves labeling of the oligonucleotide by fluorogenic molecules. In this paper we report a novel label-free electrochemical DNAzyme based biosensor for the detection of copper ions using avidin–graphite epoxy composite electrodes.[35] Electrochemical impedance spectroscopy (EIS) is a powerful and sensitive technique for following biosensing events that take place at the surface of the electrode. Any tiny disturbance at the interface would lead to impedimetric changes.[36] This method is of general use in laboratories and has already been extensively studied and applied for amperometric, enzymatic, immune and genosensing assays.[37,38] The combination of benefits of DNAzyme and electrochemical impedance spectroscopy allowed selective detection of copper with a detection limit of 6.5 μM.

[a]*Grup de Sensors i Biosensors, Departament de Química Universitat Autònoma de Barcelona, Edifici CN, 08193 Bellaterra, Spain. E-mail: manel.delvalle@uab.es; Fax: +34 935812379; Tel: +34 935813235*

[b]*CIC biomaGUNE, Parque Tecnologico de San Sebastian, Paseo Miramon 182, 20009 San Sebastian, Spain. E-mail: vpavlov@cicbiomagune.es; Fax: +34 943005314; Tel: +34 943005308*

Published on 04 February 2013 on http://pubs.rsc.org | doi:10.1039/C3AN36778A
Downloaded on 13 March 2013

Experimental

Apparatus

AC impedance measurements were performed with an IM6e Impedance Measurement Unit (BAS-Zahner, Kronach, Germany) and Autolab PGStat 20 (Metrohm Autolab B.V, Utrecht, The Netherlands). Thales (BAS-Zahner) and FRA (Metrohm Autolab) software, respectively, were used for data acquisition and control of the experiments. A conventional three-electrode system was used to perform impedance measurements: an avidin–graphite epoxy composite (Av–GEC) electrode as a working electrode, an Ag/AgCl electrode as a reference electrode and a platinum-ring auxiliary electrode (Crison 52-67 1, Barcelona, Spain) as a counter electrode. Temperature-controlled incubations were done using an Eppendorf Thermomixer 5436.

Chemicals

Potassium ferricyanide $K_3[Fe(CN)_6]$, potassium ferrocyanide $K_4[Fe(CN)_6]$, ascorbic acid, 4-(2-hydroxyethyl)piperazine-1-ethanesulfonic acid (HEPES), sodium hydroxide, potassium chloride, sodium chloride, avidin, and copper(II) chloride were purchased from Sigma-Aldrich (Spain). DNA phosphoramidites, biotin-CE phosphoramidite, spacer-CE phosphoramidite 18 and other reagents required for solid phase oligonucleotide synthesis were purchased from Link Technologies (UK). Oligonucleotide purification cartridges (OPC) and solvents for DNA purification were purchased from Applied Biosystems (Spain). DNAzyme used in this study was prepared by automated solid-phase chemical synthesis (Applied Biosystems 3400 DNA Synthesizer) and purified with oligonucleotide purification cartridges (OPC), its purity was further analyzed by MALDI-TOF mass spectroscopy. The synthesized DNAzyme has the following sequence: 5′-biotin-$(-O-CH_2-CH_2-O-)_6$ TTC TAA TAC GAT TTA GAA TAA ATC TGG GCC TCT TTT TAA GAA C-3′, where $(-O-CH_2-CH_2-O-)_6$ corresponds to spacer-CE phosphoramidite 18. Solid-state electrodes (Av–GECs) were prepared using 50 μm particle size graphite powder (Merck, Darmstadt, Germany), avidin (Sigma-Aldrich) and Epotek H77 resin and its corresponding hardener (both from Epoxy Technology, Billerica, MA, USA). All reactions were conducted in the buffer containing 50 mM HEPES, pH 7.0, 0.5 M KCl, 0.5 M NaCl. All water used in the experiments was of nanopure grade (from Millipore Milli-Q system).

Experimental

Electrode preparation procedure

Avidin–graphite epoxy composite (Av–GEC) electrodes, used for easy immobilization of biotinylated DNAzyme, were prepared using a PVC tube body (6 mm i.d.) and a small copper disk soldered at the end of an electrical connector. The working surface is an epoxy-graphite conductive composite, formed by a mixture of graphite (18%), avidin (2%) and epoxy resin (80%), deposited on the cavity of the plastic body.[39,40] The composite material was cured at 40 °C for 7 days. Before each use, the electrode surface was moistened with MilliQ water and then thoroughly smoothed with abrasive sandpaper and finally with alumina paper (polishing strips 301044-001, Orion) in order to obtain a reproducible electrochemical surface. The electrodes were then washed twice for 10 minutes in the working buffer at room temperature while stirring.

Immobilization of DNAzyme probe

An Av–GEC electrode was immersed in 160 μL of the desired concentration of biotinylated DNAzyme in 50 mM HEPES, pH 7.0, 0.5 M KCl, and 0.5 M NaCl. After incubation for 1 h at RT while stirring, the electrodes were washed twice for 10 minutes in the working buffer at room temperature.

Reaction of DNAzyme with copper

After the immobilization of DNAzyme the electrode was immersed for 20 minutes in the solution of the desired concentration of $CuCl_2$ and 30 μM concentration of ascorbic acid in the working buffer at RT while stirring. The electrodes were then washed twice for 10 minutes in the working buffer at room temperature.

Impedimetric detection

Impedance spectra were recorded between 50 kHz and 0.05 Hz, at a sinusoidal voltage perturbation of 10 mV amplitude and a sampling rate of 10 points per decade above 66 Hz and 5 points per decade at the lower range. The experiments were carried out under open circuit potential conditions in an unstirred solution of 0.1 M PBS buffer solution containing a 0.01 mM $K_3[Fe(CN)_6]/K_4[Fe(CN)_6]$ (1 : 1) mixture, used as a redox marker. The impedance spectra were plotted in the form of complex plane diagrams (Nyquist plots, $-Z_{im}$ *vs.* Z_{re}) and fitted to a theoretical curve corresponding to the equivalent circuit with Z_{view} software (Scribner Associates Inc., USA). The equivalent circuit was formed by one resistor/capacitor element in series with a resistance. The chi-square goodness of fit was calculated for each fitting by the FRA software employed (Eco Chemie, the Netherlands). In all cases impedance data were recorded in the following order after each of above described steps. In order to compare the results obtained from the different electrodes used, and to obtain independent and reproducible results, relative signals are needed.[39] Thus, the Δ_{ratio} value was defined according to the following equations:

$$\Delta_{ratio} = \Delta_s/\Delta_p$$

$$\Delta_s = R_{ct(DNAzyme-AA-Cu)} - R_{ct(electrode-buffer)}$$

$$\Delta_p = R_{ct(DNAzyme)} - R_{ct(electrode-buffer)}$$

where $R_{ct(DNAzyme-AA-Cu)}$ was the electron transfer resistance value measured after incubation with ascorbic acid and copper; $R_{ct(DNAzyme)}$ was the electron transfer resistance value measured after DNAzyme immobilization on the electrode, and $R_{ct(electrode-buffer)}$ was the electron transfer resistance of the blank electrode and buffer.

This journal is © The Royal Society of Chemistry 2013

Published on 04 February 2013 on http://pubs.rsc.org | doi:10.1039/C3AN36778A
Downloaded on 13 March 2013

Results and discussion

The analytical procedure for biosensing consists of the immobilization of the biotinylated DNAzyme onto the surface of the avidin modified GEC electrodes, followed by binding of copper ions to the –CTGGGCC– section of DNA. The reconstituted DNAzyme enhances the rate of ascorbic acid oxidation by oxygen. The accumulated oxidation products insulate the surface of Av–GEC electrodes, changing their interfacial properties, followed by electrochemical impedance spectroscopy (EIS) in the presence of the reversible redox couple $[Fe(CN)_6]^{3-}/[Fe(CN)_6]^{4-}$ as a marker as depicted in Fig. 1.

Optimization of electrode surface

First, the concentration of DNAzyme immobilized onto the Av–GEC electrode surface was optimized in order to achieve the maximum surface coverage. For this purpose, increasing concentrations of DNAzyme were used to carry out the immobilization, evaluating the changes in the Δ_p caused by the DNA layer. The curve of adsorption of DNAzyme on the electrode surface is shown on Fig. 2. It can be observed that the difference in resistance (Δ_p) asymptotically approaches its maximum value starting from 0.2 μM of DNAzyme concentration. This is due to the formation of a chemical bond between the biotin moiety of DNAzyme and avidin on the electrode surface, which followed a Langmuir isotherm. The concentration of DNAzyme equal to 0.2 μM was chosen as the optimal concentration.

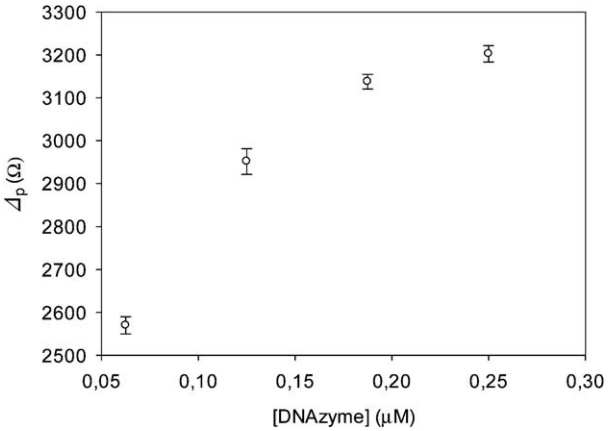

Fig. 2 Optimization of the concentration of DNAzyme placed onto the electrode. Uncertainty values corresponding to replicated experiments ($n = 5$).

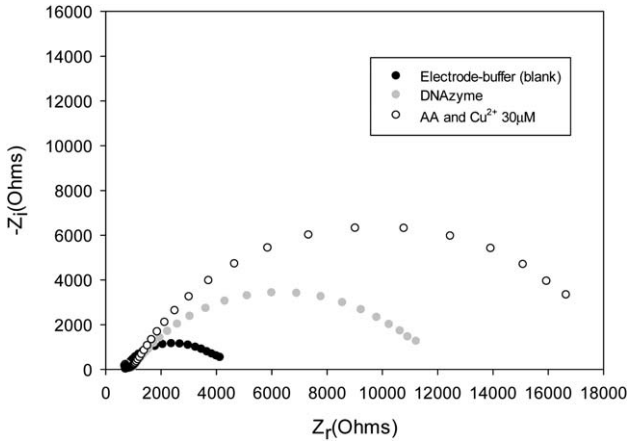

Fig. 3 Nyquist diagram of: (a) electrode–buffer ●, (b) DNAzyme, and (c) ascorbic acid and Cu^{2+} 30 μM.

Detection of Cu^{2+}

After the optimization of DNAzyme concentration, and following the above mentioned experimental protocol for the detection of copper, the biosensor response was initially evaluated. Cu^{2+} ions captured by the layer of DNAzyme significantly enhance the rate of ascorbic acid oxidation[41,42] in vicinity of the electrode, consequently the electrode surface is partially blocked due to the adsorption of oxidation products on it, resulting in an increase in the interfacial electron-transfer resistance. Representative Nyquist plots of DNAzyme in the absence and presence of Cu^{2+} are shown in Fig. 3. As can be seen, resistance R_{ct} between the electrode surface and the solution is increased. This fact is due to the effect of the kinetics of the electron transfer redox marker $[Fe(CN)_6]^{3-}/[Fe(CN)_6]^{4-}$ which is delayed at the interface of the electrode, mainly caused by steric hindrance and electrostatic repulsion presented by the oxidized products formed.

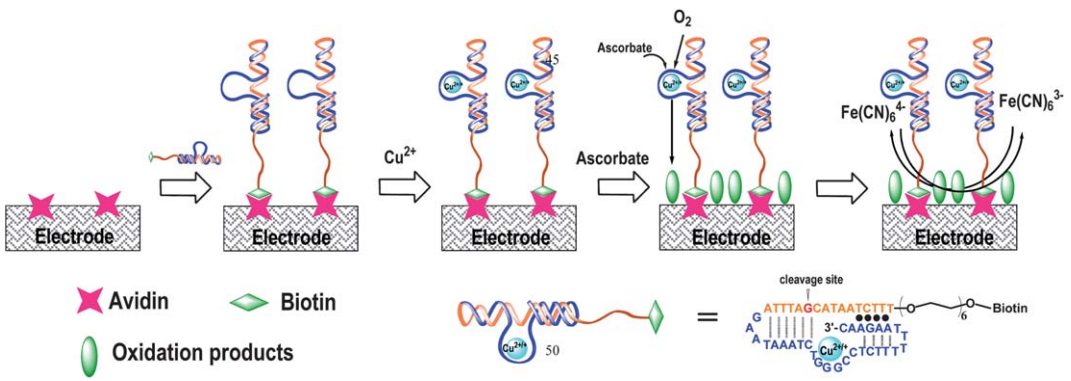

Fig. 1 Schematic illustration of an impedimetric DNAzyme sensor for Cu^{2+}.

Published on 04 February 2013 on http://pubs.rsc.org | doi:10.1039/C3AN36778A
Downloaded on 13 March 2013

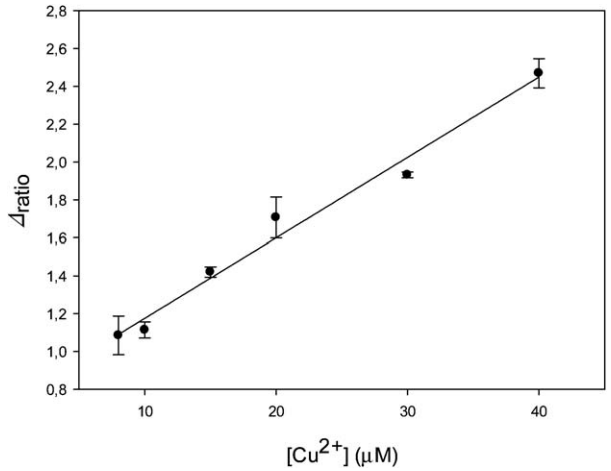

Fig. 4 Calibration curve, relative signal *versus* Cu^{2+} concentration. Uncertainty values corresponding to replicated experiments ($n = 5$).

Sensitivity of DNAzyme based sensor

To evaluate the sensitivity of the assay, new experiments with solutions containing different amounts of copper were performed and the calibration curve was built. Fig. 4 shows the evolution of the Δ_{ratio} relative signal, as extracted from the Nyquist diagrams, for the calibration of the copper sensor. To evaluate the linear range and detection limit of this DNAzyme-based copper sensor, the calibration curve was built, representing the analytical signal expressed as Δ_{ratio} *vs.* copper concentration (Fig. 4). As the copper concentration rises, the interfacial electron transfer resistance between the electrode surface and the solution also increases up to 40 μM of Cu^{2+}. As can be seen, a linear trend is obtained with a linear range from 10 μM to 40 μM for Cu^{2+}. From the least squares fitting, sensitivity appeared to be of 4×10^{-2} μM^{-1} and the detection limit of 6.5 μM. The repeatability of the method showed a relative standard deviation (%RSD) between 2 and 6%, obtained from a series of 5 replicates carried out for each standard in the linear range.

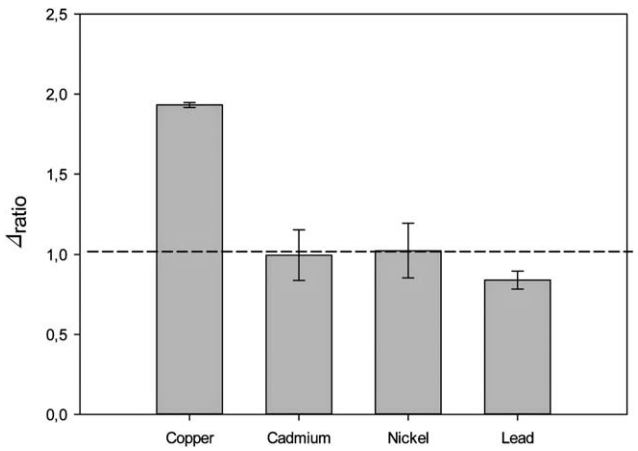

Fig. 5 Impedimetric response obtained with different metals assayed at the same concentration (30 μM). Uncertainty values corresponding to replicated experiments ($n = 5$).

Selectivity of DNAzyme based sensor

Next, the selectivity of the assay for the detection of Cu^{2+} over other divalent metal ions, frequently found together with copper, such as nickel, cadmium and lead was investigated. All concentrations tested were 30 μM. As can be seen from Fig. 5 only in the presence of copper, the primary species, does the biosensor give a significant response, so the interference with other metal ions can be considered negligible.

Conclusions

In conclusion, we have described a simple biosensor for the determination of copper(II) based on its DNAzyme immobilized by a strong non-covalent avidin–biotin interaction on the electrode surface. Upon reconstitution with Cu^{2+} this DNAzyme catalyzes oxidation of ascorbic acid with oxygen, leading to blocking of the electrode surface by the reaction products. The immobilization step, and the catalytic event inhibiting the electron-transfer kinetics of the redox probe at the electrode interface, can be monitored by labeless electrochemical impedance spectroscopy. The DNAzyme biosensor shows a linear response range of 10 μM to 40 μM Cu^{2+} and a detection limit of 6.5 μM. Interference to some related metals can be considered negligible. Advantages of the reported label-free method for Cu^{2+} detection over other conventional techniques are its simplicity and high selectivity.

Acknowledgements

This work was supported by the Spanish Ministry of Science and Innovation (projects BIO2011-26356 and CTQ2010-17099). V.P. acknowledges Ramon y Cajal contract from the Spanish Ministry of Science and Innovation. M.d.V. is supported by ICREA Academia program.

References

1 E. L. Que, D. W. Domaille and C. J. Chang, *Chem. Rev.*, 2008, **108**, 1517–1549.
2 P. G. Georgopoulos, A. Roy, M. Yonone-Lioy, R. Opiekun and P. Lioy, *J. Toxicol. Environ. Health, Part B*, 2001, **4**, 341–394.
3 United States Environmental Protection Agency Consumer Fact Sheet on Copper, http://water.epa.gov/drink/contaminants/basicinformation/historical/upload/Archived-Consumer-Fact-Sheet-on-Copper.pdf, C. i. d.-w. World Health Organization, 2004, and http://www.who.int/water_sanitation_health/dwq/chemicals/copper.pdf.
4 M.-S. Chan and S.-D. Huang, *Talanta*, 2000, **51**, 373–380.
5 A. P. S. Gonzáles, M. A. Firmino, C. S. Nomura, F. R. P. Rocha, P. V. Oliveira and I. Gaubeur, *Anal. Chim. Acta*, 2009, **636**, 198–204.
6 N. G. Beck, R. P. Franks and K. W. Bruland, *Anal. Chim. Acta*, 2002, **455**, 11–22.
7 J. Wu and E. A. Boyle, *Anal. Chem.*, 1997, **69**, 2464–2470.
8 J. Tanyanyiwa and P. Hauser, *Electrophoresis*, 2002, **23**, 3781–3786.

 This journal is © The Royal Society of Chemistry 2013

Published on 04 February 2013 on http://pubs.rsc.org | doi:10.1039/C3AN36778A
Downloaded on 13 March 2013

9 M. R. Ganjali, M. Emami and M. Salavati-Niasari, *Bull. Korean Chem. Soc.*, 2002, **23**, 1394–1398.
10 B. B. Petkovic, S. P. Sovilj, M. V. Budimir, R. M. Simonovic and V. M. Jovanovic, *Electroanalysis*, 2010, **22**, 1894–1900.
11 A. K. Singh, S. Mehtab and A. K. Jain, *Anal. Chim. Acta*, 2006, **575**, 25–31.
12 R. K. Mahajan and P. Sood, *Int. J. Electrochem. Sci.*, 2007, **2**, 832–847.
13 M. Etienne, J. Bessiere and A. Walcarius, *Sens. Actuators, B*, 2001, **76**, 531–538.
14 A. Mohadesi and M. A. Taher, *Talanta*, 2007, **72**, 95–100.
15 B. High, D. Bruce and M. M. Richter, *Anal. Chim. Acta*, 2001, **449**, 17–22.
16 S. Qiu, S. Gao, X. Zhu, Z. Lin, B. Qiu and G. Chen, *Analyst*, 2011, **136**, 1580–1585.
17 C.-L. He, F.-L. Ren, X.-B. Zhang, Y.-Y. Dong and Y. Zhao, *Anal. Sci.*, 2006, **22**, 1547–1551.
18 X.-L. Lv, Y. Wei and S.-Z. Luo, *Anal. Sci.*, 2012, **28**, 749–752.
19 H. S. Jung, P. S. Kwon, J. W. Lee, J. I. Kim, C. S. Hong, J. W. Kim, S. Yan, J. Y. Lee, J. H. Lee, T. Joo and J. S. Kim, *J. Am. Chem. Soc.*, 2009, **131**, 2008–2012.
20 Y. Xiang, A. Tong, P. Jin and Y. Ju, *Org. Lett.*, 2006, **8**, 2863–2866.
21 S. K. Silverman, *Org. Biomol. Chem.*, 2004, **2**, 2701–2706.
22 R. R. Breaker and G. F. Joyce, *Chem. Biol.*, 1994, **1**, 223–229.
23 R. R. Breaker and G. F. Joyce, *Chem. Biol.*, 1995, **2**, 655–660.
24 S. W. Santoro, G. F. Joyce, K. Sakthivel, S. Gramatikova and C. F. Barbas, *J. Am. Chem. Soc.*, 2000, **122**, 2433–2439.
25 S. H. J. Mei, Z. Liu, J. D. Brennan and Y. Li, *J. Am. Chem. Soc.*, 2003, **125**, 412–420.
26 J. Li, W. Zheng, A. H. Kwon and Y. Lu, *Nucleic Acids Res.*, 2000, **28**, 481–488.
27 V. Pavlov, Y. Xiao, R. Gill, A. Dishon, M. Kotler and I. Willner, *Anal. Chem.*, 2004, **76**, 2152–2156.
28 F. Wang, J. Elbaz and I. Willner, *J. Am. Chem. Soc.*, 2012, **134**, 5504–5507.
29 T. Lan, K. Furuyab and Y. Lu, *Chem. Commun.*, 2010, **46**, 3896–3898.
30 J. Liu, A. K. Brown, X. Meng, D. M. Cropek, J. D. Istok, D. B. Watson and Y. Lu, *Proc. Natl. Acad. Sci. U. S. A.*, 2007, **104**, 2056–2061.
31 Z. Wang, J. H. Lee and Y. Lu, *Chem. Commun.*, 2008, 6005–6007.
32 J. Liu and Y. Lu, *J. Am. Chem. Soc.*, 2007, **129**, 9838–9839.
33 M. Liu, H. Zhao, S. Chen, H. Yu, Y. Zhang and X. Quan, *Biosens. Bioelectron.*, 2011, **26**, 4111–4116.
34 Z. Fang, J. Huang, P. Lie, Z. Xiao, C. Ouyang, Q. Wu, Y. Wu, G. Liu and L. Zeng, *Chem. Commun.*, 2010, **46**, 9043–9045.
35 E. Zacco, M. I. Pividori and S. Alegret, *Biosens. Bioelectron.*, 2006, **21**, 1291–1301.
36 E. Katz and I. Willner, *Electroanalysis*, 2003, **15**, 913–947.
37 A. Merkoçi, M. Pumera, X. Llopis, B. Perez, M. del Valle and S. Alegret, *TrAC, Trends Anal. Chem.*, 2005, **24**, 341–349.
38 M. Pumera, M. Aldavert, C. Mills, A. Merkoçi and S. Alegret, *Electrochim. Acta*, 2005, **50**, 3702–3707.
39 A. Bonanni, M. J. Esplandiu, M. I. Pividori, S. Alegret and M. del Valle, *Anal. Bioanal. Chem.*, 2006, **385**, 1195–1201.
40 A. Bonanni, M. I. Pividori and M. del Valle, *Anal. Bioanal. Chem.*, 2007, **389**, 851–861.
41 N. Carmi, L. A. Shultz and R. R. Breaker, *Chem. Biol.*, 1996, **3**, 1039–1046.
42 N. Carmi, S. R. Balkhi and R. R. Breaker, *Proc. Natl. Acad. Sci. U. S. A.*, 1998, **95**, 2233–2237.

Article 8. Three different signal amplification strategies for the impedimetric detection of thrombin

C. Ocaña and M. del Valle

Biosensors and Bioelectronics (draft)

Three different signal amplification strategies for the impedimetric sandwich detection of thrombin

*Cristina Ocaña and Manel de Valle**

Sensors and Biosensors Group, Department of Chemistry, Universitat Autònoma de Barcelona, Edifici Cn, 08193 Bellaterra, Barcelona, SPAIN

Corresponding author:

Manel del Valle

Sensors and Biosensors Group

Universitat Autonoma de Barcelona,

Campus UAB, Edifici C, 08193 Bellaterra,

Spain

Telephone: +34 5813235

Fax: +24 5812477

Email: manel.delvalle@uab.cat

The total number of pages is (excluding this one): 15

Three different signal amplification strategies for the impedimetric sandwich detection of thrombin

*Cristina Ocaña and Manel de Valle**

Sensors and Biosensors Group, Department of Chemistry, Universitat Autònoma de Barcelona, Edifici Cn, 08193 Bellaterra, Barcelona, SPAIN

Abstract

In this work, we report a comparative study on three highly specific amplification strategies for the ultrasensitive detection of thrombin with the use of aptamer sandwich protocol. The protocol consisted on the use of a first thrombin aptamer immobilized on the electrode surface, the recognition of thrombin protein, and the reaction with a second biotinylated thrombin aptamer forming the sandwich. Through the exposed biotin end, three variants have been tested to amplify the electrochemical impedance signal. The strategies included (a) silver enhancement treatment, (b) gold enhancement treatment and (c) insoluble product produced by the combination of the enzyme horseradish peroxidase (HRP) and 3-amino-9-ethylcarbazole (AEC). The properties of the sensing surface were probed by electrochemical impedance measurements in the presence of the redox marker ferrocyanide/ferricyanide. Insoluble product strategy and silver enhancement treatment resulted in the lowest detection limit of the probe (0.3pM), while gold enhancement method resulted in highest reproducibility, 8.8% RSD at pM thrombin concentration levels. Results of silver and gold enhancement treatment also permitted direct inspection by scanning electron microscopy (SEM).

Keywords : impedance, nanoparticles, aptamer, biosensor, thrombin, amplification.

1.Introduction

Aptamers are single-stranded nucleic acid molecules that can bind with high affinity and specificity to a wide range of target molecules, such as drugs, proteins, or even whole cells (1,2). They are generated by an in vitro selection process called SELEX (3). This method allows the identification of a unique RNA/DNA molecules from very large population of random sequence oligomers, which bind to the target molecule with very

high affinity and specificity. They show dissociation constant typically from the micromolar to low picomolar range, comparable to those of some monoclonal antibodies (4). Not surprisingly, aptamers have found growing interest as active separation materials in chromatography (5), and electrophoresis (6), as therapeutic (7,8) or diagnostic agents, and as active materials for biosensing (9). The use of aptamers as biocomponents in biosensing, aptasensors, offers over classical affinity sensing methods mainly based on antibodies, a multitude of advantages, such as the possibility of easily regenerate the function of immobilized aptamers, their easy and homogenous preparation and the possibility of using them without labelling.

In aptasensor field, different transduction techniques can be used; optical(10), atomic force microscope(11), surface plasmon resonance(12), electrochemical(13,14) and piezoelectric(15). In the last years, among the different electrochemical techniques reported, the use of electrochemical impedance spectroscopy (EIS) has grown among these studies(16). EIS is a characterization technique which is very sensitive to changes of the interfacial properties of modified electrodes upon biorecognition events taking place at the electrode surfaces (17,18). Other important features presented by EIS are that it does not require any special reagent for the analysis, has the capacity for label-free detection and is a cost-efficient technique.

Nowadays, since many small target analytes are present at ultralow-levels, there are increasing demands for ultrasensitive detection. Nevertheless, it is sometimes difficult to obtain ultrasensitive detection of small targets. Thus, in order to carry out the sensitive detection, the exploration of novel amplification strategies is essential (19). Different amplification strategies have been used in biosensors, such as the use of gold nanoparticles (20,21), silver nanoparticles (22), enzymatic reactions (23,24), graphene (25), carbon nanotubes (26),…

In this work, we report a comparative study on three highly specific amplification strategies for the ultrasensitive detection of thrombin with the use of aptamer sandwich protocol. The strategies included (a) silver enhancement treatment, (b) gold enhancement treatment and (c) insoluble product produced by the combination of the enzyme horseradish peroxidase (HRP) and 3-amino-9-ethylcarbazole (AEC).The protocol consisted on the use of a first thrombin aptamer immobilized on the electrode surface, the recognition of thrombin protein, and the reaction with a second biotinylated thrombin

aptamer forming the sandwich. Through the exposed biotin end, the three variants have been tested to amplify the electrochemical impedance signal.

2. Experimental

2.1. Chemicals

Potassium dihydrogen phosphate, potassium ferricyanide $K_3[Fe(CN)_6]$, potassium ferrocyanide $K_4[Fe(CN)_6]$, sodium monophosphate, streptavidin gold nanoparticles, avidin horseradish peroxidase (Av-HRP), 3-amino-9-ethylcarbazole, 655nm streptavidin quantum dots (strep-QDs), avidin and the target protein thrombin (Thr), were purchased from Sigma (St. Louis, MO, USA). Poly(ethylene glycol) 1000 (PEG), sodium chloride and potassium chloride were purchased from Fluka (Buchs, Switzerland). LI silver enhancement kit was obtained from Nanoprobes (Yaphank, New York). All-solid-state electrodes (AvGECs) were prepared using 50 μm particle size graphite powder (Merck, Darmstadt, Germany), Epotek H 77 resin and its corresponding hardener (both from Epoxy Technology, Billerica, MA, USA), and avidin. All reagents were analytical reagent grade. Aptamers used in this study were purchased by Sigma Aldrich (St. Louis, MO, USA). Stock solutions of aptamers were diluted with sterilized and deionised water, separated into fractions and stored at −20 °C until required. Their base sequences were:

- AptThrBio1: 5'-GGTTGGTGTGGTTGG-Biotin-3'
- AptThrBio2: 5'-Biotin-AGTCCGTGGTAGGGCAGGTTGGGGTGACT-3'
- AptCytc:5'-Biotin-AGTGTGAAATATCTAAACTAAATGTGGAGGGTGGGACGGGAAGAAGTTTATTTTTCACACT-3’

All solutions were made up using Milli-Q water from Milli-Q System (Millipore, Billerica, MA, USA). The buffers employed were: PBS (187 mM NaCl, 2.7 mM KCl, 8.1 mM $Na_2HPO_4 \cdot 2H_2O$, 1.76 mM KH_2PO_4, pH 7.0), acetate buffer 0.5M (pH 5.5), 10nM PBS without NaCl and KCl.

2.2. Apparatus

AC impedance measurements were performed with the aid of an Autolab PGStat 20 (Metrohm Autolab B.V, Utrecht, The Netherlands). FRA (Metrohm Autolab) software was used for data acquisition and control of the experiments. A three electrode

configuration was used to perform the impedance: a platinum-ring auxiliary electrode (Crison 52–67 1, Barcelona, Spain), a Ag/AgCl reference electrode and the constructed AvGEC as the working electrode. A scanning electron microscope (SEM) (Merlin, Zeiss, Germany) was used to visualize silver and gold enhanced strep-AuNPs on electrode surface. Temperature-controlled incubations were done using an Eppendorf Thermomixer 5436.

2.3. Construction of working electrodes

The electrodes were prepared using a PVC tube body (6 mm i.d.) and a small copper disk soldered to the end of an electrical connector. The conductive part of AvGECs was an avidin epoxy graphite conductive paste, formed from graphite (18%), avidin (2%) and epoxy resin (80%), which was deposited into the cavity in the plastic body, filling it (27). The composite material was cured in an oven at 40 °C for 7 days. Before each use, the electrode surface was moistened with Milli-Q water and then thoroughly smoothed with abrasive sandpaper and finally with alumina paper (polishing strips 301044-001, Orion) in order to obtain a reproducible electrochemical surface (28,29).

2.4. Protein capture and amplification protocols

The scheme of experimental protocols for thrombin analysis, described in detail below, is represented in Fig. 1.

2.4.1. Aptamer immobilization

The first step consists of aptamer AptThrBio1 immobilization on the electrode surface. A volume of 160 µL of MilliQ water containing 35pmols of aptamer solution was heated to 80–90 °C for 3 minutes in order to promote the loose conformation of the aptamer. Then, the solution was dipped in a bath of cold water and the electrode was immersed in it, where the avidin-biotin affinity interaction took place for 15 minutes at the electrode surface. This was followed by two washing steps using PBS buffer solution for 10 minutes, in order to remove any unadsorbed aptamer.

2.4.2. Blocking step

To avoid any possible nonspecific adsorption, the electrodes were dipped in 160 µL of PEG 40 mM. This was followed by two washing steps using PBS buffer solution for 10 minutes.

2.4.3. Thrombin detection

The electrodes were dipped in a solution with the desired concentration of Thr. The incubation took place for 15 minutes. Then, the biosensors were washed twice with PBS buffer solution for 10 minutes.

2.4.4. Sandwich formation

In order to obtain the aptamer sandwich formation, the electrodes were dipped in 160 µl of PBS solution containing 12pmols of AptThrBio2. The incubation took place for 15 minutes. This was followed by two washing steps using PBS buffer solution for 10 minutes.

2.4.5 Amplification Protocols

Three different variants were used;

Silver enhancement treatment(30)

AvGEC electrodes modified with the sandwich complex were incubated in 160 µL of strep-AuNPs, from a 1/100 dilution of the stock solution in PBS buffer. The tube was incubated at 25ºC with gentle stirring for 20 minutes. This step was followed by two gentle washing steps in PBS buffer for 10 minutes at 25 ºC. Negative controls were performed for the strep-AuNPs addition step using AptCytc as aptamer without affinity.

20 µl of a solution obtained by the combination of 10 µl of enhancer and 10 µl of initiator were deposited onto the electrode surface and left for 7 minutes to facilitate the reaction. Silver enhancement occurs during the catalytic reduction of silver from one solution (e.g. the enhancer) by another (e.g. the initiator) in the presence of gold nanoparticles. The reduction reaction causes silver to build up on the surface of the gold nanoparticles. After this catalytic silver reduction, the electrodes were thoroughly washed with deionized water to stop the reaction. The silver enhancing solution was prepared immediately before each use. For silver enhancement treatment, the negative control used was a non-biotinylated AptCytc as aptamer without affinity.

153 *Gold enhancement treatment*

154 AvGEC electrodes modified with the sandwich complex were incubated in 160 µL of
155 strep-AuNPs, from a 1/100 dilution of the stock solution in PBS buffer. The tube was
156 incubated at 25ºC with gentle stirring for 20 minutes. This step was followed by two
157 gentle washing steps in PBS buffer for 10 minutes at 25 ºC. Negative controls were
158 performed for the strep-AuNPs addition step using AptCytc as aptamer without affinity.

159 The modified electrodes modified with sandwich and strep-AuNPs were immersed in a
160 solution containing a mixture of 0.01% $HAuCl_4$ and 0.4 mM $NH_2OH{\cdot}HCl$ (pH 6.0) for 2
161 min at 25ºC, rinsed, and then treated for 2 additional min. In order to prevent the non-
162 specific background of fine gold particles, the electrodes were rinsed with a solution of
163 0.6 M triethylammonium bicarbonate buffer after each amplification. Solutions were
164 freshly prepared in a lightproof container before each use.

165 *Insoluble product treatment*

166 AvGEC electrodes modified with the sandwich complex were incubated in 160 µL of av-
167 HRP, from a 1/500 dilution of the stock solution in PBS buffer, during 30 minutes with
168 gentle stirring. This step was followed by two gentle washing steps in PBS buffer for 10
169 minutes at 25ºC.

170 10 mg of AEC were dissolved in 1mL of DMF (yellow color). Then, 66 µL of the previous
171 solution were mixed in 2mL of acetate buffer 0.5M (pH 5.5). After that, 66 µL of H_2O_2
172 0.3% was added to the previous solution. Finally, 20 µL of this solution were deposited
173 onto the electrode surface for 15 minutes, a red product were deposited onto the electrode
174 surface, Figure 2. This step was followed by twice washing steps with distillated water.

175 Different selectivity experiments carried out were performed with the same protocol
176 unless where specified.

177 All incubations were carried out at controlled temperature in the thermomixer.

178

179

180

2.5. Impedimetric detection

Impedance experiments were carried out at an applied potential of 0.17V (vs. Ag/AgCl reference electrode), with a range of frequency of 50KHz-0.05Hz, an AC amplitude of 10 mV and a sampling rate of 10 points per decade above 66 Hz and 5 points per decade at the lower range. All measurements were performed in PBS buffer containing 0.01M $K_3[Fe(CN)_6]/K_4[Fe(CN)_6]$ (1:1) mixture, used as a redox marker. The impedance spectra were plotted in the form of complex plane diagrams (Nyquist plots, $-Z_{im}$ *vs.* Z_{re}) and fitted to a theoretical curve corresponding to the equivalent circuit with Z_{view} software (Scribner Associates Inc., USA).

3. Results

The modification of the electrodes surface with the sandwich formation as well as the three different amplification strategies were studied by electrochemical impedance spectroscopy using a solution of $K_3[Fe(CN)_6]/ K_4[Fe(CN)_6]$ as a redox marker in the bulk solution.

A typical spectrums obtained in these experiments are shown in Figure 3. The equivalent circuit was formed by one resistor/ capacitor element in series with a resistance. In it, the resistance in series with the capacitor element, R_s, corresponds to the resistance of the solution, the resistance in parallel with the capacitor element, Rct, is the charge transfer resistance between the solution and the electrode surface, whilst the capacitor element is the constant phase element (CPE) associated with the double-layer capacitance. The use of a CPE instead of a capacitor is required to optimize the fit to the experimental data, and this is due to the nonideal nature of the electrode surface. For all performed fittings, the chi-square goodness-of-fit test was thoroughly checked to verify calculations. In all cases, calculated values for each circuit remained in the range of 0.0003-0.15 much lower than the tabulated value for 50 degrees of freedom (67.505 at 95% confidence level). Thus demonstrating the high significance of the final fits.

The parameter of interest in our case is represented by the change transfer resistance Rct. This value in the spectrum corresponds to the diameter of the semicircle. In order to compare the results obtained from the different electrodes used, and to obtain independent

and reproducible results, a relative transformation of signals was needed (31). Thus, the Δ_{ratio} value was defined according to the following equations:

$$\Delta_{ratio} = \Delta_s / \Delta_p$$

$$\Delta_s = Rct_{(AptThrBio1\text{-}Thr/AptThrBio2/strep\text{-}AuNPs\ or\ Av\text{-}HRP/silver\ enhance.\ or\ gold\ enhance.\ or\ insoluble\ product)} - Rct_{(electrode\text{-}buffer)}$$

$$\Delta_p = Rct_{(AptThrBio1)} - Rct_{(electrode\text{-}buffer)}$$

where $Rct_{(AptThrBio1\text{-}Thr/AptThrBio2/strep\text{-}AuNPs\ or\ Av\text{-}HRP/silver\ enhance.\ or\ gold\ enhance.\ or\ insoluble\ product)}$ was the electron transfer resistance value measured after thrombin incubation, sandwich formation and different signal amplification methods; $Rct_{(AptThrBio1)}$ was the electron transfer resistance value measured after aptamer immobilization on the electrode, and $Rct_{(electrode\text{-}buffer)}$ was the electron transfer resistance of the blank electrode and buffer.

As can be seen in Fig. 3, the Rct value increased after each biosensing step. This change was due to the inhibition of the electrochemical reaction of the redox marker at the electrode surface, caused by the presence of blocking layers. Two different factors should be taken into account to properly explain this effect: electrostatic repulsion and sterical hindrance. The former is more significant in the first step of protocol; when the AptThrBio1 is immobilized onto the electrode surface by avidin–biotin affinity, a first layer is formed, where negatively charged phosphate groups of aptamer skeleton are responsible of the electrostatic repulsion of the negatively charged redox marker, thus inhibiting the interfacial transfer process and resulting in Rct increment. The addition of Thr and a second ApThrBio2 to form a sandwich complex results in a further increment of Rct due to the increased quantity of negative charge and the hindrance caused by the formation of a double layer. In Fig. 3a) and b), after the addition of strep-AuNPs an increment of Rct value was observed because of the increased space resistance due to gold streptavidin conjugates. In addition, working at pH 7, streptavidin is slightly negatively charged (pI is around pH 5) and this fact also contributes to enhancement of impedance (32). In the second amplification step, silver or gold enhancement treatment (33,34), a significant increments of Rct values were also observed and attributable to the silver or gold deposition on gold. In the case of silver treatment the increment of Rct is higher than the gold enhancement obtained due to the fact that silver deposition mechanism is faster than gold deposition mechanism.

As can be seen in Fig 3c), after the addition of av-HRP in insoluble product strategy, an increment of Rct was produced due to the sterical hindrance because of the size of the enzyme. In the enzymatic reaction step, Rct showed a higher significant increase which indicates that the precipitation has a big effect on the charge transfer reaction.

Detection of thrombin: comparison between three different amplification strategies

The aim of these experiments was to study and compare the best amplification techniques using a sandwich protocol. All steps of these experiments have been optimized separately (data not shown). The obtained calibration curves are represented in Fig. 4. As can be seen in this figure, all calibration curves increased until the value of 100pM of Thr, this could be due to the fact that concentrations larger than 100pM cause a saturation on the electrode surface.

The first amplification method used was silver enhancement treatment. This well-known method is based on the deposition of silver after the addition of strep-AuNP in the sandwich aptamer modified electrode. This strategy presented high sensitivity and reproducibility.

Secondly, the amplification method used was gold enhancement treatment. This method is based on the same protocol which have just explained before, in this case with gold deposition. This protocol showed high reproducibility and sensitivity.

Finally, the last amplification strategy used was insoluble product treatment. This method is focused on the production of an insoluble product by an enzymatic reaction. These reagents are converted to water and insoluble product, which precipitate and cause a blocking of the electrode surface, producing a high increment of Rct. This strategy presented high sensitivity and low detection limit.

All numerical results are represented in Table 1. The highest sensitivity was attained using insoluble product reaction due to the fast blocking of the electrode surface, while showed the lowest reproducibility value. In addition, this method beside silver enhancement treatment showed the lowest detection limit of the target analyte, 0.3pM, demonstrating that these methods presented ultrahigh sensitivity for the detection of thrombin. Moreover, a signal increment of up to 189 % between simple biosensing and insoluble product strategy was observed. However, gold enhancement treatment showed the best reproducibility value, 8.8 %RSD. This confirm that silver enhancement and insoluble

product strategies may reach a low detection limit and ultrahigh sensitivity for thrombin detection.

Scanning Electron Microscope characterization

In order to confirm the presence and distribution of gold nanoparticles onto the electrode surface with silver and gold enhancement treatment, SEM images were taken. These experiments also provided an image of the homogeneity and accessibility of the anchorage points supplied by the avidin entrapped in the biocomposite. SEM images taken at an acceleration voltage of 3 kV are shown in Figure 6. Figure 6 a.1) and a.2) showed positive and negative control with the use of silver enhancement method, while Figure 6 b. 1) and 6 b. 2) showed positive and negative controls of gold enhancement treatment. As can be seen, both positive controls showed a quite homogeneous distribution of the nanoparticles. That fact also implies a regular distribution of avidin molecules in the biocomposite and a well-organized formation of aptamer sandwich onto the electrode surface. While silver enhancement treatment showed monocrystalline particles, gold enhancement treatment showed sphere nanoparticles, this could be due to the fact that silver crystallized in specific directions thanks to the disposition of the streptavidin around of gold nanoparticles. Comparing these experiments with their respectives negative controls that did not use the biotinylated complementary target aptamer, a surface without nanoparticles can be observed.

Selectivity of the aptamer sandwich protocol

Selectivity of each amplify strategy was examined by challenging thrombin with different possible interfering proteins. Prothrombin, IgG, fibrinogen, BSA and cytochrome c were employed to investigate the specificity of the three methods for the detection of thrombin. As shown in Figure 7, it is observed that incubation with these proteins produced negligible response compared with 75pM Thr even at concentration four or five orders of magnitude higher than typical Thr concentration, demonstrating that the three signal amplification methods possessed sufficient specificity to thrombin detection.

4. Conclusion

In current study, three different signal amplification strategies were studied and compared for the ultrasensitive impedance detection of thrombin (silver enhancement treatment, gold enhancement treatment and insoluble product reaction produced by the combination of HRP and AEC).

With the different strategies reported, low detection limits in the pM level, ample range of responses for thrombin concentration and low %RSD values were achieved. Among the three methods proposed, insoluble product reaction and silver enhancement treatment were the best overall methods displaying low detection limits, 0.3pM, and high affinities with a sensitivity values of $6.99 \cdot 10^{-14}$ M^{-1} and $2.19 \cdot 10^{-14}$ M^{-1} respectively. In addition, whole methods showed high selectivity values. The silver and god enhancement treatment also permitted to visualize the gold nanoparticles on the electrode surface with SEM. This allowed confirming the proposed steps of the protocol and a homogeneous distribution of biosensing sites on the electrodes.

Reference

1. Jayasena, S. D. (1999) Aptamers: An emerging class of molecules that rival antibodies in diagnostics. *Clinical Chemistry* **45**, 22
2. Patel, D. J., and Suri, A. K. (2000) Structure, recognition and discrimination in RNA aptamer complexes with cofactors, amino acids, drugs and aminoglycoside antibiotics. *Reviews in Molecular Biotechnology* **74**, 39-60
3. Ellington, A. D., and Szostak, J. W. (1990) In vitro selection of RNA molecules that bind specific ligands. *Nature* **346**, 818-822
4. Jenison, R. D., Gill, S. C., Pardi, A., and Polisky, B. (1994) High-Resolution molecular discrimination by RNA. *Science* **263**, 1425-1429
5. Kotia, R. B., Li, L., and McGown, L. B. (2000) Separation of Nontarget Compounds by DNA Aptamers. *Analytical Chemistry* **72**, 827-831
6. Clark, S. L., and Remcho, V. T. (2002) Aptamers as analytical reagents. *Electrophoresis* **23**, 1335-1340
7. Biesecker, G., Dihel, L., Enney, K., and Bendele, R. A. (1999) Derivation of RNA aptamer inhibitors of human complement C5. *Immunopharmacology* **42**, 219-230
8. Hicke, B. J., Marion, C., Chang, Y. F., Gould, T., Lynott, C. K., Parma, D., Schmidt, P. G., and Warren, S. (2001) Tenascin-C aptamers are generated using tumor cells and purified protein. *Journal of Biological Chemistry* **276**, 48644-48654
9. Evtugyn, G. A., Kostyleva, V. B., Porfireva, A. V., Savelieva, M. A., Evtugyn, V. G., Sitdikov, R. R., Stoikov, I. I., Antipin, I. S., and Hianik, T. (2012) Label-free aptasensor for thrombin determination based on the nanostructured phenazine mediator. *Talanta* **102**, 156-163

10. Lee, M., and Walt, D. R. (2000) A fiber-optic microarray biosensor using aptamers as receptors. *Analytical Biochemistry* **282**, 142-146
11. Basnar, B., Elnathan, R., and Willner, I. (2006) Following aptamer-thrombin binding by force measurements. *Analytical Chemistry* **78**, 3638-3642
12. Vasilescu, A., Gaspar, S., Mihai, I., Tache, A., and Litescu, S. C. (2013) Development of a label-free aptasensor for monitoring the self-association of lysozyme. *Analyst* **138**, 3530-3537
13. Radi, A., Acero Sánchez, J. L., Baldrich, E., and O'Sullivan, C. K. (2005) Reusable Impedimetric Aptasensor. *Anal. Chem.* **77**, 6320-6323
14. Ocaña, C., Pacios, M., and del Valle, M. (2012) A Reusable Impedimetric Aptasensor for Detection of Thrombin Employing a Graphite-Epoxy Composite Electrode. *Sensors* **12**, 3037-3048
15. Srijanto, B. R., Cheney, C. P., Hedden, D. L., Gehl, A. C., Crilly, P. B., Huestis, M. A., and Ferrell, T. L. (2012) Piezoresistive Microcantilevers-Based Cocaine Biosensors. *Sensor Letters* **10**, 850-855
16. McDonald, J. R. (1987) *Impedance Spectroscopy*, John Wiley, New York
17. Bardea, A., Patolsky, F., Dagan, A., and Willner, I. (1999) Sensing and amplification of oligonucleotide-DNA interactions by means of impedance spectroscopy: a route to a Tay-Sachs sensor. *Chem. Comm.*, 21-22
18. Loo, A. H., Bonanni, A., Ambrosi, A., Poh, H. L., and Pumera, M. (2012) Impedimetric immunoglobulin G immunosensor based on chemically modified graphenes. *Nanoscale* **4**, 921-925
19. Bonanni, A., and del Valle, M. (2010) Use of nanomaterials for impedimetric DNA sensors: A review. *Anal. Chim. Acta* **678**, 7-17
20. Yuan, J., Wu, S., Duan, N., Ma, X., Xia, Y., Chen, J., Ding, Z., and Wang, Z. (2014) A sensitive gold nanoparticle-based colorimetric aptasensor for Staphylococcus aureus. *Talanta* **127**, 163-168
21. Bonanni, A., Esplandiu, M. J., and del Valle, M. (2008) Signal amplification for impedimetric genosensing using gold-streptavidin nanoparticles. *Electrochim. Acta* **53**, 4022-4029
22. Song, W., Li, H., Liang, H., Qiang, W., and Xu, D. (2014) Disposable electrochemical aptasensor array by using in situ DNA hybridization inducing silver nanoparticles aggregate for signal amplification. *Analytical Chemistry* **86**, 2775-2783
23. Zheng, Y., Chai, Y., Yuan, Y., and Yuan, R. (2014) A pseudo triple-enzyme electrochemical aptasensor based on the amplification of Pt–Pd nanowires and hemin/G-quadruplex. *Analytica Chimica Acta* **834**, 45-50
24. Kaatz, M., Schulze, H., Ciani, I., Lisdat, F., Mount, A. R., and Bachmann, T. T. (2012) Alkaline phosphatase enzymatic signal amplification for fast, sensitive impedimetric DNA detection. *Analyst* **137**, 59-63
25. Bai, L., Chai, Y., Pu, X., and Yuan, R. (2014) A signal-on electrochemical aptasensor for ultrasensitive detection of endotoxin using three-way DNA junction-aided enzymatic recycling and graphene nanohybrid for amplification. *Nanoscale* **6**, 2902-2908
26. Zhang, J., Chai, Y., Yuan, R., Yuan, Y., Bai, L., and Xie, S. (2013) A highly sensitive electrochemical aptasensor for thrombin detection using functionalized mesoporous silica@multiwalled carbon nanotubes as signal tags and DNAzyme signal amplification. *Analyst* **138**, 6938-6945
27. Bonanni, A., Pividori, M. I., and del Valle, M. (2007) Application of the avidin-biotin interaction to immobilize DNA in the development of electrochemical impedance genosensors. *Anal. Bioanal. Chem.* **389**, 851-861
28. Williams, E., Pividori, M. I., Merkoçi, A., Forster, R. J., and Alegret, S. (2003) Rapid electrochemical genosensor assay using a streptavidin carbon-polymer biocomposite electrode. *Biosens. Bioelectron.* **19**, 165-175

29. Lermo, A., Campoy, S., Barbé, J., Hernández, S., Alegret, S., and Pividori, M. I. (2007) In situ DNA amplification with magnetic primers for the electrochemical detection of food pathogens. *Biosensors and Bioelectronics* **22**, 2010-2017
30. Ocaña, C., and Del Valle, M. (2014) Signal amplification for thrombin impedimetric aptasensor: Sandwich protocol and use of gold-streptavidin nanoparticles. *Biosensors and Bioelectronics* **54**, 408-414
31. Bonanni, A., Esplandiu, M. J., Pividori, M. I., Alegret, S., and del Valle, M. (2006) Impedimetric genosensors for the detection of DNA hybridization. *Anal. Bioanal. Chem.* **385**, 1195-1201
32. Sivasankar, S., Subramaniam, S., and Leckband, D. (1998) Direct molecular level measurements of the electrostatic properties of a protein surface. *Proceedings of the National Academy of Sciences* **95**, 12961-12966
33. Cai, H., Wang, Y. Q., He, P. G., and Fang, Y. H. (2002) Electrochemical detection of DNA hybridization based on silver-enhanced gold nanoparticle label. *Analytica Chimica Acta* **469**, 165-172
34. Hanaee, H., Ghourchian, H., and Ziaee, A. A. (2007) Nanoparticle-based electrochemical detection of hepatitis B virus using stripping chronopotentiometry. *Analytical Biochemistry* **370**, 195-200

Tables

Table 1. Calibration results of the three amplification methods.

Amplification strategy	Sensitivity (M^{-1})	*RSD (%)	Detection limit (pM)	Amplification factor %	Linear Range (pM)
Silver enhancement	$2.19 \cdot 10^{-14}$	9.9	0.30	89	0.1-100
Gold enhancement	$2.02 \cdot 10^{-14}$	8.8	0.45	80	0.1-100
Insoluble product reaction	$6.99 \cdot 10^{-14}$	11	0.30	189	0.1-100

* Corresponding to five replicate experiments at 75pM thrombin.

Figure Captions

Figure 1. Scheme of the experimental procedures of the three amplification strategies.

Figure 2. Insoluble product reaction.

Figure 3. Nyquist diagrams of: a) silver enhancement treatment, b) gold enhancement treatment and c) insoluble product reaction.● bare AvGEC electrode, ○ biotinylated aptamer of thrombin 1, ▼ biotinylated aptamer of thrombin and thrombin protein, Δ sandwich complex, ■ sandwich complex modified with strep-AuNPs or av-HRP , □ sandwich complex modified with strep-AuNPs and silver enhancement treatment or modified with av-HRP and insoluble reaction. All experiments were performed in PBS solution and all EIS measurements were performed in PBS solution containing 0.01M $K_3[Fe(CN)_6]/K_4[Fe(CN)_6]$.

Figure 4. Regression curves of: a) silver enhancement treatment, b) gold enhancement treatment and c) insoluble product reaction. (1) (black circle) biotinylated aptamer of thrombin 1, (2) (white circle) sandwich complex, (3) (black triangle) sandwich complex modified with strep-AuNPs or av-HRP, (4) (white triangle) sandwich complex modified with strep-AuNPs and silver enhancement treatment. All experiments were performed in PBS solution and all EIS measurements were performed in PBS solution containing 0.01M $K_3[Fe(CN)_6]/K_4[Fe(CN)_6]$. Uncertainty values corresponding to replicated experiments (n = 5).

Figure 5. SEM images of: a.1) experiment using biotinylated aptamer of thrombin 1 + thrombin + biotinylated aptamer of thrombin 2 + strep-AuNPs + silver enhancement treatment, a.2) experiment using biotinylated aptamer of thrombin 1 + thrombin + biotinylated aptamer of cytochrome c + strep-AuNPs + silver enhancement treatment, b.1) experiment using biotinylated aptamer of thrombin 1 + thrombin + biotinylated aptamer of thrombin 2 + strep-AuNPs + gold enhancement treatment and b.2) experiment using biotinylated aptamer of thrombin 1 + thrombin + biotinylated aptamer of cytochrome c + strep-AuNPs + gold enhancement treatment. SEM images were taken at a acceleration voltage of 3 KV and a resolution of 2 μm.

Figure 6. 3D bar chart of the three amplifications methods response towards different proteins present in serum. Uncertainty values corresponding to replicated experiments (n = 5).

Fig.1

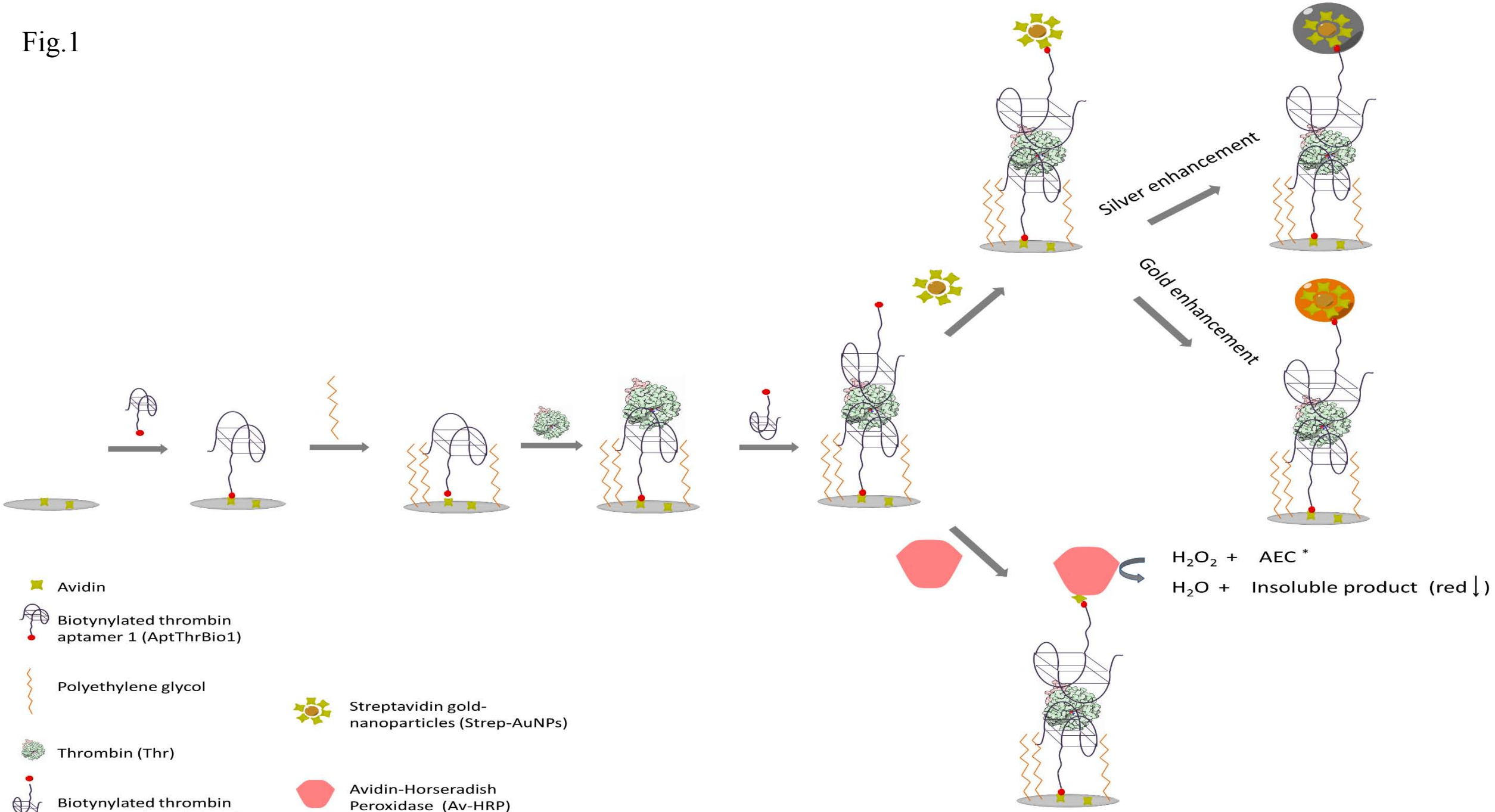
Silver enhancement
Gold enhancement
H_2O_2 + AEC *
H_2O + Insoluble product (red ↓)
Avidin
Biotynylated thrombin aptamer 1 (AptThrBio1)
Polyethylene glycol
Thrombin (Thr)
Biotynylated thrombin aptamer 2 (AptThrbio2)
Streptavidin gold-nanoparticles (Strep-AuNPs)
Avidin-Horseradish Peroxidase (Av-HRP)
AEC 3-amino-9-ethylcarbazole

Fig.2

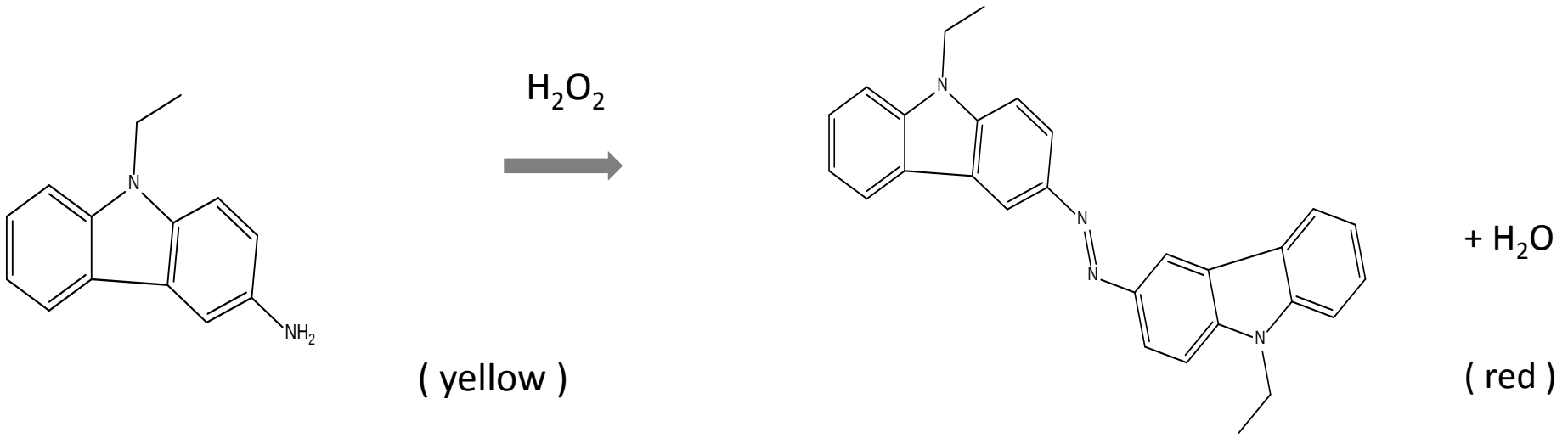

(yellow)

(red)

3-amino-9-ethylcarbazole (AEC)

Fig.3

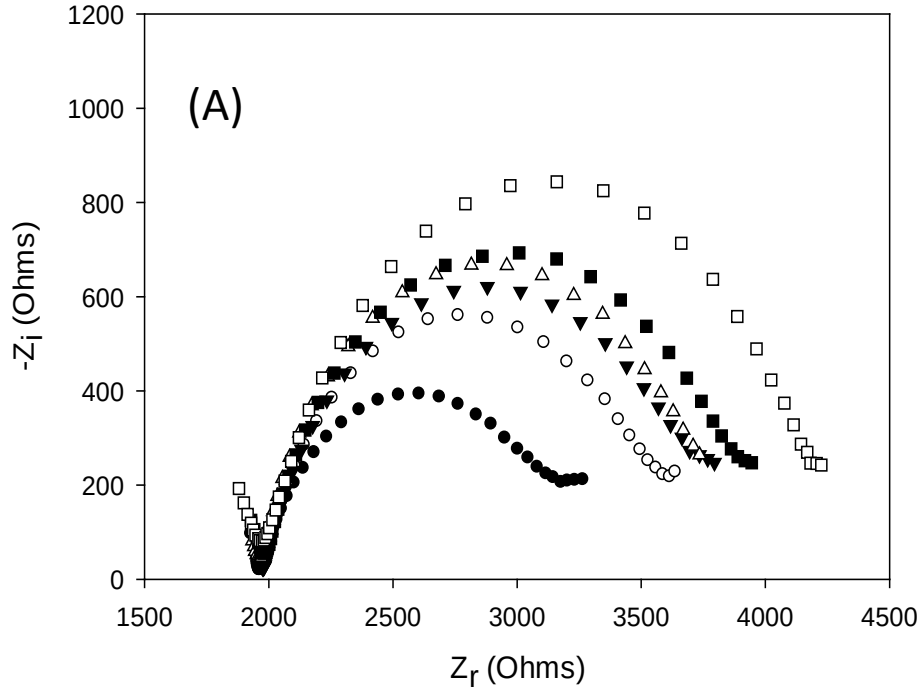
(A)
-Zi (Ohms)
Zr (Ohms)
0
200
400
600
800
1000
1200
1500
2000
2500
3000
3500
4000
4500

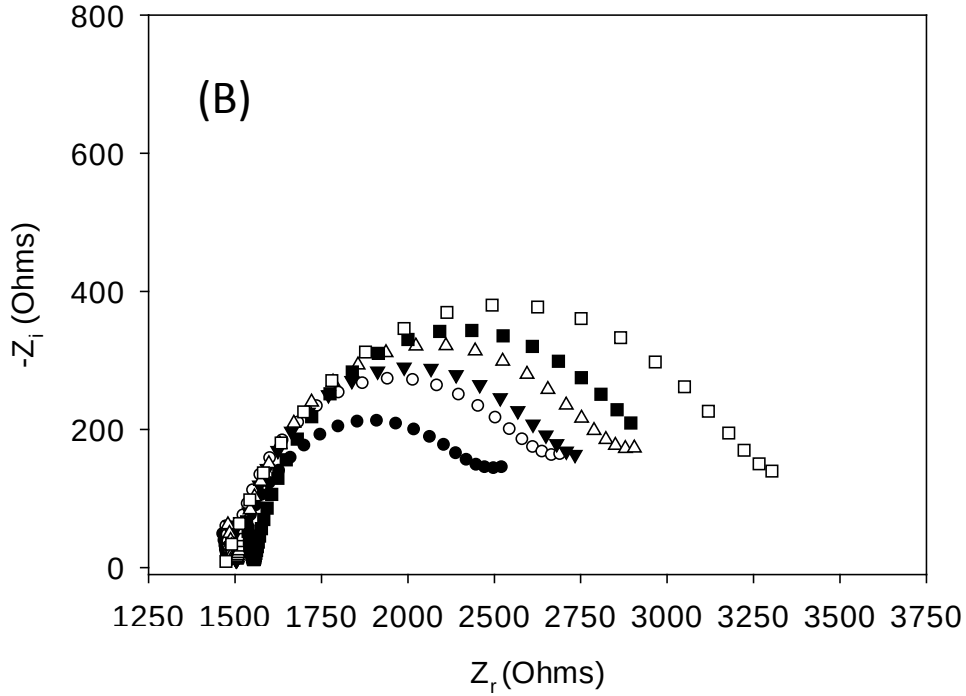
(B)
-Zi (Ohms)
Zr (Ohms)
0
200
400
600
800
1250
1500
1750
2000
2500
2750
3000
3250
3500
3750

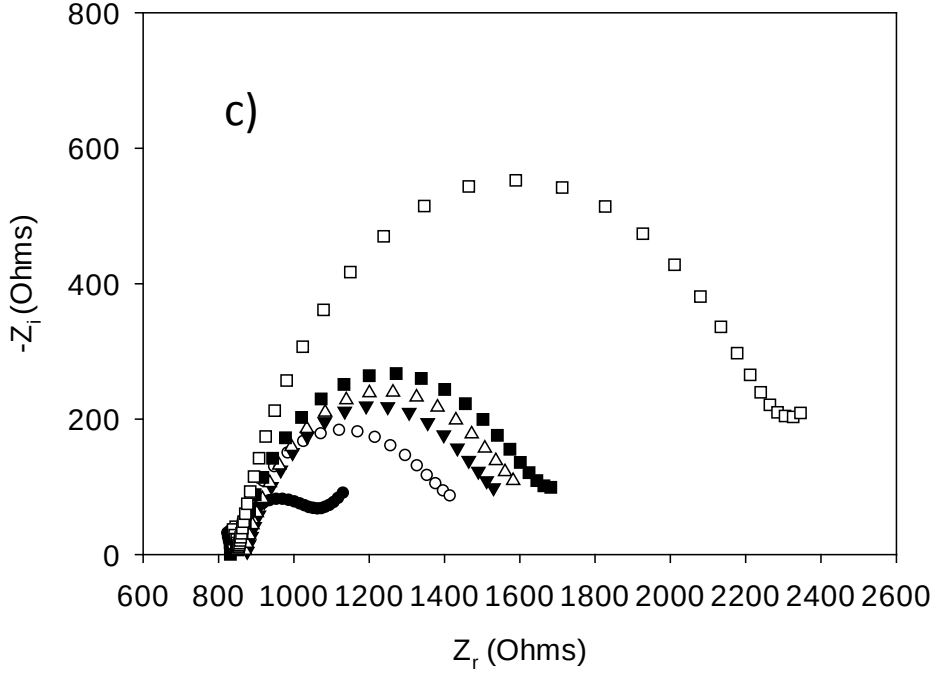
c)
-Zi (Ohms)
Zr (Ohms)
0
200
400
600
800
600
800
1000
1200
1400
1600
1800
2000
2200
2400
2600

Fig.4

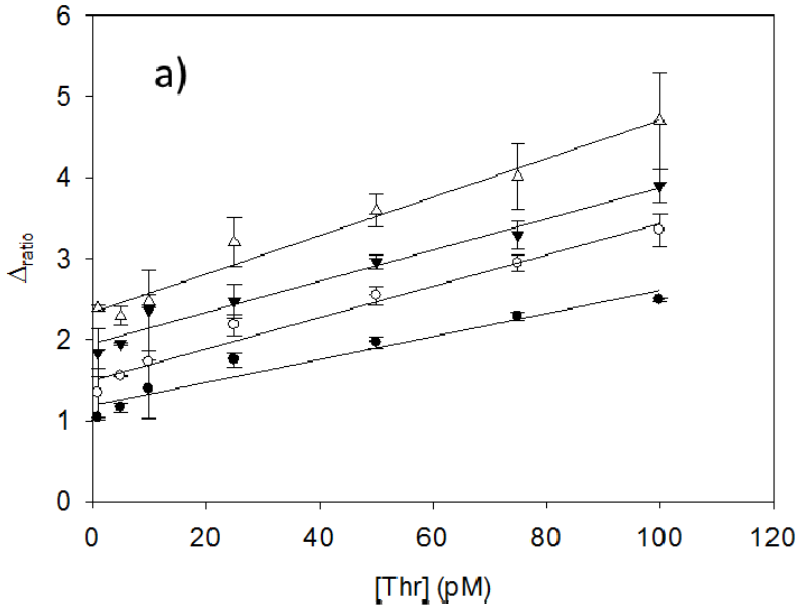

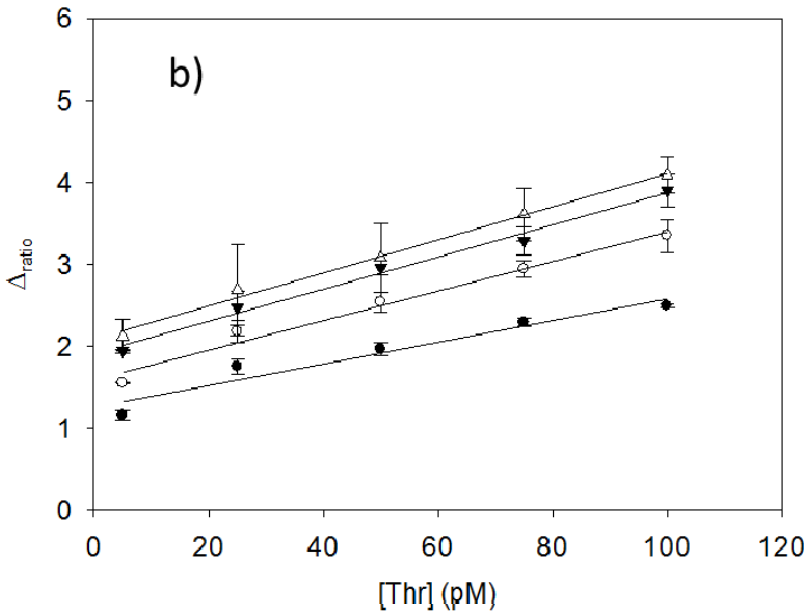

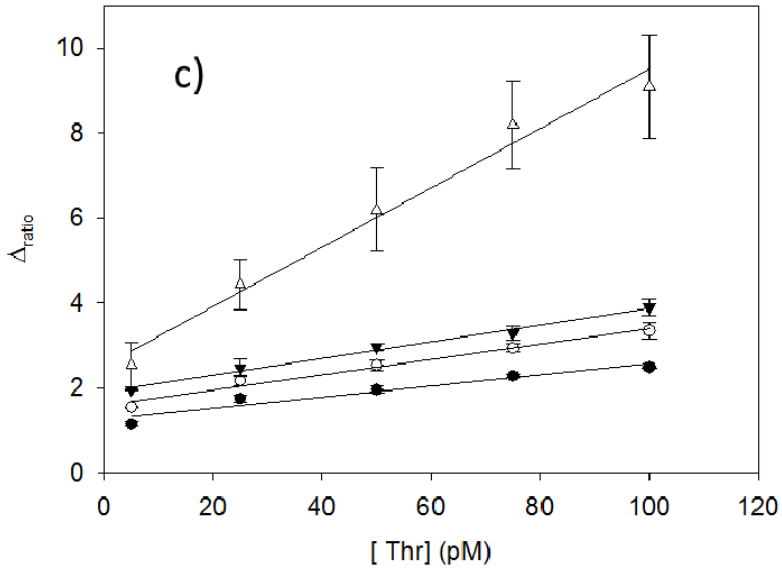

Fig. 5

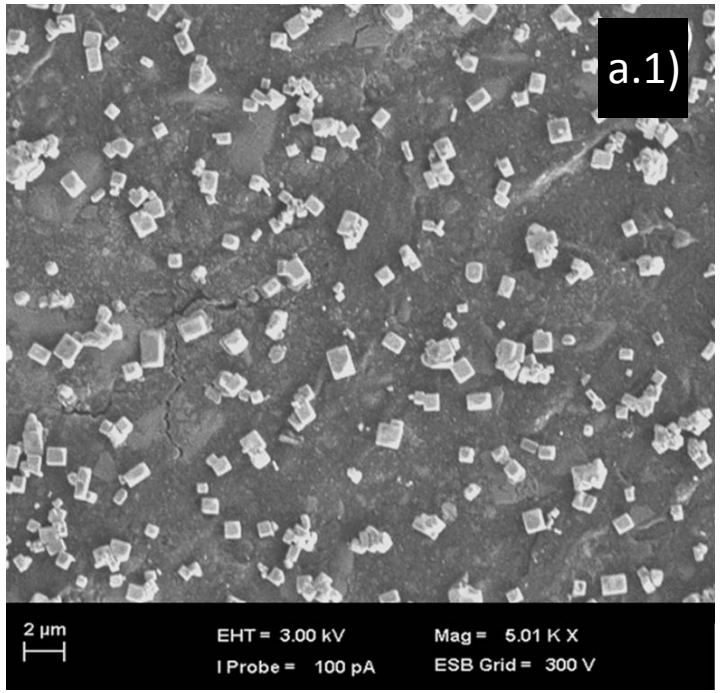
a.1)
2 µm
EHT = 3.00 kV
I Probe = 100 pA
Mag = 5.01 K X
ESB Grid = 300 V

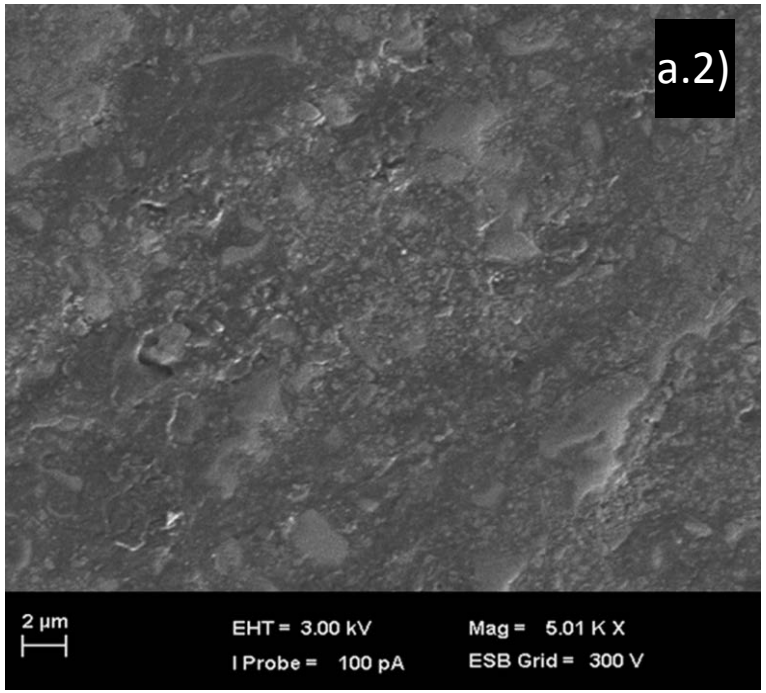
a.2)
2 µm
EHT = 3.00 kV
I Probe = 100 pA
Mag = 5.01 K X
ESB Grid = 300 V

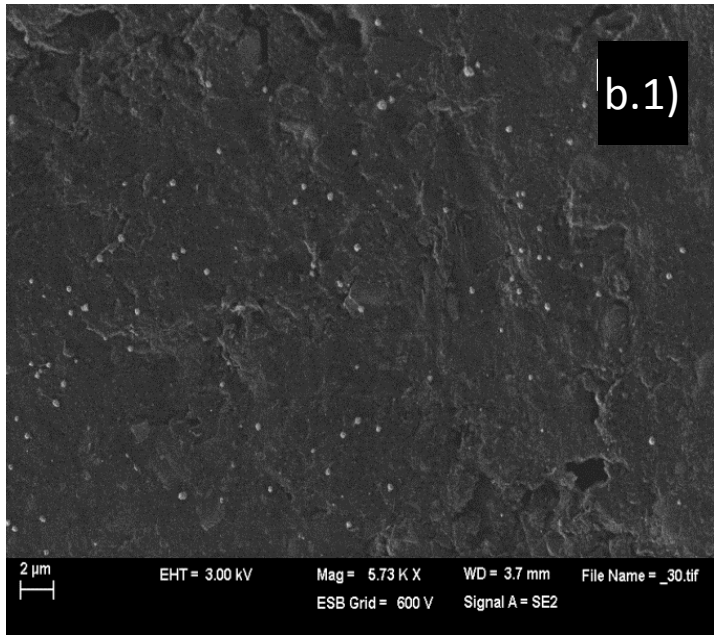
b.1)
2 µm
EHT = 3.00 kV
Mag = 5.73 K X
ESB Grid = 600 V
WD = 3.7 mm
Signal A = SE2
File Name = _30.tif

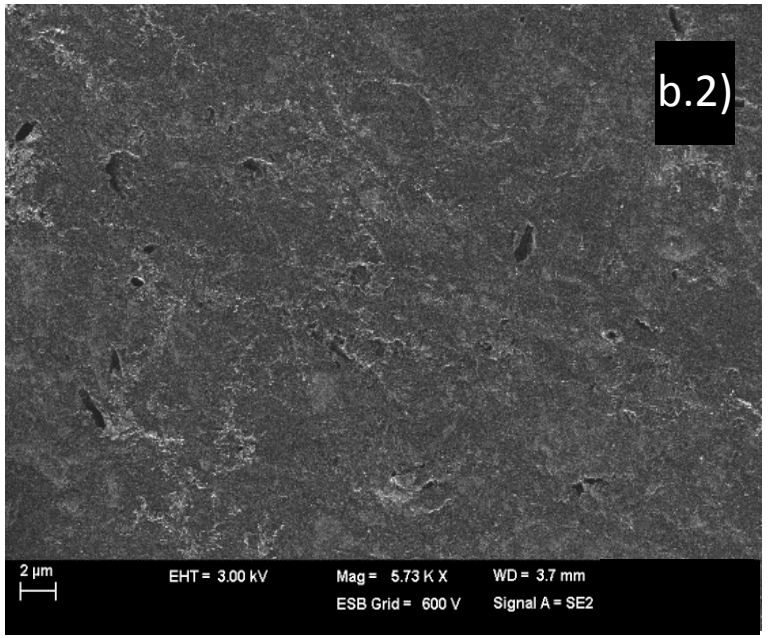
b.2)
2 µm
EHT = 3.00 kV
Mag = 5.73 K X
ESB Grid = 600 V
WD = 3.7 mm
Signal A = SE2

Fig. 6

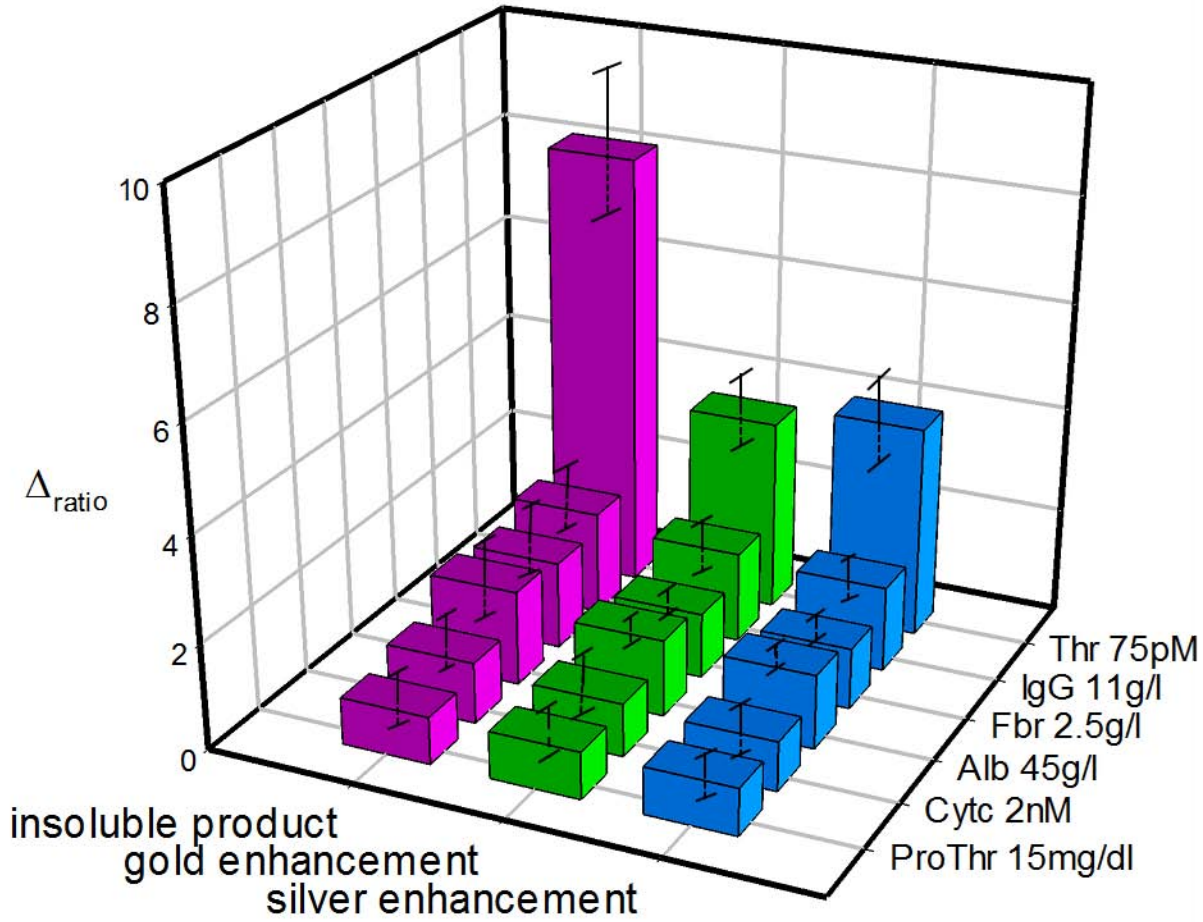
10
8
6
4
2
0
Δ_{ratio}
insoluble product
gold enhancement
silver enhancement
Thr 75pM
IgG 11g/l
Fbr 2.5g/l
Alb 45g/l
Cytc 2nM
ProThr 15mg/dl